UNIVERSITY OF SOUTHAMPTON

A multiwavelength analysis of M31's globular clusters and their low mass X-ray binaries

Mark B. Peacock
Submitted for the degree of Doctor of Philosophy
SCHOOL OF PHYSICS AND ASTRONOMY
FACULTY OF ENGINEERING, SCIENCE AND MATHEMATICS

May 24, 2010

UNIVERSITY OF SOUTHAMPTON

ABSTRACT

FACULTY OF ENGINEERING, SCIENCE AND MATHEMATICS

SCHOOL OF PHYSICS AND ASTRONOMY

Doctor of Philosophy

A multiwavelength analysis of M31's globular clusters and their low mass X-ray binaries

by Mark B. Peacock

Globular clusters (GCs) are dense groups of thousands to millions of stars. They are often very old systems with ages similar to those of their host galaxies and the early Universe. These clusters provide unique laboratories for astrophysical research and have been used by countless studies to improve our understanding of the Universe. In particular, they are ideal locations for studying stellar evolution and the formation and evolution of galaxies. They also provide unique locations for studying individual exotic objects, such as X-ray binaries. In this study, I investigate the properties of GCs in the nearby spiral galaxy, M31. This galaxy hosts the largest GC population in the Local Group. This, combined with its relative proximity to us, makes it an important bridge between studies of Galactic and extragalactic GCs. However, previous catalogues of these clusters have suffered from significant inhomogeneity and contamination from both stars and galaxies. In this contribution I present new, homogeneous, optical and near infra-red photometry of the M31 GC system. In addition to this, the structural parameters for over half of the known clusters are determined through fitting point spread function convolved King models to their density profiles. This photometry is used to remove significant contamination from non-cluster sources in previous cluster catalogues and to confirm a large population of young clusters in the M31 cluster system. Determining the properties of these clusters is very important in investigating both this, and other, GC systems. It is also of great benefit in investigating the exotic objects hosted by these clusters. I combine these data with archived *XMM Newton* observations, to study the low mass X-ray binaries (LMXBs) in M31's clusters. LMXBs are known to be relatively common in GCs and, through studying the properties of the GCs which host them, it is possible to investigate the effects of cluster environment on the formation and evolution of these systems. From this work, I demonstrate that the presence of LMXBs is proportional to the stellar collision rate of a GC. This provides good observational evidence that these LMXBs are formed through dynamical interactions. These data are also used to consider the morphology of horizontal branch stars in M31's GCs. Published *GALEX* ultraviolet observations of these clusters are used as a probe into their hot stellar populations. From this work, I propose a relationship between the core density of these clusters and their ultraviolet colour. This result suggests that the formation of (FUV bright) extreme horizontal branch stars may be enhanced in dense stellar environments through stellar interactions.

DECLARATION

ACKNOWLEDGEMENTS

I would like to start by thanking those people whose ideas and advice have helped to produce the science contained in this thesis. Obviously, I am very grateful to Tom Maccarone for initially starting me off on this interesting project, for being patient, and for providing help and guidance thoughout. Of real benefit were the *very* detailed comments provided by Arunav Kundu and Christian Knigge on some of the science presented in this thesis. As were the comments and suggestions of my other collaborators Steve Zepf, Chris Waters and Dave Zurek. I would also like to thank Chris Waters for writing, sharing and helping me to use the King model fitting code used in this work.

A special mention should go to all my office mates past and present, who have made my time at Southampton so enjoyable. The early leavers, Dave (whose acknowledgements I shall not try to compete with) and Mo (who for some reason decided Paris would be a nicer place to live than sunny Southampton). I genuinely appreciated both of your help in solving some of the 'I cant use anything problems' when I started. The earliest leaver of them all, Vanessa, who quickly moved on to the heady heights of the other corridor. Matthew, who provided endless distracting chat and yet never enough tea. Yang, who along with Simone, left me standing in the race to finish. Martin deserves a particular mention for helping me to develop my secretarial skills. Lee, who I met in the office a couple of times between 'observing trips'. Dan, who despite hiding around the corner has been a welcome addition. And last but not least, Liz and John, who made their presence felt despite arriving late. Liz, I hope you don't get too dehydrated when I leave.

I would also like to thank everyone else at Southampton for their help, advice and for being part of such a friendly environment. In particular, I'd like to thank Simon, without whom this computer wouldn't be working. Omar, for passing on this thesis template and for kindly hanging around in Southampton long enough to solve my last minute problems. Marge, for ensuring I didn't miss the daily coffee, lunch, coffee breaks (we have become slack since you left). Grace for helping me live the film star lifestyle, well a little bit of the lifestyle, for a day. A mention should also go to the Tonys for having an original name: Tony (the Tiger, if only that name had stuck); Tony (I'm not sure he's at Southampton, but he seems to be here more than me) and Tony (used to be a Pompey fan, but may have to find another club soon...). Tana, who I wish the best of luck as Tom's latest protege, I'm sure it will all go smoothly. And of course everyone else I've forgotton ...

Finally, I'd like to thank my family for all their support over the past few years and my friends, in particular Diana (because I promised I'd mention her), for providing welcome distractions.

Contents

1 Introduction **1**

1.1 Globular Clusters . . . 1

1.1.1 Stellar populations . . . 2

1.1.2 Integrated colours, age and metallicity . . . 7

1.1.3 Globular clusters and galaxy formation . . . 10

1.1.4 Exotic objects in globular clusters . . . 16

1.2 X-ray Binaries . . . 18

1.2.1 Low mass X-ray binaries . . . 19

1.2.2 Formation of low mass X-ray binaries . . . 23

1.2.2.1 Primordial formation . . . 23

1.2.2.2 Dynamical formation . . . 24

1.2.3 Low mass X-ray binaries in globular clusters . . . 26

2 The M31 globular cluster system: a WFCAM and SDSS photometric survey **30**

2.1 Abstract . . . 30

2.2 Introduction . . . 31

2.2.1 The M31 globular cluster system . . . 31

2.3 Photometry of clusters and candidates . . . 34

2.3.1 Identification of clusters . . . 34

2.3.2 Optical photometry . . . 35

2.3.2.1 *ugriz* data . . . 35

2.3.2.2 Identification and locations of clusters . . . 37

2.3.2.3 Photometry . . . 38

2.3.2.4 Comparison with previous photometry . . . 42

2.3.2.5 Variability in B383: a classical nova? . . . 45

2.3.3 Near-infrared photometry . . . 46

2.3.3.1 K-band data . . . 46

2.3.3.2 Photometry . . . 47

2.3.3.3 Comparison with previous photometry . . . 47

2.3.4 Summary of photometry . . . 50

2.4 Classification of sources . . . 51

2.4.1 Stellarity 51
2.4.2 Visual examination 54
2.4.3 Colours 54
2.4.3.1 Young clusters 56
2.4.3.2 Old globular clusters 57
2.4.3.3 Extended clusters in the halo of M31 58
2.4.4 Final classification 59
2.5 Properties of confirmed clusters 61
2.6 Conclusions 62

3 The structural parameters of globular clusters in M31 64
3.1 Abstract 64
3.2 Introduction 65
3.3 Wide Field Camera data 66
3.4 M31 globular clusters 66
3.4.1 Selection of globular clusters 66
3.4.2 Profile fitting of M31’s old clusters 67
3.5 Reliability of parameters 68
3.5.1 Consistency checks 69
3.5.2 Comparison with previous work 70
3.6 The structure of M31 globular clusters 72
3.7 Summary 76

4 Low mass X-ray binaries in M31 globular clusters 78
4.1 Abstract 78
4.2 Introduction 79
4.3 M31 globular clusters 81
4.4 The X-ray population of M31’s globular clusters 82
4.4.1 *XMM-Newton* observations of M31 82
4.4.2 The 2XMMi catalogue 83
4.4.3 M31 globular clusters in 2XMMi 84
4.4.4 Detections from previous catalogues 88
4.4.5 Candidate clusters and other sources 91
4.5 Population of LMXBs 92
4.6 LMXB-GC relationships 94
4.6.1 Stellar collision rate and mass 97
4.7 Conclusions 101

5 The ultraviolet colour of globular clusters in M31: a core density effect on the formation of extreme horizontal branch stars? 102

5.1 Abstract 102
5.2 Introduction 103
5.3 M31 globular cluster data 105
5.4 UV properties of M31 clusters 108
5.4.1 Metallicity relationships 108
5.4.2 Density/ Mass relationships 108
5.4.3 Milky Way globular cluster data 112
5.4.4 Low mass X-ray binaries and other FUV-bright sources . . . 114
5.5 Conclusions 116

6 Summary 118

APPENDICES

A Catalogue of old clusters in M31 (table 2.1: old clusters) 122

B Catalogue of young clusters in M31 (table 2.1: young clusters) 136

C Catalogue of candidate clusters in M31 (table 2.1: candidate clusters) 142

D The structural parameters of old clusters in M31 (table 3.1) 155

Bibliography 160

LIST OF TABLES

2.2 Photometry of B383 45
2.3 Classifications of sources 60
3.1 Structural parameters of old clusters in M31 (sample) 68
4.1 XMM-Newton observations of M31 83

4.2 M31 clusters in 2XMMi 85
4.3 All old clusters from P10 with proposed X-ray emission 89
4.4 Candidate clusters and non-clusters with proposed X-ray emission . 90
5.1 FUV luminosity of selected Galactic LMXBs 115

LIST OF FIGURES

1.1 The Galactic globular cluster M15. Constructed from optical *g*,*r* and *i*-band images from the Sloan Digital Sky Survey (SDSS; mosaiced together using the program MONTAGE, http://hachi.ipac.caltech.edu:8080/montage/). 3
1.2 Colour magnitude diagram of M15 based on *g* and *r*-band observations from the Sloan Digital Sky Survey. This is produced using the published photometry of An *et al.* (2008). Labelled are the main stellar populations in the cluster. These are the main sequence (MS), blue straggler (BS), red giant branch (RGB) and horizontal branch (HB) stars. 4
1.3 An example of using optical and near-infrared photometry to estimate the ages and metallicities of GCs. This figure is taken from Kundu *et al.* (2005). It shows the colour of globular clusters in NGC 4365 and NGC 1399 obtained from deep *HST* photometry. Also indicated are the expected colours of clusters with certain ages (blue, dashed lines; 1, 3, 5, 8, 11, and 15 Gyr left to right) and metallicities (red, solid lines; -1.7, -0.7, -0.4, 0, 0.4 dex from bottom to top). The predicted colours are from the SSP models of Bruzual and Charlot (2003). These data demonstrate the potential of near-infrared and optical colours to separate age and metallicity effects. It can be seen that there is a population of clusters in NGC 4365 that have colours consistent with intermediate ages of $\sim$3 Gyr. 9

1.4 The colour of GCs as a function of projected galactocentric radius. This figure is taken from Tamura *et al.* (2006b). This figure shows that both of these globular cluster systems are bimodal. It can also be seen that the relative number of red to blue clusters decreases with the distance from the centre of these two galaxies. 12

1.5 The mean metallicities of the red (top, solid points), blue (bottom, open bottom) and all globular clusters (points) as a function of luminosity of their host galaxies. This figure, taken from Peng *et al.* (2006), is the average of all galaxies observed in the ACS Virgo cluster survey. It can be seen that the average metallicity of both the red and blue cluster systems increases as a function of host galaxy luminosity. 13

1.6 The specific frequency of red GCs (*top*) and blue GCs (*bottom*) as a function of the mass of their host galaxies. Open squares are elliptical galaxies, filled squares are elliptical galaxies in clusters and open circles are spiral galaxies. It can be seen that the specific frequency of both the blue and the red cluster systems appear to be larger in massive galaxies. This figure is taken from Brodie and Strader (2006) using data from Rhode *et al.* (2007). 15

1.7 A schematic view of a low mass X-ray binary, produced by Robert Hynes. Annotated are the key features of these systems. 20

1.8 Cartoon of the possible evolution of a low mass X-ray binary system form a primordial binary. This figure is taken from Tauris and van den Heuvel (2003). 24

1.9 The magnitude (*left*) and colour (*right*) of all GCs (open) and LMXB hosting GCs (solid) in five elliptical galaxies. Taken from Kundu *et al.* (2007). 28

2.1 *(open)* The radial velocity distribution of M31's GCs, taken from the spectroscopic survey of Perrett *et al.* (2002). *(filled grey)* The radial velocity distribution of Milky Way halo stars, from Brown *et al.* (2010). To compare the populations, the number of halo stars plotted is 25% of the total Brown *et al.* (2010) sample. The dashed line indicates the radial velocity of M31 (-304 kms^{-1}; de Vaucouleurs *et al.*, 1991). 32

2.2 Coverage of the SDSS and WFCAM images used. For reference all objects listed in the RBC are shown in red. Only images covering the locations of these objects were extracted from the SDSS archive. The green ellipse indicates the D_{25} ellipse of M31. The grid represents $2^{\circ} \times 2^{\circ}$ squares on the sky (13.6×13.6 kpc at the distance of M31) and highlights the spatial extent of the GC system. 36

2.3 Difference between the location of objects in our images and their location in the RBC (solid) and C09 (open). In both cases, data are grouped into 0.2 arcsec bins. 38

2.4 The aperture radii used to measure the total *g*-band (*open*) and K-band (*solid, grey*) magnitudes of M31's clusters. 40

2.5 *Top:* comparison between our total cluster magnitudes and those from C09. *Bottom:* comparison between our total cluster magnitudes and colours and those from the Barmby catalogue (B2000). In all cases the y axis is our photometry minus that obtained previously. The highlighted point indicates the cluster B383. 43

2.6 Comparison with previous K-band photometry from the RBC (*bottom*) and profile fits to these WFCAM images from Peacock *et al.* (2009) (*top*). The errors quoted are from our photometry only, as errors are not available from the previous work. 48

2.7 WFCAM and 2MASS images of the faint cluster B041. Both images are 45 arcsec $\times$ 45 arcsec and demonstrate the improved spatial resolution and signal to noise of the WFCAM images over 2MASS. 49

2.8 Stellarity of objects classed as confirmed clusters (red) and candidate clusters (grey) in the RBC (their class 1 and 2 sources respectively) and from K07 (their class A and B/C sources respectively). Also included are the re-classifications for many of these sources from C09 (their old and young clusters). The stellarity is based on SEXTRACTOR photometry of the WFCAM images. Extended sources have a stellarity close to 0 and point sources close to 1. . . . 52

2.9 Colours of clusters and candidates from the RBC (*left*), K07 (*middle*) and C09 (*right*). Included are objects classified as confirmed old clusters (red), young clusters (blue), and candidate clusters (grey) from each catalogue. The black points show the colours of Milky Way GCs. The arrow represents a reddening of $E(B-V) = 0.1$. . . 55

2.10 *Top:* Colours of previously confirmed clusters which are confirmed here to be extended (red). *Bottom:* Colours of proposed candidate clusters which are confirmed to be extended (grey). The lines indicate linear fits to the colours of all confirmed M31 GCs. The black points indicate the colours of the Milky Way GCs and the arrow represents an extinction of $E(B-V) = 0.1$. 58

2.11 K-band GCLF for all sources classed as confirmed GCs (solid, red) and young clusters (open, blue). 61

3.1 Comparison between the core radius (r_c, *top*), integrated K-band magnitude (K, *middle*) and stellar collision rate (Γ, *bottom*) derived from fitting different observations of the same cluster. 70

3.2 Comparison between the core radii (r_c), half light radii (r_h), tidal radii (r_t) and stellar collision rates (Γ) measured in this study and those measured by Barmby *et al.* (2007, B07). The Barmby *et al.* (2007) parameters were obtained using *HST* STIS/ACS (solid circles) and WFPC2 (open circles) observations. 71

3.3 Structural parameters of M31 GCs (*top*) and Milky Way GCs (*bottom*). The dashed line indicates the GCs in the Milky Way over a similar galactocentric radius. It should be noted that the core densities are K-band luminosity densities for the M31 GCs and V-band luminosity densities for the Milky Way clusters. 73

3.4 Properties of M31's GCs (crosses) as a function of projected distance to the centre of M31 (R_{gcp}). Bold points show the median values for clusters binned on R_{gcp}. The line demonstrates the relationship found by Barmby *et al.* (2007) between r_h and R_{gcp}. 75

4.1 SDSS *i*-band (*left*) and WFCAM K-band (*right*) images of the GCs B035 (*top*), B094 (*middle*) and B146 (*bottom*, note that no K-band image is available for this cluster). The GC location from the catalogue of P10 is indicated by the red circles of radius 2 arcsec. The blue circle shows the XMM source location with its 1σ error. The Chandra positions from Di Stefano *et al.* (2002) (cross) and Williams *et al.* (2004) (plus) are shown where available. 87

4.2 Flux of cluster X-ray sources as a function of the clusters luminosity (left) and stellar collision rate (right). 92

4.3 The transient X-ray source in B128. 93

4.4 *(top)* The dereddened colour and metallicity for all clusters (open, red) and LMXB hosting clusters (solid, black). *(bottom)* the scaled cumulative frequency of the two populations. The cluster colours are taken from the catalogue of P10, while their spectroscopic metallicities taken from the collated table of Fan *et al.* (2008). It can be seen that the LMXBs tend to favour redder, higher metallicity, clusters. 95

4.5 X-ray hardness as a function of cluster metallicity (hardness ratios are defined in section 4.4). 96

4.6 Hardness of a source as a function of its flux. Red points show metal rich clusters (with $[Fe/H] < -0.7$), while blue points indicate metal poor clusters. It can be seen, particularly in the HR_2 plot, that the metal rich clusters do appear to be softer. While there is found to be a significant difference in the HR_2 between these populations, it can be seen that there are relatively few metal rich clusters in our sample. 97

4.7 *(top)* The stellar collision rate and luminosity for all clusters (open, red) and LMXB hosting clusters (solid, black). *(bottom)* the scaled cumulative frequency of the two populations. The GC data are taken from the catalogue of P10. It can be seen that the LMXBs tend to favour brighter clusters with higher stellar collision rates. 98

4.8 Stellar collision rate vs magnitude for all GCs (crosses) and LMXB hosting clusters (solid diamonds). This shows a clear relationship between the two parameters. This is in good agreement with the predicted relationship $\Gamma \propto M_{tot}^{1.5}$ (dashed line). The LMXB hosting clusters are found to have higher than average collision rates for their magnitude. 99

4.9 This shows the cumulative fractional collision rate for all GCs (small crosses) and LMXB hosting GCs (large crosses). If the formation of LMXBs is linearly proportional to GC collision rate, they should be evenly distributed along this plot. 100

5.1 Optical colour magnitude diagram for all M31 GCs with data from Peacock *et al.* (2010) and E(B-V)<0.16 from Fan *et al.* (2008). Small grey points indicate all GCs, while open black circles indicate those clusters detected in the *GALEX* FUV observations. 107

5.2 The ultraviolet colours of M31's GCs as a function of both metallicity and optical colour. Colours are dereddened using the reddening estimates of Fan *et al.* (2008). The grey points/arrows show those clusters detected in the NUV but not the FUV. 109

5.3 The ultraviolet colours of M31's GCs as a function of mass and core density. 110

5.4 The dereddened FUV-NUV colour of M31's GCs as a function of core density. Solid circles show the densest 50% of clusters. At the top of this figure, we show the distribution of all clusters (open) and the dense clusters (solid). It can be seen that the denser clusters appear to have bluer UV colours. The grey arrows show the upper limits for clusters detected in only the NUV. 112

5.5 The UV properties of Milky Way GCs. UV data taken from updated table of Sohn *et al.* (2006) from the original IUE observations of Dorman *et al.* (1995). Colours are transformed into the *GALEX* filters using equation 5.3. Grey points indicate all Galactic GCs while open red circles show those with FUV and NUV data. Due to the large extinction for many of the Galactic GCs, these UV data are only available for 22 clusters. 114

THESIS OUTLINE

This study is broken down as follows. *Chapter 1* is intended as a general introduction to the subjects addressed in this work. *Chapters 2-5* contain the research presented in this thesis. *Chapter 6* summarises the overall findings of this contribution. The research chapters constitute studies in their own right, so readers interested in a particular section should be able to read them independently. Below is a brief description of the subjects addressed in the following chapters. I have also highlighted the contributions of others to the work presented. All of the research presented was primarily performed by myself but has also benefited from the ideas and comments of Tom Maccarone.

In *Chapter 2*, I present the results of a new survey of the M31 globular cluster (GC) system based on optical images from the Sloan Digital Sky Survey and near infrared observations from the Wide Field Camera on the UK Infrared Telescope. This chapter presents the colours of these clusters, considers the old and young clusters in the galaxy and investigates potential contamination in previous catalogues.

The properties of these clusters are further considered in *chapter 3*. Here we consider their structure by fitting PSF convolved King models to the cluster profiles. The code used to perform this King model fitting was kindly provided by Chris Waters. The details of this code itself I claim no credit for. These two chapters are based on work already published in the papers Peacock *et al.* (2009, 2010). Both of these papers benefited from detailed comments from Arunav Kundu and Christian Knigge. They also benefited from comments and ideas from Steve Zepf, Chris Waters and Dave Zurek.

The X-ray properties of M31's GCs are considered in *chapter 4*. This is based on data from the 2XMMi catalogue and provides the most homogeneous, deep, high spatial resolution X-ray survey of M31's GCs to date. The properties of the clusters hosting LMXBs are investigated using these data and the cluster properties determined in chapters 2 and 3. This chapter includes some work published in Peacock *et al.* (2009), but presents new, more homogeneous, data and includes a more complete discussion.

In *chapter 5*, I consider the influence of cluster density on the far ultraviolet properties of M31's GCs. This uses the newly derived structural parameters, combined with previously published *GALEX* near and far ultraviolet luminosities of the clusters. These data are used to investigate the horizontal branch population of M31's GCs. This work has benefited from ideas and suggestions from Christian Knigge and Andrea Dieball.

1
Introduction

This study is primarily concerned with investigating the properties of extragalactic globular clusters and the X-ray binaries they host. In this chapter, a general introduction is given to both globular cluster and X-ray binary systems. A more specific introduction to the topics investigated in each of the following science chapters is provided at the start of each chapter.

1.1 Globular Clusters

Globular clusters (GCs) are dense, roughly spherical groups of thousands to millions of stars. The GCs in our Galaxy have been observed for hundreds of years and some can even be seen with the naked eye. The Milky Way is now known to contain at least 150 of these clusters (although there are likely to be $\sim$20 unknown clusters hidden behind the Galaxy, Harris, 1996). Because of their relatively faint magnitudes, and small sizes, it took significantly longer for extragalactic GCs to be identified. However, in the pioneering work of Hubble (1932), GCs were detected around the local group galaxy M31 and were subsequently suggested from an excess of point sources in the giant elliptical M87 (e.g. Baum, 1955; Sandage, 1961; Racine, 1968). Globular clusters are now identified around almost all galaxies that are observed with sufficient detail. This includes galaxies of all morphological types, including some dwarf galaxies. The number of GCs in different galaxies varies significantly. For example, M31 (the focus of this study) contains over 400 GCs (Barmby *et al.*, 2000), while M87 (the cD galaxy at the centre of the Virgo cluster) is thought to contain over 10,000 (e.g. Tamura *et al.*, 2006a). To first order, the number of GCs in a galaxy is related to its mass (discussed in more detail below). Due to their proximity to us, the Galactic GCs remain the best studied. The properties of the Galactic GC system are available from the commonly used Harris catalogue (Harris, 1996). Throughout this study (unless otherwise stated), we use data from the Harris catalogue[1] to indicate the properties of the Milky Way's GCs. Many observational results are still based primarily on these clusters. However, in the era of the *Hubble Space Telescope (HST)* and large ground based telescopes, the data available for extragalactic GCs have improved dramatically. In this study we investigate the properties of extragalactic GC systems, in particular M31's GCs.

For many years, GCs have been used to study different aspects of astrophysics. For example, in a series of papers studying the distribution and distance to known GCs, Shapley (1918) provided some of the earliest estimates of the size of the Galaxy, noting that the Sun is significantly offset from the Galactic centre. More recently, GCs have been used to determine the distances to nearby galaxies (through measurement of the luminosity distribution of their GC systems, see e.g. Kissler-Patig, 2000), to investigate galaxy formation and evolution (see e.g. the review of Brodie and Strader, 2006), to investigate star formation and evolution and to study exotic objects hosted by the clusters. The properties of GCs and their application to such studies are described below.

1.1.1 Stellar populations

Figure 1.1 shows a *gri*-band image of the Galactic GC M15, as seen by the Sloan Digital Sky Survey (SDSS; see e.g. Adelman-McCarthy *et al.*, 2007). This image demonstrates the general structure of GCs. They are roughly spherical systems with small, very dense cores extending out to regions of much lower densities. A large number of bright, red stars can also be seen in this image. These red giant stars demonstrate the evolved stellar population of this cluster.

The colour magnitude diagram (CMD) of this cluster, based on these SDSS data, is shown in figure 1.2. This diagram shows the typical stellar populations observed in GCs. The large group of stars at the bottom of the plot are the core hydrogen

[1]taken from the February 2003 version: http://physwww.physics.mcmaster.ca/ harris/mwgc.dat

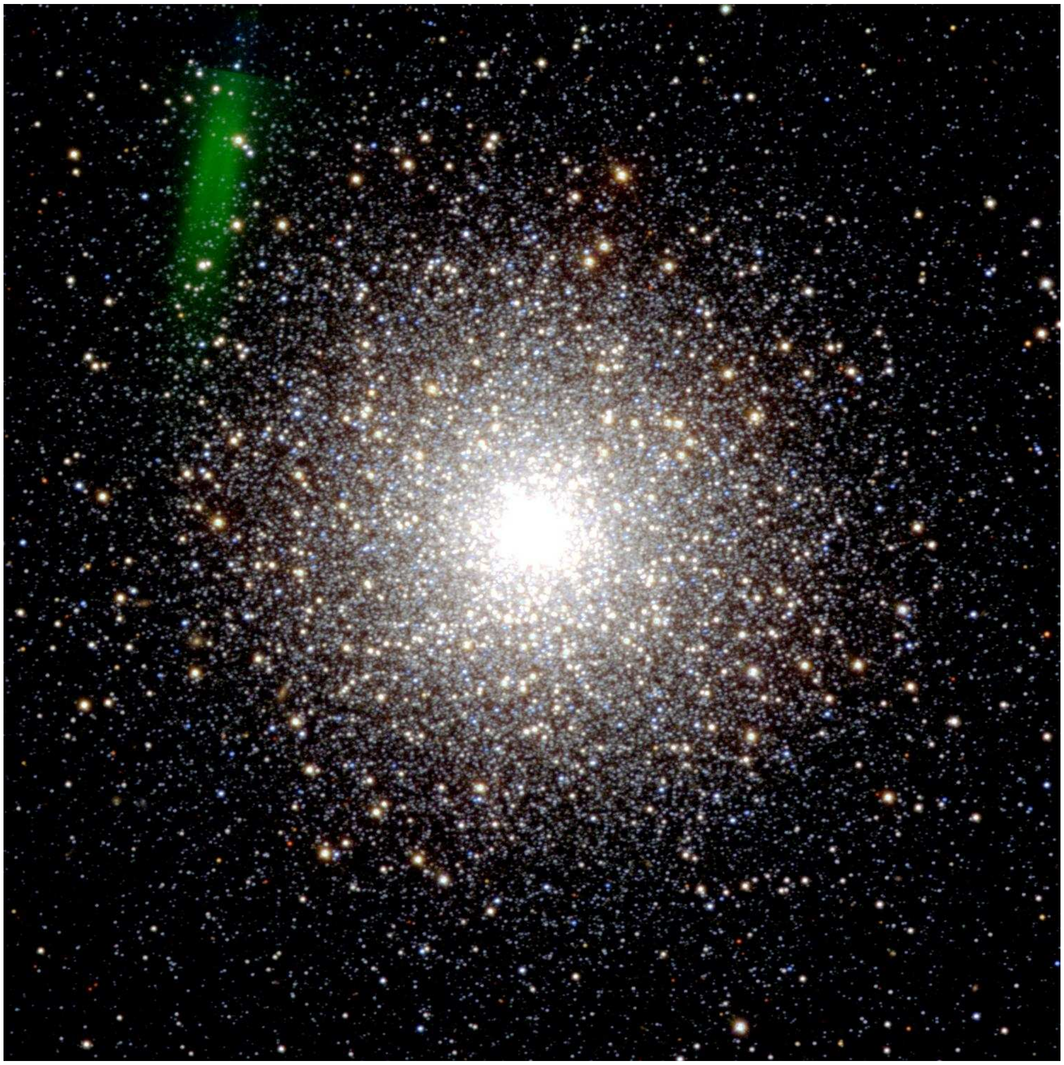

Figure 1.1: The Galactic globular cluster M15. Constructed from optical *g*,*r* and *i*-band images from the Sloan Digital Sky Survey (SDSS; mosaiced together using the program MONTAGE, http://hachi.ipac.caltech.edu: 8080/montage/).

burning main sequence (MS) stars. This CMD stops at r$\sim$21 mag, due to both crowding and the detection limits of these data. However, the MS is known to extend down to the lower right region of this plot, with decreasing stellar mass. The old age of M15's stellar population is demonstrated by the distinctive truncation of the main sequence. This is a common feature of Galactic GC CMDs and is due to massive stars evolving off of the MS to brighter, redder colours. The location of the MS turn-off, provides one of the best methods of estimating the age of a simple stellar population, with a single star formation epoch. Direct measurements of this MS turn-off have been used to determine the age of the Milky Way's GCs (with the most homogeneous estimates to date coming from the *HST* ACS survey of Marín-Franch *et al.*, 2009). Extending up from the MS to the bright, red region of figure

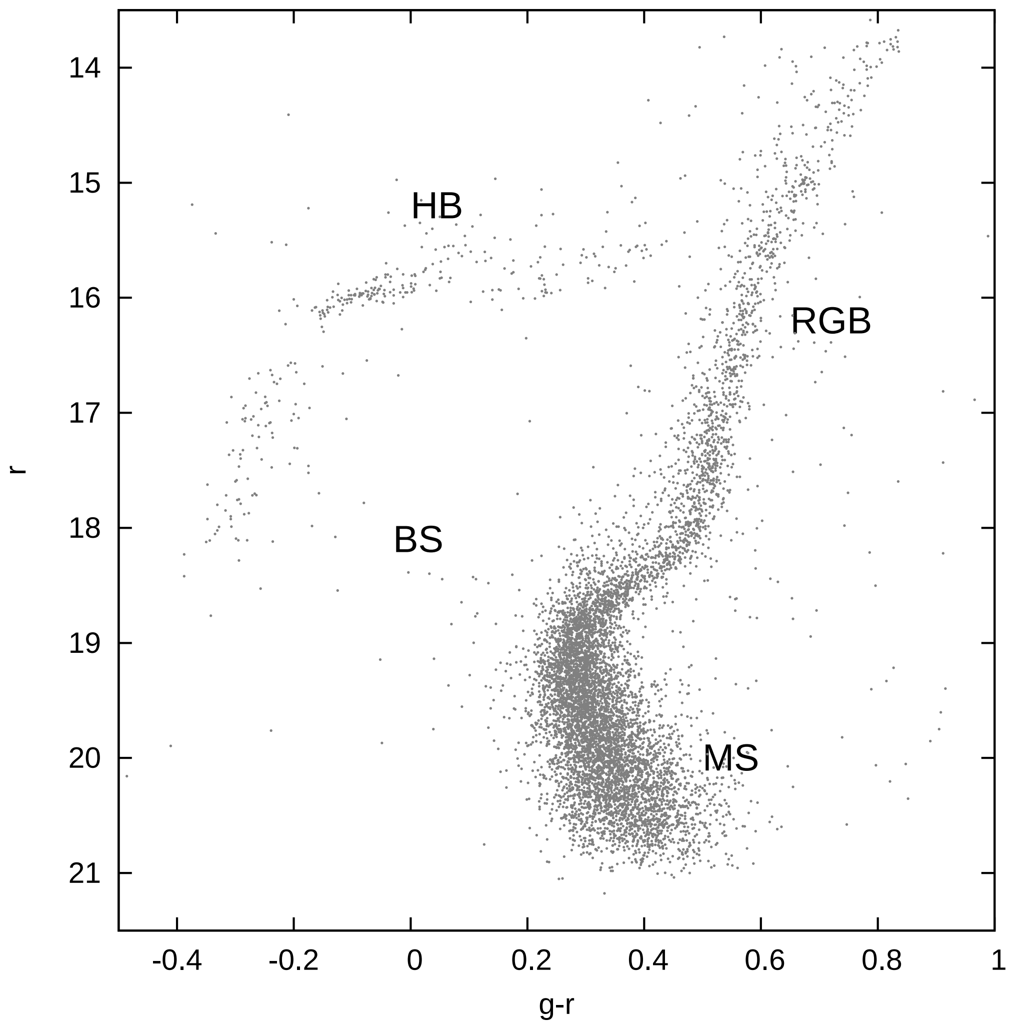

Figure 1.2: Colour magnitude diagram of M15 based on *g* and *r*-band observations from the Sloan Digital Sky Survey. This is produced using the published photometry of An *et al.* (2008). Labelled are the main stellar populations in the cluster. These are the main sequence (MS), blue straggler (BS), red giant branch (RGB) and horizontal branch (HB) stars.

1.2 are the red giant branch (RGB) stars in the cluster. The large cool envelopes of these stars gives them their distinctive colour and luminosity.

A small group of stars can be seen which lie on the MS, but beyond the observed main sequence turn-off. These are referred to as blue straggler stars (BS). Their high luminosities mean that these stars should have already evolved off the cluster main sequence long ago. It is therefore believed they must have gained mass at some stage of their evolution. The exact mechanism for the formation of these stars remains an area of active research. However, several methods have been proposed. These include: the merger of stars through stellar collisions (Hills and Day, 1976); mass transfer or coalescence of stars in binary systems (McCrea, 1964); or the evolution of triple systems, which can drive the coalescence of a very tight inner binary system (Perets and Fabrycky, 2009). No clear relationship between the stellar collision rate of a cluster and its BS population is observed in the Galactic GCs (e.g. Leigh *et al.*, 2007). Instead the core mass of a cluster is found to correlate with the BS population (Knigge *et al.*, 2009). This suggests that the binary formation scenario may be the dominant process in forming these stars. However, the fraction of BSs *is* found to increase towards the centre of some clusters, suggesting that stellar interactions in the dense cores of these clusters does play a role in their formation. It should also be noted that, the binary fraction itself may increase in clusters with high stellar collision rates. This is because of the dynamical formation of binary systems.

A further population of stars can be seen in figure 1.2, which extends blueward from the RGB. It can be seen that these stars have similar r-band luminosity, but a large spread in colour. Because of their appearance in optical CMDs (such as figure 1.2), these stars are referred to as horizontal branch (HB) stars. They were identified by Hoyle and Schwarzschild (1955) as being post RGB stars with helium burning cores and a thin hydrogen burning shell. It is currently thought that these stars have similar core masses of $\sim 0.5 M_{\odot}$ and thin hydrogen envelopes of mass 0.02-0.2$M_{\odot}$ (see e.g. Moehler, 2001). The observed spread in colour of these stars is thus related to the mass and opacity of their hydrogen envelopes. Those stars with less massive envelopes have higher effective temperatures and bluer colours. The production of these HB stars is thought to require significant mass loss while on the RGB. Furthermore, the spread in colour of HB stars, within individual clusters, probably suggests a spread in this mass loss (Rood, 1973).

Explaining the observed distribution of HB stars in Galactic GCs has been a long standing challenge, and is still not fully resolved (see e.g. the reviews of Moehler, 2001; Catelan, 2009). At an early stage in the investigation of these stars, the metallicity was identified as the primary parameter related to the HB population in a cluster (e.g. Sandage and Wallerstein, 1960). This is due to the fact that, for the same mass, metal rich HB stars will generally have redder colours than metal poor HB stars because of their increased opacity. However, the metallicity alone can not explain the observed HB populations in all Galactic GCs. Perhaps the most striking example of this is the different HBs observed in clusters with similar metallicities (e.g. NGC 288 and NGC 362: Bellazzini *et al.*, 2001). This has led to the long standing search for a 'second parameter' to explain the HB stars observed. This second parameter problem dates back as far as the proposed 'first parameter' (metallicity) (Sandage and Wallerstein, 1960). Investigating the second parameter has been the focus of many subsequent studies (as reviewed by: Fusi Pecci and Bellazzini, 1997; Catelan, 2009). Many processes have been proposed as the second parameter, and it is likely that more than one may play a role. Indeed, it has been proposed that 'non-global' parameters may also effect the HB population of individual GCs (e.g. Freeman and Norris, 1981). Some of the proposed second parameters include:

Age of the stellar population: The effect of increasing the age of a stellar population is to make the HB stars bluer (e.g. Lee *et al.*, 1994, 2000; Maraston, 2005). For GCs older than $\sim$10Gyr, the core mass of HB stars is thought to be roughly constant. Because older stellar populations will generally have lower masses, this means that, for the same mass loss on the RGB, the effective temperature of the HB stars will increase with age. The age of a cluster became one of the prime second parameter candidates following the work of Searle and Zinn (1978), where an observed variation with galactocentric radius was interpreted in terms of an age effect. The age of a stellar population certainly has an influence on the HB morphology. However, whether the age spread in the Milky Way's GCs is large enough to explain the observed HBs remains uncertain. For example, it was proposed by Rey *et al.* (2001) that the different HB populations of the clusters M13 and M3 could be produced by a difference in the age of the clusters. However, Catelan (2009) used the age estimates of Salaris and Weiss (2002) to show that the age difference between these clusters is unlikely to be large enough to explain the different HB populations. Age variations are also unlikely to explain the bimodal HBs observed in some clusters, where significant populations of both blue and red HBs are observed (e.g. NGC 6388 and NGC 6441 Rich *et al.*, 1997; Piotto *et al.*, 2002). This would require a large internal spread in ages.

Helium abundance: The helium fraction of a cluster has been another popular explanation. A stellar envelope with a higher helium fraction will have fewer electrons per unit mass. The resulting decrease in opacity will produce smaller envelopes and hence bluer colours. The helium abundance has gained impetus in recent years with the discovery of multiple main sequences in clusters, which may indicate a spread in helium abundance within the same cluster (e.g. ω Cen and NGC 2808: Lee *et al.*, 2005). Enhanced helium abundance has also been proposed as an explanation for the excess far-ultraviolet radiation observed in the brightest GCs in M87 (Sohn *et al.*, 2006; Kaviraj *et al.*, 2007).

Stellar core rotation: It is thought that stars with faster rotating cores will delay the onset of a helium flash. This results in HB stars with more massive cores and less massive envelopes. This means that faster core rotation may produce bluer HB stars (e.g. Mengel and Gross, 1976; Fusi-Pecci and Renzini, 1978; Peterson, 1985).

Mass loss: Ultimately the amount of mass loss on the RGB will determine the colour of the HB stars in a cluster. Hence a spread in this mass loss will produce a spread in the colours of HB stars (Rood, 1973; Peterson, 1982; Catelan, 2000).

Cluster core density: The stellar density in a cluster core might be expected to enhance the the mass loss from RGB stars, and hence produce bluer HB stars. Such a relationship is observed in the Milky Way's clusters for the 'blue tail' of the HB stars (extreme-HB/subdwarf B) (Fusi Pecci *et al.*, 1993; Buonanno *et al.*, 1997). This can also help to help explain the presence of extreme-HB stars in the metal rich, high density clusters, NGC 6388 and NGC 6441 (Rich *et al.*, 1997).

Due to the complexity of the observed HBs, and the limited sample of Galactic GCs, observations of extragalactic GCs would be of great benefit in investigating these parameters. Most of the observational data on HB stars is currently limited to the Galactic field, its GCs and the GCs of the LMC and SMC. This is due to the difficulty in resolving stellar populations in extragalactic GCs. It is possible to produce limited colour-magnitude diagrams for GCs at the distance of M31 using high spatial resolution *HST* images of the clusters (e.g. Mackey *et al.*, 2006). Unfortunately, for most extragalactic GCs, such colour magnitude diagrams are not available. However, it is possible to infer the HB morphology of extragalactic GCs indirectly by using UV observations (e.g. in M87 and M31 Sohn *et al.*, 2006; Rey *et al.*, 2007). Because of their sensitivity to high temperature objects, such wavelengths are known to be a good probe into the HB population of a GC (e.g. O'Connell, 1999; Brown *et al.*, 2004). In chapter 5 we investigate the effect of cluster core density on the HB stars in M31's GCs by using *GALEX* far-UV photometry.

1.1.2 Integrated colours, age and metallicity

As can be seen from figure 1.2, the Galactic GCs are found to represent a good approximation to a simple stellar population, hosting a population of stars with similar ages (as shown by the single MS turn-off) and metallicities (as demonstrated by the narrowness of the MS and RGB). This makes GCs unique locations to study stellar evolution and test models of simple stellar populations. It should be noted that recent observations suggest that the stellar populations of GCs are more complex than this. Deep *HST* observations have resolved the main sequence into multiple branches in some clusters (e.g. NGC 2808: Piotto *et al.*, 2007). Also spectroscopic abundances are found to vary between stars in the same cluster (e.g. red giants in NGC 2808; Carretta *et al.*, 2006). While this recent work provides interesting clues into the formation of GCs, these variations are small. In this study, we are concerned primarily with the properties of extragalactic GCs. Therefore such internal variation in age or metallicity of the stellar population of a cluster are likely to be much smaller than the errors on these parameters. For the remainder of this study, we therefore consider clusters to have a single age and metallicity.

Investigating the properties of extragalactic GCs is very important in order to study a larger and more diverse sample of clusters than the 150 clusters currently known in the Milky Way. However, given the increased distance of these extragalactic clusters from us, it is very difficult to resolve the individual stellar populations in these clusters. At the distance of M31, it is possible to produce colour magnitude diagrams for bright stars outside the cores of these clusters by using the superb spatial resolution of *HST* images (Mackey *et al.*, 2006; Perina *et al.*, 2009). For one of M31's GCs (B379) very deep HST exposures have been used to produce a colour-magnitude diagram for the cluster to the main sequence turn-off in the cluster. This allows a direct determination of its age (Brown *et al.*, 2004). However, this is the only cluster in M31 for which such data are available. For the majority of M31's GCs the properties of their stellar population have to be inferred from the integrated emission of the cluster. Fortunately, it is possible to estimate many cluster properties from integrated colours. With this in mind we present, as part of this study, a multiwavelength survey of the M31 GC system. This photometry, presented in chapter 2, provides self consistent, integrated colours for M31's GCs which are very useful in investigating their properties. The effects of age and metallicity on the colour of a cluster are discussed below.

It can be seen from the CMD in figure 1.2, that the integrated colour of a cluster will be strongly dependent on its stellar population. Clusters with an older stellar population will have a more truncated main sequence. This is because more massive stars exhaust their core hydrogen quicker and hence evolve off of the MS at earlier ages. The result of this is that older stellar populations will have fewer bright (blue) MS stars and more RGB stars. Hence, older GCs will have redder integrated colours than younger clusters. The metallicity of the stellar population in a cluster also has an influence on its colour. This is because, increasing the metallicity of a star increases the opacity of its atmosphere making it cooler than an equivalent metal poor star. The result of this is that both MS and RGB stars in metal rich clusters will have redder colours.

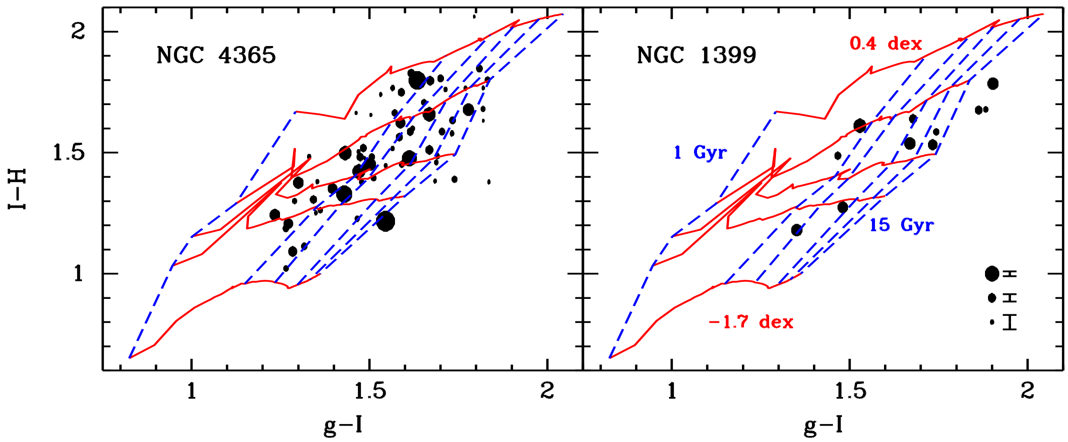

Figure 1.3: An example of using optical and near-infrared photometry to estimate the ages and metallicities of GCs. This figure is taken from Kundu *et al.* (2005). It shows the colour of globular clusters in NGC 4365 and NGC 1399 obtained from deep *HST* photometry. Also indicated are the expected colours of clusters with certain ages (blue, dashed lines; 1, 3, 5, 8, 11, and 15 Gyr left to right) and metallicities (red, solid lines; -1.7, -0.7, -0.4, 0, 0.4 dex from bottom to top). The predicted colours are from the SSP models of Bruzual and Charlot (2003). These data demonstrate the potential of near-infrared and optical colours to separate age and metallicity effects. It can be seen that there is a population of clusters in NGC 4365 that have colours consistent with intermediate ages of $\sim$3 Gyr.

These effects suggest that the integrated colours of a GC can be used to estimate the age and metallicity of the underlying stellar population. However, there is a notorious degeneracy between both of these parameters (e.g. Worthey, 1994). This is because increasing the age and the metallicity of the stars in a cluster both result in the cluster having redder colours. One method for (at least partially) breaking this degeneracy is to consider a combination of optical and near infrared colours of the cluster (e.g. Kissler-Patig, 2000; Puzia *et al.*, 2002; Kundu *et al.*, 2007). At optical wavelengths, the bright, blue stars, just below the main sequence turn-off, make a significant contribution to the total cluster luminosity. The colour of these stars is a function of both the age and the metallicity of the cluster. However, the near infrared is more sensitive to the cooler RGB stars in the cluster. The colour of these stars is primarily related to their metallicity. The result of this is that a combination of these colours can potentially discriminate between the effects of cluster age and metallicity.

Simple stellar population (SSP) models, such as those presented by Bruzual and Charlot (2003) and Maraston (2005), are found to reproduce the observed colour magnitude diagrams of GCs relatively well. These models can be used to estimate the integrated colours of a GC for a given age and metallicity. These colours are found to be in good agreement with observations of the Galactic GCs at optical and near infrared wavelengths (e.g. Bruzual and Charlot, 2003). Comparing these SSP models with optical and near infrared observations of extragalactic GCs is one of the most efficient ways of determining their ages and metallicities. An example of this method is shown in figure 1.3 (Kundu *et al.*, 2005). This shows the colour of GCs in NGC 4365 and NGC 1399 compared with the SSP models of Bruzual and Charlot (2003). It can be seen that some of the clusters in NGC 4365 have colours consistent with intermediate ages of around 3 Gyr (as originally proposed in this galaxy by Puzia *et al.*, 2002). This method has also been used to suggest a population of intermediate age GCs in several other galaxies: NGC 4365 (Puzia *et al.*, 2002; Kundu *et al.*, 2005); IC 4051, NGC 3311 (Hempel *et al.*, 2005); NGC 5813 (only a small sample: Hempel *et al.*, 2007). However, the ages determined for GCs in some other galaxies are consistent with only an old population: NGC 3115 (Puzia *et al.*, 2002); NGC 1399 (Kundu *et al.*, 2005); NGC 4472, NGC 4594, NGC 3585 (Hempel *et al.*, 2007). Spectral energy distribution (SED) fitting to SSP models from UV, optical and near infrared photometry have also been used to suggest a population of intermediate age clusters in M31 (Fan *et al.*, 2006). This is in agreement with a suggested population of old, intermediate and young clusters in 70 of M31's GCs, estimated from spectroscopy by Puzia *et al.* (2005). However, this population of intermediate age clusters in M31 is not identified in optical and near-infrared SED fitting by Jiang *et al.* (2003). It has also been noted that the spectroscopically identified intermediate age clusters in M31 may be old clusters whose spectra are effected by the population of HB stars in the clusters (e.g. Rey *et al.*, 2007; Strader *et al.*, 2009).

In this study, we do not attempt such fitting. However, we do note that the more accurate multiwavelength data of M31's GCs presented in chapter 2 should be of great use for such work in the future. We do make use of these colours, in chapter 2, to distinguish purely between young and old ($\gtrsim$1Gyr) clusters, based on the age sensitive *g*-*r* colour.

1.1.3 Globular clusters and galaxy formation

Globular cluster systems are very useful probes into galaxy formation and evolution. Because of this, we outline below some of the observed properties of GC systems and their implications in the context of galaxy formation. While the research presented in this study does not directly deal with such questions, we do note that determining the properties of M31's GCs are of benefit to such studies. This is because, along with the Milky Way's GCs, this is one of the few spiral galaxies in which the full GC system can be studied in detail. Many extragalactic GC observations focus on the cleaner, and more numerous, GC systems of early type galaxies. However, determining GC properties across a range of galaxy morphologies is very important in the context of constraining models.

Many GCs are known to have very old ages, similar to that of their host galaxies and the early Universe. It is also believed that major star formation periods in galaxies are accompanied by significant GC formation. This theory is supported by observations of interacting gas rich galaxies. In these systems significant star formation is triggered, and young, massive clusters are observed (e.g. the Antennae galaxy: Whitmore and Schweizer, 1995). Indeed, observations of massive, young clusters suggests that the number of these clusters is proportional to the star formation rate of the galaxy (Larsen and Richtler, 2000). Over time, some of these young clusters are disrupted, but the surviving systems are observable as old GC systems (for a description of the proposed evolution of a young cluster system, see e.g. Fall and Zhang, 2001). Because of the old ages of these clusters, and their link to star formation, the ages, metallicities and dynamics of a GC system provide a record of the formation and evolution of their host galaxies.

One of the most interesting observational results in the context of galaxy formation was the discovery of a bimodality in the colour of GC systems (e.g. in NGC 1399, NGC 4472 and NGC 5128; Ostrov *et al.*, 1993; Zepf and Ashman, 1993). This bimodality in colour has been attributed to a bimodality in the metallicity of these GC systems and the Milky Way is also known to host a population of metal rich and metal poor GCs. Since these early studies, cluster bimodality is now found in most galaxies observed in sufficient detail (e.g. Larsen *et al.*, 2001; Kundu and Whitmore, 2001). Bimodality has also been confirmed in M87 in the metallicity sensitive I-H bands (Kundu and Zepf, 2007). In the Milky Way, and other galaxies, it is found that the metal rich clusters are more centrally concentrated than the metal poor clusters, possibly providing a clue to their origins (e.g. Geisler *et al.*, 1996; Bassino *et al.*, 2006). This is demonstrated by figure 1.4 (taken from Tamura *et al.*, 2006b), which shows the bimodality is present in M87 and NGC 4552 and that the fraction of blue clusters increases at larger galactocentric radii. For a large survey of 100 early type galaxies in the Virgo cluster, Peng *et al.* (2006) confirmed bimodality in most bright galaxies observed. This bimodality is less obvious for the fainter galaxies, but this is likely due to it being harder to identify in the smaller GC systems of fainter galaxies. This, clearly peaked, bimodality suggests multiple major star formation episodes in the galaxies (e.g. Zepf and Ashman, 1993). The large datasets available from ACS observations of Virgo cluster galaxies have also

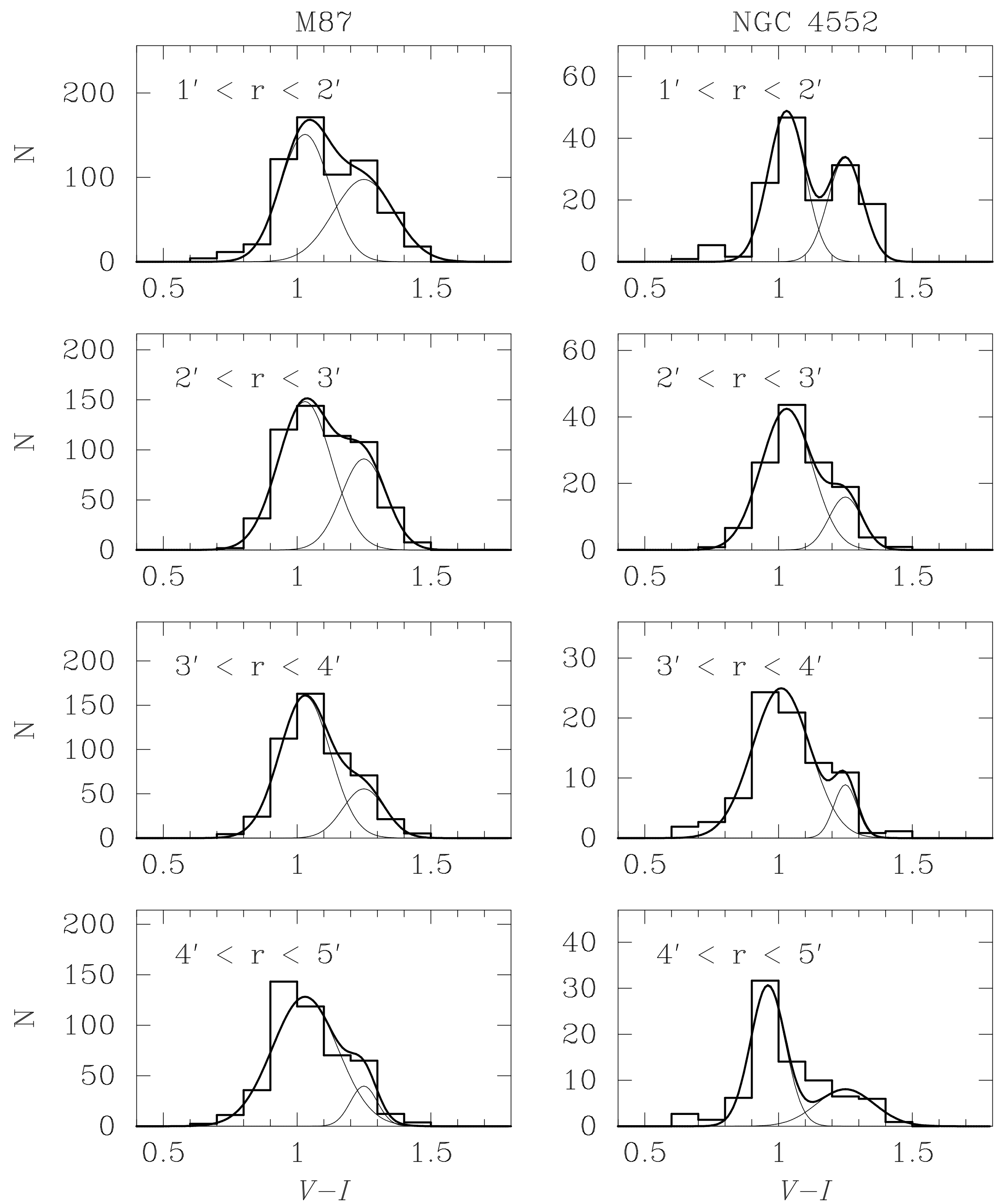

Figure 1.4: The colour of GCs as a function of projected galactocentric radius. This figure is taken from Tamura *et al.* (2006b). This figure shows that both of these globular cluster systems are bimodal. It can also be seen that the relative number of red to blue clusters decreases with the distance from the centre of these two galaxies.

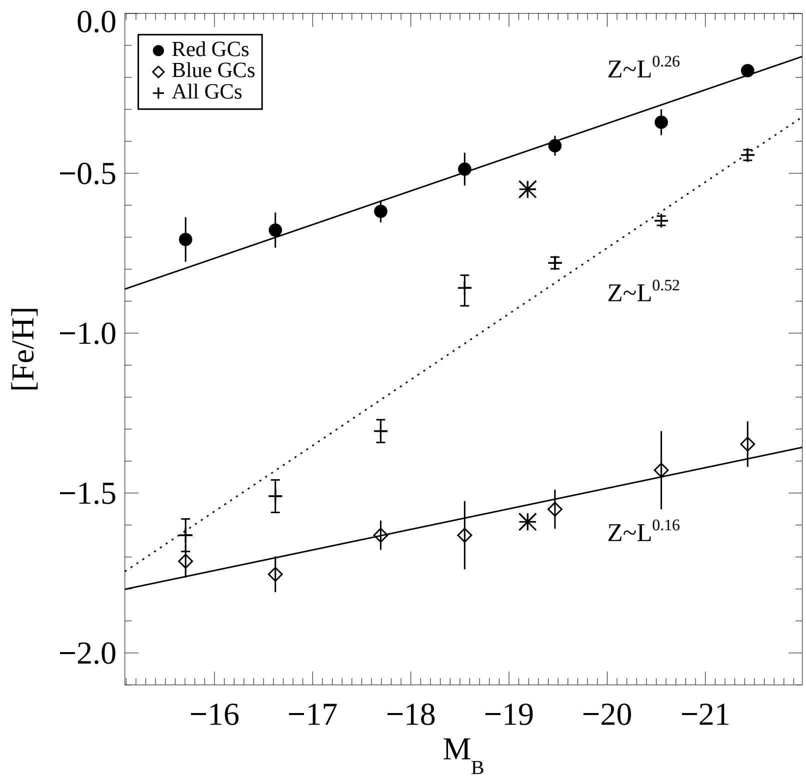

Figure 1.5: The mean metallicities of the red (top, solid points), blue (bottom, open bottom) and all globular clusters (points) as a function of luminosity of their host galaxies. This figure, taken from Peng *et al.* (2006), is the average of all galaxies observed in the ACS Virgo cluster survey. It can be seen that the average metallicity of both the red and blue cluster systems increases as a function of host galaxy luminosity.

demonstrated that, while most galaxies host a population of blue GCs, the fraction of red GCs increases significantly with the luminosity of their host galaxies (e.g. Peng *et al.*, 2006; Strader *et al.*, 2006). This result was in fact observed even before cluster bimodality was suggested. It was found that the mean metallicity of a GC system was related to the magnitude of the host galaxy (Brodie and Huchra, 1991). Interestingly, it is also found that the peak metallicity of both the metal rich and metal poor clusters increase (with similar slopes) with galaxy luminosity (Peng *et al.*, 2006; Brodie and Strader, 2006). This is demonstrated by figure 1.5 (taken from Peng *et al.*, 2006).

Ashman and Zepf (1992) predicted the bimodal (or multimodal) metallicity distribution in GC systems before it was first observed. They proposed that, in the formation of early type galaxies through major mergers between gas rich spiral galaxies, significant GC formation occurs. The resulting GC system is a combination of the original surviving metal poor GCs from the progenitor galaxies and the new GCs produced from the relatively metal rich gas. In addition to predicting the bimodality of GC systems, this scenario explains the larger specific frequency of GCs in elliptical galaxies compared with spirals. It also provides an explanation for the observed radial distributions of metal rich and metal poor clusters, with metal rich clusters being more centrally concentrated. However, there are some problems with the major merger model and additional scenarios have been proposed. Forbes *et al.* (1997) proposed in situ formation of GCs. The idea behind this model is that metal poor GCs form from fragmentation in the early stages of galaxy formation. This formation is then truncated by some process, before a second period of cluster formation occurs and produces the second population of higher metallicity clusters. The exact reason for this truncation remains unclear, although reionisation is a leading candidate (e.g. Santos, 2003). It has also been proposed that the accretion of GCs from less massive galaxies may produce the observed cluster systems (Côté *et al.*, 1998). If all galaxies host an initial population of GCs, whose metallicity is related to the mass of the galaxy, it is found that these models can produce the GC systems observed (Côté *et al.*, 2002).

It is clear that both high quality photometry and spectroscopy of extragalactic GC systems can be used to help constrain these models and provide important cosmological clues. Over the past decade, *HST* ACS observations, such as the Virgo cluster survey (Côté *et al.*, 2004) and Fornax cluster survey (Jordán *et al.*, 2007a), have produced a wealth of data on the GC systems of early type galaxies. These surveys are, by necessity of the field of view of the ACS, limited to the central regions of the massive galaxies in these clusters. Constraining the total GC systems out to larger radii is currently less well studied, although this situation is being improved through the use of large field of view detectors on ground based telescopes (e.g. Rhode and Zepf, 2004; Harris, 2009). The GC systems of extragalactic spiral galaxies are also comparatively poorly studied. This is primarily due to the increased complexity in these studies due to structure and extinction from the host galaxies. However, observations of the GC systems of spiral galaxies is improving from studies of edge on spiral galaxies (e.g. Rhode *et al.*, 2005, 2007) and improved wide field and high resolution observations of M31's GCs (partially aided by the work presented in this study and by e.g. Galleti *et al.*, 2004; Huxor *et al.*, 2008; Caldwell *et al.*, 2009).

To investigate the cluster population in different galaxies, the specific frequency (S_N) of the GCs in a galaxy was proposed by Harris and van den Bergh (1981). This is a measure of the number of GCs ($N_{\rm GC}$) normalised to the galaxies luminosity

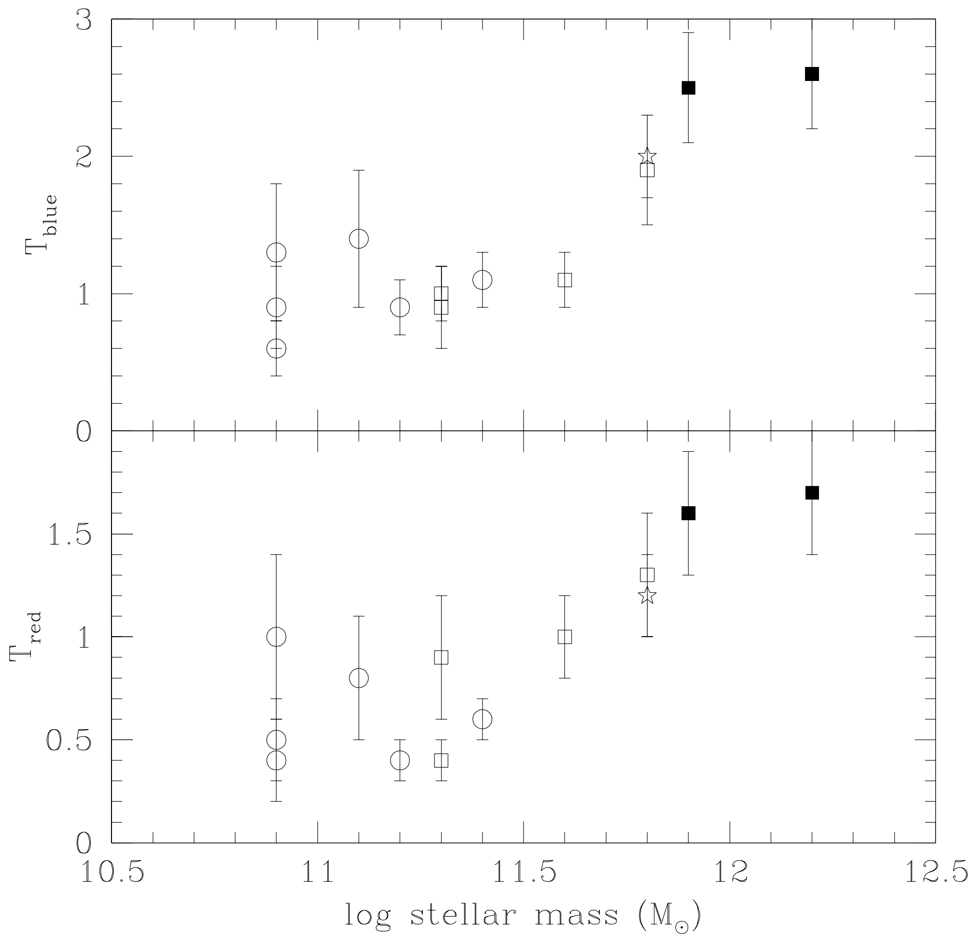

Figure 1.6: The specific frequency of red GCs (*top*) and blue GCs (*bottom*) as a function of the mass of their host galaxies. Open squares are elliptical galaxies, filled squares are elliptical galaxies in clusters and open circles are spiral galaxies. It can be seen that the specific frequency of both the blue and the red cluster systems appear to be larger in massive galaxies. This figure is taken from Brodie and Strader (2006) using data from Rhode *et al.* (2007).

(M_V). It is defined as:

$$S_N = N_{GC} 10^{-0.4(M_V+15)} \tag{1.1}$$

While this measure provides an intuitive normalisation, it scales the number of GCs to the luminosity of a galaxy and not to the desired mass. The mass-to-light ratios of different galaxies are known to vary, particularly for different morphological types. An alternative approach was used by Zepf and Ashman (1993). They defined the parameter T as:

$$T = \frac{N_{GC}}{M_G/10^9 M_\odot} \tag{1.2}$$

This has an advantage over S_N since it scales the number of clusters directly by galaxy mass (M_G). However, it should be noted that M_G is harder to estimate, and often comes from assuming a certain mass-to-light ratio for different galaxy types. Studies of both S_N (e.g. Harris, 1991) and T (e.g. Ashman and Zepf, 1998) suggested that bright elliptical galaxies appear to have higher fractions of GCs than spirals. Ashman and Zepf (1992) noted that this excess of clusters in elliptical galaxies could be explained by the formation of clusters in major mergers. Such a process would result in an increased number of red clusters in elliptical galaxies and hence make its GC system larger than the sum of its progenitor galaxies. Interestingly, it has recently been found that the specific frequency of blue GCs is also higher in more massive galaxies (figure 1.6, taken from Rhode *et al.*, 2007). Such a result is not expected from the major merger scenarios. Instead, Rhode *et al.* (2007) suggest that the result is consistent with biased hierarchical formation (West, 1993; Santos, 2003). It has also been proposed that dwarf galaxies can have high specific frequencies (e.g. Miller *et al.*, 1998; Peng *et al.*, 2008). Peng *et al.* (2008) note that the specific frequency of dwarf galaxies in the Virgo cluster increases towards the centre of the cluster, which may also suggest a bias in cluster formation due to the increased potential near the centre of the cluster. However, studying the GC systems of dwarf galaxies is very difficult due to a combination of their small GC populations, contamination from non-cluster sources and from GCs associated with nearby giant galaxies. It is important to note that, while specific frequencies are of use in constraining models of galaxy and GC formation, they remain relatively poorly constrained. This is because accurate measures of this quantity require high spatial resolution (in order to minimise contamination) and large fields of view (to measure the entire GC system). In several cases, where GC specific frequencies are remeasured, the derived specific frequencies are found to be lower than earlier studies (e.g. Rhode and Zepf, 2004; Brodie and Strader, 2006; Rhode *et al.*, 2007). There are also difficulties in determining the correct mass of the galaxies, which can influence the specific frequencies (e.g. McLaughlin, 1999; Dirsch *et al.*, 2003, 2005).

1.1.4 Exotic objects in globular clusters

Globular clusters are known to host relatively exotic objects among their stellar population. Many of these are likely to be related to the dense stellar environments at the centre of these clusters, which can be as high as $10^5 L_\odot/pc^3$. These objects include tight binary systems such as cataclysmic variables (e.g. Pooley and Hut, 2006), LMXBs and qLMXBs (e.g. Verbunt and Hut, 1987; Heinke *et al.*, 2003) and millisecond pulsars (e.g. Lyne *et al.*, 1987). All of these sources are discussed in more detail in section 1.2. As discussed above, GCs contain stellar populations with similar ages and metallicities. These stars are also at distances which are relatively easy to determine, compared with sources in the field of the Galaxy. This makes it relatively easy to determine source luminosities from fluxes in order to compare populations. For objects located in the field of the galaxy such parameters are often very difficult to estimate. This makes GCs useful locations for studying the individual objects they contain. Accurate estimates of the global properties of GCs are hence very useful in the investigation of these objects. In chapters 2 and 3, we investigate the colours and structure of M31's GCs. These are used in chapters 4 and 5 to investigate the bright LMXBs and HB stars in these clusters. These data could also be of use in investigating other sources in the future (e.g. milli-second pulsars detected by LOFAR: van Leeuwen and Stappers, 2010).

1.2 X-ray Binaries

An X-ray binary consists of a compact object accreting mass from a secondary donor star. The compact object, often referred to as the primary star, can be either a neutron star or a black hole. As such, these systems provide important locations for investigating the properties of both neutron stars and black holes. Indeed, X-ray binaries provided some of the first observational evidence for the existence of black holes (McClintock and Remillard, 1986; Casares *et al.*, 1992; Casares, 2007). They can also be used to test general relativity, in the extreme conditions around compact objects (e.g. Kaaret *et al.*, 1997; van der Klis, 2000), and to estimate the equation of state for neutron stars (e.g. Lattimer and Prakash, 2004). The properties of X-ray binary systems and accretion processes are discussed in detail in the excellent reviews of Lewin and van der Klis (2006) and Frank *et al.* (2002).

X-ray binaries are primarily split into two groups. These are based, not on the nature of their compact object, but on the mass of their *donor* stars. Low mass X-ray binaries (LMXBs) have donor stars less massive than the accreting compact object. In these systems, mass can be transferred, from the donor star to the compact object, via Roche lobe overflow. In this process, an accretion disk forms around the compact object. The hot inner regions of this disk make LMXBs very bright at X-ray wavelengths, while the cooler outer regions of the disk often dominate the system's optical emission. It is also possible for a compact object to accrete matter from a star which does not fill its Roche lobe. In these systems, known as high mass X-ray binaries (HMXBs), accretion can occur via a stellar wind from a very massive ($\gtrsim 10 M_{\odot}$) donor star. The X-ray emission from HMXBs is also dominated by the inner regions of an accretion disk around the compact object. However, their optical or near infrared emission can be dominated by the massive (and hence very bright) donor stars in the system. The magnitude of the donor stars in HMXBs makes it relatively easy to associate X-ray emission with an optical counterpart. Because of the high mass of the donor star in HMXBs, they have relatively short lifetimes compared with LMXBs. This is confirmed by the distribution of HMXBs and LMXBs in the Galaxy, where HMXBs are found in a thinner disk than LMXBs (Grimm *et al.*, 2002). An additional class of X-ray binaries exist in which the compact object is a white dwarf star. Known as cataclysmic variables (CVs), these systems also accrete mass via Roche lobe overflow. However, they are generally fainter than LMXBs due to the lower mass, and larger size, of the compact object.

In chapter 4 the X-ray emission from M31's GCs is considered. These clusters are not expected to host HMXBs. This is because massive donor stars should not be present in these old stellar populations. Instead, the X-ray emission from GCs is likely to originate from a combination of: LMXBs ($L_x \lesssim 10^{38}$erg/s); LMXBs which are not in outburst, 'quiescent' LMXBs (qLMXBs: $L_x \lesssim 10^{35}$erg/s); and CVs ($L_x \lesssim 10^{32}$erg/s). All of these X-ray binaries are observed to be relatively common in the Galactic GCs [e.g.: LMXBs, Verbunt and Hut (1987), Liu *et al.* (2001); qLMXBs, Heinke *et al.* (2003) and CVs, Pooley and Hut (2006)]. As can be seen from these luminosities, if a GC hosts LMXBs in outburst, then these systems are expected to be the dominant source of X-ray emission from the cluster. For Galactic GCs, the sub-arcsecond spatial resolution of the *Chandra* observatory makes it is possible resolve and detect these different X-ray sources in the cores of GCs [e.g. 47 Tuc (Grindlay *et al.*, 2001a); NGC 6397 (Grindlay *et al.*, 2001b); NGC 6752 (Pooley *et al.*, 2002a); NGC 6440 (Pooley *et al.*, 2002b); ω Cen (Rutledge *et al.*, 2002); NGC 6626 (Becker *et al.*, 2003); NGC 6121, M4 (Bassa *et al.*, 2004); M15 (Hannikainen *et al.*, 2005); NGC 288 (Kong *et al.*, 2006); NGC 2808 (Servillat *et al.*, 2008)]. However, for extragalactic GCs, the detection limits of the available observations usually limit us to studying only the (relatively bright) LMXBs in outburst. It is also not possible to resolve the individual X-ray sources in extragalactic GCs. Instead, X-ray surveys of extragalactic GCs (such as that presented in chapter 4) study the integrated X-ray luminosity. They therefore study whether a cluster hosts one, or more, LMXBs in outburst. Because LMXBs are the dominant X-ray sources in extragalactic GCs we focus on these systems in more detail below.

1.2.1 Low mass X-ray binaries

Our current understanding of an LMXB system is illustrated by figure 1.7. The compact object is in a binary system with a donor star which is close enough to fill its Roche lobe. This means that matter can be transferred from the donor star onto the compact object. However, the angular momentum of this accreting material is too large for it to accrete directly onto the compact object. Instead, it forms a ring of material orbiting the compact object at a radius consistent with its angular momentum. As this material accumulates it is subject to dissipative processes which cause it to lose some of its orbital potential energy. This causes the material to spiral closer to the compact object, forming an accretion disk around it. For this to occur the gas must also lose angular momentum. In the absence of external torques (for example from magnetic fields), this requires that angular momentum is transferred outwards within the disk. Thus we have a situation where the inner accretion disk loses angular momentum and spirals inwards, while the outer accretion disk

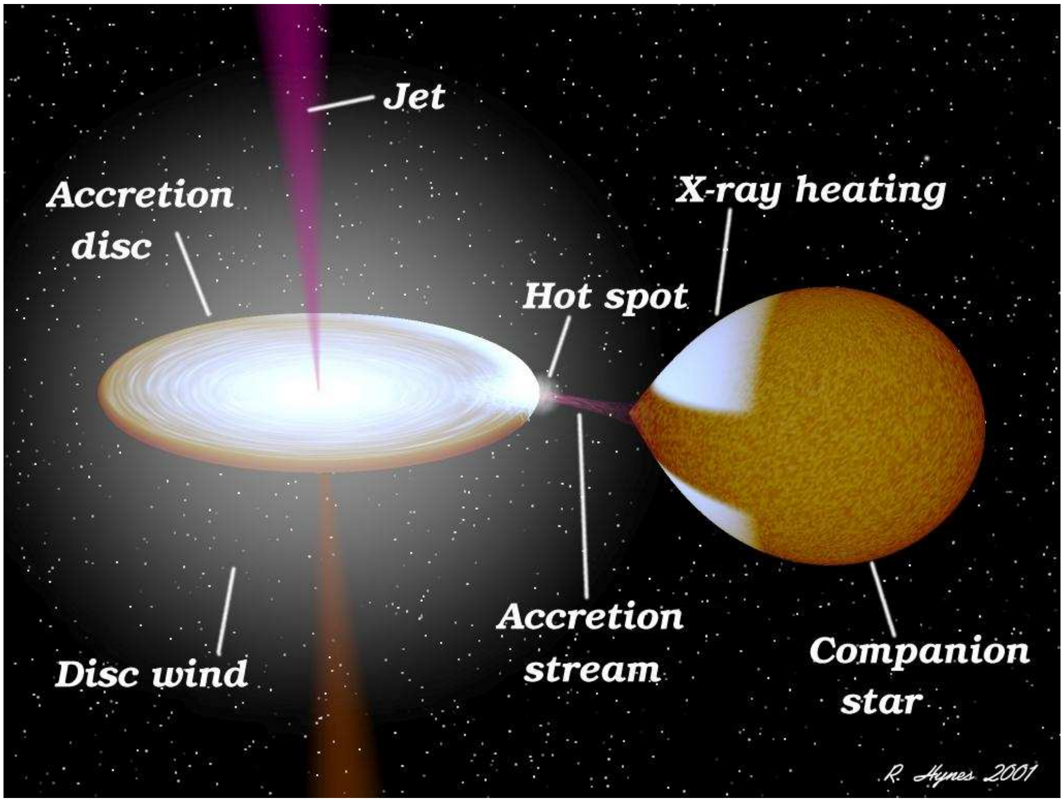

Figure 1.7: A schematic view of a low mass X-ray binary, produced by Robert Hynes. Annotated are the key features of these systems.

gains angular momentum and spirals outwards. This material forms an accretion disk around the compact object which increases in temperature as the material falls further into the potential of the compact object. These hot inner regions emit high energy radiation, which may irradiate and heat the outer disk and inner face of the donor star. Highly energetic outflows (*jets*) are observed from some LMXBs. These are observed in both black hole and neutron star systems, although they are much stronger in black hole systems. While these jets are interesting in their own right, they are beyond the scope of this work and not considered further here.

An estimate of the theoretical limit on the luminosity of an accreting object is set by the Eddington limit. As matter accretes onto the compact object it experiences a force due to radiation pressure. This force is due to Thompson scattering off the electrons in the material. The force on the protons is negligible, since the Thompson cross section is $\propto 1/(\text{mass of particle})^2$. However, the accretion of protons is also resisted due to the electrostatic attraction between the protons and electron. The Eddington limit is defined as the maximum luminosity the system can have before the radiation pressure balances the gravitational force, hence stopping further accretion. By assuming steady accretion flow and spherical symmetry, this limit is found to be:

$$L_{Edd} = \frac{4\pi \mathrm{G} M m_{\mathrm{p}} c}{\sigma_{\mathrm{T}}} \approx 1.3 \times 10^{38} \left(\frac{\mathrm{M}}{\mathrm{M}_{\odot}}\right) \mathrm{erg/s} \tag{1.3}$$

Here M is the mass of the compact object, $\mathrm{M}_{\odot}$ is the mass of the Sun, m_{p} is the mass of a proton, c is the speed of light and σ_{T} is the Thompson cross section. For neutron stars with M$\sim$1.4$\mathrm{M}_{\odot}$, this corresponds to $\sim 2 \times 10^{38}$erg/s. This provides a relatively crude, order of magnitude, estimate of the maximum luminosity of an X-ray binary. Systems with anisotropic accretion can exceed this limit. However, if an object is observed with luminosities significantly larger than this limit, then this suggests that the compact object is larger than the theoretical limit for a neutron star and may be a black hole.

The energy of photons emitted from these LMXB systems can be estimated by considering the likely temperatures of the inner accretion disk. For an optically thick accretion disk, the emission will have a black body spectrum. The total flux (F_{bb}) from a black body of temperature (T_{bb}) is given by $F_{bb} = \sigma T_{bb}^4$, where σ is the Stefan-Boltzmann constant. From this, T_{bb} can be estimated via:

$$T_{bb} = \left(\frac{L_{acc}}{4\pi R_\star^2 \sigma}\right)^{1/4} \tag{1.4}$$

where L_{acc} is the luminosity of the system and $R_\star$ is the radius of the black body. This provides an estimate for the lowest temperature of the emitted radiation. However, if the accretion disk is not optically thick, then the radiation temperature can be higher than this. It is also possible to estimate an upper limit on temperature of the emitted radiation by assuming that all the gravitational energy gained by the accreting material (E_{grav}) is converted to thermal energy (E_{th}). This temperature (T_{th}) can be estimated via:

$$\begin{aligned} E_{th} &= E_{grav} \\ 2 \times (3/2) k_{\mathrm{B}} T_{th} &= \mathrm{G}M(m_{\mathrm{p}} + m_{\mathrm{e}})/R_\star \\ T_{th} &= \frac{\mathrm{G}M m_{\mathrm{p}}}{3 k_{\mathrm{B}} R_\star} \end{aligned} \tag{1.5}$$

where m_{p} is the mass of a proton, m_{e} is the mass of an electron (assumed to be negligible) and k_{B} is the Boltzmann constant. The radiation temperature of the emitted photons (T_{rad}, where the typical emitted photon energy, hν=kT_{rad})

should lie in this temperature range. Hence, for a typical neutron star (with mass, $M=1.4M_\odot$ and radius, $R_\star$=10km) with $L_{acc} \sim L_{Edd}$, the expected radiation temperature is $\sim 10^7 < T_{rad} < 10^{11}$K. This corresponds to photon energies of ∼1keV-60MeV. As such, LMXBs are expected to be X-ray to soft gamma ray sources.

When in outburst, the X-ray to optical emission from LMXBs is usually dominated by emission from the accretion disk. The high energy emission from the central regions of an accreting LMXB is likely to irradiate both the outer accretion disk and inner face of the donor star, heating it to higher temperatures (e.g. de Jong *et al.*, 1996; van Paradijs, 1996). This has been observed in some X-ray binaries as a lag of a few seconds between the X-ray and optical variability of the systems (e.g. Hynes *et al.*, 2006). In this explanation the optical variability lags behind that of the X-ray variability due to the time it takes the X-rays to reach the outer disk. Irradiated disk models can also be used to explain the very high far ultraviolet luminosity of some of these systems. In this regime a larger region of the accretion disk is heated to very high temperatures, making LMXBs very bright in the far-ultraviolet. For black hole LMXBs, outbursts are often accompanied by strong jets. These jets often influence the near and far infrared emission from the systems. In quiescent LMXBs the donor star in the system often dominates the emission; this provides an opportunity to study the donors.

Many of the LMXBs observed in the Galaxy (e.g. Bradt *et al.*, 2000; Lewin and van der Klis, 2006) and GCs (e.g. Jordán *et al.*, 2004; Verbunt and Lewin, 2006) are transient in nature. These systems can remain in a faint quiescent state for months or years between periods of bright outburst. It is currently thought that the transient behaviour of LMXBs is due to instabilities in the accretion disk due to hydrogen ionisation. If the accretion disk is hot enough that hydrogen is ionised, then the accretion flow can be stable and the source persistent. It is thought that irradiation of the accretion disk is capable of keeping the outer disk temperatures above this limit in some neutron star LMXBs, hence producing the observed persistent sources (van Paradijs, 1996; King *et al.*, 1996; King, 1999). However, if disk temperatures are lower than this limit, then regions of neutral hydrogen are present. This lowers the viscosity of the disk which can suppress the accretion of matter. Instead, this material builds up in the outer accretion disk. It has also been noted that, while both persistent and quiescent neutron star LMXBs are observed, most proposed black hole LMXBs are transient systems (King *et al.*, 1996). This may be a result of black hole LMXBs being less efficient at irradiating their accretion disks (since the lower temperatures of non-irradiated disk models predict transient behaviour). In the Galactic GCs, it has been suggested that the proportion of qLMXBs to LMXBs in outburst is $\sim 7:1$ (Heinke *et al.*, 2003).

In neutron star LMXBs, type I X-ray bursts are sometimes observed. These occur when the accreting material accumulates on the surface of the neutron star. As this material builds up it can reach temperatures and densities high enough for thermonuclear burning to occur. The result is that the system's luminosity rapidly increases for periods of seconds. Since the production of these bursts requires the presence of a surface for the accreting material to collect on, it provides a good method for distinguishing between neutron star and black hole binary systems. A similar phenomenon is observed in CVs, where material accumulates on the surface of a white dwarf. The resulting thermonuclear explosion, known as a classical nova, rapidly increases the luminosity of the system for a short period (e.g. Warner, 1995).

1.2.2 Formation of low mass X-ray binaries

1.2.2.1 Primordial formation

Many of the LMXBs in the Galaxy may have been formed through the evolution of primordial binary systems. The theories of such formation have to overcome two major obstacles. Firstly, the formation of the compact object in the binary system must be proceeded by a supernova explosion. This may disrupt the binary system if too much mass is lost. The survival of such systems has been explained by significant mass transfer prior to this supernova (the explanation originally proposed for Cyg X-3 van den Heuvel and Heise, 1972). Secondly, the formation of observed X-ray binaries with orbital periods of minutes to hours requires the loss of significant angular momentum to tighten the binary. Most theories of binary evolution achieve this loss of angular momentum through a common envelope phase (first proposed by Ostriker *et al.*, 1976; Paczynski, 1976). During this phase, the binary orbit decreases substantially due to frictional drag. It also results in significant mass loss from the stellar envelope; aiding the survival of the binary post supernova. Figure 1.8 shows a diagram for the potential formation mechanism of an LMXB from a primordial binary (taken from the review of Tauris and van den Heuvel, 2003). The initial binary system must clearly contain a star massive enough to produce the compact object. A period of mass loss and tightening of the binary must then follow (likely involving a common envelope phase). A supernova explosion then produces the neutron star, which the binary must survive. Another period of binary tightening may then be necessary in order for the secondary star to fill its Roche lobe, before accretion can occur and the X-ray binary is produced. The final stage expected in

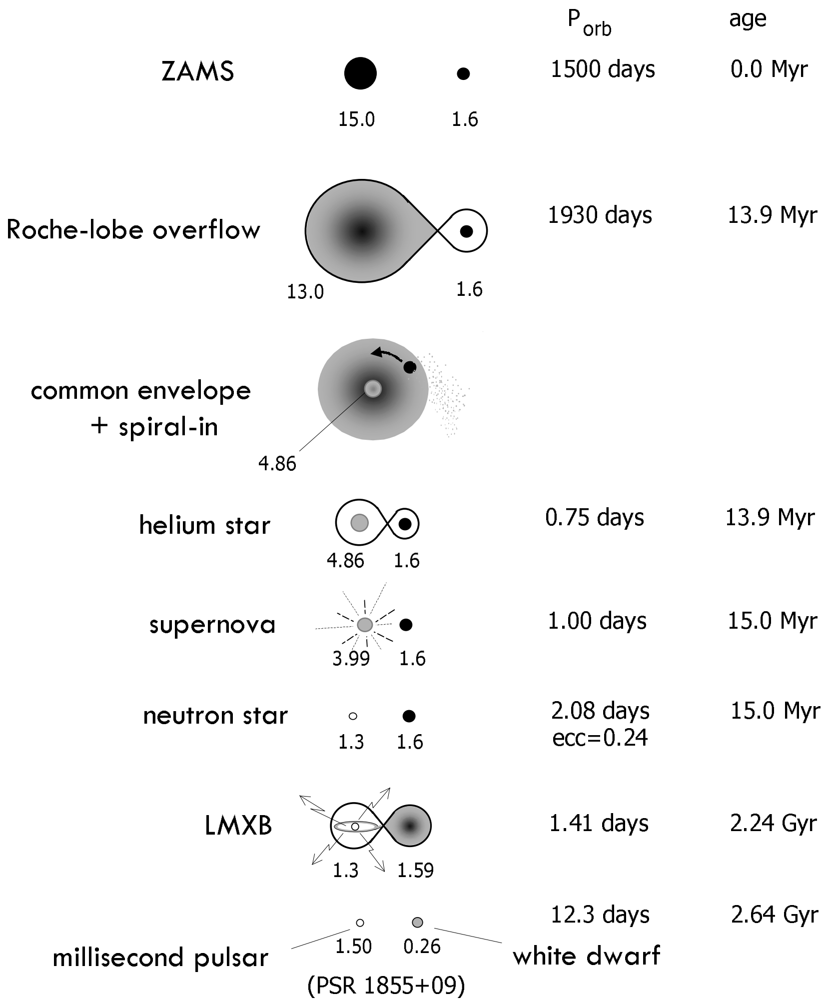

Figure 1.8: Cartoon of the possible evolution of a low mass X-ray binary system form a primordial binary. This figure is taken from Tauris and van den Heuvel (2003).

the evolution of an LMXB, shown in this figure, is the production of a millisecond pulsar. This is predicted due to the 'spin up' effect of sustained accretion onto the neutron star.

1.2.2.2 Dynamical formation

The production of LMXBs in the Galaxy is relatively inefficient, with only ∼150 currently known (Liu *et al.*, 2001). However, in GCs, it has long been proposed that the formation of LMXBs will be more efficient. This is because LMXBs may be formed via dynamical interactions in the dense cores of the GCs (e.g. Clark, 1975; Katz, 1975). In these mechanisms, isolated neutron stars can be captured by donor stars to form LMXBs. Three primary methods have been proposed for dynamical formation of these systems. They may be formed via the tidal capture of a neutron star in a close encounter with a main sequence star (Fabian *et al.*, 1975), via direct collisions of a neutron star with a giant star (Sutantyo, 1975) or they could be formed through three body interactions between a neutron star and a primordial binary system (Hills and Day, 1976; Hut and Verbunt, 1983). These dynamical formation mechanisms are strongly related to the density of stars and so they will be most important in the cores of the GCs, where the stellar densities can be very high. Dynamical formation may be further enhanced by mass segregation, which is likely to enhance the number of neutron stars in the cores of the clusters. For the Galactic GCs Verbunt and Hut (1987) investigated how the stellar collision rate in a cluster effected the presence of an LMXB. The stellar collision rate (Γ) of a GC can be studied via:

$$\Gamma = \int n_{\rm NS} n_{\rm MS} \sigma_{12} v_{12} {\rm dV}$$

where the integral is over the volume of the cluster, $n_{\rm NS}$ and $n_{\rm MS}$ are the number density of neutron stars and main sequence stars, σ_{12} ($\propto 1/v_{12}^2$) is the cross section for the interaction and v_{12} is the velocity between the stars. The velocity between the interacting stars will be similar to the velocity dispersion (σ) in the cluster. This equation can be simplified by assuming that the stellar collision rate in the cluster is dominated by collisions occurring in a constant density core. This is a reasonable assumption for a typical cluster where the stellar density is similar across the core region, but decreases rapidly at larger radii. From this approximation it is found that:

$$\Gamma \propto \rho_c^2 r_c^3 / \sigma$$

where r_c is the cluster core radius and ρ_c is the cluster core density. Measuring the velocity dispersion of a cluster requires accurate spectroscopy, which is often not available. However, σ can be estimated as $\rho_c^{1/2} r_c$ by assuming virial equilibrium. This implies that Γ can be estimated via:

$$\Gamma \propto \rho_c^{3/2} r_c^2 \tag{1.6}$$

This equation can be used to estimate Γ from photometry alone. Verbunt and Hut

(1987) demonstrated that the formation of the known Galactic GC LMXBs was proportional to this stellar collision rate. This result lends excellent support to the theory that LMXBs are formed via dynamical interactions. It was further explored by Pooley *et al.* (2003) who demonstrated that the number of X-ray sources in a GC scales with the stellar collision rate of the cluster. This work included all X-ray sources with $L_x \gtrsim 10^{31} erg/s$. Because of the low luminosity limit, this study includes contributions from CVs, qLMXBs and LMXBs in the clusters. The strong correlation found by Pooley *et al.* (2003) suggests that the formation of these binaries is likely to be related to dynamical interactions. In chapter 4 we investigate the relationship between the stellar collision rate of M31's GCs and the formation of LMXBs.

1.2.3 Low mass X-ray binaries in globular clusters

Globular clusters are very interesting locations to study LMXBs. Firstly, they are found to be a rich source of LMXBs which is a likely consequence of the dynamical formation described above. Also, the distance to, metallicity, and stellar densities of sources in GCs are much easier to estimate than those of LMXBs in the field of the Galaxy. The effects of such parameters are often very hard to study using field LMXBs. The Galactic GC system is relatively small, with 14 LMXBs currently known in 12 GCs. Despite the small number of systems, they have provided a useful dataset for many studies. Over recent years the study of GC LMXBs has been extended to extragalactic GCs due to the availability of large ground based telescopes, high spatial resolution *HST* photometry and high resolution X-ray data from *Chandra*. The study of LMXBs in the larger GC systems of nearby galaxies has greatly enhanced our understanding of these systems.

Given the efficiency of GCs in forming LMXBs, it has been proposed that some, if not all, LMXBs in galaxies may have been originally formed in GCs (Grindlay and Hertz, 1985; Mirabel *et al.*, 2001; Mirabel and Rodrigues, 2003; White *et al.*, 2002). In this situation, these LMXBs are either ejected from their host clusters or have had their host clusters disrupted due to tidal interactions. If *all* LMXBs are formed primarily in a galaxies GCs, then we expect the number of LMXBs detected in both the GCs and the field of these galaxies to be related to the size of their GC population. This would imply that the ratio of LMXBs in a galaxies GCs to the LMXBs in the field of the galaxy should be similar for different galaxies. This is not consistent with current observations (Verbunt and Lewin, 2006). The fraction of GC to field LMXBs is found to vary from ∼10% in the Milky Way (e.g. Verbunt and Hut, 1987) and M31 (e.g. Di Stefano *et al.*, 2002; Trudolyubov and Priedhorsky, 2004, ; and chapter 4) to ∼50% in some elliptical galaxies (e.g. White *et al.*, 2002; Randall *et al.*, 2004; Jordán *et al.*, 2004; Kundu *et al.*, 2007). However, considering only elliptical galaxies, White *et al.* (2002) demonstrated that the luminosity of all X-ray sources in a galaxy scales with the number of GCs. While this suggests that a large number of LMXBs in elliptical galaxies may come from their GCs, there are uncertainties in this relationship and the results are not yet conclusive (Kim and Fabbiano, 2004; Verbunt and Lewin, 2006). These uncertainties mainly arise from errors in the estimated GC systems of these galaxies and contamination in the X-ray data from non-LMXB sources. Another test for the ejection of LMXBs from GCs is the spatial distribution of field LMXBs and GC LMXBs. If field LMXBs are ejected from GCs then they should follow the same radial distribution as GC LMXBs and the GC system. Kundu *et al.* (2007) find that, for their sample of galaxies, the field LMXBs are more centrally concentrated than the GC system. This suggests that they are unlikely to have been ejected from GCs. However, it is noted that, this does not rule out the disruption of clusters hosting LMXBs. Indeed, this disruption is likely to be more severe in inner regions of the galaxies.

Figure 1.9 shows the colour and luminosity of LMXB hosting clusters in a sample of elliptical galaxies, taken from Kundu *et al.* (2007). This figure identifies two of the key properties of LMXB hosting GCs that are observed. Firstly, it can be seen that the LMXBs favour the brighter (more massive) clusters. This is a result also seen in the Milky Way, M31 (e.g. Trudolyubov and Priedhorsky, 2004), Cen A (Jordán *et al.*, 2007b), M87 (e.g. Jordán *et al.*, 2004) and many other galaxies (e.g. Angelini *et al.*, 2001; Kundu *et al.*, 2002; Sarazin *et al.*, 2003; Kim *et al.*, 2006; Kundu *et al.*, 2007). Kundu *et al.* (2002) noted that such a relationship is likely to be the result of the larger number of stars in a more luminous GC. The luminosity of a cluster correlates well with its stellar collision rate (e.g. Davies *et al.*, 2004, and figure 4.8 in chapter 4), so it would be expected that dynamical formation would lead to a relationship between luminosity and the formation of LMXBs. However, it is also possible that LMXBs will favour high mass clusters because they may retain more of the neutron stars they produce. Neutron stars that are formed by core collapse may be formed with large kick velocities (e.g. Hobbs *et al.*, 2005). In this case, the higher escape velocities of high mass clusters, may result in more neutron stars being retained by these clusters. However, it is also possible that neutron stars with lower kick velocities can be formed via electron capture (e.g. Pfahl *et al.*, 2002; Ivanova *et al.*, 2008). Smits *et al.* (2006) demonstrated that the GC systems in their sample are consistent with these clusters retaining neutron stars from a low

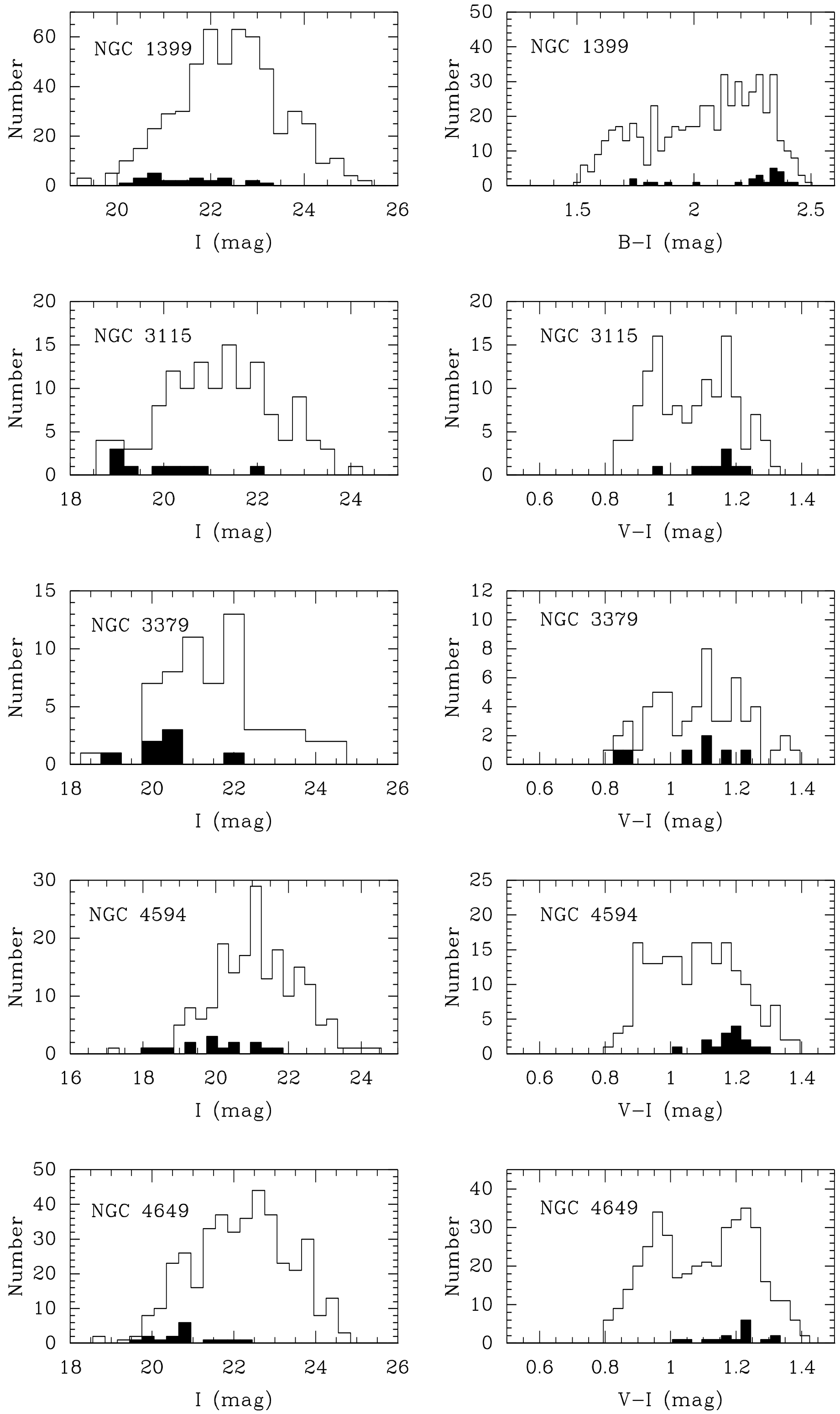

Figure 1.9: The magnitude (*left*) and colour (*right*) of all GCs (open) and LMXB hosting GCs (solid) in five elliptical galaxies. Taken from Kundu *et al.* (2007).

kick mode.

It is also found that LMXBs are preferentially formed in metal rich GCs. Such a trend is suggested in observations of GCs in the Milky Way and M31 (Bellazzini *et al.*, 1995). However, the significance of this relationship in these galaxies is limited due to the low number of metal rich clusters in both of these galaxies. Most of the metal rich clusters are also located at low galactocentric radii. This makes it hard to distinguish between tidal and metallicity effects. The data available for M31's GCs are improved slightly by the work presented in this study (section 4.6). However, the significance of this result is still much stronger when considering the GCs of early type galaxies. The large GC population of these galaxies and particularly their larger fraction of metal poor clusters, make it easier to study such a relationship. This relationship is demonstrated by the right panel of figure 1.9. It can be seen from this figure that, with the exception of NGC 3379, the GC LMXBs favour metal rich clusters. Kundu *et al.* (2002) find that the metal rich clusters in NGC 4472 are around three times more likely to host LMXBs than metal poor clusters. A similar fraction is found between the red and blue clusters in M87 (e.g. Jordán *et al.*, 2004) and the effect is observed in many other galaxies (e.g. Angelini *et al.*, 2001; Sarazin *et al.*, 2003; Kim *et al.*, 2006; Kundu *et al.*, 2007).

As discussed above, it is likely that LMXBs in GCs form primarily through dynamical mechanisms. If this is the case, then one would expect to see a direct relationship between the stellar collision rate (as defined by equation 1.6) and the formation of LMXBs. Such a relationship is observed in the Milky Way. However, this relationship is limited to the relatively small sample of 14 LMXBs in 12 Galactic GCs. Investigating this relationship in extragalactic GCs, while highly desireable, has proved relatively problematic. This is primarily due to the need to determine the core size and density of the GCs in order to estimate their stellar collision rate (see equation 1.8). To date, this has only been attempted using the excellent spatial resolution of *HST* images of selected GCs in M31 (Barmby *et al.*, 2007), and GCs in Cen A (Jordán *et al.*, 2007b) and in M87 (e.g. Jordán *et al.*, 2004; Waters, 2007). In Cen A, Jordán *et al.* (2007b) demonstrated that the GC LMXBs do favour higher collision rate clusters. However, this result is limited by signal-to-noise to the brighter clusters. A relationship is also suggested in M87, although the increased distance of GCs in Virgo cluster galaxies make measurements of the GC core radii less reliable. In chapter 3 we present the structural parameters for M31's GCs. These are estimated from deep ground based photometry. Using these data, the effect of stellar collision rate on the formation of LMXBs in these clusters is discussed in chapter 4.

2

The M31 globular cluster system: a WFCAM and SDSS photometric survey

2.1 Abstract

In this chapter, we present an updated catalogue of globular clusters (GCs) in M31 based on images from the Wide Field Camera (WFCAM) on the UK Infrared Telescope and from the Sloan Digital Sky Survey (SDSS; Adelman-McCarthy *et al.*, 2007). Our catalogue includes new, homogeneous *ugriz* and K-band photometry of these clusters. We discuss the difficulty of obtaining accurate photometry of clusters projected against M31 due to small scale background structure in the galaxy. We consider the effect of this on the accuracy of our photometry and provide realistic photometric error estimates. We investigate possible contamination in the current M31 GC catalogues using the excellent spatial resolution of these WFCAM images combined with the SDSS multicolour photometry. We identify a large population of clusters with very blue colours. Most of these have recently been proposed by other work as young clusters. We distinguish between these, and old clusters, in the final classifications. Our final catalogue includes 416 old clusters, 156 young clusters and 373 candidate clusters. One GC (B383) is found to be significantly brighter in

previous observations than observed here. We investigate all of the previous photometry of this GC and suggest that this variability appears to be genuine and short lived. We propose that the large increase in its luminosity may have been due to a classical nova in the GC at the time of the previous observations in 1989.

2.2 Introduction

As discussed in section 1.1, GCs are among the oldest known stellar systems. They typically have ages similar to those of their host galaxies, making them ideal probes into galaxy formation and evolution. The properties of GCs vary significantly. However, individual clusters contain populations of stars with similar ages and metallicities. This makes them unique locations for studying stellar evolution. While the study of GCs in the Milky Way has led to many advances, the Milky Way contains relatively few GCs ($\sim$150 GCs: Harris, 1996), many of which have high foreground extinction, making them hard to study. By determining the properties of extragalactic GCs, we are able to study a more diverse population and ensure our current conclusions are not biased by the Milky Way's clusters being atypical.

For extragalactic GCs, it is very difficult to resolve individual stars in the clusters. However, it is possible to estimate many properties of a GC from its integrated light. For example: the masses of GCs can be estimated by assuming a mass to light ratio; combined optical and near infrared colours of GCs can be used to (at least partially) break the age and metallicity degeneracy and estimate these parameters (e.g. Puzia *et al.*, 2002; Jiang *et al.*, 2003; Hempel *et al.*, 2007); and their structural parameters can be estimated by fitting their density profiles (e.g. Barmby *et al.*, 2007; Jordán *et al.*, 2007b; McLaughlin *et al.*, 2008; Peacock *et al.*, 2009). The colours of GCs and GC candidates are also very useful in selecting genuine GCs from stellar asterisms and background galaxies. Good multi-wavelength photometry of GCs is therefore highly desireable.

2.2.1 The M31 globular cluster system

The proximity of M31, and its relatively large GC population compared with the Milky Way ($\sim$400: Barmby *et al.*, 2000), makes it the ideal location to study extragalactic globular clusters. Its clusters have been the focus of many studies dating back to the early work of Hubble (1932) and Vetešnik (1962). However, attempts to study its clusters have faced several challenges. Photometry of these clusters is complicated by many of them being projected against the bright and non-uniform

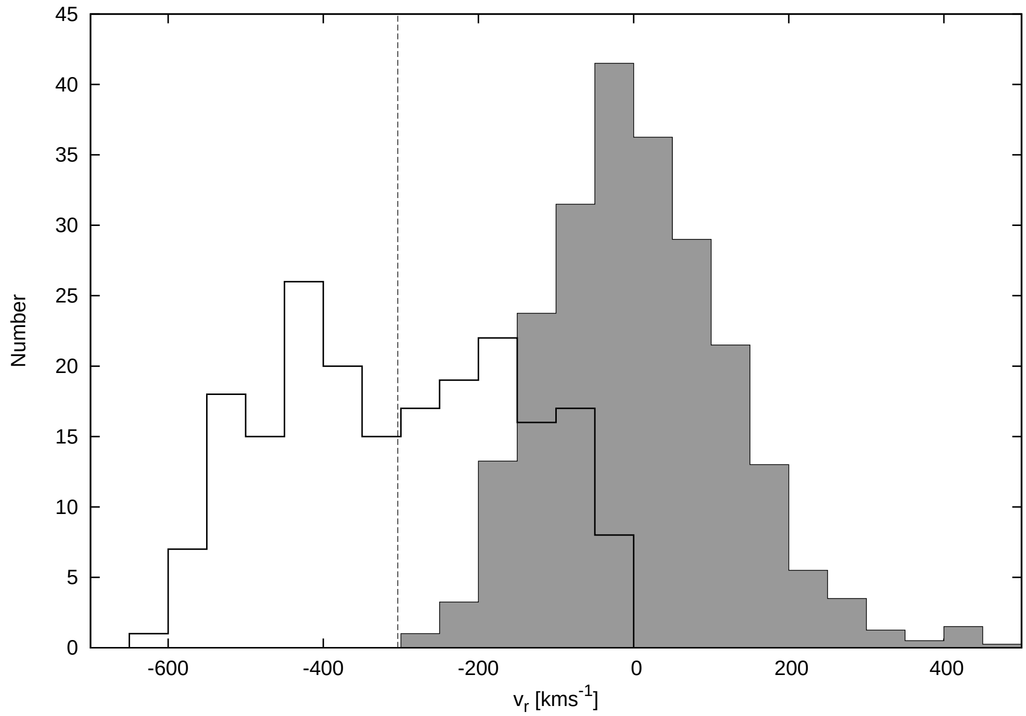

Figure 2.1: *(open)* The radial velocity distribution of M31's GCs, taken from the spectroscopic survey of Perrett *et al.* (2002). *(filled grey)* The radial velocity distribution of Milky Way halo stars, from Brown *et al.* (2010). To compare the populations, the number of halo stars plotted is 25% of the total Brown *et al.* (2010) sample. The dashed line indicates the radial velocity of M31 (-304 kms^{-1}; de Vaucouleurs *et al.*, 1991).

structure of M31 itself. The galaxy's proximity also results in the GC system extending over a wide region of the sky, with clusters recently found beyond 4° from the centre of the galaxy (Huxor *et al.*, 2008). This means that surveys with large fields of view are required in order to study the GC system. It is also difficult to confirm GCs in M31 based on spectroscopy alone. Figure 2.1 compares the velocities of known GCs in M31 (taken from Perrett *et al.*, 2002) with the velocities of stars in the halo of the Milky Way (Brown *et al.*, 2010). It can be seen that the radial velocity distribution of M31's GC system overlaps that of Milky Way halo stars.

Over the past decades there have been several large catalogues of M31's GCs including those of: Battistini *et al.* (1987); Barmby *et al.* (2000); Galleti *et al.* (2004); Kim *et al.* (2007). In addition to these catalogues many new clusters and candidates have been proposed (e.g. Battistini *et al.*, 1993; Mochejska *et al.*, 1998; Barmby *et al.*, 2002; Galleti *et al.*, 2006, 2007; Huxor *et al.*, 2008; Caldwell *et al.*, 2009). These studies have made considerable progress in removing contamination from the cluster catalogues due to either background galaxies (e.g. Racine, 1991;

Barmby *et al.*, 2000; Perrett *et al.*, 2002; Galleti *et al.*, 2004; Kim *et al.*, 2007; Caldwell *et al.*, 2009) or stars and asterisms both in the Milky Way and M31 itself (e.g. Barmby *et al.*, 2000; Cohen *et al.*, 2005; Huxor *et al.*, 2008; Caldwell *et al.*, 2009). However, despite this work, it is likely that there remains significant contamination in the current catalogues of M31 clusters, especially at the faint end of the GC luminosity function. These studies have also resulted in a large number of unconfirmed candidate clusters (currently over 1000: Galleti *et al.*, 2004) whose true nature remains uncertain.

It has been known for many years that some of the proposed GCs in M31 have very blue colours. Recent work has identified that a large number of the clusters in the current catalogues are young clusters (e.g. Beasley *et al.*, 2004; Fusi Pecci *et al.*, 2005; Rey *et al.*, 2007). A comprehensive catalogue of young clusters in M31 has recently been published from the spectroscopic survey of Caldwell *et al.* (2009). Compared with the young open clusters in the Milky Way, these clusters have relatively high masses ($< 10^5 M_\odot$), akin to the young clusters observed in the Large Magellanic Cloud. A recent *Hubble Space Telescope (HST)* study of 23 of these young clusters suggested that on average they are larger and more concentrated than typical old clusters (Barmby *et al.*, 2009). Most of the clusters studied by Barmby *et al.* (2009) are found to have dissolution timescales (the time that it takes dissipative process to disrupt the cluster) of less than a few Gyr. Therefore, they are not expected to evolve into typical old globular clusters. Whether these clusters are massive open clusters, young globular clusters or a mix of both, it is clear that they represent a different population to the classical old GCs also observed in M31 (which are the focus of this study). We therefore distinguish between the two populations in our classifications and conclusions.

While these previous studies have provided a wealth of information on the M31 GC system they have also resulted in a rather heterogeneous sample. For example, the excellent and commonly used Revised Bologna Catalogue (hereafter RBC) of M31 GCs by Galleti *et al.* (2004) includes photometry from many different authors using different telescopes and in some cases different (homogenised) filters. This has been previously noted by Caldwell *et al.* (2009) (hereafter C09) who recently published new V-band photometry for many RBC sources which were located in the Local Group Galaxy Survey images of M31 (LGGS: Massey *et al.*, 2006). While this work provides excellent deep V-band photometry, the survey does not cover the outer clusters and candidates and does not provide colour information. The most complete set of optical colours, derived in a consistent manner, is still that of the Barmby catalogue (Barmby *et al.*, 2000). This work presented homogeneous

UBVRI colours for many of their clusters. However, it is incomplete in some of these bands and only provides new photometry for 285 clusters. For these reasons we chose to produce new, homogeneous, optical photometry for the proposed GCs and GC candidates in the RBC using images from the Sloan Digital Sky Survey (SDSS). The excellent calibration and large field of view of this survey is ideal for studying such an extended system. Details of this photometry are presented in section 2.3.2.

The study of M31's GCs in the near infrared (NIR) is very useful both for confirming genuine GCs and for estimating their ages and metallicities (e.g. Barmby *et al.*, 2000; Galleti *et al.*, 2004; Fan *et al.*, 2006). The first major survey of M31's GCs in the NIR was by Barmby *et al.* (2000) who used pointed observations of individual clusters to obtain K-band photometry of 228 clusters. More recently Galleti *et al.* (2004) obtained NIR photometry in the J,H and K-bands of 279 of their confirmed GCs from the 2 Micron All Sky Survey (2MASS). The spatial coverage of 2MASS makes it ideal for such a project. However, the survey is relatively shallow and has relatively poor spatial resolution. We have obtained new deep K-band photometry using the Wide Field Camera on the UK Infrared Telescope to determine the K-band magnitude of M31's GCs across the entire GC luminosity function. Some results of this survey are already published in Peacock *et al.* (2009). In addition to providing the first K-band photometry for 126 GCs marked as confirmed in the RBC, the excellent spatial resolution of these images is very useful for removing stellar sources from genuine clusters, and for investigating the density profiles of the clusters. Details of this new K-band photometry are presented in section 2.3.3, while the classifications of the proposed clusters and candidates are considered in section 2.4.

2.3 Photometry of clusters and candidates

2.3.1 Identification of clusters

In the following analysis we consider all the GCs and GC candidates listed in the RBC [their confirmed clusters (class 1), confirmed extended clusters (class 8) and candidate clusters (class 2)]. Based on the original catalogue of Battistini *et al.* (1987), this catalogue has been regularly updated to include the results from most new studies. This version of the catalogue (v3.5) includes the newly discovered GCs in the outer regions of M31 (Mackey *et al.*, 2006; Huxor *et al.*, 2008) and the new GCs and candidates from Kim *et al.* (2007) (hereafter K07: their class A and

B/C objects, respectively). We also consider the catalogue of C09 which includes some additional clusters and gives updated locations and classifications for many of the objects in the RBC based on images from the LGGS or Digital Sky Survey and/or Hectospec spectroscopy. This combined catalogue is used to identify the known GCs and candidates in the following analysis.

2.3.2 Optical photometry

2.3.2.1 *ugriz* data

To obtain homogeneous optical photometry of M31's clusters and candidates we extracted images of M31 from the SDSS archive. Since M31 is at a relatively low Galactic latitude of -21°, it is not included in the standard survey field. However drift scan images of M31 were obtained by the SDSS 2.5m telescope (Adelman-McCarthy *et al.*, 2007) in 2002 as part of a special run during a period when the survey's primary field was not available (Zucker *et al.*, 2004). The runs used (3366, 3367, 6426 and 7210) provide images in the five SDSS bandpasses (*ugriz*: Fukugita *et al.*, 1996). Each of the observations takes images in these bands simultaneously meaning that they are taken under the same atmospheric conditions. The seeing for different observations varied significantly between 1.1-2.1 arcsec in *g* (meaning that faint GCs could appear as point sources in some of these images). The 3σ detection limits of these images were verified to be similar to the standard survey ($u < 22.0, g < 22.2, r < 22.2, i < 21.3, z < 20.5$). These data were found to cover and detect 92% (*gri*), 90% (*z*) and 73% (*u*) of the 1558 clusters and candidates in the current RBC. Two of these GCs were saturated in the *r* and *i* bands and one was saturated in the *g*-band. We do not provide new photometry for these clusters but good photometry is already available for these very bright clusters from previous studies.

We extracted all images covering the locations of confirmed and candidate clusters from the SDSS Supplemental Archive. Figure 2.2 shows the coverage of these data and demonstrates that most known clusters and candidates (red circles) are covered. These images have been processed through the standard SDSS pipeline (Stoughton *et al.*, 2002) which both reduces the raw images and produces a catalogue of sources in each image. Since the SDSS extraction and photometry routines are not designed to work in crowded fields (like M31), the default catalogues produced by the pipeline can not be used for photometry of the clusters. Instead we performed photometry on the images as described in the next section.

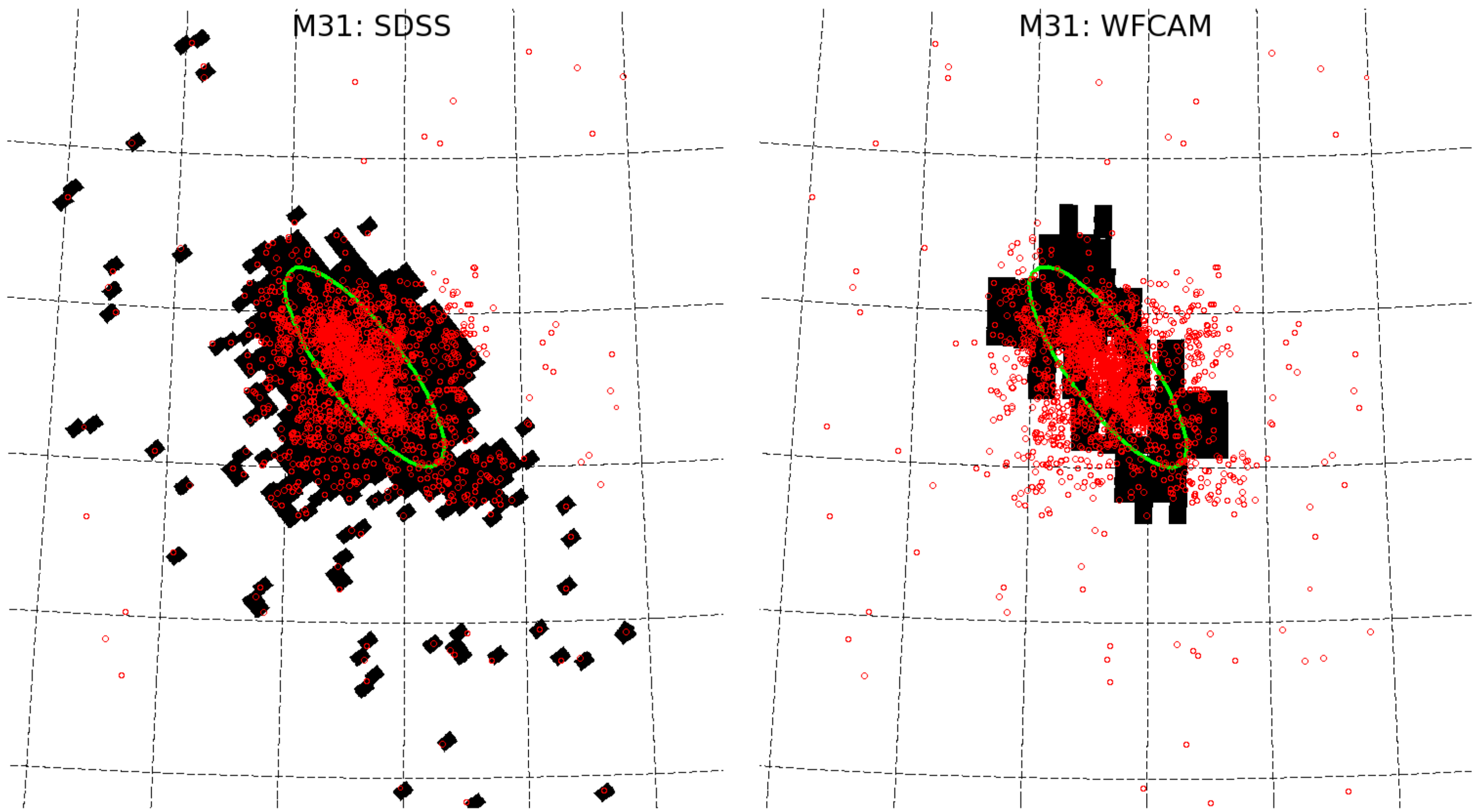

Figure 2.2: Coverage of the SDSS and WFCAM images used. For reference all objects listed in the RBC are shown in red. Only images covering the locations of these objects were extracted from the SDSS archive. The green ellipse indicates the D_{25} ellipse of M31. The grid represents $2^{\circ} \times 2^{\circ}$ squares on the sky (13.6×13.6 kpc at the distance of M31) and highlights the spatial extent of the GC system.

The photometric zero points for these images were calculated using the calibration coefficients produced by the pipeline. These calibrations place the magnitudes on the AB photometric system [Oke and Gunn (1983); the *u*-band zeropoint has previously been found to be slightly offset from the AB system by $u_{\mathrm{AB}} = u_{\mathrm{SDSS}} - 0.04$ mag (Bohlin *et al.*, 2001), this correction is *not* applied to our photometry]. This calibration is known to give magnitudes accurate to $\sim$0.01 mag.

2.3.2.2 Identification and locations of clusters

Catalogues of all sources in each of the *ugriz* images were produced using the program SEXTRACTOR (Bertin and Arnouts, 1996). This detected and located every source in each filter, performed initial aperture photometry, and gave an estimate of the stellarity of each source based on the PSF of its host image. Sources were identified using a minimum detection area (DETECT_MINAREA) of 3 pixels and a detection (DETECT_THRESH) and analysis threshold (ANALYSIS_THRESH) of 1.5σ. Through examination of the resulting catalogues, these values were found to detect the majority of sources in the images and to include the majority of their profiles in our analysis. It is important to identify and resolve as many sources as possible in order to distinguish between stellar and extended sources as accurate as possible.

This source catalogue was matched to our combined catalogue of known M31 GCs and candidates (described in section 2.3.1) based on astrometry. We identified all objects within 3 arcsec of the locations quoted in the RBC and (separately) to their locations in C09. Some genuine clusters in the SDSS images may not appear extended due to the poor angular resolution of some of the images. Also, we wish to provide photometry for potentially misclassified stars in addition to the extended clusters. The M31 GC catalogue was therefore matched to sources with stellar profiles in addition to those with extended profiles. In the few cases where multiple sources were located within 3 arcsec of the quoted location, priority was given first to sources flagged as extended and then to the closest source to the quoted location.

Figure 2.3 shows the difference between our positions and the positions quoted in RBC (solid) and C09 (open). We find excellent agreement between our locations and those of C09. However, we find that the difference in the positions of many sources in the RBC are greater than 1 arcsec. The offsets between the proposed cluster locations are found to be in all directions. They are therefore unlikely to be due to a single systematic offset. The large errors in the positions of some sources in the RBC were noted and discussed by C09. We note the strong agreement between our locations and those of C09 and use their locations to identify GCs and

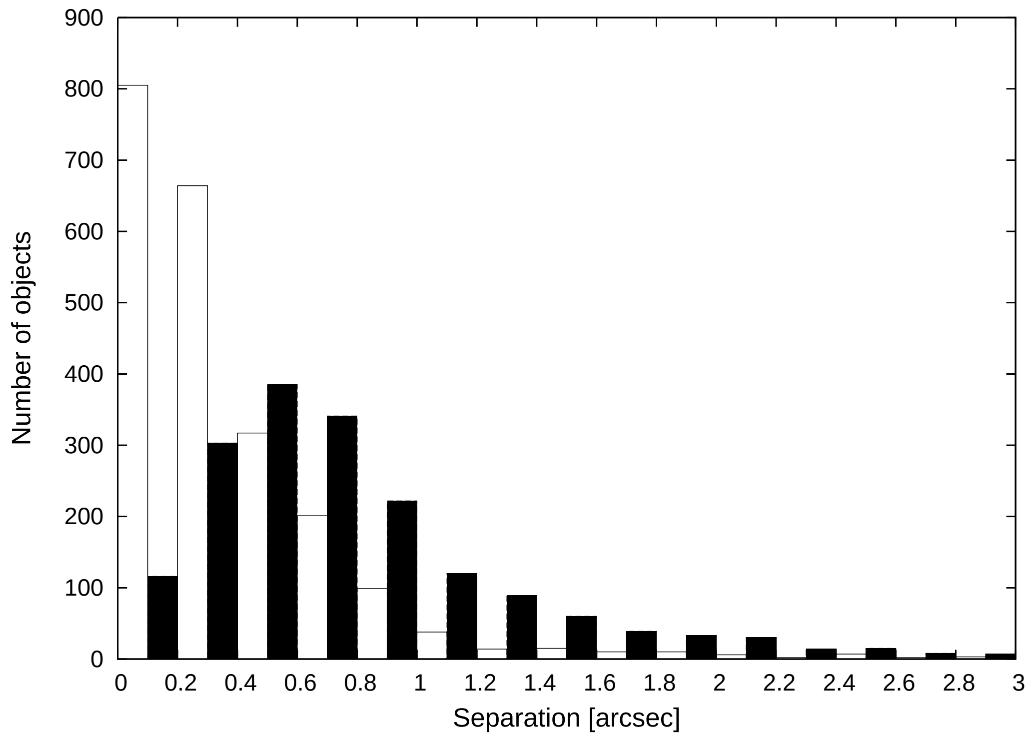

Figure 2.3: Difference between the location of objects in our images and their location in the RBC (solid) and C09 (open). In both cases, data are grouped into 0.2 arcsec bins.

candidates.

2.3.2.3 Photometry

Photometry of all clusters and candidates was obtained using SExtractor's simple aperture photometry. We also considered using the IRAF:APPHOT routines to perform the aperture photometry but SExtractor was found to deal better with contamination from neighbouring sources. This is a significant problem when using aperture photometry to obtain magnitudes of extended sources in a crowded region like M31. To minimise the effects of neighbouring sources within the GC aperture, SExtractor masks all other sources detected in the aperture and replaces them with pixels from symmetrically opposite the source.

For background estimation we considered the use of both local and global solutions. To produce a global estimate of the background SExtractor produces a smoothed background map for each image. We chose to create this with a BACK_FILTERSIZE of 3 and a BACK_SIZE of 64 pixels. By examination of the background maps produced by SExtractor, this method was found to give a good estimation of genuine background variation (due mainly to structure in M31 itself) without subtracting flux from the sources of interest. This was compared with the photometry produced using local backgrounds (calculated around the isophotal limits of the sources). In most cases good agreement was found between the two methods. However the local background estimates were found to deal better with the most strongly varying background regions (near the centre of the galaxy and its spiral arms). For this reason local background estimation was used for the final photometry.

To determine the total luminosity of each cluster, we produced curves of growth from g-band photometry obtained through apertures with radii in the range $2.8 - 10.6$ arcsec with 0.6 arcsec increments. These were used to determine the aperture size required to enclose the total cluster light. The best aperture was determined independently for each object. This method ensures that we measure the total cluster luminosity correctly for the largest clusters. The use of smaller apertures for smaller clusters also maximises the signal to noise and minimises the contamination from nearby sources. The aperture size used to determine the total magnitude of each cluster is quoted in table 2.1. Figure 2.4 shows the aperture sizes used to obtain the total g-band (and K-band) magnitude of all GCs located in our images. The average aperture radius used was $\sim$5.8 arcsec, with 87% of the apertures $\leq$8.2 arcsec. The *ugriz* colours of the clusters were measured through 4 arcsec apertures. We also measured the colours using the aperture determined for the total g-band magnitude. This confirmed that there were no significant aperture effects due to the use of smaller apertures. For the final colours we chose to use the smaller aperture size in order to maximise the signal to noise and minimise the contamination from nearby sources.

The statistical errors across the GC luminosity function are in most cases less than 0.05 mag in *gri*. In general the u and z bands have slightly larger errors as they have slightly lower signal to noise. However, there are additional systematic errors which need to be considered.

Firstly, the errors in the zero point calculation are estimated at 0.01 mag. This error dominates over the statistical errors for many of the bright clusters. The other significant source of error for some of the clusters is due to contamination from nearby sources and the error on the background estimation. In the bluer wavelengths there is significant small scale structure in M31. For clusters projected against the densest regions of the galaxy, this makes background subtraction difficult as it can vary on scales smaller than the cluster of interest. The issue of background estimation is found to be particularly significant for the g-band photometry. In this filter there is significant small scale structure across M31 (this structure is less significant in the shallower u-band images where the statistical errors are larger). In order to

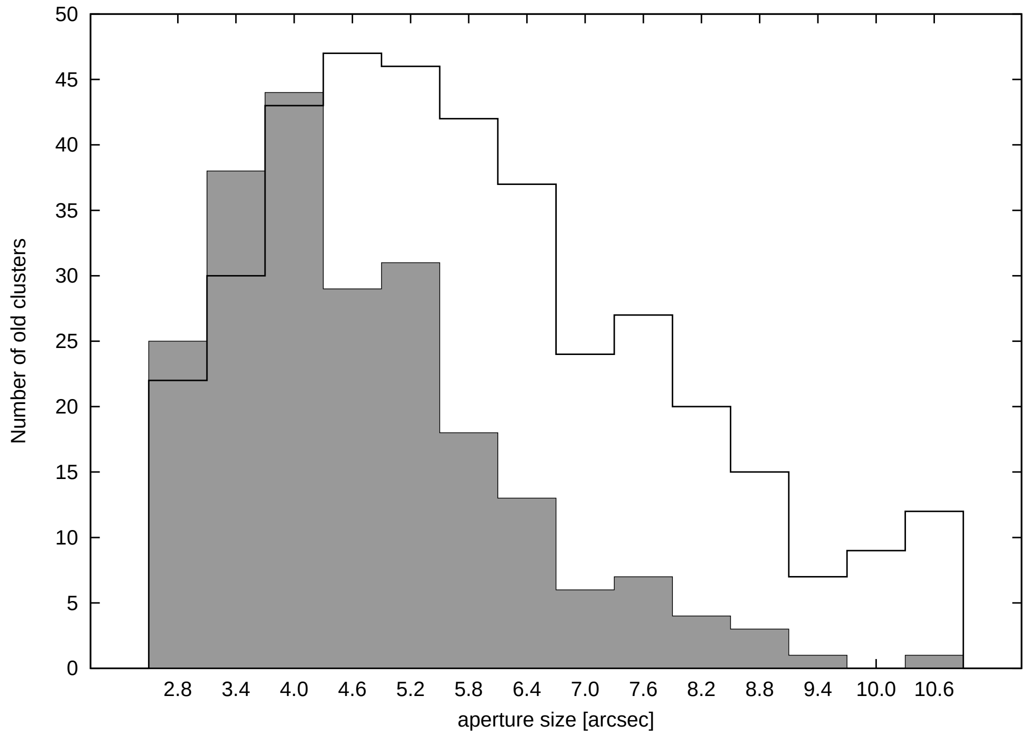

Figure 2.4: The aperture radii used to measure the total g-band (*open*) and K-band (*solid*, *grey*) magnitudes of M31's clusters.

estimate the error on our background estimation we repeated our photometry with apertures 1.8 arcsec larger than the aperture used for the total magnitudes. With perfect background estimation, the determined flux should be the same through both apertures (within the photometric errors). The difference in luminosity of the cluster through each aperture can therefore be used to give an estimation of the error on the background estimation. In most cases this estimated error is quite small, with a median value $\sim$0.015 mag, but for a few clusters it can reach $\sim$0.1 mag. This additional error is combined with the calibration and statistical error and included in table 2.1 as $\sigma_{g,tot}$.

The error on the *ugriz* colours should be less affected by these effects. This is because they are often taken through smaller apertures, also we expect that possible errors in the background level in each filter should, at least partially, cancel. For this reason the errors in the colours quoted in table 2.1 are only the statistical errors.

Table 2.1: Classifications and photometry of clusters in M31 (sample)

GC Name[1]	RA[2]	DEC[2]	Classification[3]			Photometry													
			f	f_{RBC}	f_{C09}	R_g^4	g	$(u-g)$	$(g-r)$	$(r-i)$	$(i-z)$	$\sigma^5_{g,tot}$	$\sigma_{(u-g)}$	$\sigma_{(g-r)}$	$\sigma_{(r-i)}$	$\sigma_{(i-z)}$	R_K^4	K_s	$\sigma^5_{K,tot}$
...	...	...	...	...	...	...	...	...	...	...	...	...	...	...	...	...	...	...	...
H13	9.64018	41.74805	1	1	old	5.8	18.009	0.960	0.449	0.229	0.070	0.061	0.052	0.020	0.022	0.042	-	-	-
HEC6	9.64833	44.28028	1	8	old	-	-	-	-	-	-	-	-	-	-	-	-	-	-
H14	9.70587	42.37969	1	1	old	5.8	18.747	1.324	0.684	0.429	0.307	0.087	0.117	0.027	0.027	0.048	-	-	-
B304-G028	9.73726	41.17456	1	1	old	6.4	17.172	1.309	0.591	0.279	0.162	0.022	0.033	0.015	0.015	0.021	5.2	14.510	0.052
B305-D024	9.74522	40.27559	1	1	young	6.4	18.152	1.776	0.598	0.296	0.219	0.038	0.093	0.022	0.023	0.042	4.6	15.075	0.048
SK005A	9.74647	41.67426	1	1	unknown	4.6	19.771	1.095	0.728	0.213	0.434	0.081	0.178	0.047	0.053	0.099	-	-	-
B306-G029	9.78627	40.57250	1	1	old	8.8	16.880	1.890	1.125	0.606	0.395	0.021	0.047	0.014	0.013	0.016	8.2	12.521	0.030
B307-G030	9.82689	40.54948	1	1	interm	7.6	17.582	1.631	0.600	0.384	0.153	0.056	0.070	0.019	0.020	0.035	5.2	14.691	0.055
B309-G031	9.85262	40.24141	1	1	old	6.4	17.903	1.501	0.694	0.326	0.201	0.037	0.063	0.019	0.020	0.033	4.6	15.096	0.056
B310-G032	9.85724	41.39256	1	1	old	6.4	17.398	1.295	0.598	0.287	0.201	0.028	0.037	0.016	0.016	0.023	-	-	-
B436	9.87773	40.30570	1	2	interm	6.4	18.619	1.809	0.743	0.369	0.241	0.074	0.142	0.027	0.028	0.050	4.6	15.461	0.085
B181D	9.87860	41.47394	1	2	old	3.4	18.193	1.326	0.610	0.242	0.129	0.031	0.055	0.019	0.020	0.033	-	-	-
B311-G033	9.89052	40.52075	1	1	old	10.0	15.846	1.407	0.719	0.391	0.227	0.021	0.021	0.012	0.012	0.014	7.6	12.764	0.033
B312-G035	9.91738	40.95068	1	1	old	9.4	15.947	1.457	0.751	0.385	0.255	0.018	0.022	0.012	0.012	0.015	7.6	12.705	0.032
B313-G036	9.93587	40.88195	1	1	old	8.8	16.764	1.701	0.877	0.452	0.328	0.030	0.041	0.015	0.014	0.018	7.6	13.105	0.029
B001-G039	9.96253	40.96963	1	1	old	7.6	17.576	1.806	0.967	0.540	0.374	0.020	0.069	0.017	0.016	0.022	5.8	13.720	0.050
B316-G040	9.97329	40.69416	1	1	interm	9.4	17.159	1.439	0.621	0.265	0.179	0.023	0.049	0.017	0.019	0.031	5.2	14.806	0.117
B317-G041	9.98030	41.79614	1	1	old	8.8	16.915	1.277	0.537	0.252	0.141	0.019	0.029	0.015	0.015	0.021	-	-	-
B002-G043	10.01072	41.19822	1	2	old	4.6	17.857	1.289	0.516	0.283	0.160	0.025	0.053	0.019	0.021	0.040	2.8	15.469	0.099
...	...	...	...	...	...	...	...	...	...	...	...	...	...	...	...	...	...	...	...

The locations, classifications and photometry of clusters in M31. The full version of this table is printed in appendix A, it is also available electronically from the VizieR archive or from the supplementary material accompanying Peacock *et al.* (2010). The optical photometry (in the *ugriz*-bands) is described in section 2.3.2 and the near-infrared photometry (in the K-band) is described in section 2.3.3 .

[1]Cluster name, taken from the Revised Bologna Catalogue (Galleti *et al.*, 2004)

[2]Position of the object in SDSS *r*-band image [J2000, degrees]

[3]Classification of source as described in section 2.4. Options for flag, f: 1-old globular cluster; 2-candidate cluster (21-candidate old cluster, 23-candidate young cluster); 3-young cluster; 4-galaxy; 5-HII region; 6-stellar source. Flags f_{RBC} and f_{C09} indicate the previous classifications of the source from the RBC v3.5 of Galleti *et al.* (2004) and from the catalogue of Caldwell *et al.* (2009), respectively.

[4]Aperture size used to measure the total magnitude of the cluster [arcsec]

[5]Error on the total magnitude, includes the statistical, calibration and systematic errors

2.3.2.4 Comparison with previous photometry

To date the best set of optical colours of M31 GCs derived in a homogeneous manner is that of the Barmby catalogue. This includes colours for 285 clusters in the Johnson UBVRI bands obtained through 8 arcsec apertures. The catalogue also contains photometry for an additional 160 clusters collated from other studies. This collated photometry is taken mainly from the work of: Reed *et al.* (1992, 1994); Battistini *et al.* (1993); Mochejska *et al.* (1998); Sharov and Liutyi (1983); Sharov *et al.* (1987, 1992); Sharov and Alksnis (1995). For full details of the sources and reliability of this additional photometry we refer the reader to the description in Barmby *et al.* (2000) and the references therein.

There is little previous optical photometry in the *ugriz* bands with which to compare our results. However it is possible to compare our colours with those of the Barmby catalogue by transforming between the UBVRI and *ugriz* bands. This was done using the following the transformations from Jester *et al.* (2005)

$$V = g - 0.59 \times (g - r) - 0.01 \pm 0.01 \tag{2.1}$$

$$u - g = 1.28 \times (\mathrm{U} - \mathrm{B}) + 1.13 \pm 0.06 \tag{2.2}$$

$$g - r = 1.02 \times (\mathrm{B} - \mathrm{V}) - 0.22 \pm 0.04 \tag{2.3}$$

$$r - i = 0.91 \times (\mathrm{Rc} - \mathrm{Ic}) - 0.20 \pm 0.03 \tag{2.4}$$

These transformations are based on all stars studied by Jester *et al.* (2005). Applying these to the colours of globular clusters may introduce a slightly larger error than the quoted rms residuals as globular clusters are stellar populations rather than single stars. However, they can be used to check for consistency with this previous work.

Figure 2.5 compares our colours for confirmed clusters with the transformed colours from the Barmby catalogue. The errors quoted include the residual from the transformations and the errors in our photometry only. The scatter is therefore expected to be larger than 1σ due to errors in the previous photometry. It can be seen that reasonable agreement is found between the *u-g* and *r-i* colours of the clusters. For the *g-r* colours a slight offset of 0.035 mags is found. However, this is within the rms scatter of the transformations. We believe this offset may be due to the errors in the transformations (due to the difference in the spectrum of a typical globular cluster compared with a single star), rather than a genuine offset between the colours. We therefore believe that for most clusters our colours are consistent with the previous UBVRI colours in the Barmby catalogue.

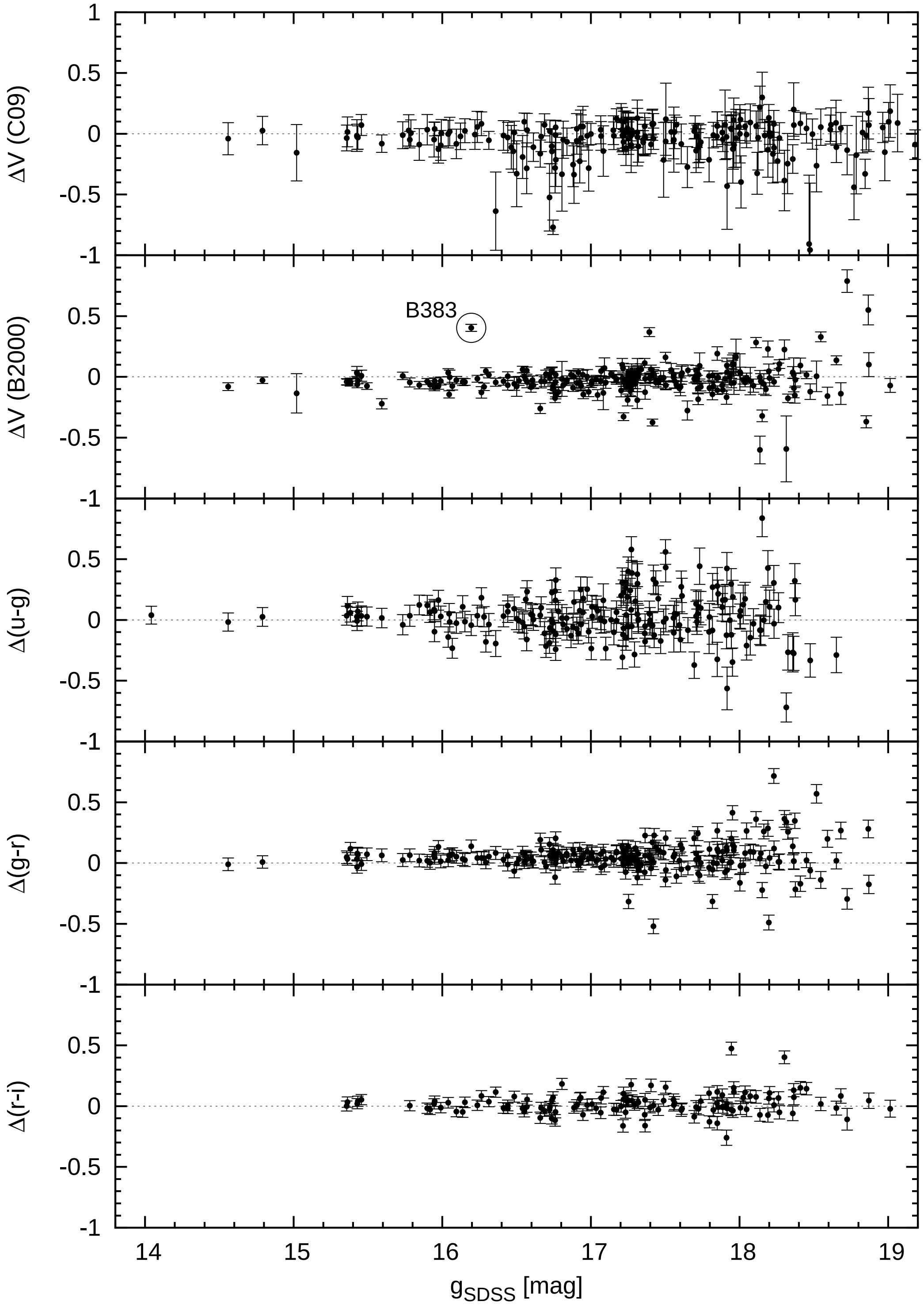

Figure 2.5: *Top:* comparison between our total cluster magnitudes and those from C09. *Bottom:* comparison between our total cluster magnitudes and colours and those from the Barmby catalogue (B2000). In all cases the y axis is our photometry minus that obtained previously. The highlighted point indicates the cluster B383.

The top panels of figure 2.5 compare the total magnitudes of the clusters obtained here with V-band photometry from the Barmby catalogue and the more recent photometry of C09. To compare the total magnitudes of the clusters, our g-band photometry was transformed to the V-band using equation 2.1. For most clusters good agreement is found between our magnitudes and those in the Barmby catalogue (again errors in the Barmby catalogue photometry are not included). However, it can be seen that there are some significant outliers. Three of the brightest clusters are brighter in our photometry than found previously. This is likely due to our use of larger apertures for larger clusters. Many of these bright clusters are found to extend beyond the 8 arcsec apertures used to obtain the Barmby catalogue photometry. For the fainter clusters we identify a group of 7 clusters which are fainter than expected. These clusters all have nearby neighbours, the effects of which we attempt to remove from our photometry but believe are included in the previous photometry. We therefore believe our values for these clusters to represent the actual cluster magnitudes better. Another group of faint clusters are found which are brighter than expected. The majority of these clusters are in dense regions near the galaxy centre or spiral arms and we believe the differences are due to errors in the background estimation. It is very difficult to estimate the background accurately for regions with variations on the scales of the clusters themselves. It is unclear which photometry is more accurate for these few clusters, although our use of smaller apertures for smaller clusters should minimise this effect. In the Barmby catalogue they subtract light from the bulge of M31 before performing photometry using a ring median filter. We repeated our photometry using a similar method but did not find significant differences in our photometry. Background estimation for clusters in these dense regions is an inherent problem in finding their absolute magnitudes. It should be noted that, while we attempt to account for this in the quoted errors in our photometry, the errors for some clusters in these dense regions may be larger than quoted.

It can also be seen that excellent agreement is found between between our photometry and that of C09. The errors in this comparison are larger due to the inclusion of the errors quoted by C09. The group of clusters which were fainter in our photometry than the Barmby catalogue are found to agree well with this photometry. This is likely due to C09 also subtracting the effects of nearby sources from their photometry. They also use a similar method of increasing their aperture size for larger clusters, and our photometry for brighter clusters agrees with theirs. We again identify a few clusters in dense background regions whose magnitudes are slightly fainter than expected. However, not all of these are the same outliers as

Table 2.2: Photometry of B383

Source of photometry	Observation date	Detector	ΔU	ΔB	ΔV	ΔR	
SDSS (This study)	2002 October 06	CCD	[17.15	16.70	15.72	15.06	]*
Sharov *et al.* (1992)	1990 October 15-18	Photoelectric	-0.13	-0.06	-0.06	-	
Reed *et al.* (1992)	1989 August 23-30	CCD	-	0.54	0.39	0.18	
Sharov and Liutyi (1983)	1980 October 8-13	Photoelectric	-0.05	-0.03	-0.06	-	
Battistini *et al.* (1987)	1977-1981	Plate	0.16	0.07	0.16	-	

The magnitude difference between the SDSS photometry presented here and that found by previous work.
* The total magnitude of the cluster in the SDSS images (transformed to Johnson filter system)

those found in the Barmby catalogue. This highlights the difficulty of accurately obtaining integrated magnitudes for clusters in these regions.

2.3.2.5 Variability in B383: a classical nova?

Figure 2.5 identifies one relatively bright cluster (B383) which is significantly fainter ($\Delta V = 0.39$) in our photometry than found in previous photometry. This cluster was not observed by Barmby *et al.* (2000) and its BVR band photometry in both the Barmby catalogue and the RBC are from the work of Reed *et al.* (1992). This cluster has high signal to noise, a relatively clean background, and its magnitude was obtained through a similar sized aperture to that used previously (7.8 arcsec). The cluster is present in two different SDSS observations and the magnitudes obtained from each agree very well. Table 2.2 compares our photometry with other previous observations of B383. It can be seen that there is good agreement between our photometry and the previous photometry of Sharov and Liutyi (1983), Sharov *et al.* (1992) and Battistini *et al.* (1987). We therefore believe that our photometry of this cluster is reliable.

We note that, for other clusters our photometry agrees well with that of Reed *et al.* (1992) and that B383 is brighter in all of their observations (B, V and R bands). We therefore believe that this discrepancy is unlikely to be due to an error in their photometry. This raises the possibility that the cluster luminosity may have genuinely varied between our observations. The increase in luminosity of B383 could have been produced by a transient in the cluster. To explain the observed variability, this transient would have to have bluer colours than the cluster and a brightness of $M_V \sim -7.9$.

A potential candidate for this increase would be a classical nova in the cluster at the time of the Reed *et al.* (1992) observations. Novae have typical luminosities of $-6 < M_V < -9$ and could explain this blue excess in the Reed *et al.* (1992) observations. A classical novae of this brightness would be expected to have a very short outburst duration (e.g. Warner, 1995) and would therefore be expected to have faded by the time of our observations and even those of Sharov *et al.* (1992) $\sim$10 months later.

Globular clusters are expected to host classical novae. There is evidence for Classical novae in the Galactic GCs M80 (Pogson, 1860; Wehlau *et al.*, 1990) and (possibly) M14 (Hogg, 1964; Margon *et al.*, 1991). Classical novae have also been detected in a GC in M87 (Shara *et al.*, 2004) and two of M31's other GCs [B111: Quimby *et al.* (2007); Shafter and Quimby (2007) and B194: Henze *et al.* (2009)]. Confirmation of a classical nova in B383 is very difficult as any remaining signatures of the event will be very faint. However, it offers a plausible explanation for such a large brightness variation.

2.3.3 Near-infrared photometry

2.3.3.1 K-band data

To obtain K-band photometry of M31's GCs, images across M31 were obtained using the Wide Field CAMera (WFCAM) on the UK Infrared Telescope (UKIRT) under the service program USERV1652. The large field of view of the WFCAM makes it ideal for such a project. The coverage of these data is shown in figure 2.2. They do not currently cover the whole GC system, missing both the most central and most distant clusters. The details of these observations were originally presented in Peacock *et al.* (2009) but are summarised again below.

The data were taken on the nights of 2005 November 30 and 2007 August 06 with K-band seeing of 0.85-1.00 arcsec and 0.6-0.8 arcsec respectively. To ensure the images were well sampled, each observation was taken with 2×2 microstepping to give an effective pixel size of 0.2 arcsec. Five observations were taken of each field giving a total exposure time of 225s and a 3σ detection limit of $\sim$19 mag.

The images were reduced using the standard WFCAM pipeline (see e.g. Dye *et al.*, 2006). The pipeline processing reduced and stacked the raw images and interlaced (Fruchter and Hook, 2002) the microstepped images together. The pipeline also applies an accurate astrometric solution to the images based on matching sources to the 2MASS catalogue. This method has been shown to give positions accurate to 80mas (Dye *et al.*, 2006). We determined the photometric zero point for each observation by calibrating against the 2MASS catalogue. This was done by comparing instrumental magnitudes of bright, unsaturated, stars in each field with the 2MASS Point Source Catalogue. This places the K-band photometry on the standard 2MASS (Vega-based) photometric system. This method has previously been shown to give zero points for K-band WFCAM images to better than 0.02 mag (Hodgkin *et al.*, 2009).

2.3.3.2 Photometry

Photometry was obtained for all GCs and candidates with WFCAM images using SExtractor. SExtractor was run in the same way used to obtain the optical magnitudes (described in section 2.3.2.3). The aperture required to determine the total K-band luminosity was again selected for each cluster from curves of growth. The aperture size was selected independently of the aperture used to determine the total *g*-band magnitude of the cluster. In many cases a smaller aperture was required to enclose all the K-band light of the cluster, with an average aperture size of $\sim$4.6 arcsec selected and 84% of the apertures $\leq$ 6 arcsec. The use of smaller apertures for the K-band images is expected because of the smaller PSF of these images.

As with the *ugriz* photometry, it was found that the error in the K-band photometry was often dominated by non statistical errors. The zero point calibration error of the WFCAM images is estimated to be 0.02 mag. This is larger than the statistical errors for most of the clusters. The K-band luminosity of the clusters also suffers from errors in the background estimation and contamination from neighbouring sources. We estimate the effect of this on the accuracy of our photometry using the same method used for the total *g*-band magnitude (by retaking photometry through a larger aperture). The median estimated error, due to contamination, was found to be 0.025 mag. The estimated error due to contamination and background variation was combined with the statistical and calibration errors and quoted as the final error $\sigma_{K,tot}$ in table 2.1.

2.3.3.3 Comparison with previous photometry

The most complete NIR data currently available for M31's GCs is that from the RBC. This includes K-band magnitudes of 279 confirmed GCs in the RBC obtained from the 2MASS archive (Galleti *et al.*, 2004). This 2MASS photometry is from either the 2MASS Point Source Catalogue or Extended Source Catalogue and measured through apertures with radii of 4 and 5 arcsec respectively. The bottom panel of figure 2.6 compares our K-band photometry of all confirmed GCs with the K-band photometry in the RBC obtained from 2MASS. Errors are not included for the K-band photometry in the RBC, so only the total errors in our photometry are

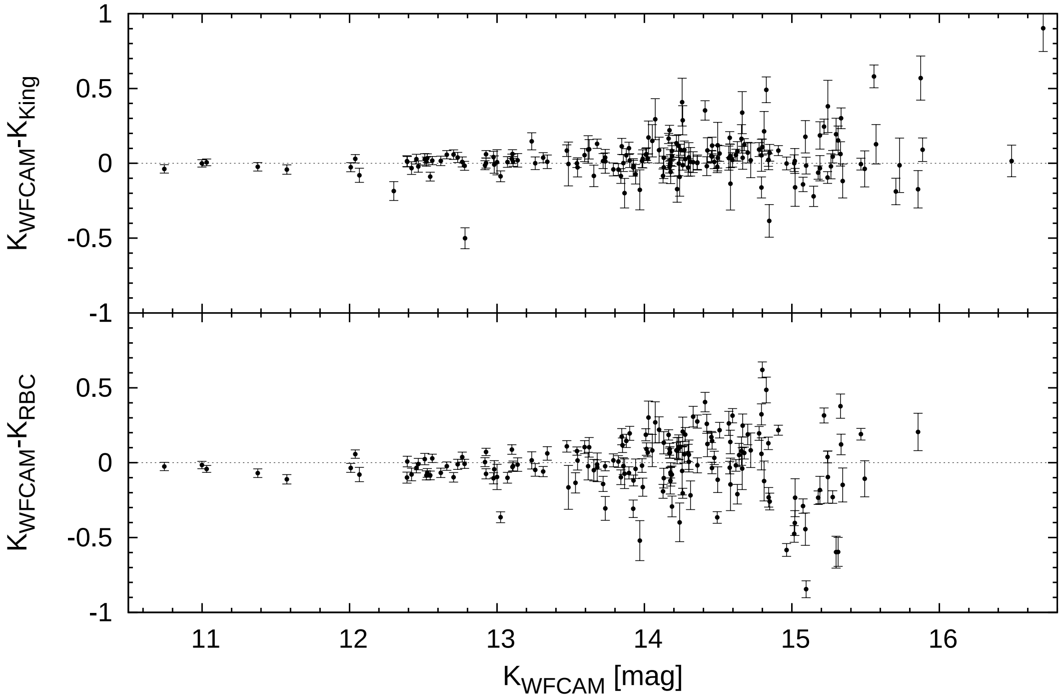

Figure 2.6: Comparison with previous K-band photometry from the RBC (*bottom*) and profile fits to these WFCAM images from Peacock *et al.* (2009) (*top*). The errors quoted are from our photometry only, as errors are not available from the previous work.

included in these plots.

Two clusters are found to have very different magnitudes and lie off this plot. One of these (B090) is very faint in the previous photometry and has a very blue J-K colour. We therefore believe the previous photometry for this object is unlikely to be accurate. The other (B041) is found to be fainter in our photometry. The WFCAM and 2MASS images for this cluster are shown in figure 2.7. This comparison demonstrates the superior depth and spatial resolution of the WFCAM images over 2MASS. The circles show the aperture sizes used for our photometry and the 2MASS photometry. The improved spatial resolution helps to separate clusters from nearby sources and allows the use of significantly smaller apertures. It is clear from this image that the previous photometry for these faint sources is unlikely to be as reliable as that presented here. From examination of the 2MASS catalogues we can only identify this source in the 'reject' catalogue. We therefore believe that the 2MASS photometry of this cluster is unreliable.

The errors in the 2MASS photometry are expected to be larger than those obtained here since 2MASS is significantly shallower than our data. Taking this into account, most of our photometry is found to be consistent, although there are several outliers. We believe that most of these differences are due to the improved spatial

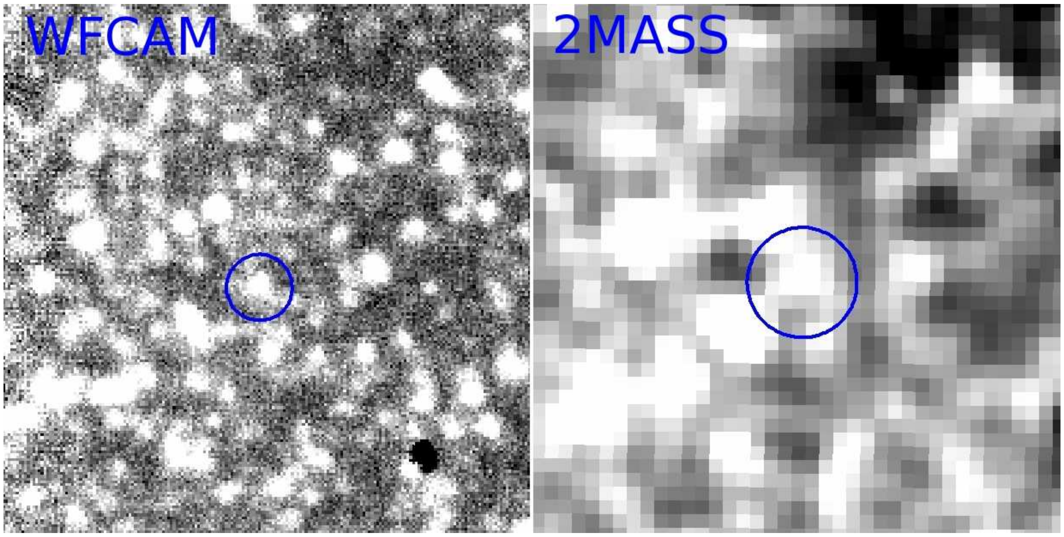

Figure 2.7: WFCAM and 2MASS images of the faint cluster B041. Both images are 45 arcsec $\times$ 45 arcsec and demonstrate the improved spatial resolution and signal to noise of the WFCAM images over 2MASS.

resolution of our data over 2MASS which makes it easier for us to remove contamination from nearby sources and to estimate the background level more reliably. The poorer resolution could result in both overestimation of the cluster magnitudes (if nearby sources are included in the cluster aperture) and underestimation of their magnitudes (if unresolved background sources result in an overestimation of the background level). This highlights the importance of spatial resolution, even in obtaining integrated magnitudes. The brightest clusters are also found to be ~ 0.05 mag brighter in our photometry than in the RBC. We believe this is due to our use of larger apertures for larger clusters. This was identified and discussed by Galleti *et al.* (2004) who attempt to apply aperture corrections to these clusters. However, we believe our use of larger apertures should be more reliable.

An alternative method to aperture photometry is to fit the profile of the clusters and find their integrated magnitudes. This method removes aperture affects because it integrates the magnitude out to the tidal radius of the cluster. It also accounts for contamination from nearby sources since it assumes the cluster to have a smooth profile. This provides a very useful independent method of estimating the total magnitudes of the clusters. The results of fitting the profiles of these clusters are presented in chapter 3 and in Peacock *et al.* (2009). The top panel of figure 2.6 compares this integrated K-band magnitude with the aperture magnitudes found here. Errors are not available for the profile fit magnitudes (as discussed in chapter 3) but are expected to be of a similar size to the errors obtained from aperture photometry. Three of these clusters are found to be brighter in our photometry. Examination of these clusters revealed that they all have very bright nearby neighbours. Since these cause significant background gradients across the cluster profiles, we believe that the model fits to these will be less reliable and the aperture photometry is probably more accurate. Some of the fainter clusters are also found to lie slightly outside 2σ. As discussed in chapter 3, we believe this is due to the King model fits being less reliable for these faint clusters (which have relatively low signal-to-noise). For these faintest clusters it is likely that aperture photometry gives more accurate magnitudes.

The scatter in these comparisons highlights the difficulty in determining the NIR magnitudes of clusters projected onto stars and surface brightness fluctuations from M31. We believe our approach gives the best estimate of their magnitudes and the most realistic errors to date. In total we present K-band photometry for 319 and 603 sources classified as confirmed and candidate clusters in the RBC respectively. This includes the first K-band photometry for 126 confirmed clusters and 429 candidate clusters.

2.3.4 Summary of photometry

The *ugriz* colours, total *g* and total K-band luminosity of M31's GCs and candidates are presented in table 2.1. This table includes the statistical errors in the *ugriz* colours and the errors in the total *g* and K-band luminosity (which include the calibration errors and estimated error due to background variation and contamination from nearby sources).

It should be noted that the *ugriz* photometry presented here is on the standard SDSS (AB) photometric system, while the K-band photometry is on the standard 2MASS (Vega-based) photometric system. The magnitudes can be converted between the two systems using the following offsets taken from Hewett *et al.* (2006):

$$u_{\rm Vega} = u_{\rm AB} - 0.927 \tag{2.5}$$

$$g_{\rm Vega} = g_{\rm AB} + 0.103 \tag{2.6}$$

$$r_{\rm Vega} = r_{\rm AB} - 0.146 \tag{2.7}$$

$$i_{\rm Vega} = i_{\rm AB} - 0.366 \tag{2.8}$$

$$z_{\rm Vega} = z_{\rm AB} - 0.533 \tag{2.9}$$

$$\rm K_{AB} = K_{Vega} + 1.900 \tag{2.10}$$

Errors on these transformations are not presented by Hewett *et al.* (2006). However, since these transformation only involve applying the filter bandpasses to the SED of Vega, their errors are likely to be relatively small (compared with observational errors).

The names of the objects in table 2.1 are taken from the RBC. The positions of the sources are taken from their locations in our *r*-band images and should be accurate to better than 1 arcsec. Some of the proposed clusters are not detected (or not located) in the SDSS images. The names, locations and classifications of these clusters (taken from the RBC or C09) are included in table 2.1. This table lists all previously proposed clusters and candidates in the RBC. Many of these objects are found by this (and other) studies not to be genuine clusters. The classifications of these sources are discussed in the next section. Only those objects with classification flag, f=1 should be considered confirmed old GCs.

2.4 Classification of sources

2.4.1 Stellarity

The WFCAM images of M31 have a FWHM of 0.6 – 0.95 arcsec corresponding to a spatial resolution of 2.3-3.6 pc at the distance of M31. This is a significant improvement over most of the images previously used to classify clusters. Typical GCs at the distance of M31 will have half light radii between 0.5 – 1 arcsec and should be detected beyond this radius. These data therefore allow us to investigate possible contamination in the previous GC catalogues from single stars and previously unresolved asterisms of stars. Figure 2.8 shows the SExtractor K-band stellarity flag for confirmed and candidates clusters in the RBC (left) and, separately, the clusters and candidates from K07 (middle). Also included is the stellarity of old and young clusters from C09 (most of which are re-classifications of sources in the other two catalogues).

The majority of sources can be identified as either having stellar profiles (with a stellarity close to 1) or extended profiles (with stellarity close to 0). It can be seen that some objects with K$>$15 have uncertain stellarity flags. The ability of SExtractor to determine the stellarity of a source is mainly dependent on the signal to noise of the source, the PSF of the image and crowding around the source. From visual examination of the sources with uncertain stellarity flags, it was found that the majority of them have nearby sources contaminating their profiles. In gen-

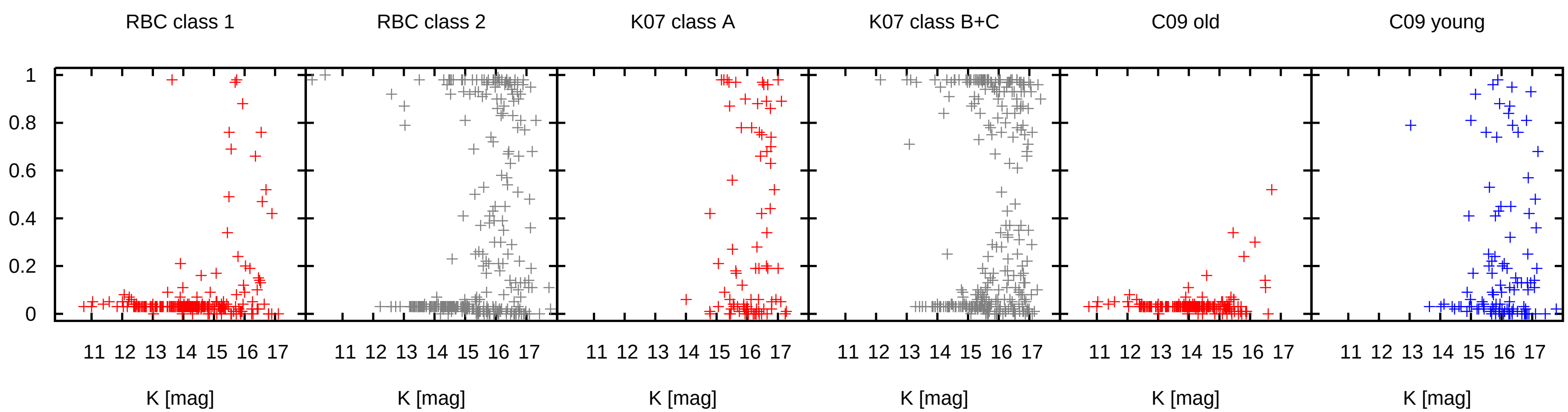

Figure 2.8: Stellarity of objects classed as confirmed clusters (red) and candidate clusters (grey) in the RBC (their class 1 and 2 sources respectively) and from K07 (their class A and B/C sources respectively). Also included are the re-classifications for many of these sources from C09 (their old and young clusters). The stellarity is based on SEXTRACTOR photometry of the WFCAM images. Extended sources have a stellarity close to 0 and point sources close to 1.

eral we consider objects with a stellarity <0.4 to be extended. This choice is relatively arbitrary. However, as can be seen from figure 2.8, the exact choice of this boundary between stellar and extended has little influence on the classification of most sources. For the fainter sources, it is clear that this stellarity flag is less reliable. For these objects we rely on visual examination of the cluster to estimate their nature (as described in the next section).

It can be seen from figure 2.8 that excellent agreement is found between our data and the classifications of C09 with all sources they classify as old being extended. We also find that the majority of confirmed clusters in the RBC are extended. However, there are 12 RBC *class 1* objects which have either stellar or uncertain stellarity flags. We note that some of these clusters have already been reclassified by C09 as stars. It can also be seen that many of the sources classed as confirmed clusters by K07 are found to be unresolved. We note that their work was based on images with poorer spatial resolution and we reclassify many of these objects as being stellar sources.

Some of the young clusters from C09 are found to be extended and look like normal centrally concentrated GCs. However, it can be seen from figure 2.8 that many of the proposed young clusters have stellar, or uncertain, stellarity flags. This is likely because these young clusters can appear as resolved asterisms in the K-band images. This has previously been noted by Cohen *et al.* (2005) who used K-band images taken with adaptive optics to demonstrate that 4 proposed young clusters may be asterisms. However, as discussed by C09, young clusters are generally faint in K and may be dominated by only a few bright (resolved) supergiants making them appear as resolved asterisms of stars, rather than an extended cluster. Many of these objects have subsequently been confirmed by *HST* images to be genuine clusters. We therefore do not reclassify any of the proposed young clusters which appear as resolved stellar sources in our K-band images.

Our data also allow us to classify many of the previously unclassified candidate clusters. In total we classify 368 previous candidates as likely to be stellar sources. For the above reasons, it is possible that we may potentially include some genuine young clusters in this classification. Figure 2.8 demonstrates that a large group of the proposed candidates are extended in our images. These objects are therefore likely to be either genuine clusters or background galaxies. These candidates represent ideal targets for followup spectroscopy in order to confirm their nature.

2.4.2 Visual examination

As discussed above, the stellarity flag for some of the fainter objects is relatively uncertain. Visual examination of these objects can help in deciding whether they are extended or stellar sources. Visual examination of the clusters and candidates which are confirmed as extended also provides a method of identifying background galaxies. These were identified as either having spiral structure, or extended ellipticity. While this method is relatively subjective, it is helpful in classifying an object. Inspecting the images of the objects also provides a useful check on our otherwise automated classifications. During this process, we also ensured that our automated photometry had selected a reasonable aperture size for each cluster, in order to measure its total luminosity.

We examined the *ugriz* and K-band images of every cluster and candidate studied[1]. We first examined the objects in our sample which have recently been classified from the spectroscopic study of C09 as being background galaxies. We then examined the previously classified confirmed clusters, followed by the proposed candidate clusters. In this way, we were able to reclassify some of the objects based on their appearance. We note that some of the newly confirmed galaxies look very similar to typical GCs. This highlights the limitations of visual examination on identifying galaxies. We do not reclassify any of the previously confirmed clusters as galaxies based on this visual examination. However, we did identify 3 candidate clusters with clear spiral structure and 30 other candidates which are likely background elliptical galaxies (this is in addition to the candidates confirmed to be galaxies from the spectroscopic study of C09). During this visual examination it was also found that some of the clusters and candidates with uncertain stellarity flags from our SExtractor photometry are likely to be asterisms of stellar sources, rather than extended clusters.

2.4.3 Colours

Figure 2.9 shows the colours of objects previously classified as confirmed GCs (red) and candidate GCs (grey) in the RBC (left) and by K07 (middle). The right panel shows the colours of the objects which are confirmed by C09 to be old clusters. Shown in blue are the proposed young clusters from C09 and the confirmed clusters from the RBC which are flagged as being potentially young. For comparison, the black points indicate the colours of the Milky Way's GCs. The *g*-K colour for the

[1]Thumbnail images of these clusters are available at http://www.astro.soton.ac.uk/~m.b.peacock/m31gc.html

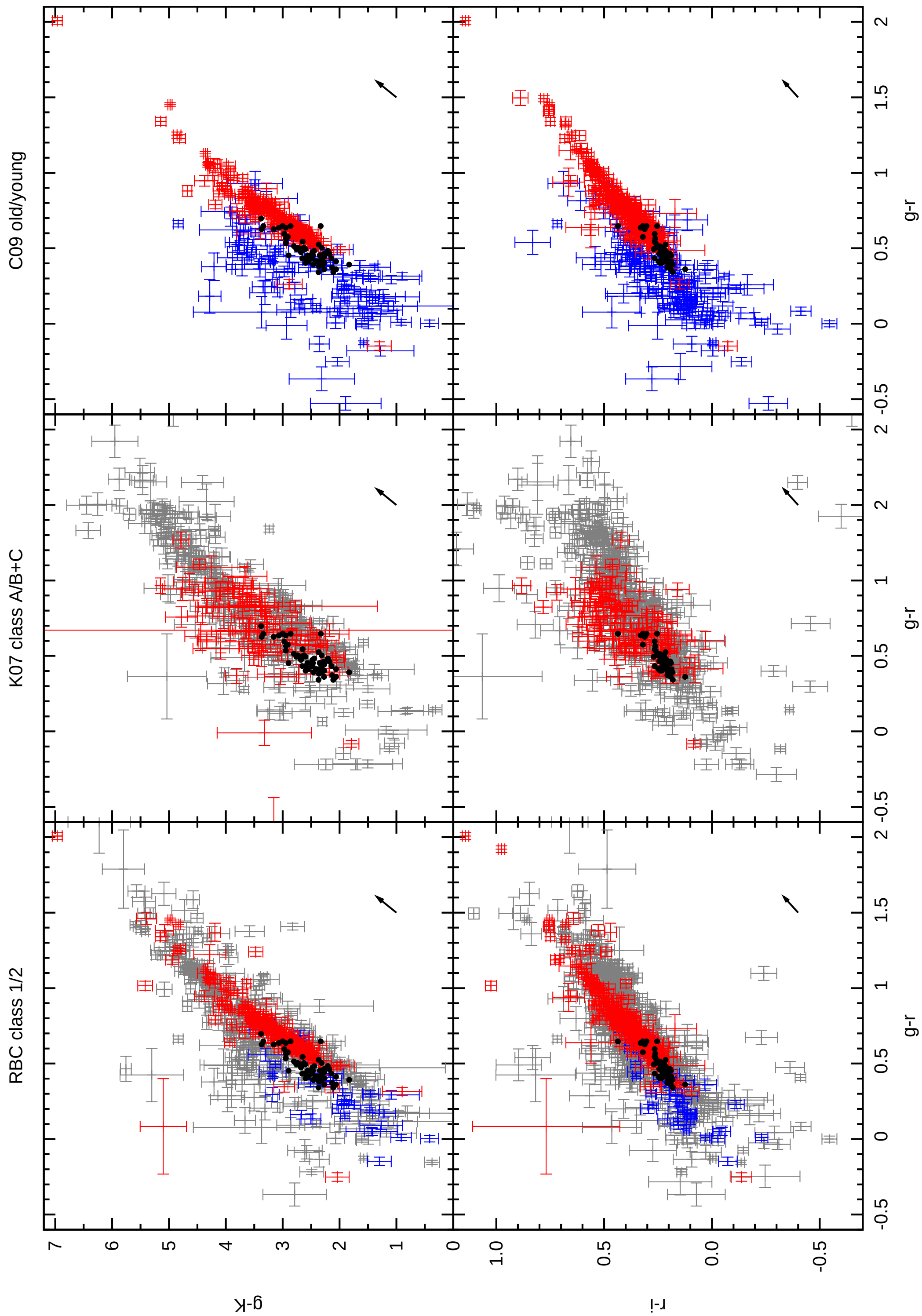

Figure 2.9: Colours of clusters and candidates from the RBC (*left*), K07 (*middle*) and C09 (*right*). Included are objects classified as confirmed old clusters (red), young clusters (blue), and candidate clusters (grey) from each catalogue. The black points show the colours of Milky Way GCs. The arrow represents a reddening of $E(B-V) = 0.1$.

Milky Way GCs were taken from Cohen *et al.* (2007) and optical colours from the Harris catalogue (Harris, 1996). The colours of the Milky Way's GCs were transformed into the *ugriz* filters using the transformations of Jester *et al.* (2005) and dereddened using the values for $E(B-V)$ quoted in the Harris catalogue. Only the Milky Way clusters with $E(B-V) < 0.4$ are included. The Galactic GC system contains relatively few metal rich clusters and most of these are at a relatively low galactocentric radius (and hence have relatively high extinction). The Milky Way clusters plotted are therefore limited to mainly low metallicity clusters. It can be seen that the Milky Way's GCs define a tight region in the colour-colour plots. For this reason, the colours of the proposed GCs and candidates in M31 are very useful in classifying the objects.

It should be noted that the colours of M31's GCs are reddened due to both Galactic extinction and extinction intrinsic to M31. The Galactic reddening in the direction of M31 is relatively uncertain, but it is estimated for the region around the disk of M31 to be $E(B-V) \sim$0.062 mag (Schlegel *et al.*, 1998). However, the extinction due to M31 itself can be much larger and varies significantly between GCs due to their locations in (and line of sight depths through) the galaxy. Previous work (e.g. Barmby *et al.*, 2000; Fan *et al.*, 2008) has demonstrated that the reddening for some of these clusters can be substantial. For example, the very red cluster in figure 2.9 with *g*-K=6.95 is B037 which is known to be heavily reddened [$E(B-V) = 1.38$: Barmby *et al.* (2000)].

Figure 2.9 shows that our colours are in good agreement with the classifications of C09. It can be seen that most of the objects classified by C09 as old clusters define a tight region which is consistent with the (reddened) colours of the Milky Way's GCs. In most cases the confirmed clusters in the RBC also have colours consistent with the Milky Way's GCs. Many of the confirmed clusters from K07, and a few of the confirmed clusters from the RBC, have colours which are not consistent with the Milky Way's GCs or the majority of the confirmed GCs in M31. This is in agreement with our conclusions from the previous section that some of the previously confirmed clusters may be misclassified stars. The colours also suggest that many of the unclassified candidate clusters may be stars, asterisms of stars or background galaxies.

2.4.3.1 Young clusters

These colours clearly identify the population of very blue clusters that have been noted by previous studies. It can be seen that our colours are in excellent agreement with the spectroscopic classifications of C09. We also find good agreement with the confirmed clusters in the RBC which are flagged as potential young clusters (flag *yy*=1,2 or 3 in the RBC). This flag is based on the work of Fusi Pecci *et al.* (2005). Most of the previously identified young clusters are much bluer in g-r than any GC in the Milky Way. Using a similar method to Fusi Pecci *et al.* (2005), we define all objects with g-$r<0.3$ to be young clusters.

Some of the proposed young clusters have colours which are consistent with being old clusters. However, these objects are also consistent with being young clusters with reddened colours. These clusters are also found in high density regions of M31 and look similar to the other young clusters we have observed. We therefore choose to keep the previous (spectroscopic) classification for these clusters and suspect that their colours may be reddened. It can also be seen from figure 2.9 that two clusters classified as old by C09 (B386 and PHF7-1) have very blue colours. We reclassify these two objects as young clusters.

2.4.3.2 Old globular clusters

Figure 2.10 shows the colours of all confirmed and candidate clusters following the removal of all stellar objects based on their stellarity flag or visual examination of the cluster images. We have also removed those objects identified in the previous section as being young clusters. It can be seen that, having removed these objects, the colours of the confirmed clusters are now consistent with the colours of the old GC system of the Milky Way. The clusters extend to much redder colours, but this is consistent with the expected reddening due to extinction from M31.

The grey points in the bottom panels of figure 2.10 show the colours of the remaining candidate clusters after the removal of non-extended objects. Comparison with the confirmed old clusters shows that many of the candidates have colours consistent with being old clusters. These clusters are flagged as old candidates in table 2.1 and should be considered the strongest candidate clusters. We also identify candidates with very blue colours, consistent with the other young clusters identified. These are flagged as young candidate clusters in table 2.1. It can be seen that, despite removing objects identified as stars, the colours of many of the candidate clusters are inconsistent with being either old or young clusters. As we are uncertain of the classification of these objects, we retain their classification as candidates. However, it is likely that many of these candidates are either background galaxies or unresolved asterisms.

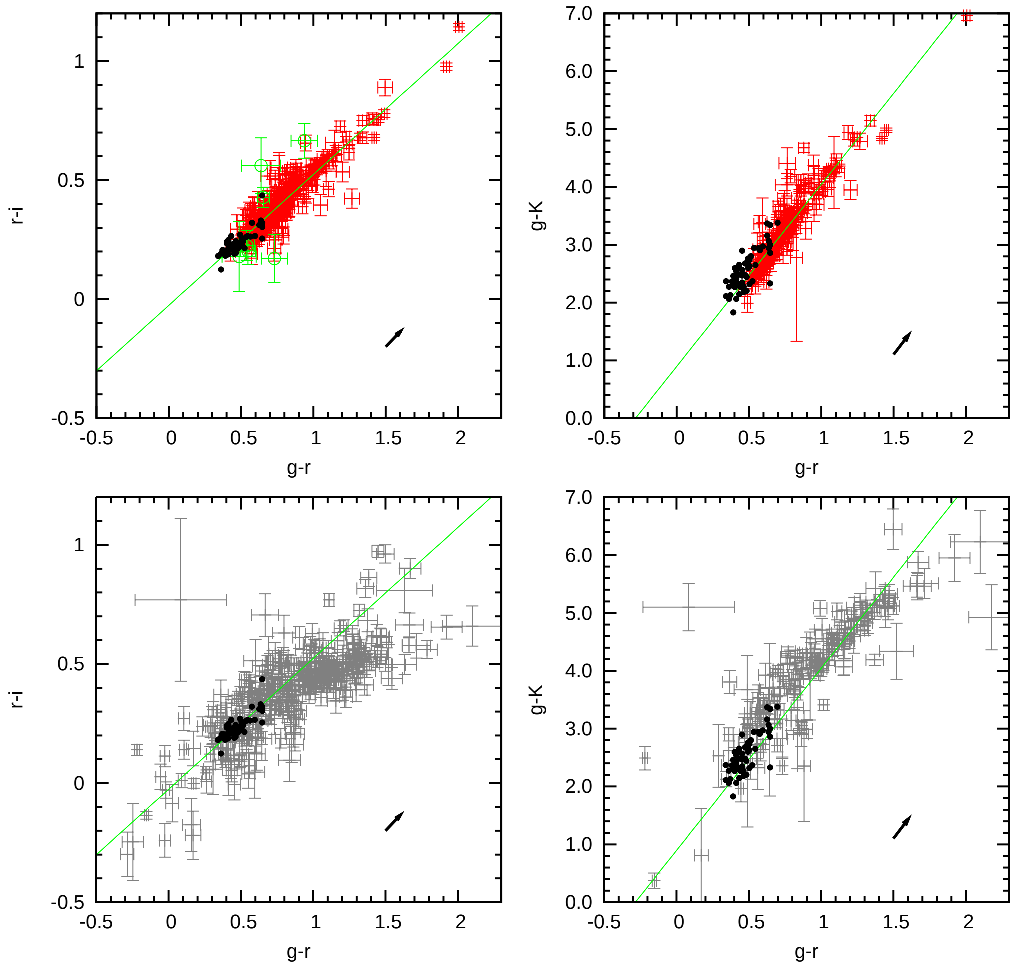

Figure 2.10: *Top:* Colours of previously confirmed clusters which are confirmed here to be extended (red). *Bottom:* Colours of proposed candidate clusters which are confirmed to be extended (grey). The lines indicate linear fits to the colours of all confirmed M31 GCs. The black points indicate the colours of the Milky Way GCs and the arrow represents an extinction of $E(B-V) = 0.1$.

2.4.3.3 Extended clusters in the halo of M31

Recent studies of the halo of M31 have identified a population of very extended clusters (Huxor *et al.*, 2005; Mackey *et al.*, 2006; Huxor *et al.*, 2008). These clusters have relatively low surface brightness and larger half light radii than the majority of the clusters in M31. Colour magnitude diagrams of these clusters suggest that, beyond their extended nature, they appear to be similar to typical old clusters. These clusters are similar to the Galactic GC NGC 2419 and begin to fill the 'gap' between classical GCs (which are thought to contain little dark matter) and the (dark matter dominated) dwarf spheroidal galaxies (see e.g. Huxor *et al.*, 2005). For a description of these clusters we refer the reader to Huxor *et al.* (2008, and references therein).

Seven of these clusters are located in our SDSS images and can be identified in table 2.1 from their names which have the prefix HEC ('Halo Extended Cluster'). Our colours of these clusters were found to be less reliable than the other clusters studied. This is because they are resolved, due to the diffuse nature of the clusters, into multiple sources.

The colours for these clusters were therefore re-measured through 12 arcsec apertures using the IRAF:APPHOT task PHOT. A smaller aperture of 8 arcsec was used for HEC11 due to a bright neighbouring star. This method gives reliable results for clusters in the halo of M31 where there is little contamination from neighbouring sources and the background is relatively smooth. None of these extended clusters are identified in the inner regions of M31. However, it should be noted that detecting such extended (and low surface brightness) clusters, projected against more central regions of M31, would be very difficult.

These clusters are identified in figure 2.10 as open green points. It can be seen that the colours of these clusters are now consistent with the other old GCs in M31. The errors in the colours of the HECs are larger than those of the other GCs. This is due to their diffuse nature and the use of large apertures, which increases the total sky background.

2.4.4 Final classification

Our final classification is based on: the stellarity of the object; its colours; visual examination of the object in our 6 bands; velocity information and classifications from previous studies. Table 2.1 lists these classifications for all GCs and candidates. For comparison we also include the previous classifications from the RBC and C09. For consistency we have tried to keep our classifications similar to those used in the RBC. If we have no reason to reclassify the sources, we keep the original classifications (where available from C09, which were found to agree best with our classifications, otherwise from the RBC). The classifications used are:

1: old globular cluster: extended and has colours consistent with the Milky Way's GCs. Its velocity is confirmed from previous work (K07, C09 or the RBC) to be consistent with being in the M31 GC system, or the object is confirmed from high resolution *HST* images.
2: candidate cluster: not confirmed, but previously proposed as being a cluster or candidate and is found here to be extended (or have uncertain stellarity). Candidate is sub-divided, depending on whether its colours are consistent with being an old

Table 2.3: Classifications of sources

Classification	Number in this study	Previous classification of these objects RBC *1*	RBC *2*	K07 *A*	K07 *B/C*	C09 *old*	C09 *young*
1: old globular cluster	**416**	342	41	27	0	336	0
2: candidate cluster	**373**	6	101	9	256	3	0
3: young cluster	**156**	46*	78	2	0	2	151
4: background galaxy	**189**	5	170	4	10	0	0
5: HII region	**17**	0	14	3	0	0	0
6: stellar source	**444**	10	153	66	215	1	0
Total (previous catalogues):		409	557	111	481	342	151

* Many of these RBC *class 1* clusters are flagged separately in the RBC as potentially young clusters.

cluster (*21*), consistent with being a young cluster (*23*) or inconsistent with being a cluster (*2*).

3: young cluster: has colours consistent with being young. If previously classified, may appear as a resolved asterism in K, but looks like a cluster in the SDSS images.

4: background galaxy: previously classified from spectroscopy by C09 or identified from our visual examination.

5: HII region: from previous classification of C09.

6: stellar source: object appears to be a single stellar source or a previously unresolved asterism of stellar sources.

The total number of sources of each class is shown in table 2.3. For reference we include whether these objects were previously classified as: clusters or candidates in the RBC (RBC 1 and RBC 2 respectively); clusters or candidates by K07 (K07 A and K07 B/C respectively); old or young clusters by C09 (C09 old and C09 young respectively). It can be seen that we have reclassified 10 previously confirmed clusters in the RBC as likely stellar sources. We also reclassify 6 of these objects as candidate clusters, as we are uncertain of their nature, or they lack spectroscopic confirmation. Some of the candidate clusters in the RBC are confirmed to be old or young clusters. This is based on the new spectroscopic confirmations by C09. We are also able to classify many of the candidate clusters in the RBC as stars. In most cases we find good agreement with the new classifications of C09. Their catalogue includes fewer objects because they do not provide classifications for the whole GC system. All objects classed as young clusters by C09 are retained in our classification.

We have reclassified many of the confirmed clusters from K07 as likely stellar sources. We have also been able to classify nearly half of the cluster candidates from this catalogue as being stellar. We believe this is due to our improved spatial

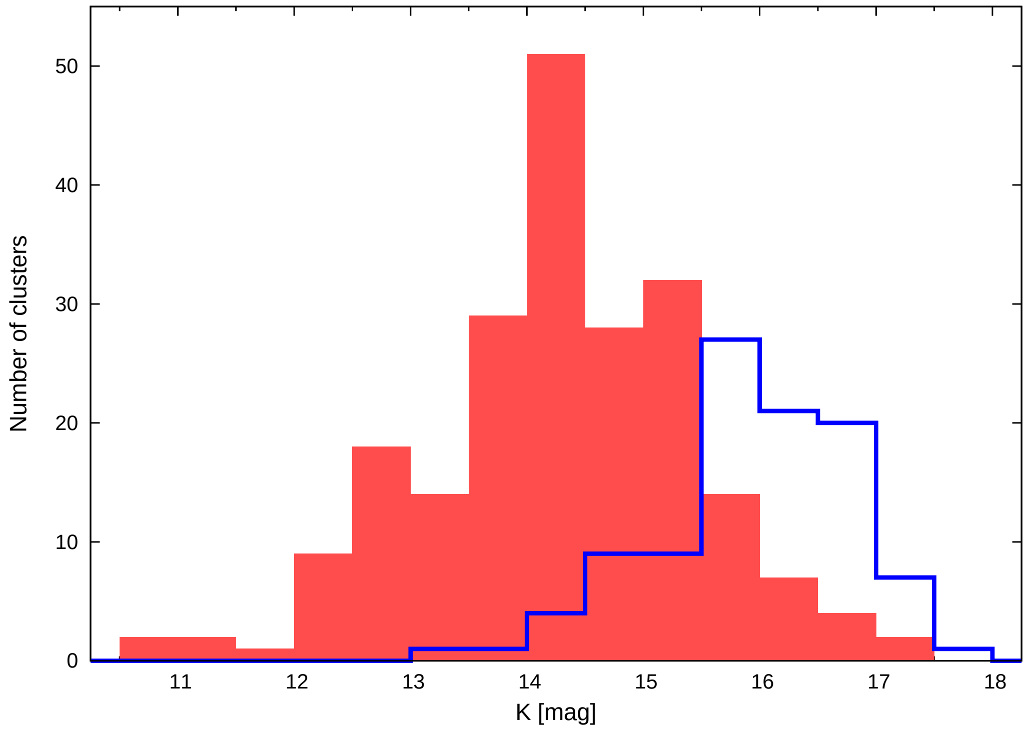

Figure 2.11: K-band GCLF for all sources classed as confirmed GCs (solid, red) and young clusters (open, blue).

resolution compared with the images used for this previous catalogue. We identify and remove 8 objects from the catalogue of K07 which are within 2 arcsec of another previously identified object in the RBC and we believe are now duplicated in the RBC. A further 5 objects from the catalogue of K07 appear to be associated with objects in the catalogue of C09. The names for these objects in table 2.1 are the combination of their identifications in each catalogue.

2.5 Properties of confirmed clusters

Figure 2.11 shows the GC Luminosity Function (GCLF) for all confirmed GCs (solid bars) and young clusters (open bars) with K-band photometry. These clusters are not corrected for extinction. However, extinction is not very significant in the K-band where the maximum correction for the most extreme case of B037 is only 0.5 mag (the width of the bins used). The peak of the GCLF is found to be at K∼14.2 mag. The K-band luminosity of a cluster is a useful estimate of its mass. This is because, in addition to being less effected by extinction, the K-band mass to light ratio (M/L) is less affected by metallicity than optical bands. The mass to light ratio of a 12 Gyr cluster in the K-band has previously been estimated to be 0.9<*M/L*<1.3 for metallicities in the range 0>[Fe/H]>-2 (Bruzual and Charlot, 2003; Forbes *et al.*, 2008). To estimate the peak mass of the old GCs in M31, we assume a K-band M/L ratio of 1.1 for all clusters (as the metallicities are not known for all of the clusters). At the distance of M31 (780 kpc; McConnachie *et al.*, 2005) and assuming the K-band magnitude of the sun to be $M_{K_s\odot}$=3.29 mag [this is taken from Cox (2000, $M_{K\odot}$=3.33) and corrected to the K 'short' filter (K_s) via $M_{K_s\odot}=M_{K\odot}-0.04$ (Carpenter, 2001)], this implies a peak mass of $M_{peak} \sim 3 \times 10^5 M_\odot$. This is slightly higher than that found for Milky Way GCs (e.g. Cohen *et al.*, 2007). However, this difference is relatively small compared with the expected uncertainty in the peak mass. This is due to errors in accurately estimating the peak in the GCLF combined with errors in the distance to M31 and the value used for the mass to light ratio.

For the fainter GCs, it is likely that masses estimated from their integrated K-band luminosities are less accurate due to stochastic effects. Stars at the tip of the red giant branch at the distance of M31 are expected to reach magnitudes of K=17.5 (Ferraro *et al.*, 2000; Tabur *et al.*, 2009). Stars this bright are relatively rare. However, it is possible that the integrated light of some fraction of these faint clusters can be dominated by a relatively low number of these stars. It is also likely that some of the faintest clusters in M31 are missing from our catalogue. These clusters should be detected in our data. However, identifying these faint clusters in front of M31 would be very difficult.

As expected the proposed young clusters peak at fainter magnitudes than the old GCs. Some of these clusters are found to be relatively bright, reaching luminosities similar to the peak of the GCLF. This suggests they are more massive than typical young open clusters in the Milky Way. While this is in agreement with the conclusions of other work (e.g. Fusi Pecci *et al.*, 2005), it should be noted that our conclusions based on this K-band luminosity are limited. The M/L ratio of these clusters is likely to be significantly lower than the M/L ratio for the older clusters in the galaxy. Also stochastic effects in these young and faint clusters are likely to be significant in the K-band.

2.6 Conclusions

Our final catalogue includes 416 old GCs. Where detected, we provide self consistent *ugriz* and K-band photometry for the proposed clusters and candidate clusters. We note the difficulty in providing accurate photometry for some of these clusters due to the complex background of M31. We highlight the need for good spatial resolution in order to remove contamination from non cluster light when obtaining integrated magnitudes. Where available, we find our photometry to be consistent with that previously published. From our multicolour photometry, we confirm the population of very blue clusters identified previously. We show that these colours are consistent with their spectroscopic classification by C09 as young clusters. We note that many of these clusters look like resolved asterisms in our K-band images. However, some of these are confirmed by HST images to be genuine clusters. Higher spatial resolution optical images than available here are required in order to confirm their nature as genuine young clusters.

We have identified that many of the confirmed clusters from Kim *et al.* (2007) are likely stellar sources (we retain only 27 of their 111 confirmed clusters as old clusters). We also identify 10 confirmed clusters in the RBC as likely stellar sources. While we have considered the classifications from K07 and the RBC separately in this paper, we caution that *all* of the objects confirmed by K07 to be clusters are included as confirmed clusters in the current version of the RBC (v3.5). We also provide new classifications for many of the cluster candidates proposed by this previous work. We identify many of these candidates to be stars and reduce the number of unclassified candidate clusters to 357.

3

The structural parameters of globular clusters in M31

3.1 Abstract

In this chapter, we present the structural parameters for a spatially limited sample of 213 of M31's old globular clusters. These parameters are based on fitting King (1966) models (convolved with an estimate of the point spread function of the cluster image) to Wide Field Camera (WFCAM) images of these clusters. We consider the reliability of the derived parameters and show them to be consistent with those of 33 clusters which were previously determined using higher spatial resolution *HST* observations. We note that the reliability of the structural parameters decreases significantly for the faintest clusters considered. This is likely to be due to the relatively low signal to noise of these clusters. We caution on the use of this method for low signal to noise images. We demonstrate that the structural parameters of old globular clusters in M31 are similar to those of the globular clusters in the Milky Way. We investigate the relationship between the structure of these clusters and galactocentric radius. This confirms the relationship found by some other studies of half light radius increasing with galactocentric radius.

3.2 Introduction

Determining the structure of globular clusters (GCs) is useful for investigating both the initial formation of the clusters and their subsequent dynamical evolution. The density profiles of clusters in the Milky Way are known to be relatively well modelled by King models (King, 1966). The structure of globular clusters is best investigated via direct counts of all stars in the clusters. However, even for Galactic clusters, it is difficult to resolve stars in the dense cores of the clusters. Also the number counts often suffer from incompleteness for faint stars. For extragalactic clusters the integrated luminosities of the clusters can be used to give a good estimate of the structure of the clusters. Due to the relatively small size of the Milky Way's cluster system, determining the structural parameters for extragalactic GCs is highly desireable. These can be used to help constrain models of cluster formation for a much larger sample of clusters than is available from the Milky Way alone. It is also of interest to consider any differences in the structure of clusters in different galaxies, as this can give insights into different formation or evolutionary histories.

The structure of a cluster is also likely to affect the population of stars contained in the cluster. For example the dense cores of GCs are likely to be ideal locations for forming tight binary systems through stellar interactions. These include exotic objects such as low mass X-ray binaries, cataclysmic variables and blue straggler stars.

The proximity of M31 makes it the ideal location for studying the structure of extragalactic GCs. The structural parameters for some of M31's GCs have been measured using *Hubble Space Telescope (HST)*: Faint Object Camera (FOC) images of 13 clusters (Fusi Pecci *et al.*, 1994); Wide Field Planetary Camera (WFPC2) images of 50 clusters (Barmby *et al.*, 2002); Advanced Camera for Surveys (ACS) and Space Telescope Imaging Spectrograph (STIS) images of 15 and 19 clusters respectively (Barmby *et al.*, 2007). However, the large angular size of the M31 GC system, combined with the small field of view of the *HST* cameras, means that many of M31's clusters do not have estimates of their structural parameters. Here we use ground based images obtained using the Wide Field Camera (WFCAM) on the UK Infrared Telescope (UKIRT) to estimate the structural parameters for a much larger sample of clusters. The core radii of GCs at the distance of M31 are typically smaller than the PSF of these WFCAM images of them. However, it is possible to infer their structure by fitting PSF convolved King models to their profiles. This method has previously been used in order to estimate the structure of GCs in M31 (Barmby *et al.*, 2007; Peacock *et al.*, 2009), Cen A (Harris *et al.*, 2006;

Jordán *et al.*, 2007b; McLaughlin *et al.*, 2008), M87 (Waters, 2007) and other Virgo cluster galaxies (e.g. Jordán *et al.*, 2009).

3.3 Wide Field Camera data

To investigate the properties of the GCs in M31, we obtained K-band photometry using the Wide Field Camera (WFCAM) on the UK Infrared Telescope (UKIRT) under the service program USERV1652. These data cover most of the disk of M31, but avoid the central regions where surface brightness fluctuations are largest. They also do not cover some of the clusters in the outer halo of M31. The regions covered by these WFCAM images were shown previously in chapter 2 (figure 2.2).

Each observation consisted of microstepped 5s exposures with a nine point jitter pattern. The 2$\times$2 microstepping was used to give an effective pixel size of 0.2 arcsec and ensure the images were well sampled. Five observations were taken of each field to give a total exposure time of 225s. This gives a detection limit of K=19 at 3σ. Our observations were taken on the nights of 2005-11-30 and 2007-08-06 with seeing of 0.85-1.00 arcsec and 0.6-0.8 arcsec, respectively. This corresponds to a spatial resolution of 3.21-3.78 pc and 2.26-3.04 pc at the distance of M31.

The images were processed using the standard WFCAM pipeline (for details on the WFCAM and its pipeline see e.g. Dye *et al.*, 2006). The pipeline reduces and stacks the raw images and adds an accurate astrometric solution to the final images by fitting sources to the Two Micron All Sky Survey (2MASS). For combining our microstepped images we chose not to use the standard pipelines interleaving method. Instead the reduced images were drizzled together (Fruchter and Hook, 2002) using the IRAF STSDAS task DRIZZLE. Drizzling has the advantage that it produces combined images with smoother PSFs than interlacing.

3.4 M31 globular clusters

3.4.1 Selection of globular clusters

We select M31 clusters from the catalogue of Peacock *et al.* (2010) (see chapter 2 for details). This catalogue provides sub-arcsec locations and updated classifications for all clusters identified in most major M31 cluster surveys to date (including those of: Battistini *et al.*, 1987; Barmby *et al.*, 2000; Galleti *et al.*, 2004; Kim *et al.*, 2007; Caldwell *et al.*, 2009). Our observations cover 213 of the 417 old clusters in this catalogue; allowing us to study over half of M31's GCs.

3.4.2 Profile fitting of M31's old clusters

To investigate the structure of the clusters in our observations, we must first consider the effects of seeing on their appearance. The images of the clusters studied are the result of a convolution of their physical size with the point spread function (PSF) of the observations. To account for this, we create a model for the PSF of each image so that we can convolve it with our model for the underlying structure of the cluster. We modelled the PSF for the images with a Moffat profile using the DAOPHOT tasks ALLSTAR/SEEPSF. To determine the shape of the PSF we fit the brightest 40 stars in each image which were unsaturated, had no bright neighbours and were greater than 100 pixels from the detector edges (where the noise is significantly higher). No significant variation in the PSF was observed across the images so we select a single PSF model for each detector of each observation.

The structural parameters of the clusters were determined by identifying the best fitting King model to their profiles using the program SUPERKING (Waters, 2007). Details of this code are presented in Waters (2007), where its application to HST observations of M87's GCs is also presented. For a given cluster image and PSF model, this code selects the best fitting King model to fit the data based on χ^2 minimisation. Three parameters are required in order to constrain a King model. We use this code to fit the clusters based on their central potentials (W_0), total K-band magnitudes (K) and tidal radii (r_t). In addition to these parameters, it is also necessary to fit the center of the clusters (x_o,y_o) and the flux of the clusters backgrounds. Before fitting the GC profiles, bright stars (above 5σ) were removed from the region around the cluster using the DAOPHOT task ALLSTAR. Each cluster was fit out to a radius of 20 arcsec. This was chosen to extend beyond the expected tidal radius for 85% of the clusters (based on Milky Way GCs in the Harris catalogue; Harris, 1996). This allows for the tidal radius and background level to be accurately computed.

In table 3.1 (for full table see appendix D), we present the best fitting structural parameters for the 213 old clusters studied. Where clusters were present and in more than one observation, we select the observation with the best seeing. We assign a flag to each cluster based on visual examination of the cluster and its residual after subtraction of our best fitting model. These flags are used to identify poorly fitting models, as well as clusters contaminated by very bright stars. The parameter Γ in

Table 3.1: Structural parameters of old clusters in M31 (sample)

GC Name(1)	$\chi^2/\nu^{(2)}$	$W_0^{(3)}$	c(3)	K(4)	$r_c^{(5)}$	$r_h^{(5)}$	$r_t^{(5)}$	$\log(\rho_c)^{(6)}$	$\log(\Gamma)^{(6)}$	Flag(7)
B001-G039	1.07	6.25	13.70	1.31	1.25	2.71	25.9	3.87	6.00	1
B002-G043	1.07	8.10	15.34	1.86	0.34	1.93	24.8	4.55	5.90	1
B003-G045	1.15	9.55	14.91	2.25	0.24	4.05	42.7	4.82	5.99	1
B004-G050	1.69	6.45	14.18	1.37	0.92	2.13	21.4	4.05	6.01	1
B005-G052	1.20	8.25	12.54	1.91	0.36	2.27	29.1	5.57	7.47	12
B006-G058	0.85	9.60	12.64	2.26	0.20	3.47	36.2	5.97	7.55	1
B008-G060	11.15	4.30	14.04	0.89	2.16	2.77	16.8	3.31	5.63	1
B009-G061	1.35	7.40	14.63	1.65	0.56	2.00	24.6	4.35	6.02	1
B010-G062	1.02	6.00	14.00	1.25	2.70	5.37	48.2	2.79	5.05	1
B011-G063	1.28	7.00	14.20	1.52	0.63	1.84	21.1	4.44	6.26	1
B012-G064	0.95	7.25	12.69	1.60	0.91	3.00	36.1	4.52	6.70	1
B013-G065	1.06	3.35	14.47	0.73	4.90	5.08	26.1	2.21	4.70	1
B015-V204	1.33	6.30	13.48	1.33	1.78	3.91	37.9	3.50	5.74	1
...	...	...	...	...	...	...	...	...	...	...

The full version of this table is presented in appendix D. This table is also available in electronic form from the VizieR archive or from the supplementary material of Peacock *et al.* (2009).
[1]Cluster names are taken from table 2.1 and are the same as those in the Revised Bologna Catalogue of M31 GCs (Galleti *et al.*, 2004).
[2]The χ^2 per degree of freedom for the best fitting model to the cluster profile.
[3]The central potential (W_0) and concentration parameter [$c = \log(r_t/r_c)$] of the cluster.
[4]The K-band magnitude of the cluster (from profile fits *not* aperture photometry) [mag].
[5]The core, half light and tidal radii of the cluster (assuming the distance of M31 to be 780 kpc McConnachie *et al.*, 2005) [pc].
[6]The cluster core density [$L_{K,\odot}pc^{-3}$] and stellar encounter rate [as defined by equation 1.6; $L^2_{K,\odot}pc^{-3}km^{-1}s$].
[7]Flag based on visual examination of the cluster image and its residual after subtraction of the best fitting model. Flags are: 1-clean cluster image and residual; 2-elliptical profile; 3-poor residual after subtraction; 4-bright source close to the cluster which may potentially influence its profile; 5-potential asterism; 6-potentially stellar profile/ unphysical parameters.

table 3.1 is an estimate of the stellar collision rate in the cluster, as defined in section 1.2.2.2. This is calculated from equation 1.6: $\Gamma \propto \rho_c^{3/2} r_c^2$.

3.5 Reliability of parameters

Having identified the best fitting King model to describe each cluster, we investigate the reliability of the parameters found. The reliability of this method of modelling the cluster profile is primarily dependent on the spatial resolution of the GC images, the accuracy of the PSF model used in the deconvolution and the signal-to-noise (S/N) of the cluster images. The spatial resolution of the WFCAM images at the distance of M31 is 2.3-3.8 pc. This is only slightly larger than the spatial resolution of *HST* observations of Cen A (∼1.8 pc) and significantly smaller than that of *HST* observations of Virgo cluster galaxies (∼8 pc). The effect of S/N on the reliability of PSF convolved King model fits to *HST* images of GCs at the distance NGC 3597, NGC 1275 and the Virgo cluster were investigated by Carlson and Holtzman (2001).

By simulating GCs with varying S/N, they suggested that an integrated S/N∼90 was required to recover the correct cluster concentration 50% of the time for clusters at the distance of Virgo. The reliability of the fits was found to improve significantly with S/N, increasing to ∼80% for a S/N∼150. Our WFCAM images of M31's GCs benefit from better spatial resolution than *HST* observations of GCs in Virgo cluster galaxies. However, for the WFCAM images this S/N limit corresponds to a magnitude of K∼15.3. Carlson and Holtzman (2001) also found that the profile fits were more reliable for lower concentration clusters as their larger cores are easier to measure.

3.5.1 Consistency checks

Due to the small spatial scale of the clusters we are fitting, it is likely that the errors on these parameters will be dominated by errors in the PSF model which is convolved with the cluster.

To investigate the magnitude of the typical measurement errors, we compare the results obtained from fitting the same cluster from different observations. In total, 115 clusters are present in multiple images. These observations have all been taken under slightly different conditions and will have different PSF models. Therefore, by fitting these clusters independently and comparing the resulting parameters, we can estimate the reliability of the parameters calculated. Figure 3.1 shows the differences between the derived parameters for the clusters fit in more than one image.

For clusters brighter than K∼15mag we find good agreement between the parameters measured. However it can be seen that the scatter increases significantly for clusters with K$>$15mag. This suggests that the errors on the parameters found for these faint clusters are significantly higher. This compares well with the expected reliability limit due to signal-to-noise proposed by Carlson and Holtzman (2001).

We expect that the variation observed in figure 3.1 gives a reasonable estimate of the errors on the parameters found for all the GCs studied. In the following analysis, we include all 213 GCs studied but note that the errors on individual parameters for the faintest clusters will be large. Since most of the GCs studied are brighter than this limit, we do not believe our conclusions are sensitive to this increased error on the faintest clusters.

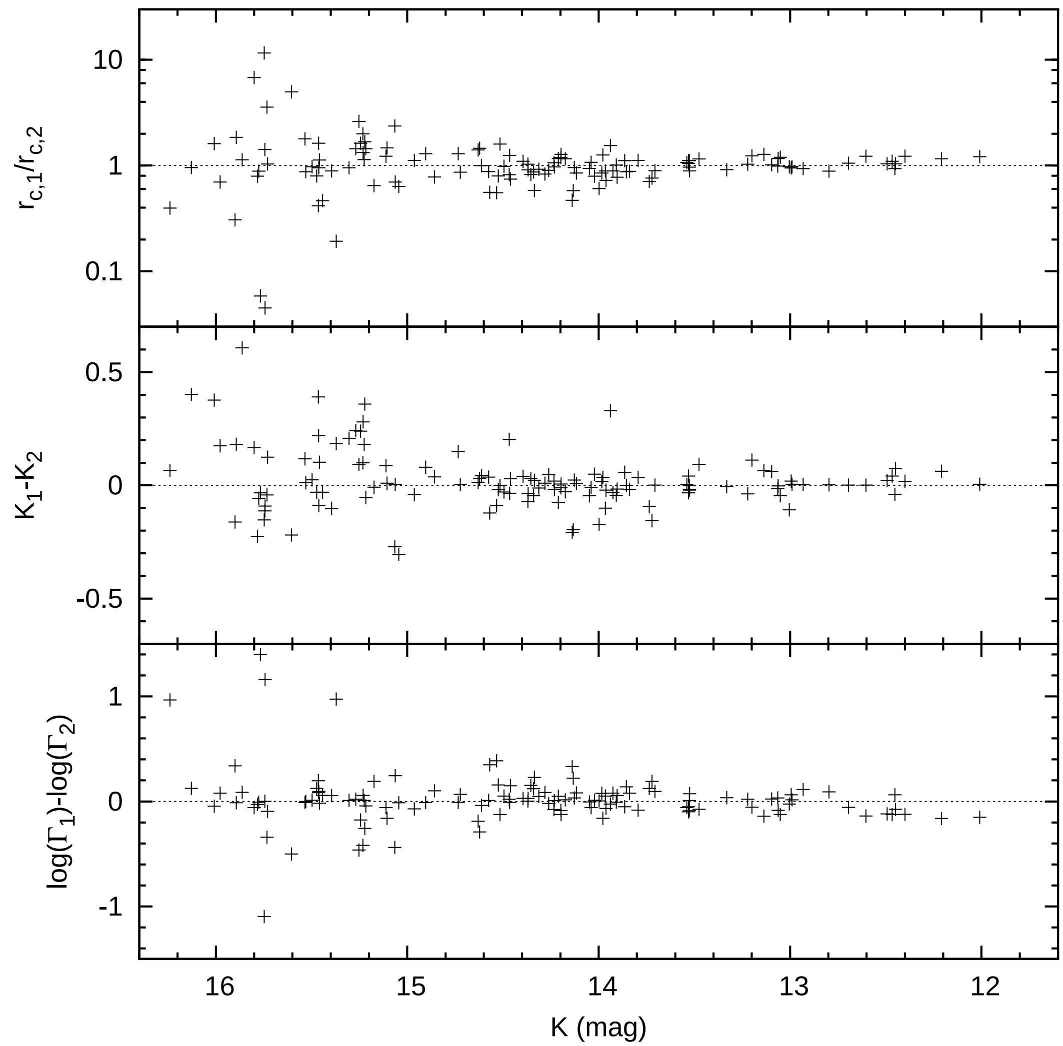

Figure 3.1: Comparison between the core radius (r_c, *top*), integrated K-band magnitude (K, *middle*) and stellar collision rate (Γ, *bottom*) derived from fitting different observations of the same cluster.

3.5.2 Comparison with previous work

Some of the GCs in M31 have been observed by the *HST* under several different programs. Using these data the structural parameters for 96 clusters have already been estimated from either ACS, STIS or WFPC2 observations (Barmby *et al.*, 2002, 2007). As these observations have better spatial resolution than those used in this study, they provide a useful test for this method of PSF convolution. Figure 3.2 compares these previously determined parameters with those found in this study. There are 33 clusters present in both datasets.

For clusters brighter than K∼15 mag, we find reasonable agreement between the radii found in this study and those found by Barmby *et al.* (2007). For clusters fainter than this we find significant differences between both the core and tidal radii

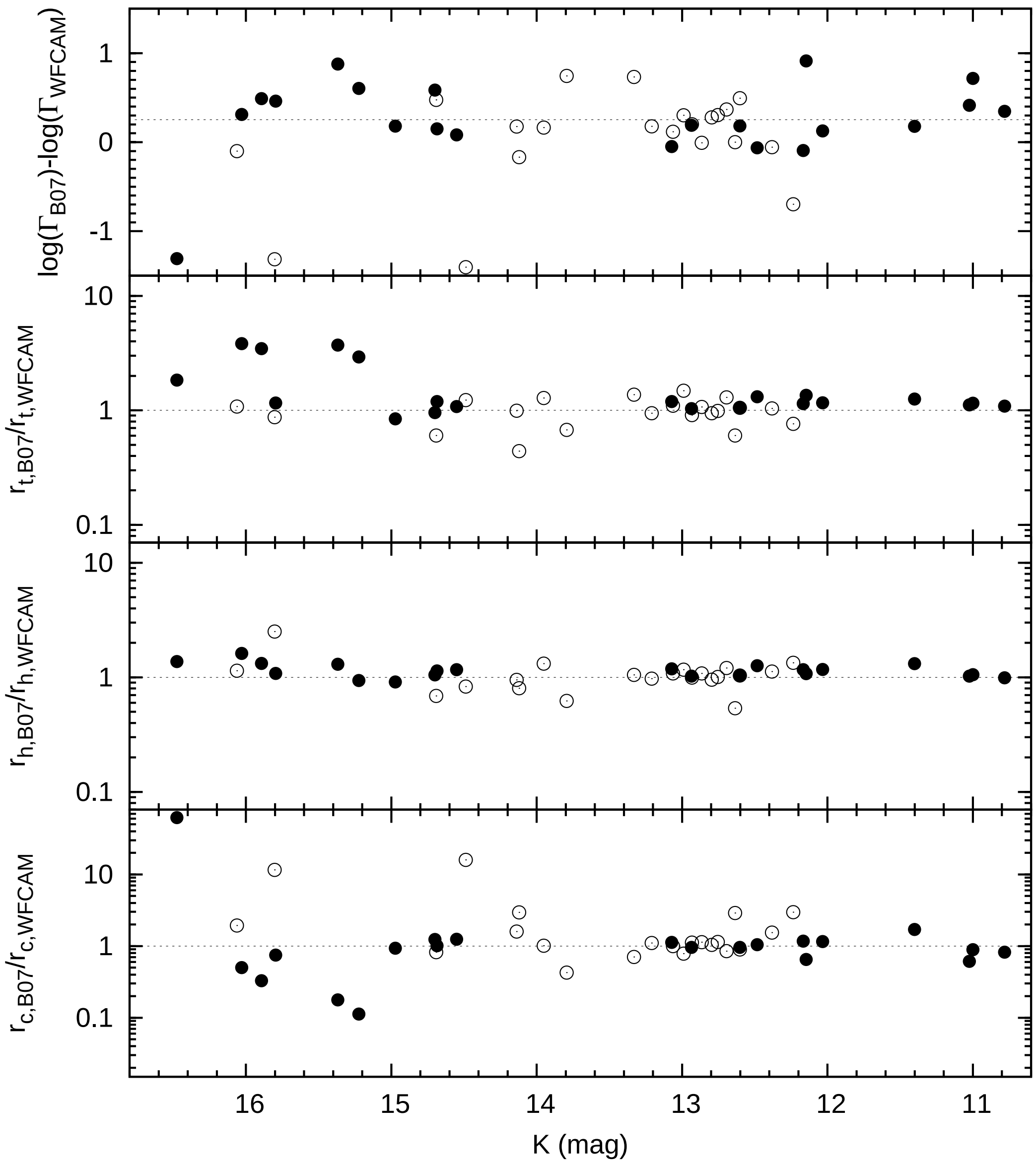

Figure 3.2: Comparison between the core radii (r_c), half light radii (r_h), tidal radii (r_t) and stellar collision rates (Γ) measured in this study and those measured by Barmby *et al.* (2007, B07). The Barmby *et al.* (2007) parameters were obtained using *HST* STIS/ACS (solid circles) and WFPC2 (open circles) observations.

found. However, this is within the large errors predicted in the previous section for these fainter clusters. It can be seen that the derived core radius of the faintest cluster in this comparison (B041), is significantly smaller than that previously found. This is a very faint and diffuse cluster, projected against a relatively crowded region of M31, as such it is likely that our fits to this cluster are unreliable.

For all the cluster parameters compared we find greater discrepancies between our results and those based on WFPC2 observations (open circles). The likely reason for this is the differing methods used to estimate these parameters. We fit the whole profile of the cluster and select the best fitting tidal radius, where as the WFPC2 observations are fit to the inner region of the cluster (where the signal to noise is greater) and the tidal radius is inferred from the best fitting model (Barmby *et al.*, 2002). The tidal radius inferred from the second method is much more susceptible to slight deviations from a pure King model. We therefore believe our tidal radii may better represent the actual tidal radii of the clusters.

It can be seen that the half light radii are found to be the most reliable of the structural parameters. These radii compares well, even for clusters with relatively low S/N. This has been found by other studies (e.g. Kundu and Whitmore, 1998; Carlson and Holtzman, 2001) and is likely due to the half light radius being relatively robust to errors on the concentration of the cluster.

The stellar collision rates found by both studies show a clear scaling difference. The stellar collision rate is calculated from the cluster core density (using equation 1.6). The core density is a luminosity density and *not* a mass density. This offset is therefore expected because, in this study, we measure the K-band core density, whereas the previous work presents V-band core densities. This offset is therefore most likely due to the difference between the V and K-band mass-to-light ratios of the clusters. Since our analysis is relative only to values measured in this study, this offset should not affect our conclusions. Also since stellar mass is more closely correlated with K-band luminosity than any optical band, comparisons of the collision rates within our data are likely to be robust.

3.6 The structure of M31 globular clusters

Figure 3.3 shows the concentration [$c = \log(r_t/r_0)$], core radii (r_0), half light radii (r_h), tidal radii (r_t) and core density (ρ_0) of M31's GCs. For comparison the same parameters for the Milky Way's GCs are shown on the bottom row (Harris, 1996). Before comparing these populations there are two important differences which need

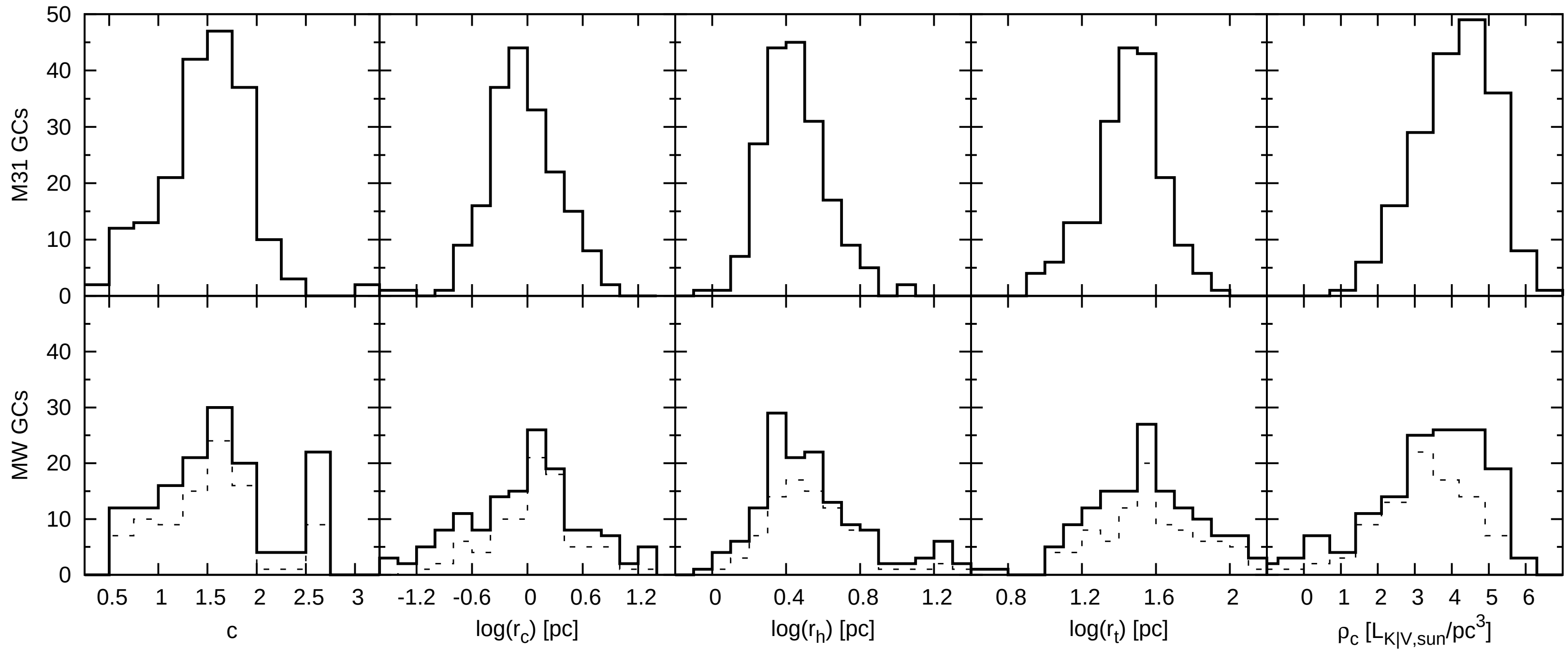

Figure 3.3: Structural parameters of M31 GCs (*top*) and Milky Way GCs (*bottom*). The dashed line indicates the GCs in the Milky Way over a similar galactocentric radius. It should be noted that the core densities are K-band luminosity densities for the M31 GCs and V-band luminosity densities for the Milky Way clusters.

to be considered. Firstly, the M31 parameters are based on the K-band, rather than the V-band luminosity of the clusters. As a result we expect offsets in parameters such as the core luminosity density due to the different mass to light ratios. However, this is unlikely to have a significant effect on the size of the clusters (Cohen *et al.*, 2007). Secondly, due to a lack of WFCAM data, the sample of M31 GCs does not include the most central or distant GCs in the galaxy. For the Milky Way GCs it is known that several structural parameters are correlated with galactocentric radius (Djorgovski and Meylan, 1994).

It can be seen that, compared with the Milky Way, there is a lack of very concentrated clusters in our sample. The group of clusters that can be seen in the Milky Way data to have concentration, c=2.5 is actually an artificial peak. All clusters in the Harris catalogue which have c$>$2.5 are set to this limit. These clusters are known as the core collapsed clusters. They have no clear core region (instead their density profiles continue to increase towards the center of the clusters). None of these core collapsed clusters are observed in our sample of M31 clusters. This can be partially explained by the exclusion of the innermost GCs (where most core collapsed GCs are located in the Milky Way). Taking this into account, we still find fewer of these clusters than expected. Potentially some faint core collapsed clusters may be missed by GC surveys as they would be the most difficult clusters to resolve. However, it is also possible that these clusters may be present, but have their concentrations underestimated. This is because their core radii will be much smaller than the PSF of our images, making it very hard to deconvolve and measure them. Comparison of the core radii of the clusters does show that we are missing, or overestimating, the core radii of some of the very smallest core radii clusters. A lack of core collapsed clusters can also be seen in similar profile fits to *HST* images of Cen A clusters (Jordán *et al.*, 2007b). Allowing for these effects, we see no strong evidence for differences between the structure of the old GCs in M31 and Milky Way.

In the Milky Way, it is known that some GC properties are related to position in the Galaxy. In figure 3.4 we plot the structural parameters of M31's GCs as a function of their projected galactocentric radius ($R_{\rm gcp}$: taken from the RBC). To help identify potential trends in these plots, we have binned the clusters into groups of 25 and determined the median value of their parameters for each group (bold points). It can be seen that the luminosity of the GCs appears to decrease slightly with $R_{\rm gcp}$. This is confirmed by a Spearman-rank test (run over the raw data) which suggests a significant correlation (with number of clusters, N=191, Spearman rank correlation coefficient, ρ_s=0.25 and P-value for non-correlation, P=5$\times$10^{-4}). How-

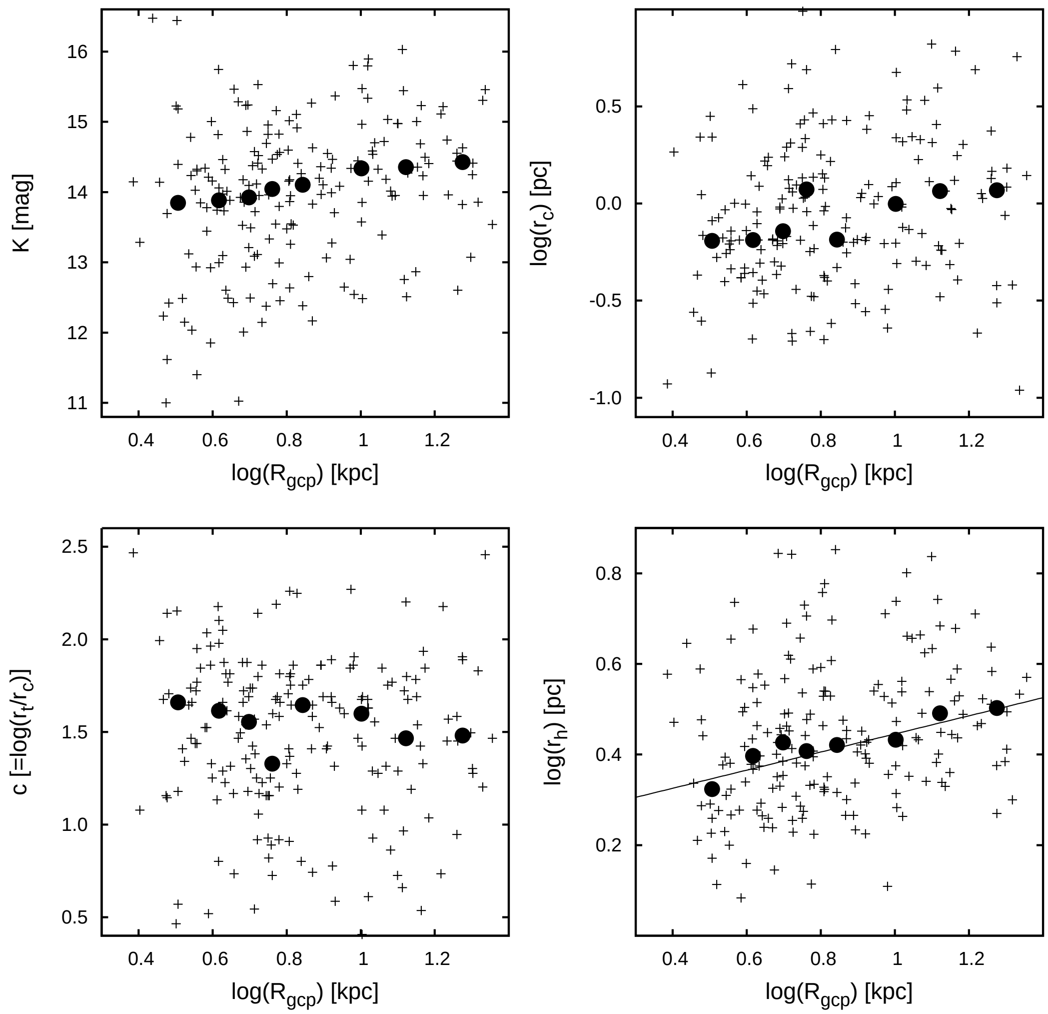

Figure 3.4: Properties of M31's GCs (crosses) as a function of projected distance to the centre of M31 (R_{gcp}). Bold points show the median values for clusters binned on R_{gcp}. The line demonstrates the relationship found by Barmby *et al.* (2007) between r_h and R_{gcp}.

ever, this correlation is mainly driven by a deficit of faint clusters in central regions. This is likely due to selection effects, as it is very difficult to identify fainter clusters projected against the dense central regions of M31. It is therefore likely that some of these clusters are missing from our catalogue. The most massive clusters also appear to be centrally located. Selection effects can not explain the lack of very massive clusters in the outer regions. However, there are few of these very bright clusters. These data also suggests that more central clusters have smaller cores (with N=191, ρ_s=0.20 and P=0.005). This relationship may be expected from the evolution of the GC system (because central GCs are expected to evolve more quickly due to greater interactions with their host galaxy). This effect is observed in the Milky Way's GCs (Djorgovski and Meylan, 1994). However, we again caution that this correlation may be artificially enhanced by selection effects (which could potentially prejudice us against the identification of extended, low density clusters in the inner regions).

The half light radius is found to be strongly correlated with $R_{\rm gcp}$ (with N=191, ρ_s=0.28 and P=1×10^{-4}). This correlation has previously been observed for a smaller number of GCs in M31, but over a greater range of $R_{\rm gcp}$ by Barmby *et al.* (2007). The line included in the bottom right panel of 3.4 is not a fit to our data, but the relationship found by Barmby *et al.* (2007):

$$log(r_h) = C + \gamma log(R^*_{\rm gcp}) \tag{3.1}$$

Where $C = 0.43$, $\gamma = 0.20$ and $R^*_{\rm gcp} = (11/92)R_{\rm gcp}$ for M31. Figure 3.4 demonstrates the excellent agreement between this relationship and that found here for a larger number of clusters. A similar trend is also found for GCs in the Milky Way (van den Bergh *et al.*, 1991; Djorgovski and Meylan, 1994) and in Virgo cluster galaxies (Jordán *et al.*, 2005). Unlike other cluster sizes, the half light radius of a cluster is thought to be largely unaffected by evolution (e.g. Spitzer Jr. and Thuan, 1972; Lightman and Shapiro, 1978; Murphy *et al.*, 1990; Aarseth and Heggie, 1998). Therefore this relationship may be related to the properties of the globular cluster system at the time of formation.

3.7 Summary

We present the structural parameters of 213 of M31's old clusters. We consider the reliability of these parameters and show our fitting to be self consistent by comparing the results obtained from fitting different images of the same cluster. Where available, the derived parameters are compared with those published from fits to higher spatial resolution *HST* images. While some scatter is seen in the derived parameters, we consider them to be relatively robust. However, we note that the errors on these parameters are hard to estimate and caution that the particular parameters of some individual GCs may have large errors. It is also found that the parameters obtained for the faintest clusters are relatively unreliable. We attribute this to the lower signal-to-noise of these clusters. Taking selection effects into account, we find the structure of M31's old cluster system to be similar to that of the Milky Way's. We note a potential lack of both core collapsed and very extended

GCs in our M31 sample. We caution that some (or all) of this effect may be due to selection effects in identifying these clusters, or difficulties in accurately measuring their parameters, rather than an intrinsic difference in the populations. We confirm the relationship previously observed in a smaller sample of M31 clusters, between the half light radius of a cluster and its distance from the centre of the galaxy. These data show no significant evidence for other trends with galactocentric radius.

4

Low mass X-ray binaries in M31 globular clusters

4.1 Abstract

We investigate low mass X-ray binaries (LMXBs) in the M31 globular cluster (GC) system using data from the 2XMMi catalogue. These X-ray data are based on all publicly available *XMM-Newton* observations of the galaxy. This survey therefore provides the most complete and homogeneous X-ray survey of M31's GCs to date, covering $>$ 80% of the confirmed old clusters in the galaxy. We associate 41 X-ray sources with confirmed old clusters in the M31 cluster catalogue of Peacock *et al.* (2010). Comparing these data with previous surveys of M31, it is found that three of these clusters are newly identified, including a bright transient source in the cluster B128. A further four clusters are found in the literature which are not detected in these data, resulting in a total catalogue of 45 clusters associated with X-ray emission. By considering the latest optical GC catalogues, we identify that three of the previously proposed X-ray clusters are likely to be background galaxies and two have stellar profiles. We consider the properties of LMXB-hosting clusters and demonstate a highly significant trend between the presence of an LMXB and

the mass and stellar collision rate of a cluster. A weaker trend is also confirmed between the metallicity and the presence of an LMXB. Considering the relationship between the luminosity and stellar collision rate of a cluster, we note that LMXB hosting clusters have higher than average stellar collision rates for their mass. This strongly suggests that the stellar collision rate is the dominant parameter related to the presence of LMXBs. This finding is consistent with the formation of LMXBs in GCs through dynamical interactions with little direct dependence on the neutron star retention fraction or cluster mass.

4.2 Introduction

Globular clusters (GCs) are known to be a rich source of low mass X-ray binaries (LMXBs). In early studies of the Milky Way's X-ray population, it was realised that many more LMXBs were located in GCs than would be expected based on their masses alone. Of the $\sim$150 bright LMXBs known in the Milky Way, 14 reside in 12 of its GCs (Liu *et al.*, 2001; Heinke and Budac, 2009). Since GCs contain only about 0.1% of the stars in the Galaxy but 10% of the LMXBs, this suggests that the formation of LMXBs is two orders of magnitude more efficient in GCs than in the field of the Galaxy. It has long been proposed that this extra efficiency is due to dynamical formation of these binaries in the dense cluster cores (Clark, 1975). The proposed mechanisms for dynamical formation of LMXB systems include: a donor star capturing the neutron star through tidal capture (e.g. Fabian *et al.*, 1975); exchange interactions between a neutron star and a primordial binary system (Hills and Day, 1976; Hut and Verbunt, 1983); and direct collisions of a neutron star with the envelope of a giant star (Verbunt and Hut, 1987). These interactions are more likely to occur in the cores of GCs due to their high stellar densities.

The properties of LMXB hosting clusters can be used to investigate the formation and evolution of these systems. For example, if dynamical formation is the primary method of forming LMXBs in GCs, then it is expected that there should be a direct relationship between the stellar collision rate in a cluster and the presence of an LMXB. Studies of LMXBs in the Milky Way's GCs are consistent with dynamical formation scenarios for these tight binaries (e.g. Verbunt and Hut, 1987; Pooley *et al.*, 2003). While work based on the Galactic GC system is very useful in investigating such relationships, it is limited to a relatively low number of GCs and LMXBs.

In the era of *Chandra* and *XMM-Newton* it has become possible to study many more GC LMXB systems by looking at extragalactic sources. These observations of nearby galaxies confirm that their GCs also contain a large fraction of the galaxies' LMXBs. Unfortunately, investigating dynamical formation in extragalactic clusters is difficult due to the small angular sizes of typical cluster cores. However, relationships between the collision rate and presence of LMXBs have been suggested in Cen A (Jordán *et al.*, 2007b) and possibly in M87 (Jordán *et al.*, 2004; Waters, 2007). It is also found, both in the Milky Way and nearby galaxies, that LMXBs favour brighter (and hence more massive) GCs (e.g. Kundu *et al.*, 2002; Sarazin *et al.*, 2003; Kim *et al.*, 2006; Kundu *et al.*, 2007). The likely reason for this is that higher mass clusters will generally have more stellar interactions and therefore form more LMXBs through dynamical interactions. However, it is also possible that LMXBs will favour high mass clusters because they may retain more of the neutron stars they produce. Neutron stars that are formed by core collapse may be formed with large kick velocities (e.g. Hobbs *et al.*, 2005). In this case, the higher escape velocities of high mass clusters, may result in more neutron stars being retained by these clusters. However, it is also possible that neutron stars with lower kick velocities can be formed via electron capture (e.g. Ivanova *et al.*, 2008).

Previous work on extragalactic LMXBs has also identified that metal rich clusters are more likely to host LMXBs than metal poor clusters (e.g. Bellazzini *et al.*, 1995; Kundu *et al.*, 2002, 2003). Several explanations for this have been proposed. Metal rich stars are likely to be physically larger, which may result in more LMXBs forming through tidal interactions and direct collisions (Bellazzini *et al.*, 1995). It was shown by (Maccarone *et al.*, 2004) that this effect alone is unlikely to explain the observed factor 3 enhancement of LMXBs in metal rich clusters. They propose that the irradiation induced winds in these binaries may explain the observed differences between metal rich and metal poor clusters. These winds are likely to be stronger in metal poor systems due to decreased line cooling. Ivanova (2006) suggested that the metallicity relationship is a natural consequence of the properties of $\sim$M$_{\odot}$ donor stars. In this mass range, they show that low metallicity stars lack an outer convective zone. This is likely to reduce the rate of tidal captures and also make it harder for a binary to tighten (and hence form an LMXB system).

In this study, we investigate LMXBs in M31's cluster system using archival *XMM-Newton* observations. For these clusters we are able to make use of the cluster properties presented in Peacock *et al.* (2009, 2010, see chapters 2 and 3 for details) to investigate the mass, colour and stellar collision rate of LMXB hosting clusters.

4.3 M31 globular clusters

The M31 GC system has been the focus of many studies. Despite this work, it is likely that some contamination and incompleteness currently exists in the M31 cluster catalogues (see chapter 2 for a discussion of the difficulties of investigating clusters in M31). To identify clusters in M31 we use the recent catalogue of Peacock *et al.* (2010) (hereafter P10; see chapter 2 for details). This catalogue includes all clusters and candidates identified in most major studies of the M31 GC system (including those of: Battistini *et al.*, 1987; Barmby *et al.*, 2000; Galleti *et al.*, 2004; Kim *et al.*, 2007; Caldwell *et al.*, 2009). It provides updated locations and classifications for all of these clusters. The locations of these clusters are found to be in good agreement with those of Caldwell *et al.* (2009), but are more accurate than those used previously to match with X-ray catalogues (e.g. Barmby *et al.*, 2000; Galleti *et al.*, 2004). The work of P10 and Caldwell *et al.* (2009) has also identified and removed significant contamination in the previous catalogues from stellar sources, background galaxies and young disk clusters.

M31 has been extensively surveyed by most recent X-ray observatories including: *Einstein* (e.g. Trinchieri and Fabbiano, 1991); *ROSAT* (e.g. Supper *et al.*, 1997, 2001); *XMM-Newton* (e.g. Shirey *et al.*, 2001; Trudolyubov and Priedhorsky, 2004) and *Chandra* (e.g. Kaaret, 2002; Williams *et al.*, 2004). Many of the resulting X-ray source catalogues have attempted to identify which sources are associated with GCs. Supper *et al.* (2001) associated 33 sources in their *ROSAT* survey with known GCs from the combined GC catalogues of Battistini *et al.* (1987), Battistini *et al.* (1993) and Magnier (1993). *Chandra* observations were used by Di Stefano *et al.* (2002), Kong *et al.* (2002), Kaaret (2002) and Williams *et al.* (2004) to identify 28, 25, 25 and 26 GC X-ray sources respectively. Currently the most complete M31 GC X-ray catalogue was produced by Trudolyubov and Priedhorsky (2004). They combined *XMM-Newton* observations along the disk of M31 with archived *Chandra* observations, to investigate 43 X-ray sources which they associated with GCs (from the GC catalogues of: Battistini *et al.*, 1987; Magnier, 1993; Barmby and Huchra, 2001; Galleti *et al.*, 2004). Most recently, Fan *et al.* (2005) collated the results of these previous studies to identify 54 unique GCs associated with X-ray sources.

In this study, we consider the X-ray properties of M31's GCs using all publicly available *XMM-Newton* observations of the galaxy. Since the study of Trudolyubov and Priedhorsky (2004), the *XMM-Newton* coverage of M31 has increased significantly and now covers the entire D_{25} ellipse of the galaxy. These data provide more accurate source locations than the *ROSAT* study of Supper *et al.* (2001) and cover many more clusters than the previous X-ray studies of M31 GCs (Di Stefano *et al.*, 2002; Trudolyubov and Priedhorsky, 2004). In this study we restrict our analysis to only those clusters classed as confirmed clusters in the recent optical catalogue of M31 GCs of P10. The previous GC X-ray associations have generally considered all cluster candidates in the galaxy. While the presence of an X-ray source in a cluster does increase the probability of it being a genuine cluster, the inclusion of such sources is also likely to increase contamination.

4.4 The X-ray population of M31's globular clusters

4.4.1 *XMM-Newton* observations of M31

Over the past decade, M31 has been the target of several *XMM-Newton* observations. The first 10 observations of M31 were obtained as part of the science verification of the telescope. These observations included five observations along the disk of the galaxy, four observations of the core of the galaxy and a shorter observation of the halo GC G1. These data are described by Trudolyubov and Priedhorsky (2004), who use it for their study of the galaxy's GCs. Since these initial observations, several other fields of the galaxy have been observed. These include: repeated observations of the X-ray sources RXJ20042.6+4115 (a bright Z-source in M31 Barnard, 2003) and the GC B375 (which hosts the brightest X-ray source in the galaxy's GC system; Kong, 2005); an observation of the dwarf galaxy NGC 205 (di Stefano, 2003); an observation on the minor axis of M31 (Bregman, 2005); and four observations to cover the recently discovered extended halo GCs in the galaxy (Tanvir, 2006). In addition to these observations a survey was recently completed to cover the entire D_{25} ellipse of the galaxy (e.g. Pietsch, 2008). All of these observations are summarised in table 4.1.

The initial observations along the disk of the galaxy, combined with these new observations covering the outer regions, provide a relatively homogeneous survey across the entire D_{25} ellipse of the galaxy. These observations, identified by the flag *survey*=y in table 4.1, provide the basis for our primary survey. It should be noted that, some of the LMXBs in M31's GCs are expected to be transient in nature. For this reason we also search for GC LMXBs in the other observations available. This allows us to identify as many LMXB hosting clusters as possible. However, it does bias the detection of transient LMXBs to regions which have been more frequently observed (such as the central region of the galaxy). We therefore flag in our final table whether the observed GC X-ray sources would have been identified in our

Table 4.1: XMM-Newton observations of M31

Obs. date	Target name	Rev no.	Obs. ID	RA (deg)	DEC (deg)	PN exp (s)	M1 exp (s)	survey
2000-06-25	M31Core	100	112570401	10.65	41.28	26.6	31.8	n
2000-12-28	M31Core	193	112570601	10.71	41.24	9.8	12.2	n
2001-01-11	G1	200	65770101	8.23	39.56	5.0	7.4	y
2001-06-29	M31Core	285	109270101	10.65	41.28	30.8	46.7	n
2002-01-05	M31North1	380	109270701	11.03	41.58	54.8	57.3	y
2002-01-06	M31Core	381	112570101	10.71	41.25	61.1	63.6	y
2002-01-12	M31South1	384	112570201	10.39	40.91	56.1	58.1	y
2002-01-24	M31South2	390	112570301	10.06	40.58	38.1	51.2	n
2002-01-26	M31North2	391	109270301	11.37	41.92	27.3	32.5	n
2002-06-29	M31North3	468	109270401	11.63	42.29	52.7	57.1	y
2003-02-06	M31-Halo1	579	151581101	8.44	39.51	8.0	9.7	n
2003-02-06	M31-Halo4	579	151580401	11.57	41.34	11.3	13.1	n
2003-07-01	M31-Halo2	652	151581201	10.77	39.82	1.6	3.1	n
2003-07-01	M31-Halo3	652	151581301	11.47	40.73	1.9	4.4	n
2004-01-02	NGC205	745	204790401	10.12	41.67	10.7	12.9	n
2004-07-16	RXJ0042.6+4115	843	202230201	10.63	41.28	18.3	19.5	n
2004-07-19	RXJ0042.6+4115	844	202230501	10.63	41.28	9.1	13.1	n
2004-07-19	RXJ0042.6+4115	844	202230401	10.63	41.28	14.3	18.5	n
2005-08-01	5C3.1	1034	300910201	10.44	40.37	8.7	3.1	n
2006-06-28	M31S3	1200	402560101	9.69	40.27	8.6	16.0	y
2006-07-01	M31SN1	1201	402560301	10.15	41.32	47.3	54.8	y
2006-07-01	M31SS1	1201	402560201	10.84	40.94	16.4	30.0	y
2006-07-03	M31nc2	1202	404060201	11.3	40.98	21.1	29.0	n
2006-07-08	M31SS2	1205	402560401	10.54	40.64	25.3	45.5	y
2006-07-08	Bo375	1205	403530201	11.41	41.68	0.0	5.3	n
2006-07-10	Bo375	1206	403530301	11.41	41.68	0.0	10.5	n
2006-07-12	Bo375	1207	403530401	11.41	41.68	0.0	9.9	n
2006-07-14	Bo375	1208	403530501	11.41	41.68	0.0	10.0	n
2006-07-16	Bo375	1209	403530601	11.41	41.68	0.0	12.7	n
2006-07-20	M31SN2	1211	402560501	9.89	40.99	52.9	58.6	y
2006-07-23	M31SN3	1212	402560701	9.73	40.64	25.1	56.1	y
2006-07-28	M31SS3	1215	402560601	10.16	40.36	31.9	37.8	y
2006-12-25	M31S2	1290	402560801	10.05	40.57	48.9	51.4	y
2006-12-26	M31NN1	1291	402560901	10.5	41.59	44.9	51.9	y
2006-12-30	M31NS1	1293	402561001	11.19	41.18	51.9	55.9	y
2007-01-01	M31NN2	1294	402561101	10.82	41.9	47.8	50.8	y
2007-01-01	M31NS2	1294	402561201	11.46	41.51	40.6	43.3	y
2007-01-03	M31NN3	1295	402561301	11.22	42.14	36.1	38.6	y
2007-01-03	M31NS3	1295	402561401	11.69	41.88	45.2	50.0	y
2007-01-05	M31N2	1296	402561501	11.36	41.92	43.7	46.2	y
2007-07-25	CXOM31J004059.2+41	1396	410582001	10.21	41.27	13.3	17.2	n

All *XMM-Newton* observations of M31 which are included in the 2XMMi catalogue. The coordinates indicate the approximate centre of each observation. The final column indicates whether the observation is considered part of our 'homogeneous' survey of M31 GCs.

primary dataset (which essentially gives a single epoch survey across M31).

It can be seen from table 4.1 that the exposure times for each field do vary slightly. The homogeneous detection limit across this survey is $\sim L_x = 10^{36}$ erg/s corresponding to the relatively short observation of G1. In total, the *XMM-Newton* observations considered here cover ∼82% of the confirmed old GCs from P10.

4.4.2 The 2XMMi catalogue

To identify sources in these observations we use the 'incremental second *XMM-Newton* serendipitous source catalogue' (2XMMi: for details see e.g. Watson *et al.*, 2009). This is a pipeline produced catalogue of sources which are identified in over

4000 publically available *XMM-Newton* observations [1]. The catalogue includes the location, flux and reliability of sources detected in all of the M31 observations listed in table 4.1.

4.4.3 M31 globular clusters in 2XMMi

The confirmed old, young and candidate clusters from P10 were matched to the 2XMMi catalogue using a matching radius of 2 arcsec+1 arcsec+$\sigma_{\rm pos,2XMMi}$. This matching radius was chosen to cover the errors in the optical cluster locations (conservatively estimated to be $<$2 arcsec, to account for systematic and centring errors for these extended sources) and systematic errors on the X-ray locations ($<$1 arcsec). This identified X-ray sources in 43 old clusters and 2 candidate clusters. No X-ray sources were identified in the young clusters listed in this catalogue.

We investigated chance associations between the clusters and X-ray sources by shifting the cluster locations by $\pm$5 arcsec. The four resulting cluster locations were matched to the X-ray sources using the same matching criteria. Only two associations were found from this, with a relatively large offset of >3 arcsec. We therefore do not believe that there is significant contamination from chance associations in the sample. Table 4.2 lists all old and candidate clusters associated with X-ray sources in the 2XMMi catalogue.

It can be seen that most clusters are well matched, with separations of $\leq$2 arcsec. However, three of the old clusters have relatively large separations of $\geq$3 arcsec and may be less reliable. These clusters are shown in figure 4.1. This shows *i* and K-band images of the clusters and their locations from the M31 cluster catalogue. The locations and error circles from the 2XMMi catalogue are marked in blue. It can be seen that all three sources are located outside of the quoted 1$\sigma_{\rm pos,2XMMi}$ error. Comparison with published *Chandra* observations (marked in figure 4.1 as blue crosses and discussed in the next section) confirms that two of these sources (B094 and B146) are associated with the clusters. This justifies the addition of a systematic error to the 2XMMi locations. The source associated with B094 (and the Chandra location) is slightly offset from the centre of the cluster. This does appear to align with an optical source on the edge of the cluster. LMXBs are expected to reside in the cores of the clusters (where the density is highest), it is therefore possible that this source is a chance alignment. However, given its proximity to the cluster, we keep this source in our analysis, but note that its association is relatively uncertain. It can be seen from this figure that the cluster B035 does not appear to be associated

[1]The catalogue was taken from http://xmmssc-www.star.le.ac.uk/Catalogue/2XMMi/

Table 4.2: M31 clusters in 2XMMi

GC NAME[1]	f^1_{P10}	SC_NAME	SC_RA	SC_DEC	SC_POS$_{err}$	SC_L$_x^2$	SC_L$_{x,err}$	SC_HR_1^3	SC_HR_2^3	SC_HR_3^3	SC_HR_4^3	SC_SUMFLG[4]	ΔPOS[5]	survey[6]
			deg	deg		10^{35}erg/s	10^{35}erg/s					arcsec	arcsec	
G001-MII	1	2XMM J003246.5+393440	8.194110	39.577931	1.22	17.8	4.6	0.36	0.28	-0.39	-0.83	0	0.61	y
B005-G052	1	2XMM J004020.1+404358	10.083819	40.732910	0.71	2528.7	26.5	0.57	0.33	-0.17	-0.30	3	2.19	y
B024-G082	1	2XMM J004111.7+414547	10.299454	41.763552	0.76	12.2	4.2	0.40	-0.00	-0.52	-0.16	1	0.53	y
B045-G108	1	2XMMi J004143.1+413419	10.429738	41.572200	0.35	2317.5	20.0	0.59	0.32	-0.14	-0.41	3	0.38	y
B050-G113	1	2XMMi J004146.3+413218	10.442963	41.538495	0.63	31.4	3.7	0.71	0.35	-0.10	-0.23	0	0.33	y
B055-G116	1	2XMM J004150.3+411211	10.459870	41.203495	0.44	26.0	2.8	0.83	0.75	0.03	-0.14	1	0.36	y
B058-G119	1	2XMM J004152.9+404708	10.470541	40.786082	0.79	15.7	4.0	0.43	-0.07	-0.27	0.29	1	0.82	y
MITA140	1	2XMM J004209.4+411744	10.539309	41.295845	0.27	82.3	2.8	0.87	0.49	-0.29	-0.52	1	0.88	y
B078-G140	1	2XMM J004212.0+411757	10.550226	41.299417	0.27	98.6	3.0	0.90	0.64	-0.19	-0.41	1	1.57	y
B082-G144	1	2XMM J004215.7+410114	10.565752	41.020601	0.21	2828.8	34.9	0.78	0.63	-0.02	-0.16	1	0.67	y
B086-G148	1	2XMM J004218.6+411401	10.577680	41.233678	0.22	672.0	6.6	0.48	0.35	-0.18	-0.39	1	0.78	y
B094-G156	1	2XMM J004224.9+405720	10.603903	40.955641	0.94	21.4	6.1	0.37	0.36	-0.23	-0.54	1	2.95	y
B096-G158	1	2XMM J004225.9+411914	10.608139	41.320638	0.25	106.2	2.6	0.80	0.45	-0.28	-0.51	0	1.36	y
B098	1	2XMM J004227.3+405936	10.613964	40.993580	1.01	16.3	6.1	0.47	0.13	-0.27	0.18	0	0.95	y
B107-G169	1	2XMM J004231.1+411938	10.629791	41.327346	0.24	231.6	3.6	0.65	0.37	-0.25	-0.46	0	1.26	y
B110-G172	1	2XMM J004233.0+410328	10.637729	41.057884	0.31	57.3	4.3	0.48	0.35	-0.35	-0.27	2	0.55	y
B117-G176	1	2XMMi J004234.3+405710	10.642969	40.952834	1.48	14.2	10.3	0.10	0.84	-0.19	-0.25	0	1.10	y
B116-G178	1	2XMMi J004234.5+413251	10.644032	41.547694	0.39	561.0	19.8	0.73	0.66	-0.02	-0.37	0	0.49	y
B123-G182	1	2XMM J004240.6+411033	10.669252	41.175928	0.44	14.0	1.4	0.70	0.26	-0.43	-0.16	2	0.44	y
B124-NB10	1	2XMM J004241.3+411524	10.672199	41.256867	0.42	49.1	3.4	0.59	0.06	-0.21	-0.59	3	1.40	y
B128-G187	1	2XMM J004247.6+411113	10.698577	41.187145	0.55	570.2	12.6	0.46	0.23	-0.23	-0.36	1	1.66	n
BH18	1	2XMM J004250.8+411032	10.711702	41.175787	1.31	6.0	2.1	0.62	0.81	-0.03	-0.31	0	1.21	y
B135-G192	1	2XMM J004251.9+413108	10.716459	41.519072	0.25	4775.9	45.9	0.69	0.50	-0.11	-0.34	3	0.48	y
B143-G198	1	2XMM J004259.5+411919	10.748114	41.322081	0.22	395.2	4.3	0.46	0.20	-0.30	-0.53	1	1.05	y
B144	1	2XMM J004259.8+411606	10.749205	41.268360	0.22	513.8	5.2	0.49	0.23	-0.19	-0.36	3	0.63	y
B091D-D058	1	2XMM J004301.4+413017	10.755850	41.504758	0.24	860.8	21.8	0.48	0.43	0.09	-0.11	2	0.40	y
B146	1	2XMM J004303.0+411525	10.762521	41.257129	0.22	421.3	4.4	0.48	0.18	-0.32	-0.48	3	3.17	y
B147-G199	1	2XMM J004303.2+412121	10.763346	41.355999	0.24	161.7	3.7	0.43	0.10	-0.39	-0.41	1	1.10	y
B148-G200	1	2XMM J004303.7+411805	10.765745	41.301462	0.23	303.2	4.2	0.44	0.21	-0.31	-0.38	3	0.95	y
B150-G203	1	2XMM J004307.3+412019	10.780786	41.338813	0.36	28.5	1.9	0.49	0.23	-0.28	-0.40	1	1.34	y
B153	1	2XMM J004310.5+411451	10.793951	41.247775	0.22	1176.8	8.0	0.47	0.21	-0.21	-0.36	3	0.94	y
B158-G213	1	2XMM J004314.3+410721	10.809660	41.122499	0.20	1381.5	14.7	0.43	0.42	0.19	-0.02	3	0.82	y
B159	1	2XMM J004314.4+412513	10.810355	41.420344	0.68	13.5	2.7	0.78	0.70	-0.36	-0.17	0	1.73	y
B161-G215	1	2XMM J004315.4+411125	10.814321	41.190373	0.43	16.2	2.1	0.47	0.04	-0.38	-0.34	0	0.48	y
B182-G233	1	2XMM J004336.6+410813	10.902912	41.136951	0.71	57.2	8.6	0.50	0.46	-0.18	-0.07	0	0.95	y
B185-G235	1	2XMM J004337.1+411443	10.905050	41.245554	0.19	867.1	9.5	0.50	0.27	-0.19	-0.25	1	0.90	y
B193-G244	1	2XMM J004345.4+413656	10.939501	41.615799	0.45	52.8	3.6	0.33	0.14	-0.16	-0.52	0	0.82	y
B204-G254	1	2XMM J004356.3+412203	10.985118	41.367648	0.41	62.5	6.6	0.37	0.25	-0.37	-0.25	0	0.64	y
B225-G280	1	2XMMi J004429.5+412136	11.123257	41.360027	0.36	1175.4	22.6	0.45	0.24	-0.26	-0.31	1	0.44	y
B375-G307	1	2XMMi J004545.4+413941	11.439532	41.661614	0.28	7013.5	40.2	0.56	0.35	-0.18	-0.46	3	0.94	y
B386-G322	1	2XMM J004626.9+420153	11.612469	42.031350	0.19	1573.8	18.5	0.54	0.27	-0.17	-0.27	3	0.24	y
[B035	1	2XMMi J004132.8+413830	10.386671	41.641724	0.58	14.2	2.0	0.47	0.12	-0.26	-0.79	0	3.36	y]
SK091C	2	2XMMi J004057.1+402155	10.238103	40.365344	1.54	5.7	2.2	0.77	-0.64	0.83	-0.28	0	1.86	y
SK182C	2	2XMMi J004527.2+413253	11.363430	41.548188	0.35	143.0	7.2	0.67	0.41	-0.22	-0.36	1	1.23	y

Top: Old GCs associated with an X-ray source in the 2XMMi catalogue. *Bottom:* candidate GCs associated with an X-ray source in the 2XMMi catalogue. Columns with an 'SC_' prefix are taken from the slim version of the 2XMMi catalogue.

[1]Cluster name and classification, as in table 2.1 and Peacock *et al.* (2010).

[2]X-ray Luminosity (0.2-12keV), assuming all sources to be at 780kpc (McConnachie *et al.*, 2005). [3]X-ray hardness ratios, as defined in section 4.4.3.

[4]Quality flag from the 2XMMi pipeline, as described in section 4.4.3.

[5]Offset between the optical and X-ray source locations.

[6]Indicates whether the source was detected in our 'primary survey' observations.

with the X-ray source. Another faint optical counterpart can be seen which is in good agreement with the X-ray source. We therefore believe that this may be a chance alignment with a non-cluster object and remove it from our analysis.

For each GC X-ray source, table 4.2 includes hardness ratios for the source and its total luminosity ($L_x, 0.2 - 12keV$). These data are taken from the 2XMMi 'slim' catalogue. This is a reduced version of the main catalogue and contains only unique sources. Many of these sources are expected to vary during the observations and some are located in more than one observation. For these sources, this catalogue quotes the mean locations and fluxes. The hardness ratios (HR) of a source are defined as:

$$\mathrm{HR}_i = \frac{(\mathrm{B}_{i+1} - \mathrm{B}_i)}{(\mathrm{B}_{i+1} + \mathrm{B}_i)} \tag{4.1}$$

Here, B_i are the narrow energy bands: B_1=0.2-0.5keV; B_2=0.5-1.0keV; B_3=1.0-2.0keV; B_4=2.0-4.5keV; B_5=4.5-12 keV. Table 4.2 also includes the summary flag (SC_SUMFLG) from the 2XMMi catalogue. This gives an indication of the reliability of the detection. The relevant flags (taken from Watson *et al.*, 2009) are:
0 = good
1 = source parameters may be affected
2 = possibly spurious
3 = located in a region where spurious detections may occur
It can be seen that many of the detections have non-zero warning flags. This is likely due to the crowded nature of M31, with most of the SC_SUMFLG=3 sources near the centre of M31. Watson *et al.* (2009) suggest that sources with flags 0-2 should be genuine, although sources with flags 1 or 2 have some of the automated spurious detection flags set. Class 3 sources are confirmed by 'manual' flagging. However, they have all of the 2XMMi automated detection flags set to spurious, and may be spurious detections. Of the 43 old clusters associated with X-ray sources, 13 have SC_SUMFLG=3. We note, from comparison with previous observations, that 10 of these 13 GCs have already been identified independently from *Chandra* observations. These sources are therefore unlikely to be spurious. The *XMM Newton* thumbnail images for all of the 2XMMi GC detections[2] were also visually examined to identify any artifacts (for example due to chip gaps). This examination suggested that the source in the cluster AU010 was unlikely to be reliable and we remove it from our catalogue.

[2]from http//www.ledas.ac.uk/data/2XMMi/

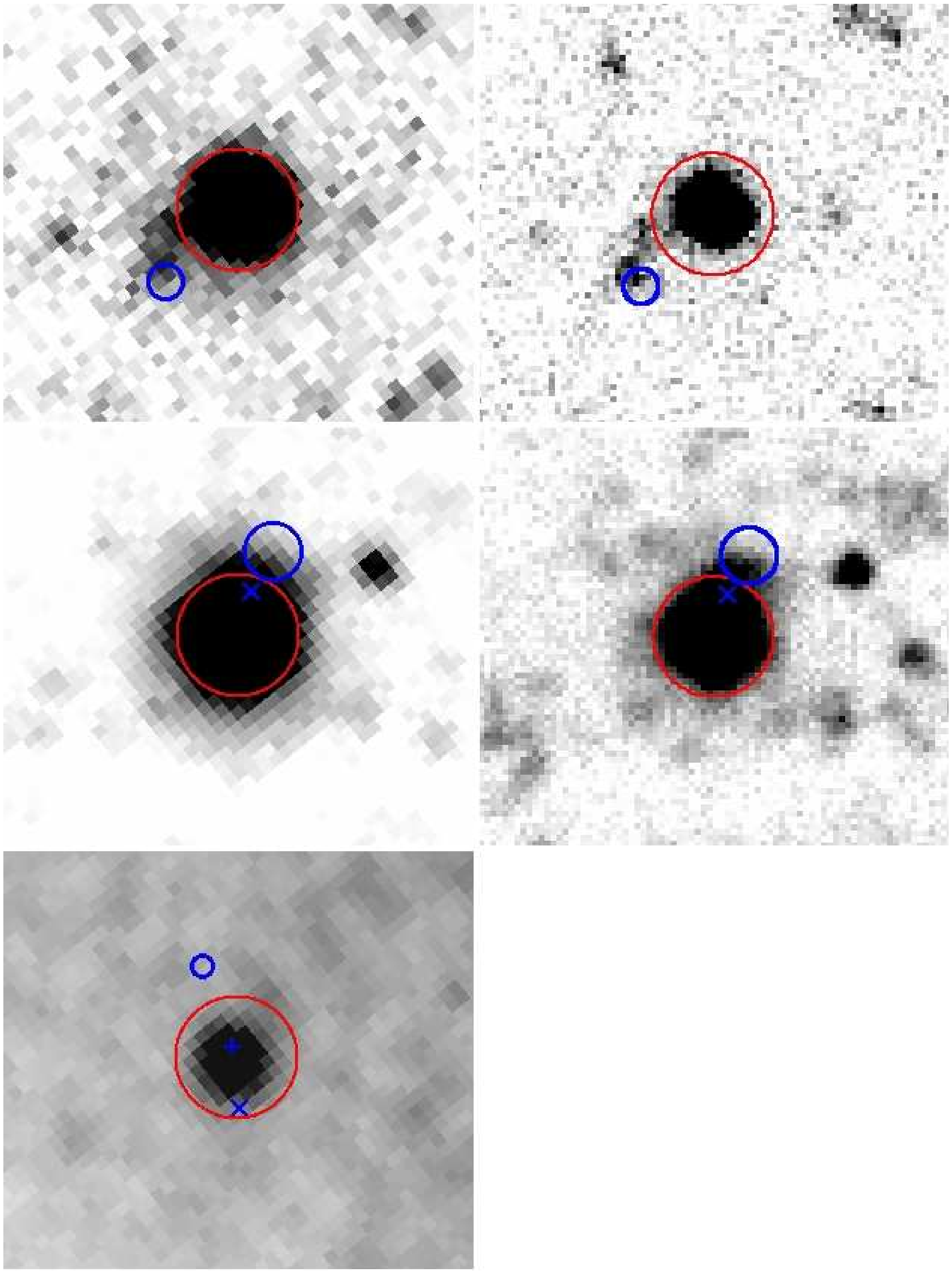

Figure 4.1: SDSS *i*-band (*left*) and WFCAM K-band (*right*) images of the GCs B035 (*top*), B094 (*middle*) and B146 (*bottom*, note that no K-band image is available for this cluster). The GC location from the catalogue of P10 is indicated by the red circles of radius 2 arcsec. The blue circle shows the XMM source location with its 1σ error. The Chandra positions from Di Stefano *et al.* (2002) (cross) and Williams *et al.* (2004) (plus) are shown where available.

4.4.4 Detections from previous catalogues

In addition to the *XMM-Newton* observations used here, other X-ray observations of M31 have associated X-ray sources with M31's GCs. This previous work is summarised in section 4.3. As discussed in chapter 1 (section 1.2.1), some LMXBs are expected to be transient nature, spending periods in quiescence. During these periods their X-ray emission will fall below our detection limit. It is therefore likely that some of the LMXBs in M31's clusters will only be detected at certain epochs. For this reason, we consider which clusters in table 4.2 were previously detected and identify any additional clusters with proposed X-ray emission.

All confirmed clusters were matched to sources identified from *ROSAT* observations by Supper *et al.* (2001), *Chandra* observations by Di Stefano *et al.* (2002); Kong *et al.* (2002); Kaaret (2002); Williams *et al.* (2004) and *XMM-Newton and Chandra* observations by Trudolyubov and Priedhorsky (2004). The cluster catalogue used in this study has more accurate locations, and some additional clusters, compared with those used in these previous studies. We therefore consider all X-ray sources in these previous catalogues. It can be seen that 38 of the clusters identified in the 2XMMi catalogue were identified previously by one of these studies, while three are newly identified. Table 4.3 lists all confirmed clusters which are associated with X-ray sources from the 2XMMi catalogue or these previous studies.

We identify four GC X-ray sources in the previous work which are not identified in the 2XMMi catalogue. The cluster B163 was previously detected by *ROSAT* and in one of the *Chandra* observations of it. This cluster is discussed by Trudolyubov and Priedhorsky (2004), where they demonstrate its transient nature. The cluster B213 was detected in a deep *ROSAT* HRI observation of the centre of M31 by Primini *et al.* (1993). The two other clusters, B164 and B293, were identified in the *ROSAT* PSPC survey of Supper *et al.* (2001). These sources have relatively large offsets from the cluster locations of 10.5 and 9.5 arcsec respectively. One of these sources is outside the region covered by the *XMM* observations. The other three have no 2XMMi counterparts within the X-ray positional error. Since these sources have no 2XMMi associations, they are likely to be transient in nature. These clusters are included in our catalogue of X-ray clusters. However, it should be noted that the larger size of the *ROSAT* positional error increases the probability of a chance association.

Table 4.3: All old clusters from P10 with proposed X-ray emission

GC NAME	$flag_{P10}$	RA	DEC	2XMMi		mixed	ROSAT		Chandra							
				(this study)	ΔPOS	T04/F05[1]	S01[2]	ΔPOS	D02[3]	ΔPOS	Ko02[4]	ΔPOS	Ka02[5]	ΔPOS	W04[6]	ΔPOS
				(0.2-12keV)		(mixed)	(0.1-2.0keV)	-	(0.3-7keV)	-	(0.3-7keV)	-	(0.1-10keV)	-	(0.3-7keV)	-
G001-MII	1	8.19389	39.57791	17.8	0.61	6	-	-	-	-	-	-	-	-	-	-
B005-G052	1	10.08462	40.73287	2528.7	2.19	1990	1127.3	1.82	-	-	-	-	-	-	1469.0	0.28
B024-G082	1	10.29938	41.76369	12.2	0.53		-	-	-	-	-	-	-	-	-	-
B045-G108	1	10.42961	41.57224	2317.5	0.38	450	1173.0	2.20	-	-	-	-	-	-	-	-
B050-G113	1	10.44285	41.53846	31.4	0.33		-	-	-	-	-	-	-	-	-	-
B055-G116	1	10.45994	41.20341	26.0	0.36	2.4-2.9	-	-	-	-	-	-	-	-	-	-
B058-G119	1	10.47083	40.78602	15.7	0.82	1-24	-	-	13.0	1.17	-	-	-	-	-	-
MITA140	1	10.53956	41.29600	82.3	0.88	40-114	-	-	117.0	1.92	83.0	0.52	55.0	1.33	62.0	0.50
B078-G140	1	10.55068	41.29969	98.6	1.57	24-300	-	-	26.0	2.63	101.0	0.68	25.0	0.54	108.0	0.27
B082-G144	1	10.56597	41.02069	2828.8	0.67	1735-2330	777.6	3.04	1197.0	0.61	-	-	838.0	1.48	747.0	0.37
B086-G148	1	10.57773	41.23389	672.0	0.78	498-763	409.3	7.87	469.0	2.66	456.0	0.59	247.0	0.12	430.0	0.42
B094-G156	1	10.60434	40.95489	21.4	2.95	19	26.0	5.44	17.0	1.47	-	-	-	-	-	-
B096-G158	1	10.60863	41.32072	106.2	1.36	28-174	-	-	74.0	1.00	93.0	0.91	45.0	0.42	114.0	0.85
B098	1	10.61408	40.99333	16.3	0.95	1-12	-	-	8.0	0.24	-	-	-	-	-	-
B107-G169	1	10.63022	41.32748	231.6	1.26	56-290	268.9	4.96	44.0	1.10	114.0	0.35	115.0	0.05	115.0	0.32
B110-G172	1	10.63793	41.05787	57.3	0.55	41-52	109.0	2.04	-	-	-	-	-	-	-	-
B117-G176	1	10.64321	40.95259	14.2	1.10	14	-	-	-	-	-	-	-	-	-	-
B116-G178	1	10.64390	41.54760	561.0	0.49	234	137.6	2.24	-	-	-	-	-	-	234.0	3.67
B123-G182	1	10.66941	41.17595	14.0	0.44	16-27	-	-	28.0	2.51	14.0	1.16	11.0	1.11	20.0	0.62
B124-NB10	1	10.67261	41.25663	49.1	1.40	34-137	-	-	11.0	1.89	25.0	0.11	39.0	0.15	35.0	0.54
B128-G187	1	10.69919	41.18718	570.2	1.66		-	-	-	-	-	-	-	-	-	-
BH18	1	10.71132	41.17596	6.0	1.21	3	-	-	5.0	1.47	5.0	0.20	-	-	-	-
B135-G192	1	10.71653	41.51895	4775.8	0.48	3093-4009	1519.2	1.51	-	-	-	-	1679.0	0.78	2125.0	0.52
B143-G198	1	10.74850	41.32206	395.2	1.05	152-555	298.4	6.20	279.0	1.49	315.0	0.45	259.0	0.11	364.0	0.29
B144	1	10.74942	41.26829	513.8	0.63	216-512	-	-	268.0	1.97	255.0	0.28	266.0	0.14	285.0	0.07
B091D-D058	1	10.75598	41.50481	860.8	0.40	553-692	166.4	4.71	-	-	-	-	225.0	2.32	-	-
B146	1	10.76212	41.25630	421.3	3.17	74-414	731.7	1.80	218.0	1.68	269.0	0.53	237.0	0.15	302.0	0.33
B147-G199	1	10.76375	41.35604	161.7	1.10	52-194	165.4	5.64	109.0	1.35	119.0	0.69	78.0	0.23	153.0	0.52
B148-G200	1	10.76607	41.30136	303.2	0.95	105-418	504.8	6.50	183.0	1.10	221.0	0.50	209.0	0.46	233.0	0.40
B150-G203	1	10.78128	41.33883	28.5	1.34	16-72	-	-	27.0	0.79	37.0	0.57	47.0	1.30	37.0	0.14
B153	1	10.79421	41.24760	1176.8	0.94	373-1248	701.8	4.48	843.0	1.37	832.0	0.65	506.0	0.22	943.0	0.34
B158-G213	1	10.80996	41.12253	1381.5	0.82	600-1880	251.6	5.54	91.0	4.89	197.0	4.39	366.0	0.31	483.0	0.73
B159	1	10.81099	41.42040	13.5	1.73	2	24.5	6.84	-	-	12.0	0.63	-	-	-	-
B161-G215	1	10.81421	41.19027	16.2	0.48	16-22	-	-	6.0	0.98	14.0	1.00	-	-	-	-
B182-G233	1	10.90280	41.13670	57.2	0.95	46	-	-	-	-	-	-	-	-	-	-
B185-G235	1	10.90534	41.24543	867.1	0.90	454-1981	418.1	6.74	183.0	1.56	425.0	0.49	364.0	1.95	350.0	0.29
B193-G244	1	10.93962	41.61601	52.8	0.82	44	153.8	4.89	-	-	-	-	-	-	42.0	1.50
B204-G254	1	10.98510	41.36747	62.5	0.64	37	105.3	2.52	-	-	-	-	-	-	-	-
B225-G280	1	11.12316	41.35993	1175.4	0.44	1130	650.3	1.80	-	-	-	-	-	-	-	-
B375-G307	1	11.43983	41.66175	7013.5	0.94	5148-10372	2936.4	5.59	2994.0	1.81	-	-	-	-	4967.0	0.89
B386-G322	1	11.61255	42.03132	1573.8	0.24	1496	822.2	3.89	-	-	-	-	-	-	-	-
B293-G011	1	9.08691	40.89363	-	-	5.1	13.3	9.54	-	-	-	-	-	-	-	-
B163-G217	1	10.82346	41.46252	-	-	1-1010	377.9	4.96	-	-	-	-	-	-	-	-
B164-V253	1	10.82553	41.20813	-	-	13	33.4	10.54	-	-	-	-	-	-	-	-
B213-G264	1	11.01463	41.51075	-	-	201	-	-	-	-	-	-	-	-	-	-

All old clusters in M31 with proposed X-ray associations. The position is the optical location of the cluster. For each X-ray catalogue considered, the source luminosity ($\times 10^{35}$ergs/s) and its offset from the cluster location are shown. In addition to the 2XMMi catalogue, we list matches to the catalogues of [1] (Trudolyubov and Priedhorsky, 2004)/(Fan *et al.*, 2005), [2] (Supper *et al.*, 2001), [3] (Di Stefano *et al.*, 2002), [4] (Kong *et al.*, 2002), [5] (Kaaret, 2002) and [6] (Williams *et al.*, 2004). It should be noted that some of the X-ray luminosities are in different bands.

Table 4.4: Candidate clusters and non-clusters with proposed X-ray emission

GC NAME	$flag_{P10}$	RA	DEC	2XMMi		mixed	ROSAT		Chandra							
				(this study)	ΔPOS	T04/F05[1]	S01[2]	ΔPOS	D02[3]	ΔPOS	Ko02[4]	ΔPOS	Ka02[5]	ΔPOS	W04[6]	ΔPOS
				(0.2-12keV)		(mixed)	(0.1-2.0keV)	-	(0.3-7keV)	-	(0.3-7keV)	-	(0.1-10keV)	-	(0.3-7keV)	-
SK091C	2	10.23810	40.36534	5.7	1.86	-	-	-	-	-	-	-	-	-	-	-
SK182C	2	11.36383	41.54835	143.0	1.23	15	39.5	12.91	-	-	-	-	-	-	-	-
NB63	2	10.63016	41.33662	-	-	5	-	-	-	-	5.0	3.55	-	-	-	-
BH16	2	10.69204	41.29333	-	-	9	-	-	31.0	1.41	9.0	0.43	-	-	-	-
B138	2	10.73165	41.30981	-	-	8-84	-	-	-	-	20.0	0.37	23.0	0.12	35.0	0.19
B007	4	10.10750	41.48667	72.5	16.05	71.5	187.4	20.4	-	-	-	-	-	-	-	-
B042D	4	10.52536	41.04669	62.4	0.40	31-73	42.4	8.29	85.0	0.18	-	-	-	-	42.0	0.69
B044D-V228	4	10.52963	41.00458	158.3	0.78	40-100	45.2	2.52	71.0	0.50	-	-	-	-	38.0	1.51
SK059A	5	10.79109	41.31692	14.4	0.47	212	615.3	4.17	-	-	74.0	0.33	212.0	0.47	70.0	0.96
B063D	6	10.64586	40.81090	155.0	0.46	154	85.4	5.80	-	-	-	-	-	-	154.0	1.25
SK119B	6	10.77379	41.26622	-	-	43	-	-	-	-	-	-	-	-	-	-
MIT311*	0	10.92917	41.48111	58.8	2.81	52	55.5	2.1	-	-	-	-	-	-	-	-
MIT380*	0	11.10667	41.60778	21.1	6.42	27	71.2	5.8	-	-	-	-	-	-	-	-
MIT16*	0	10.13500	40.55778	14.9	14.83	9.0	23.6	3.8	-	-	-	-	-	-	-	-
MIT317*	0	10.9525	41.46278	14.3	15.86		43.2	39.9	-	-	-	-	-	-	-	-
MIT165/166*	0	10.58167	41.36472	-	-	5	-	-	8.0	-	-	-	-	-	-	-

Candidate clusters (flag=2) and non-clusters associated with X-ray emission. Non-cluster sources include: background galaxies (flag=4); HII region (flag=5); stars (flag=6). Columns are as in table 4.3.

*These clusters are from the study of Magnier (1993) and are not listed in P10 (flag=0). The names and locations of these cluster candidates are taken from Supper *et al.* (2001) or Trudolyubov and Priedhorsky (2004).

4.4.5 Candidate clusters and other sources

As discussed in section 4.3, there has been significant work in classifying and studying the properties of M31's clusters since the previous X-ray cluster catalogue of Trudolyubov and Priedhorsky (2004). In this section, we therefore consider the current classifications of previously proposed clusters. Table 4.4 lists all X-ray sources associated with unconfirmed candidate clusters and previously proposed X-ray clusters which have subsequently been reclassified.

Of the 33 *ROSAT* sources associated with clusters by Supper *et al.* (2001), 26 are associated with confirmed old clusters from P10. Two of the sources are now known to be background galaxies (B007 and B042D) and one is an unconfirmed candidate cluster. The other four clusters are from the catalogue of Magnier (1993) and do not have new classifications from P10. We believe that these clusters are not confirmed through spectroscopy or high resolution imaging. We therefore consider them as candidate (rather than confirmed) clusters.

The study of Trudolyubov and Priedhorsky (2004) identified 43 X-ray clusters in M31, 37 of which are confirmed as old clusters by P10. Two of the clusters from P10 (B138 and SK100C) and two from Magnier (1993) (MIT165/166 and MIT133) are currently unconfirmed candidate clusters. The other two proposed GC X-ray sources in this catalogue are now thought to be background galaxies (B042D and B044D). We also note that these two galaxies, and an additional unconfirmed cluster (BH16), are included in the catalogue of M31 GC X-ray sources of Di Stefano *et al.* (2002). In addition to the GC X-ray sources in these catalogues, the collated work of Fan *et al.* (2005) identifies three other GC X-ray sources which are not listed as clusters the catalogue of P10. One of these, B063D, has been reclassified as stellar. This source is detected in these 2XMMi data and is associated with the object. This object may potentially be an unresolved background galaxy or possibly a foreground flare star. Another source (SK059A) has been reclassified as an HII region by Caldwell *et al.* (2009). This source represents an interesting object for follow up investigation to determine its true nature. Finally, the source “WSB85/S3-14” in Fan *et al.* (2005) is detected in these XMM data, but has no counterparts in P10. Examination of SDSS images of this cluster location shows no optical counterpart within the X-ray error circle. These images should detect the entire GC luminosity function at the distance of M31. We therefore believe that this source is unlikely to be associated with a cluster and exclude it from table 4.4.

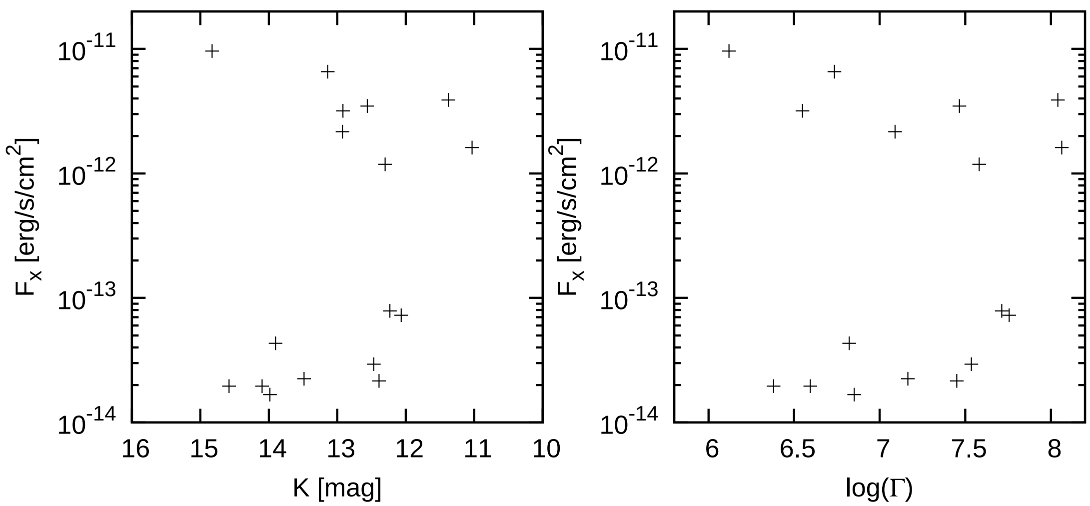

Figure 4.2: Flux of cluster X-ray sources as a function of the clusters luminosity (left) and stellar collision rate (right).

4.5 Population of LMXBs

We associate X-ray sources with $\sim 11\%$ of the old clusters in M31. In addition to these clusters, it is very likely that some clusters which host transient LMXBs, were not detected in these observations. It should also be noted, when considering M31's total cluster system, that there is likely to be significant incompleteness in the current catalogues; especially at the faint end of the GC luminosity function. However, the total fraction of clusters hosting LMXBs is consistent with that of the Milky Way.

It can be seen from table 4.2 that, compared with the Milky Way, a relatively large number of these LMXBs are very luminous, with $\sim 15\%$ having $L_x > 10^{38}$erg/s. However, it should be noted that the LMXB AC 211, in the Galactic GC M15, is an eclipsing (or near eclipsing) source. As such, a large fraction of its X-ray emission will be reprocessed to longer wavelengths. The intrinsic X-ray luminousity of this source is estimated to be $L_x \sim 10^{38}$erg/s (Naylor *et al.*, 1988). Given that there are only 12 LMXB hosting GCs in the Milky Way, it is possible that the lack of bright systems in the Milky Way may be related to the small sample, rather than a difference in the populations. We also note that LMXBs this bright are also observed in the field of the Milky Way and in other extragalactic GCs (e.g. Liu *et al.*, 2001; Kundu *et al.*, 2002). In principle multiple unresolved LMXBs in M31's GCs could explain the high luminosities of some of these LMXBs. It is likely that some of these clusters will host more than one LMXBs. For example, 2 of the 12 LMXB hosting clusters in the Milky Way are known to host 2 LMXBs in outburst (White and

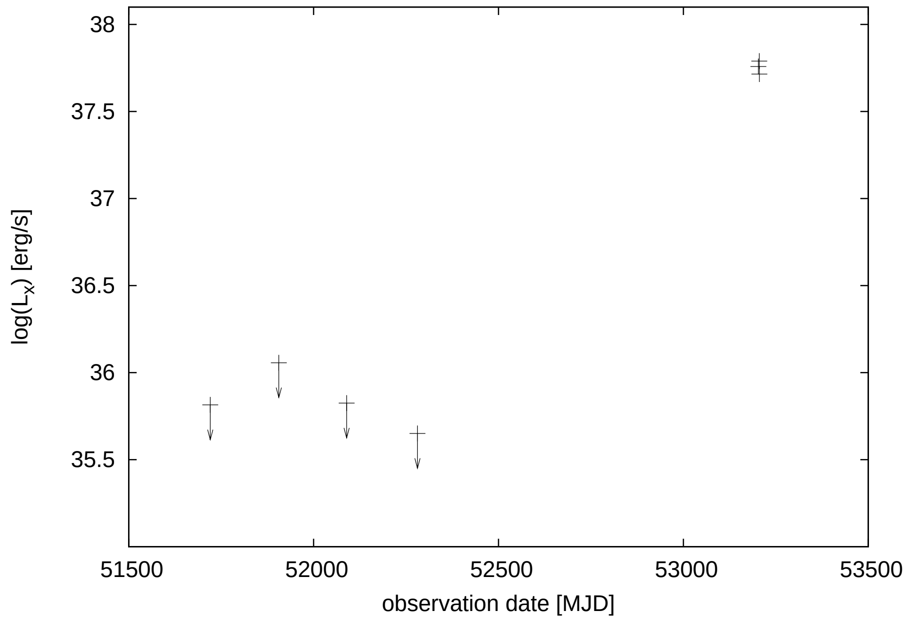

Figure 4.3: The transient X-ray source in B128.

Angelini, 2001; Heinke and Budac, 2009). However, variability observed in some of M31's LMXBs, suggests that one object is dominating the integrated luminosity. It can also be seen from figure 4.2 that we find no evidence of X-ray luminosity increasing as a function of the stellar collision rate or the mass of a cluster. Such a relationship might be expected if the number of LMXBs in a cluster is $\gg 1$. This is because the formation of LMXBs is known to be more efficient in these clusters (see section 4.6). This suggests that, for these data, the variability in the luminosity of individual LMXBs appears to dominate over the effects of multiple LMXBs.

Only one of the cluster X-ray sources detected in these observations would not have been detected in our primary survey observations. This cluster (B128) was observed, but not detected, in three previous *XMM Newton* observations of the 'core' of the galaxy. Figure 4.3 shows the observations of this cluster. The upper limits in this plot are taken from the FLIX[3] web tool and demonstrate that the source has increased in luminosity by over two orders of magnitude. This source demonstrates the benefit of re-observing clusters to identify LMXBs in outburst. In particular, elusive GC black hole LMXBs are likely to be transient in nature (e.g. King *et al.*, 1996).

To consider the spatial distribution of LMXB hosting clusters, we consider only those clusters covered by the observations selected as our primary survey. Of the 341 confirmed old clusters covered by these observations, 40 are associated with

[3]http://www.ledas.ac.uk/flix/flix.html

an X-ray sources from our 'primary survey'. It is found that the fraction of LMXB hosting clusters increases slightly towards the centre of the galaxy. However, it is also found that both the stellar collision rate and the metallicity of the clusters increase towards the centre of the galaxy. As shown in the next section, both of these parameters are expected to increase the formation of LMXB systems. Selection effects in the most central region of the galaxy also bias us against the detection of faint clusters (which are less likely to host LMXBs). As a result, this incompleteness may also result in such a relationship. For these reasons we believe these data do not provide evidence of a direct relationship between galactocentric radius and the production of LMXBs.

4.6 LMXB-GC relationships

The properties of LMXB hosting clusters provide a useful insight into the effect of these properties on the formation and evolution of LMXBs. Figure 4.4 shows the spectroscopic metallicities for all clusters with data collated by Fan *et al.* (2008) (from the studies of: Huchra *et al.*, 1991; Barmby *et al.*, 2000; Perrett *et al.*, 2002). These data cover $\sim$ 50% of the confirmed old clusters. The currently available spectroscopy for M31's clusters is heavily biased towards the more massive (brighter) clusters. However, LMXBs are known to reside primarily in more massive clusters, so this work provides metallicities for 72% of the LMXB hosting clusters. We also consider the (*i*-K) colour of these clusters from Peacock *et al.* (2010). These colours are dereddened using the values of Fan *et al.* (2008) and provide an alternative estimation of the metallicity of the clusters. It can be seen from figure 4.4 that LMXBs favour redder, metal rich clusters. A Kolmogorov-Smirnov (K-S) test between the colour of all clusters and the LMXB hosting clusters suggests that there is a 98% likelihood that these clusters are drawn from different populations. For the spectroscopic metallicities this probability is 91%. This relationship and its confidence is similar to that found in the previous work of Bellazzini *et al.* (1995) and Trudolyubov and Priedhorsky (2004). Despite the statistical significance of this relationship being relatively weak, it is consistent with the stronger relationship observed in elliptical galaxies (Kundu *et al.*, 2002; Kim *et al.*, 2006). There are several reasons why this relationship may be weaker in M31. Firstly, there are relatively few metal rich clusters in M31 compared with many early type galaxies. It should also be noted that the spectroscopic metallicities of M31's clusters have relatively large errors (with a mean error of $\sim$0.25 dex). The effect of this would be to

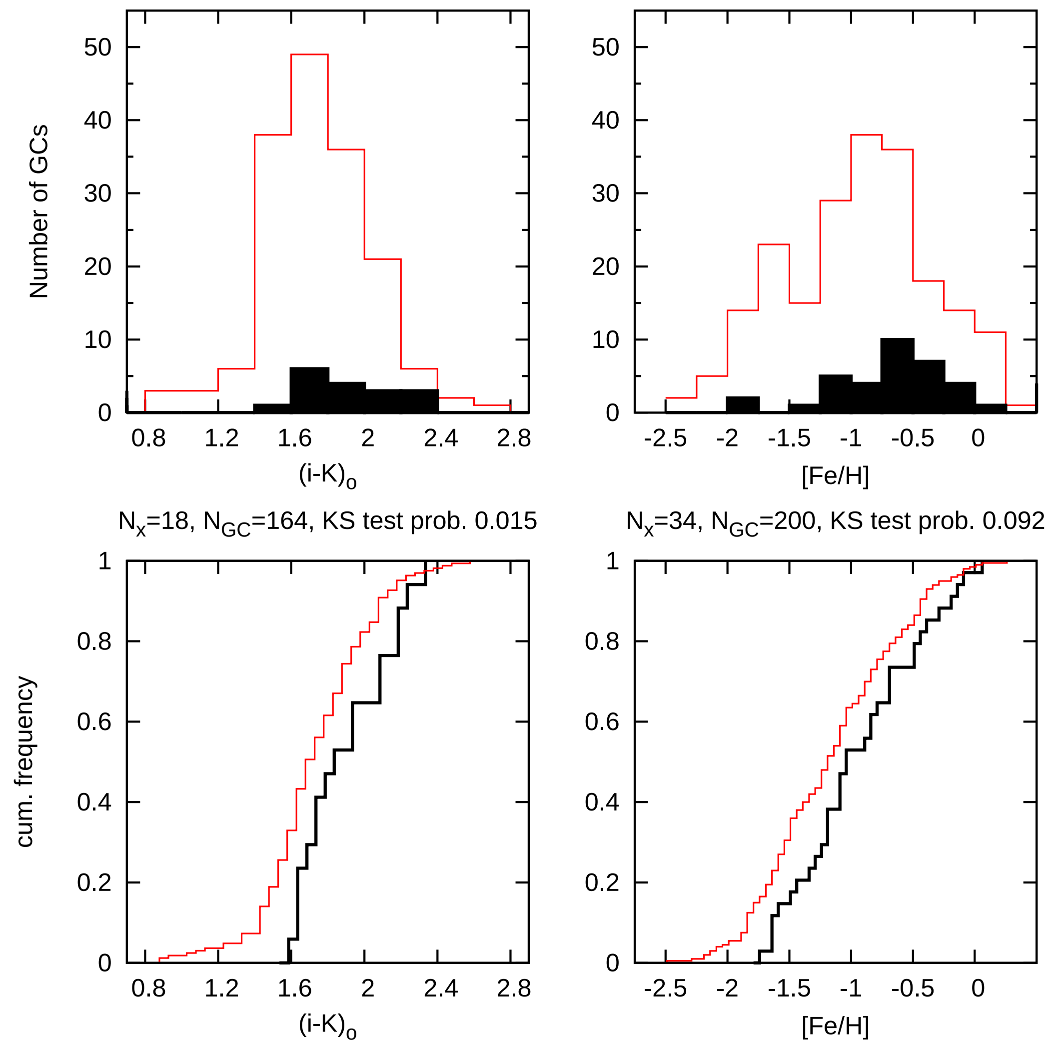

Figure 4.4: *(top)* The dereddened colour and metallicity for all clusters (open, red) and LMXB hosting clusters (solid, black). *(bottom)* the scaled cumulative frequency of the two populations. The cluster colours are taken from the catalogue of P10, while their spectroscopic metallicities taken from the collated table of Fan *et al.* (2008). It can be seen that the LMXBs tend to favour redder, higher metallicity, clusters.

weaken any genuine relationships between the clusters. In principle the colours of the clusters may give a more accurate measure of metallicity. However, the colours of M31's clusters are complicated due to variable extinction across the galaxy.

It has also been proposed that decreasing metallicity may lead to hardening of the soft X-ray emission from GC LMXBs (Irwin and Bregman, 1999; Maccarone *et al.*, 2004). In figure 4.5 we investigate this using the hardness ratios presented in table 4.2. It can be seen from this plot that there are no clear relationships between the parameters. A Spearman Rank test shows that the strongest correlation is for HR_2, which has a probability of correlation of 92%. To investigate any poten-

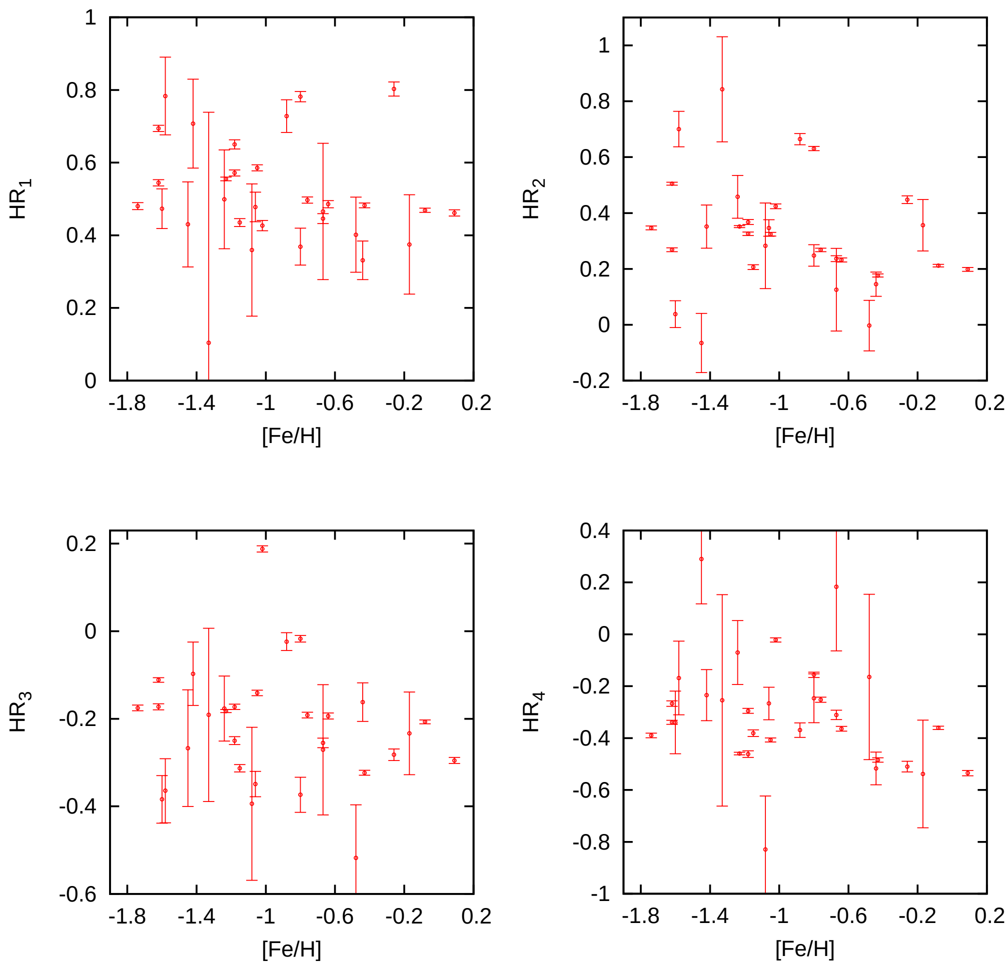

Figure 4.5: X-ray hardness as a function of cluster metallicity (hardness ratios are defined in section 4.4).

tial relationships further, we split these data into metal rich ($[Fe/H] > -0.7$) and metal poor clusters. The choice of this split is based on the bimodal peaks in the metallicity identified by Perrett *et al.* (2002). The fluxes of the X-ray sources, as functions of hardness ratio for the rich and poor clusters, are shown in figure 4.6. The only significant trend identified between the metal rich and poor clusters was in the HR_2 (0.5-1keV and 1-2keV). This relationship has a confidence of 99% but is based primarily on only 5 metal rich clusters. While significant, we do not see evidence for the relatively strong relationship observed in *ROSAT* observations of these clusters by Irwin and Bregman (1999). It is possible that this previous relationship may be due to the difficulty in modelling the soft excess emission due to M31 in these *ROSAT* data. This could potentially have a greater effect on the more centrally concentrated metal rich clusters.

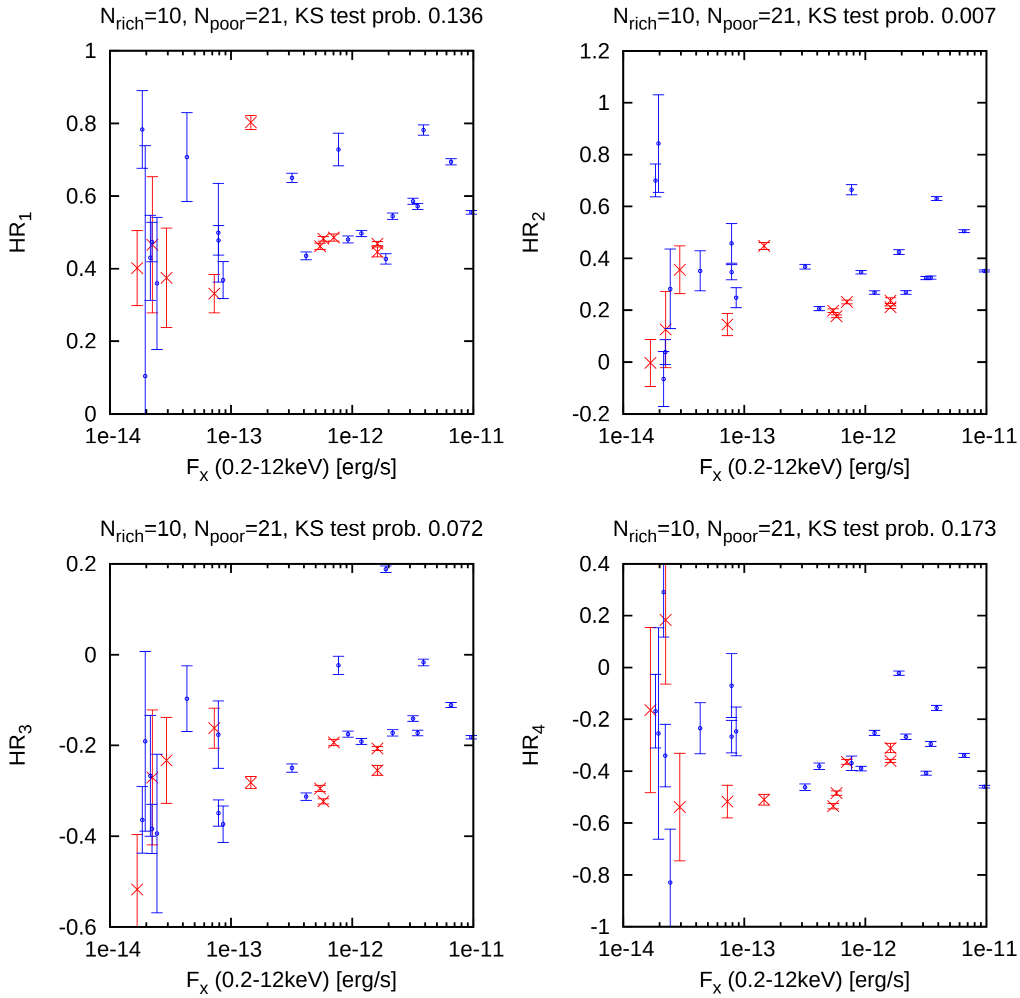

Figure 4.6: Hardness of a source as a function of its flux. Red points show metal rich clusters (with $[Fe/H] < -0.7$), while blue points indicate metal poor clusters. It can be seen, particularly in the HR_2 plot, that the metal rich clusters do appear to be softer. While there is found to be a significant difference in the HR_2 between these populations, it can be seen that there are relatively few metal rich clusters in our sample.

4.6.1 Stellar collision rate and mass

Using the stellar collision rates and K-band luminosities of these clusters presented in Peacock *et al.* (2009) (for details see chapter 3), we consider the effect of these parameters on the formation of LMXBs. Stellar collision rates are available for a spatially limited sample of 213 of M31's old clusters. Figure 4.7 shows the stellar collision rate and K-band luminosity of these clusters. It can be seen that the LMXBs are found to favour both brighter (and hence more massive) clusters and those with higher stellar collision rates. A K-S test demonstrates that these rela-

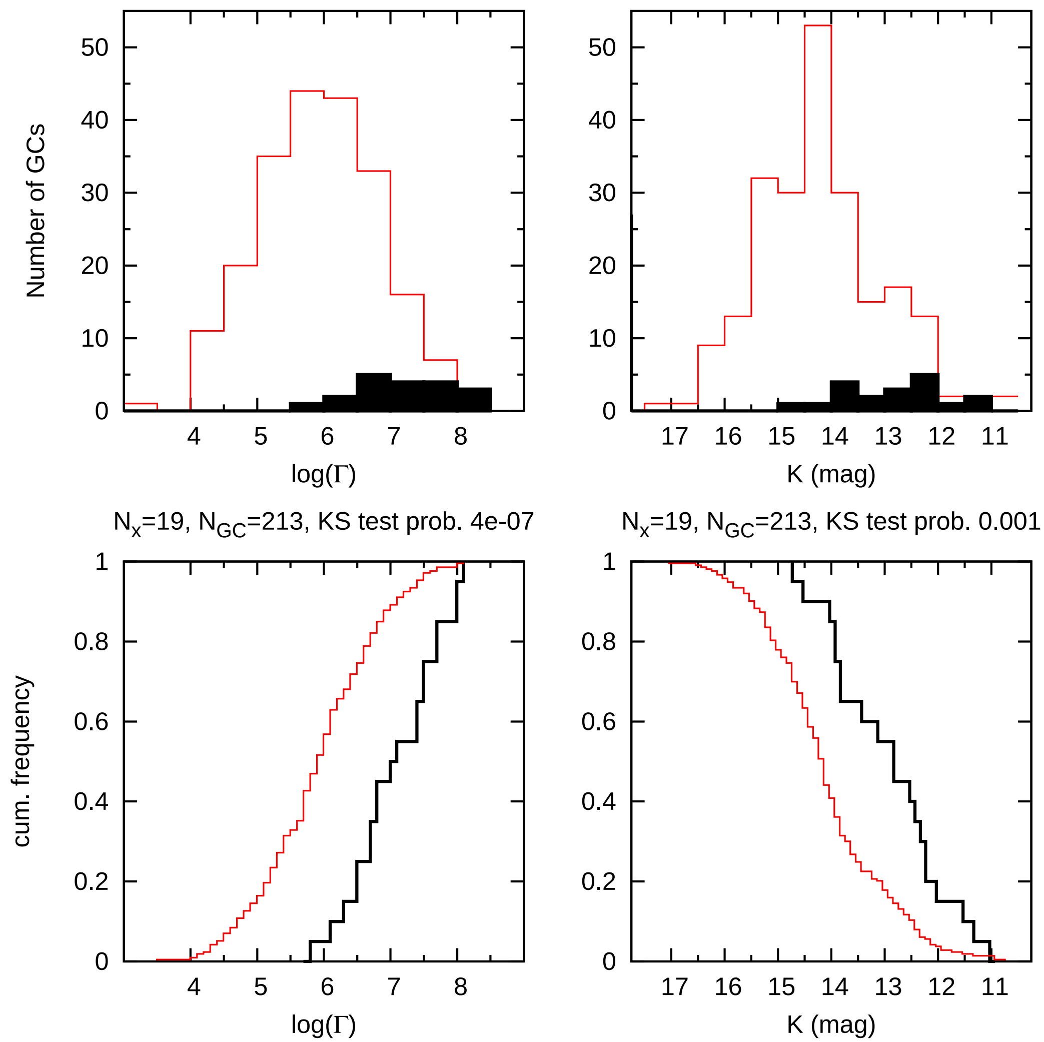

Figure 4.7: *(top)* The stellar collision rate and luminosity for all clusters (open, red) and LMXB hosting clusters (solid, black). *(bottom)* the scaled cumulative frequency of the two populations. The GC data are taken from the catalogue of P10. It can be seen that the LMXBs tend to favour brighter clusters with higher stellar collision rates.

tionships are highly significant with probabilities that they are drawn from the same population of 1×10^{-3} and 4×10^{-7} for luminosity and stellar collision rate, respectively. While still strongly significant, the mass relationship is slightly weaker than that found by Peacock *et al.* (2009). This is likely due to the new identification of several X-ray sources in fainter than average clusters. In this study, we also consider an updated cluster catalogue in which young clusters have been removed from our data (all of these young clusters are relatively faint and not associated with any X-ray sources). This confirms the result found previously, in M31 and other galaxies, that LMXBs are found preferentially in more massive clusters. However, from these data we are also able to demonstrate that the stellar collision rate of the

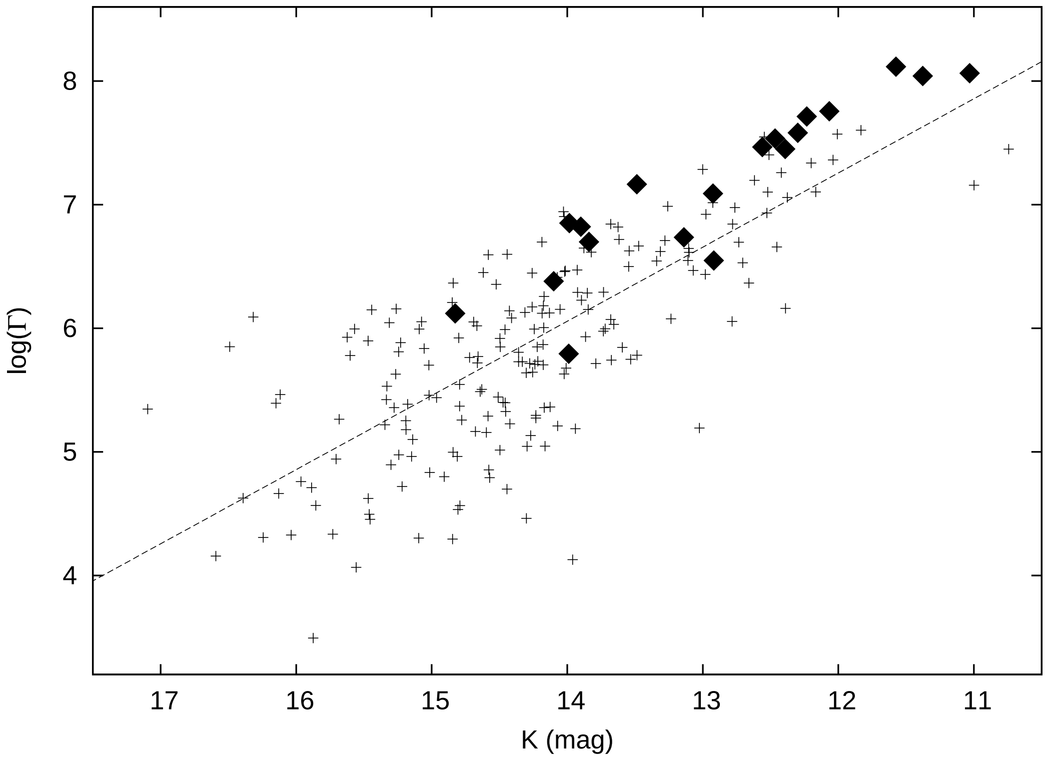

Figure 4.8: Stellar collision rate vs magnitude for all GCs (crosses) and LMXB hosting clusters (solid diamonds). This shows a clear relationship between the two parameters. This is in good agreement with the predicted relationship $\Gamma \propto M_{tot}^{1.5}$ (dashed line). The LMXB hosting clusters are found to have higher than average collision rates for their magnitude.

clusters is found to be the best discriminator in selecting LMXBs.

Figure 4.8 shows the stellar collision rate as a function of magnitude for all GCs studied (crosses) and those containing an LMXB (diamonds). It can be seen that there is a clear relationship between the luminosity of a GC and its stellar collision rate. In order to explore the relative effects of these parameters on LMXBs, we need to consider this relationship. Assuming a power law relationship between these parameters and a K-band mass (M) to light ratio of 1, we find that $\Gamma \propto M_{tot}^{1.53}$. This is consistent with the relationship found for the Milky Way's GCs and the theoretical approximation that $\Gamma \propto M_{tot}^{1.5}$ (Davies *et al.*, 2004).

It can be seen from figure 4.8 that the LMXB hosting clusters have higher than average collision rates for their mass. To investigate whether this is a statistically significant effect, we first detrend the data using the derived relationship between Γ and mass. We then run a K-S test between all GCs and the LMXB hosting GCs and find a probability of 10^{-4} that they are drawn from the same distribution. We note that there is some uncertainty in the actual relationship between Γ and mass due to the scatter in figure 4.8. To ensure our results are robust to errors in this relationship,

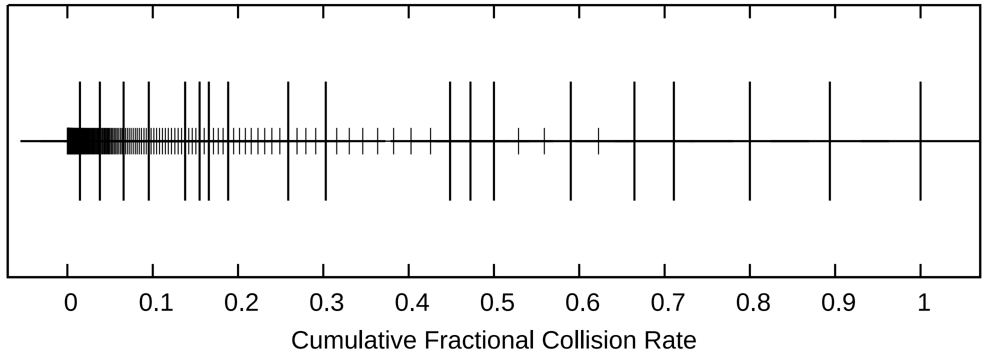

Figure 4.9: This shows the cumulative fractional collision rate for all GCs (small crosses) and LMXB hosting GCs (large crosses). If the formation of LMXBs is linearly proportional to GC collision rate, they should be evenly distributed along this plot.

we rerun the tests assuming $\Gamma \propto M_{tot}^{1.25,1.75}$. This results in probabilities of 10^{-5} and 10^{-3} respectively that they are from the same distribution. This demonstrates that, even for the steepest reasonable relationship, the LMXBs favour GCs with higher than average stellar collision rates for their mass. This result implies that the stellar collision rate is the primary parameter related to the presence of an LMXB. This is consistent with dynamical formation of these systems in clusters, with little direct influence from the mass (and hence escape velocity) of the cluster.

If these LMXBs are formed by dynamical formation, then their formation should be directly proportional to this stellar collision rate. To investigate this, we follow the method of Verbunt and Hut (1987). First we divide all cluster collision rates by the total collision rate of all of the clusters considered. We then sort the clusters by this fractional collision rate and find the cumulative value for each cluster, such that the cluster values run from 0 to 1. The result of this is that the total collisions occurring in the GC system should now be evenly distributed between 0 and 1 (i.e. we expect 10% of the total collisions to occur in clusters with values in the range 0-0.1). In this way, if the formation of LMXBs is linearly proportional to collision rate, their host clusters should be evenly spaced in this plot. It can be seen from figure 4.9 that the LMXB hosting clusters (large crosses) are consistent with this. The data do suggest a slight excess of LMXB hosting clusters in low collision rate clusters. However, a K-S test (run between these data and a linear relationship) suggests that this is not very significant (with a null hypothesis probability of 12%).

4.7 Conclusions

We associate LMXBs with 41 of M31's confirmed old clusters using the 2XMMi catalogue. In addition to these clusters, we identify four other clusters in the literature which have previously been proposed to host LMXBs. Three of these clusters are newly identified and for two other clusters, which were previously identified only in *ROSAT* observations, we confirm their association with the proposed clusters. By using updated optical catalogues of M31's clusters, we show that three of the previously proposed LMXB hosting clusters are now known to be background galaxies.

LMXBs are identified in $\sim 11\%$ of the clusters surveyed. It is likely that the true fraction of LMXB hosting clusters is lower than this because of incompleteness in the current M31 GC catalogues. We confirm the previously identified result that M31's GCs contain many more very bright LMXBs than the Milky Way's GCs. This result is likely due to the small number of GC LMXBs in the Milky Way, rather than a difference in the LMXB population.

By considering the properties of GCs which host LMXBs, the previously proposed relationship between the metallicity of M31's clusters and the presence of an LMXB is identified. This relationship is weaker than, but consistent with, that found in early type galaxies. Our data suggest some evidence for the proposed relationship between metallicity and the hardness ratio of the observed X-ray emission, but this is relatively weak compared with the previously proposed trend.

We show highly significant relationships between the presence of an LMXB and both the stellar collision rate and mass of its host GC. The stellar collision rate is found to be the best discriminator in selecting LMXB hosting GCs. We suggest that the weaker relationship between mass and LMXB presence may be primarily due to the relationship between mass and stellar collision rate. Our results demonstrate that the stellar collision rate is likely to be a fundamental parameter related to the formation of LMXBs. This result is in agreement with previous studies of GCs in the Milky Way and Cen A. The linear relationship found between the presence of an LMXB and the stellar collision rate is in good agreement with the systems being formed by dynamical interactions. This also suggests that the current dynamical properties of the GCs are related to their current LMXB populations.

5

The ultraviolet colour of globular clusters in M31: a core density effect on the formation of extreme horizontal branch stars?

5.1 Abstract

We investigate the effect of cluster core density on the far-ultraviolet (FUV) and near-ultraviolet (NUV) emission from M31's GCs. Published FUV-NUV colours from *Galaxy Evolution and Explorer (GALEX)* observations of these clusters are used as a probe into the temperature of the horizontal branch (HB) stars in these clusters. From these data, we demonstrate a significant relationship between the core density of a cluster and its FUV-NUV colour, with dense clusters having bluer ultraviolet colours. These results are consistent with a population of (FUV bright) extreme-HB (EHB) stars, the production of which is related to the stellar density in the clusters. Such a relationship may be expected if the formation of EHB stars is enhanced in dense clusters due to dynamical interactions. We caution that, while

potentially important, this result is based on a relatively low number of clusters. Further investigation of this effect would benefit from deeper ultraviolet data, more spectroscopic metallicity measurements and more reddening estimates for the clusters. We also consider the contribution of low mass X-ray binaries (LMXBs) to the integrated FUV luminosity of a cluster. We note that two of the three metal rich clusters, identified by Rey *et al.* (2007) as having a FUV excess, are known to host LMXBs in outburst. Considering the FUV luminosity of Galactic LMXBs, we suggest that a single LMXB is unlikely to produce more than 10% of the observed FUV luminosities of these clusters.

5.2 Introduction

Horizontal branch (HB) stars are core helium-burning stars that have evolved off the red giant branch (RGB). In globular clusters (GCs) they are so named because of their appearance on optical colour-magnitude diagrams, where they trace a horizontal path blueward of the RGB. These stars are thought to have similar core masses of $\sim 0.5 M_{\odot}$. Their location along the HB is therefore determined primarily by the mass and opacity of their thin stellar envelopes. To explain the observed HB stars in GCs, it is thought that substantial mass loss must occur during a star's RGB phase (e.g. Rood, 1973). The HB morphologies of different Galactic GCs are known to vary significantly. This suggests that the cluster environment has a significant effect on the evolution of stars onto the HB. The metallicity of a GC has long been proposed as the 'first parameter' related to the morphology of a GCs HB, with metal poor clusters often having bluer HB stars than metal rich GCs (e.g. Sandage and Wallerstein, 1960; Dorman *et al.*, 1995). The likely reason for this is that, for a given envelope mass, metal rich stars will have cooler envelopes because of their higher opacity. However, the metallicity of a cluster alone is insufficient to explain the HB morphology in all Galactic GCs. Firstly, the clusters which host the bluest HBs actually have intermediate metallicities (e.g. O'Connell, 1999). Also, some clusters are observed to have very different HB morphologies, but similar metallicities (e.g. NGC 288 and NGC 362: Bellazzini *et al.*, 2001). This has led to the notorious search for a 'second parameter' to describe HB morphology. Many different parameters have been proposed as a second parameter, all of which may play some role. These include a cluster's age, its helium abundance, the stellar core rotation, mass loss on the RGB and cluster core density (for a discussion of proposed second parameters, see e.g. Fusi Pecci and Bellazzini, 1997; Catelan, 2009). Despite decades of reseach, the relative effects of these different parameters are yet to be fully understood.

The bluest HB stars observed in GCs are the ‘blue tail’ or ‘extreme-HB’ (EHB) stars. These are analogues to the subdwarf B (sdB) stars observed in the Galactic field and are considered here to be those stars with T_{eff} >20,000K (Brown *et al.*, 2001). These stars have become increasingly important as the leading contenders in explaining the ‘ultraviolet excess’ (UVX) observed in elliptical galaxies (e.g. Code, 1969; Dorman *et al.*, 1995; O’Connell, 1999). Because of their high effective temperatures, they make an important contribution to the FUV emission from old stellar populations, often dominating the emission. EHB stars are observed in both metal rich and metal poor clusters (e.g. D’Cruz *et al.*, 1996; Rich *et al.*, 1997) and it is likely that the metallicity may have little direct effect on the formation of these stars (e.g. Heber *et al.*, 1986; Dorman *et al.*, 1993; O’Connell, 1999). Due to their very low envelope masses ($\lesssim 0.02 M_{\odot}$; Heber *et al.*, 1986), it is likely that their formation is more strongly related to the efficiency of mass loss mechanisms than the metallicity.

In this study, we investigate the effect of a cluster’s core density on its HB population. A relationship has previously been proposed between core density and the extent of the HB population in the Milky Way’s GCs (Fusi Pecci *et al.*, 1993; Buonanno *et al.*, 1997). There are several reasons to suspect that dense stellar environments will enhance the formation of EHB stars. Firstly, mass loss may be enhanced through tidal interactions in dense stellar encounters. Close encounters may also increase mixing in RGB stars and lead to helium enrichment, which will make the HB stars bluer (Suda *et al.*, 2007). It has also been proposed that EHB stars may be formed in binary systems either via white dwarf-white dwarf mergers or from mass loss through either Roche lobe overflow or common envelope mechanisms (Han *et al.*, 2002, 2003, 2007). This theory is supported by observations of Galactic subdwarf B (sdB) stars, a large fraction of which are found to be binary systems (e.g. Maxted *et al.*, 2001; Reed and Stiening, 2004). Interestingly, current observations suggest that the binary fraction among EHB stars may be much lower in GCs (Moni Bidin *et al.*, 2009). This may be due to the relative contributions of different formation mechanisms evolving with time, with white dwarf-white dwarf mergers becoming increasingly import for old stellar populations, such as GCs (Moni Bidin *et al.*, 2008; Han, 2008). If EHB stars do have a binary origin, then a relationship between the core density of a cluster and the population of EHB stars it hosts may be expected. This is because of dynamical formation of these binary systems in the cores of these clusters.

Only a few of M31's GCs have colour magnitude diagrams which allow direct observation of their HB stars, and these are generally incomplete (e.g. Rich *et al.*, 2005). Even in the Milky Way, measuring all the HB stars in a cluster, particularly EHB stars, from optical colour-magnitude diagrams is complicated due to the large bolometric correction for these very hot stars. In the absence of direct stellar counts, we consider the integrated far-ultraviolet (FUV) and near-ultraviolet (NUV) colours of M31's clusters. This photometry provides an indirect probe of the hot stellar populations in these GCs. Main sequence and RGB stars are too cool to have significant emission at these wavelengths and a cluster's FUV and NUV luminosity are likely to be dominated by objects brighter than ∼10,000K. If a cluster hosts a population of blue-HB or EHB stars, then these will likely dominate the cluster luminosity at these wavelengths. In the Milky Way, the FUV-V colour is found to correlate with the HB morphology of the cluster (e.g. fig. 3 of Catelan, 2009).

Recent *GALEX* FUV and NUV observations of M31 have been presented by Rey *et al.* (2005, 2007). They use this FUV-V colour as an indicator of the HB morphology of some of M31's GCs. In this work, the expected relationship between the clusters metallicity and both its FUV-V and NUV-V colour were shown. However, there is significant scatter in the FUV relationship. This confirms the need for a second parameter to describe the FUV luminosity of clusters in M31. Rey *et al.* (2007) also identify three metal rich clusters which have a FUV excess, compared with both stellar models and other metal rich clusters in the galaxy. To help explain their observations, they consider the effects of age and helium abundance on the FUV luminosities of M31's GCs. Helium abundance is also used by Sohn *et al.* (2006) and Kaviraj *et al.* (2007) to explain the FUV observations of M87's GCs. In this study, we consider correlations between the core density of a GC and its FUV properties.

5.3 M31 globular cluster data

In the following analysis, we use data from the recent catalogue of the M31's GCs from Peacock *et al.* (2010). This catalogue (described in chapter 2) provides updated classifications, *ugriz* and K-band photometry and structural parameters for objects in the Revised Bologna Catalogue of GCs in M31 (RBC: Galleti *et al.*, 2004). We use this catalogue to identify confirmed old clusters in the galaxy. This identifies 416 old clusters, of which a spatially limited sample of 213 clusters have estimates of their structural parameters. As the primary aim of this work is to investigate the effect of stellar density on the UV properties of the clusters, we restrict our sample to those clusters with structural parameters. We note that this should represent a relatively unbiased sample.

We combine this catalogue with the spectroscopic metallicities collated by Fan *et al.* (2008) from the studies of Huchra *et al.* (1991); Barmby *et al.* (2000); Perrett *et al.* (2002). Where these metallicities are available from more than one study, the values from the larger catalogue of Perrett *et al.* (2002) are chosen over Barmby *et al.* (2000). We reject the cluster B235 because of a large discrepancy (0.6 dex) between the metallicities available from Barmby *et al.* (2000) and Perrett *et al.* (2002). We also remove those clusters with large errors ($>$0.6 dex) on their metallicities (this removes the clusters B214, B229, B352 and BA11 from our analysis). This gives spectroscopically estimated metallicities for 219/416 confirmed old GCs in our catalogue. Fan *et al.* (2008) also present reddening estimates for these clusters based on this spectroscopy and on photometry from the RBC. We use these estimates of $E(B-V)$ to deredden our photometry using the extinction curves of Cardelli *et al.* (1989). The relative extinction in the different bands were evaluated from these curves by Schlegel *et al.* (1998) (for the *ugriz* filters) and by Rey *et al.* (2007) (for the *GALEX* FUV, R_{FUV}=8.16 and NUV, R_{NUV}=8.90). These values are relatively uncertain. This is because the reddening curve in the UV is known to vary along different lines of sight in the Milky Way. It is also not guaranteed that M31 has the same extinction curve as the Milky Way, although Barmby *et al.* (2000) found no evidence of significant differences in the optical bands. To minimise the effects of this on our UV colours, we limit our analysis to the clusters with relatively low extinction ($E(B-V)$ $<$0.16, consistent with the limit adopted by Rey *et al.*, 2007).

The FUV and NUV magnitudes of these clusters are taken from Rey *et al.* (2005, 2007). These data provide integrated FUV and NUV magnitudes for 104 and 210 of the 416 confirmed old clusters in Peacock *et al.* (2010). For full details of these UV observations, we refer the reader to Rey *et al.* (2005, 2007). The *GALEX* FUV (1344-1786Å) and NUV (1771-2831Å) filters have effective wavelengths of 1528Å and 2271Å respectively (Morrissey *et al.*, 2005). The photometry is on the standard *GALEX* ABmag photometric system, where:

$$\mathrm{FUV_{AB}} = -2.5 \times \log_{10}(\mathrm{F_{FUV}}/1.40 \times 10^{-15}) + 18.82 \tag{5.1}$$

$$\mathrm{NUV_{AB}} = -2.5 \times \log_{10}(\mathrm{F_{NUV}}/2.06 \times 10^{-16}) + 20.08 \tag{5.2}$$

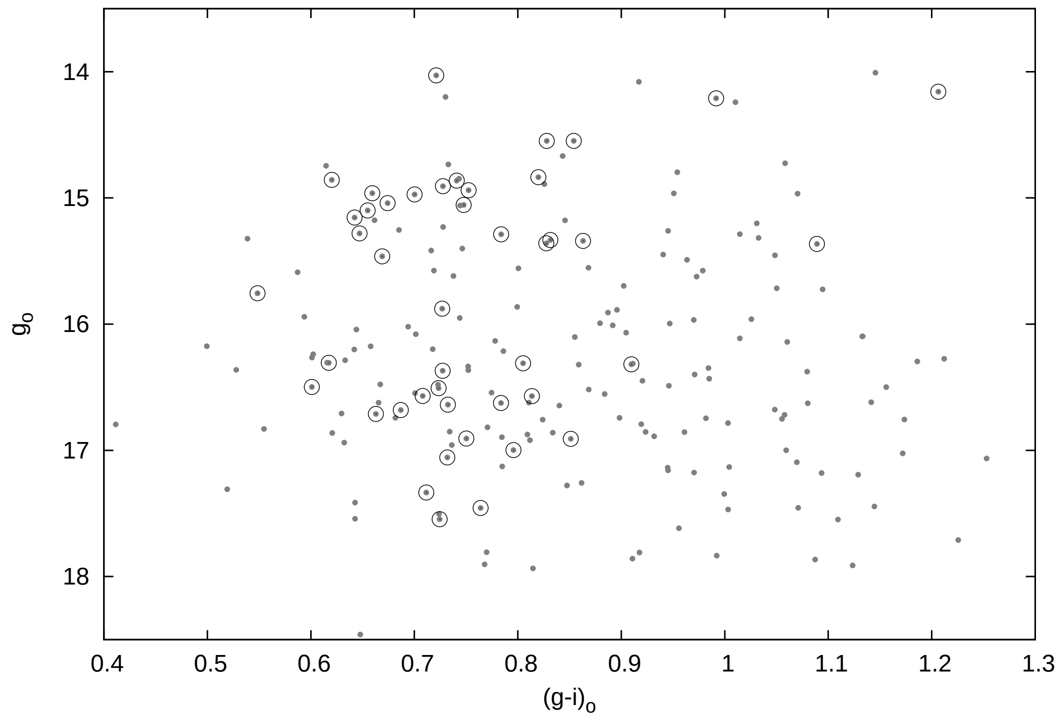

Figure 5.1: Optical colour magnitude diagram for all M31 GCs with data from Peacock *et al.* (2010) and E(B-V)<0.16 from Fan *et al.* (2008). Small grey points indicate all GCs, while open black circles indicate those clusters detected in the *GALEX* FUV observations.

Here, F is the flux of the source (erg sec^{-1}cm^{-2}Å^{-1}). The sample of clusters is magnitude limited to $\sim$22.5 in both the FUV and NUV. As highlighted by figure 5.1, this does not correspond to a homogeneous optical magnitude limit. It can be seen that the blue (metal poor) clusters are detected across the GC luminosity function. However, very few of the red (metal rich) clusters are detected in the FUV. This is discussed by Rey *et al.* (2007) and highlights the effect of metallicity on the HB properties, and hence FUV brightness, of a cluster. This plot also identifies the three metal rich clusters that are detected due to proposed excess FUV emission, as discussed by Rey *et al.* (2007).

Our final dataset contains 51 confirmed old clusters with which have $E(B-V) < 0.16$, NUV and ugriz photometry, core densities and spectroscopic [Fe/H] estimates. Of these clusters 29 have FUV photometry.

5.4 UV properties of M31 clusters

5.4.1 Metallicity relationships

Figure 5.2 shows the NUV-*g* and FUV-*g* properties of the M31's clusters as a function of metallicity. It can be seen that the NUV-*g* and FUV-*g* colours are correlated with metallicity. The relationship between the FUV-*g* and metallicity is relatively weak, but clear, especially with the inclusion of clusters with upper limits placed on the FUV magnitude. These relationships are to be expected and highlight the effect of metallicity on the HB population in a cluster. This result was already identified by Rey *et al.* (2007). It is included here for completeness, but for a more detailed discussion, we refer the reader to this work.

The right panel of figure 5.2 shows the metallicity as a function of FUV-NUV colour. It can be seen that the relationship is much less clear in this colour. A Spearman rank test actually shows metal rich clusters appear to be slightly bluer (with number of clusters, N=29, Spearman rank correlation coefficient, ρ_s=-0.39 and P-value for non-correlation, P=0.03). There is no obvious reason for such a relationship and it should be noted that selection effects, which bias us against FUV faint, metal rich clusters, could result in such a relationship. Also, this relationship is dominated by the two metal rich clusters in our sample. The FUV luminosity of these metal rich clusters may follow a different relationship to metal poor and intermediate metallicity clusters. However, it can be seen from these data that, unlike the optical-UV colour, there is no evidence for the FUV-NUV colour increasing with the metallicity of a cluster. This suggests that the effect of metallicity is much weaker on the average colour of the blue HB distribution.

The two metal rich clusters in our sample have very blue UV colours. This could result from selection effects, as these bias us against all but the FUV brightest metal rich clusters. However, the blue colours of these clusters could indicate that the FUV output of metal rich clusters (which generally have redder horizontal branches and few blue-HB stars) may be dominated by a population of EHB stars. EHB stars will have similar (or brighter) FUV luminosities to BHB stars. However, they have significantly bluer FUV-NUV colours (as shown by the UV CMD of e.g. NGC 2808 and M15: Brown *et al.*, 2001; Dieball *et al.*, 2007).

5.4.2 Density/ Mass relationships

As discussed in section 5.2, one may expect that the density of a cluster could affect its FUV luminosity. Figure 5.3 shows the optical-UV and UV colour of M31's GCs

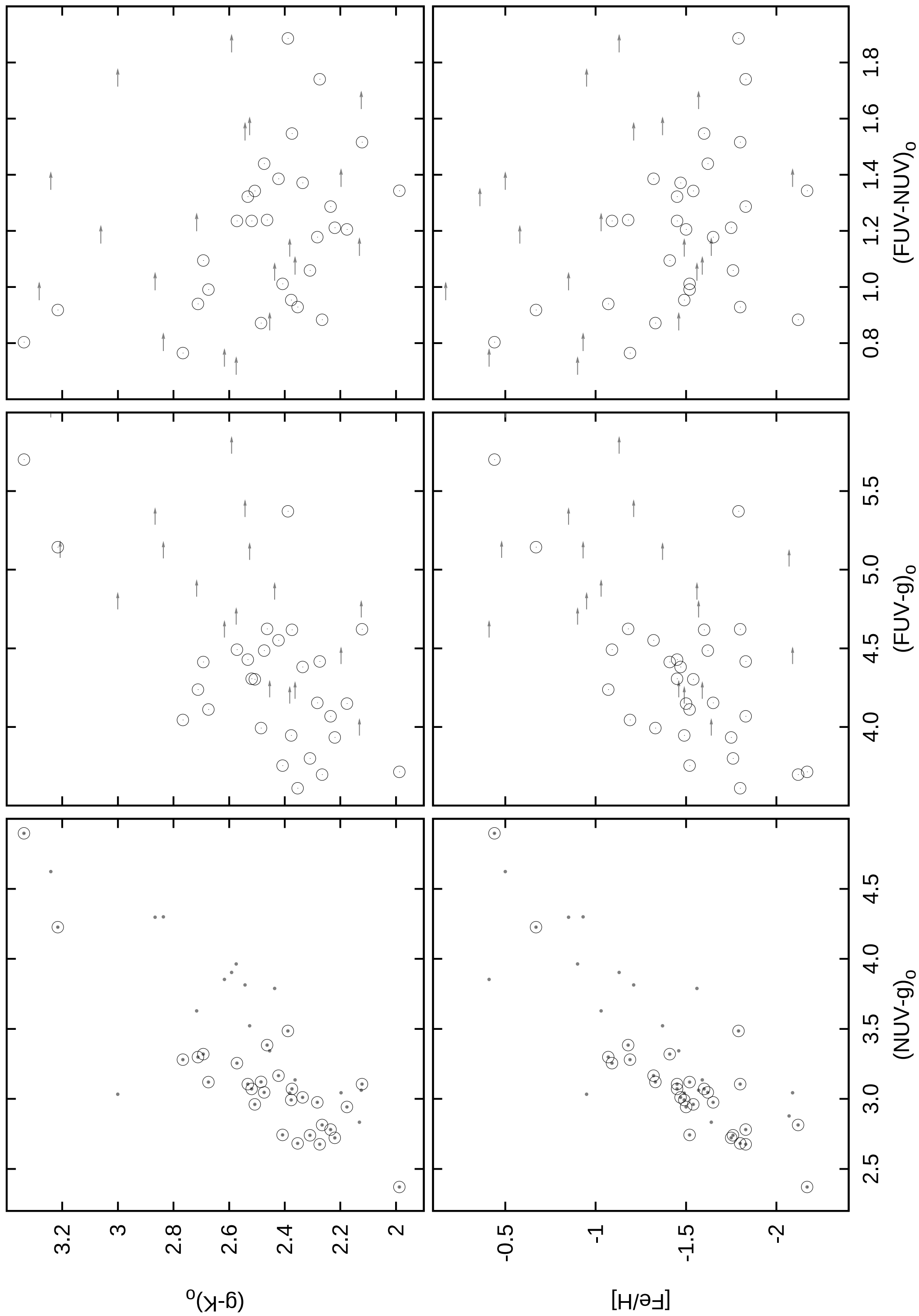

Figure 5.2: The ultraviolet colours of M31's GCs as a function of both metallicity and optical colour. Colours are dereddened using the reddening estimates of Fan *et al.* (2008). The grey points/arrows show those clusters detected in the NUV but not the FUV.

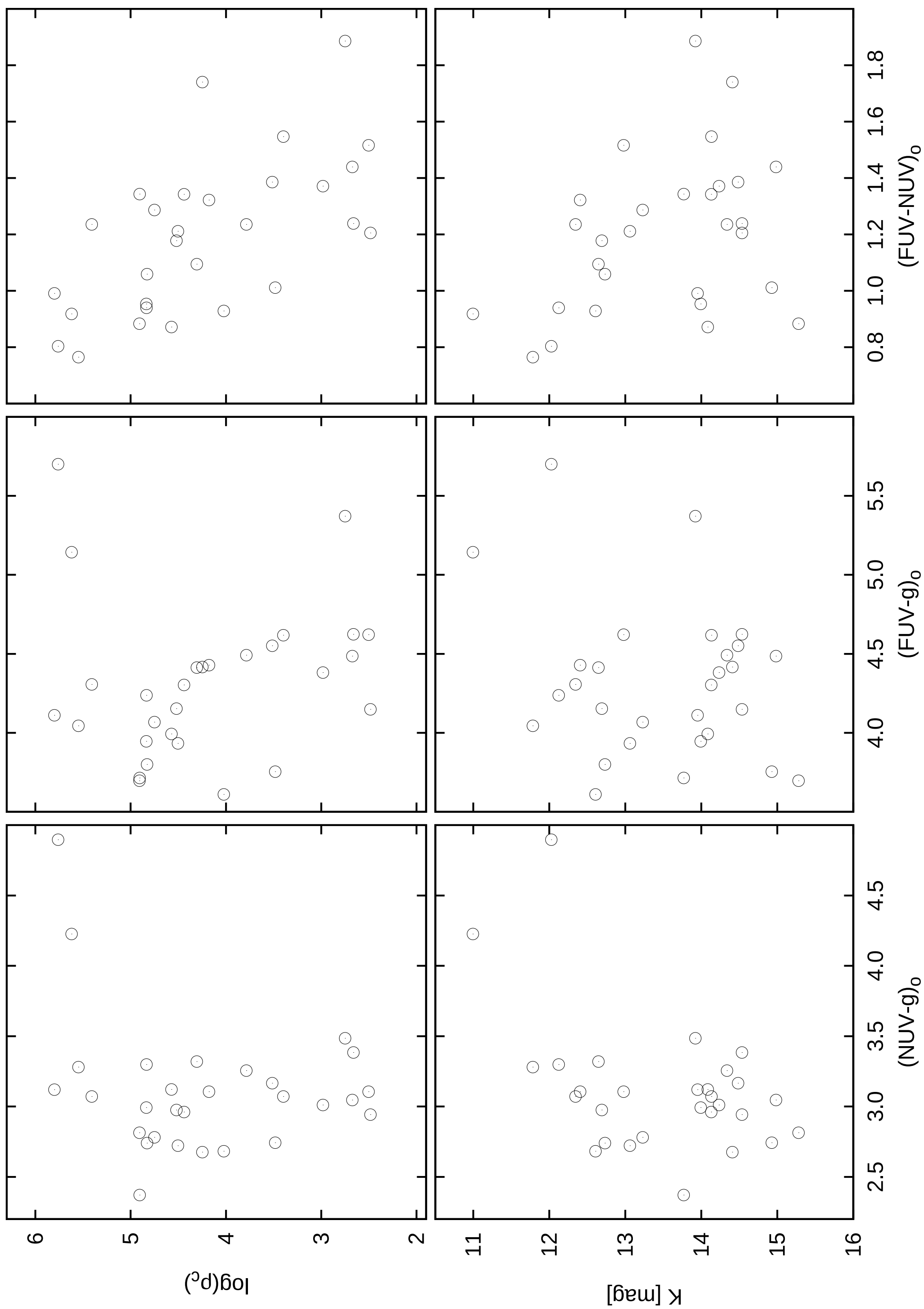

Figure 5.3: The ultraviolet colours of M31's GCs as a function of mass and core density.

as a function of luminosity and core density.

No significant trends are observed between either the luminosity or core density and UV-optical colours. This suggests that the total UV luminosity of a cluster is dominated by other effects. Since the total UV luminosity is likely dominated by the average colour of the HB stars, this result is not supprising. As can be seen from figure 5.2, the metallicity is strongly related to the UV luminosity (although additional parameters, not considered here, may be involved).

It can be seen from 5.3 that the cluster core density appears to correlate with the UV colour of the clusters. A Spearman rank test does identify a significant relationship, with higher density clusters having bluer UV colours (with N=29, ρ_s=-0.65 and P=1×10^{-4}). Since EHB stars are relatively bright at FUV wavelengths, bluer UV colours could be produced by a larger fraction of EHB stars with respect to blue-HB stars. The observed relationship is thus suggestive of a population of EHB stars, the formation of which is related to the core density of the cluster. This relationship is shown in more detail in figure 5.4. In this figure we have also split the population based on their density. It can be seen that the densest group of clusters do appear to be offset to bluer colours. Included in this plot are the upper limits for all metal poor clusters detected in the NUV but not the FUV. It can be seen that selection effects can not explain this relationship. This is because the densest clusters are also the brighter clusters, and hence generally detected. However, it can be seen that there is significant scatter in the observed relationship. This is to be expected for two reasons. Firstly, if there is a relationship between the extent of the HB in a cluster and its core density, this is very unlikely to be the only parameter involved. Secondly, the UV colour is an indirect measure of the distribution of HB stars in a cluster. Because of this, other hot populations may weaken genuine trends.

A weaker and less significant correlation is also observed between the total K-band luminosity of a cluster and its UV colour, with the brightest clusters having blue UV colours (with N=29, ρ_s=0.39 and P=0.04). This relationship is dominated by a lack of FUV faint, massive clusters. Such a relationship is again unlikely to be due to selection effects, as much fainter clusters are detected in both the NUV and FUV. This trend could be due to the same reasons as the core density relationship, because of the strong relationship between the density and mass of a cluster (as discussed in chapter 4). However, the relationship may also be suggestive of self enrichment. The greater potential of the most massive clusters may result in them retaining more of the helium they produce. Since higher helium fractions are known to produce bluer HB stars, this could potentially produce the observed trend. Because of the relatively close relationship between the mass and density of a clus-

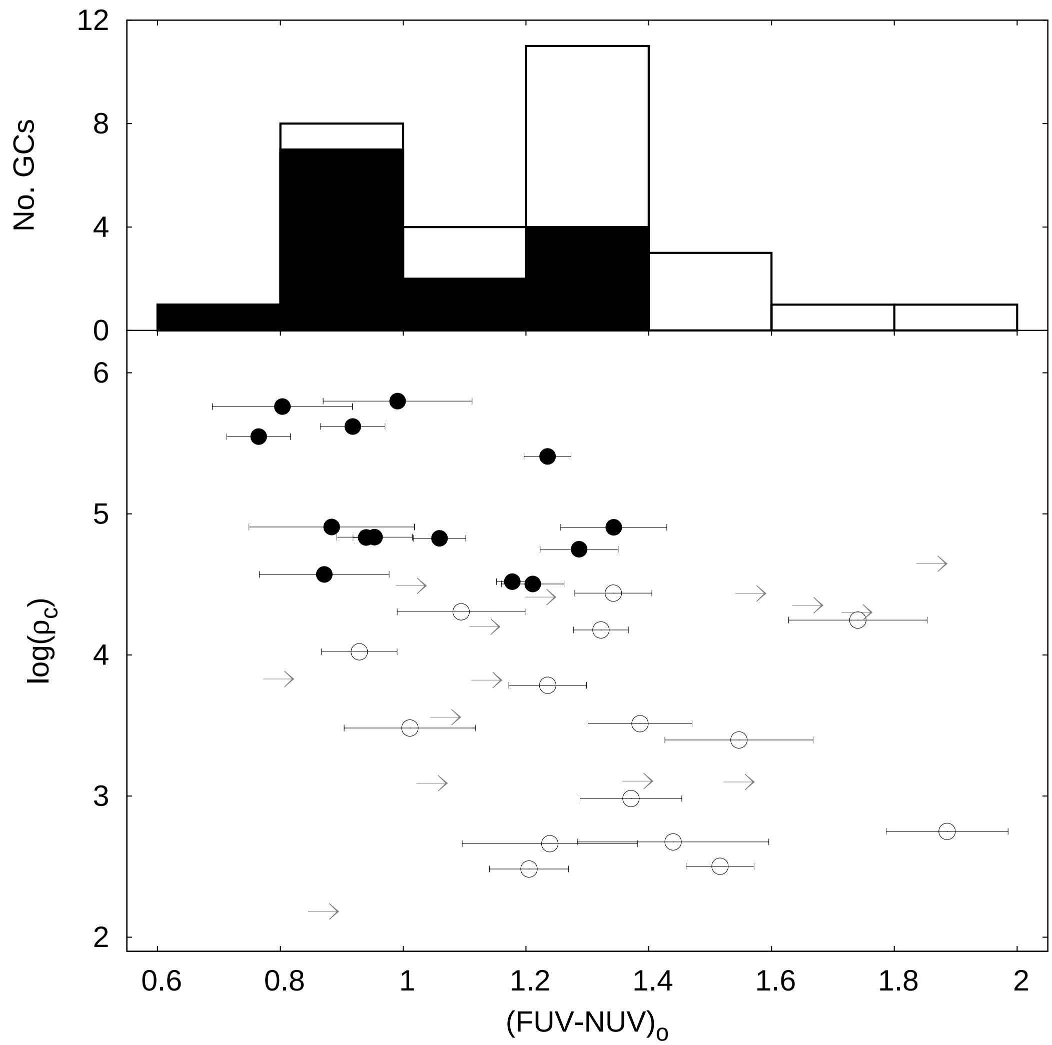

Figure 5.4: The dereddened FUV-NUV colour of M31's GCs as a function of core density. Solid circles show the densest 50% of clusters. At the top of this figure, we show the distribution of all clusters (open) and the dense clusters (solid). It can be seen that the denser clusters appear to have bluer UV colours. The grey arrows show the upper limits for clusters detected in only the NUV.

ter, and the weakness of the observed relationships, it is very difficult to refine the relative effects of mass and density.

5.4.3 Milky Way globular cluster data

Given the relatively low number of clusters in our sample, and the observed (and expected) subtlety of any relationships, it is interesting to consider the UV properties of the Milky Way's clusters. The distances, metallicities and structural parameters of the Milky Way GCs were taken from the Harris catalogue (Harris, 1996). Ultraviolet observations of the Milky Way's GCs are complicated due to both contamination (from foreground stars and background active galactic nuclei) and the high (and often variable) extinction in the direction of some of these clusters. This means that data are currently only available for a small sample of clusters. However, integrated FUV and NUV photometry of the Milky Way's GCs are available for 22 clusters from a combination of observations from the Astronomical Netherlands Satellite (ANS), Orbiting Astronomical Observatory (OAO) and International Ultraviolet Explorer (IUE) (published in Dorman *et al.*, 1995; Sohn *et al.*, 2006). These data, taken from Sohn *et al.* (2006), are on the STmag system and can be transformed to the *GALEX* ABmag system using the relationship quoted in their paper:

$$(\mathrm{FUV}-\mathrm{NUV})_{\mathrm{AB}} = (\mathrm{FUV}-\mathrm{NUV})_{\mathrm{STmag}} + 0.854 \quad (5.3)$$

Figure 5.5 shows the UV colour of the Milky Way's GCs as a function of metallicity, luminosity, and core density. It can be seen that the UV colour does not get redder with increasing metallicity. In fact, the data again suggest a slight anti-correlation, although this is not significant (with N=22, ρ_s=-0.3, P=0.17). In particular there appears to be a lack of FUV bright, metal poor, clusters. This general trend is in agreement with the observations of M31's clusters and adds strong support to metallicity having less of an influence on the UV colour than it does on the UV-optical colour.

No significant relationships are observed between UV colour of the clusters and either their luminosity or core density. It can be seen that the three most massive clusters are all FUV bright. Unfortunately, the lack of clusters this massive stops us from drawing significant conclusions from this. However, it is interesting to note that the most massive clusters in both the Milky Way and M31 are FUV bright. While the Milky Way data do not confirm the density relationships suggested from the M31 data, it is possible that such a relationship may not be observed in these data. This could be due to a combination of the lower number of clusters in the Milky Way sample, the less homogeneous UV dataset and the increased errors on the UV colour due to the difficulty of obtaining accurate UV photometry in the Galaxy. We note that, a relationship between the length of a cluster's 'blue tail' and its core density is observed in colour magnitude diagrams of the Milky Way's clusters.

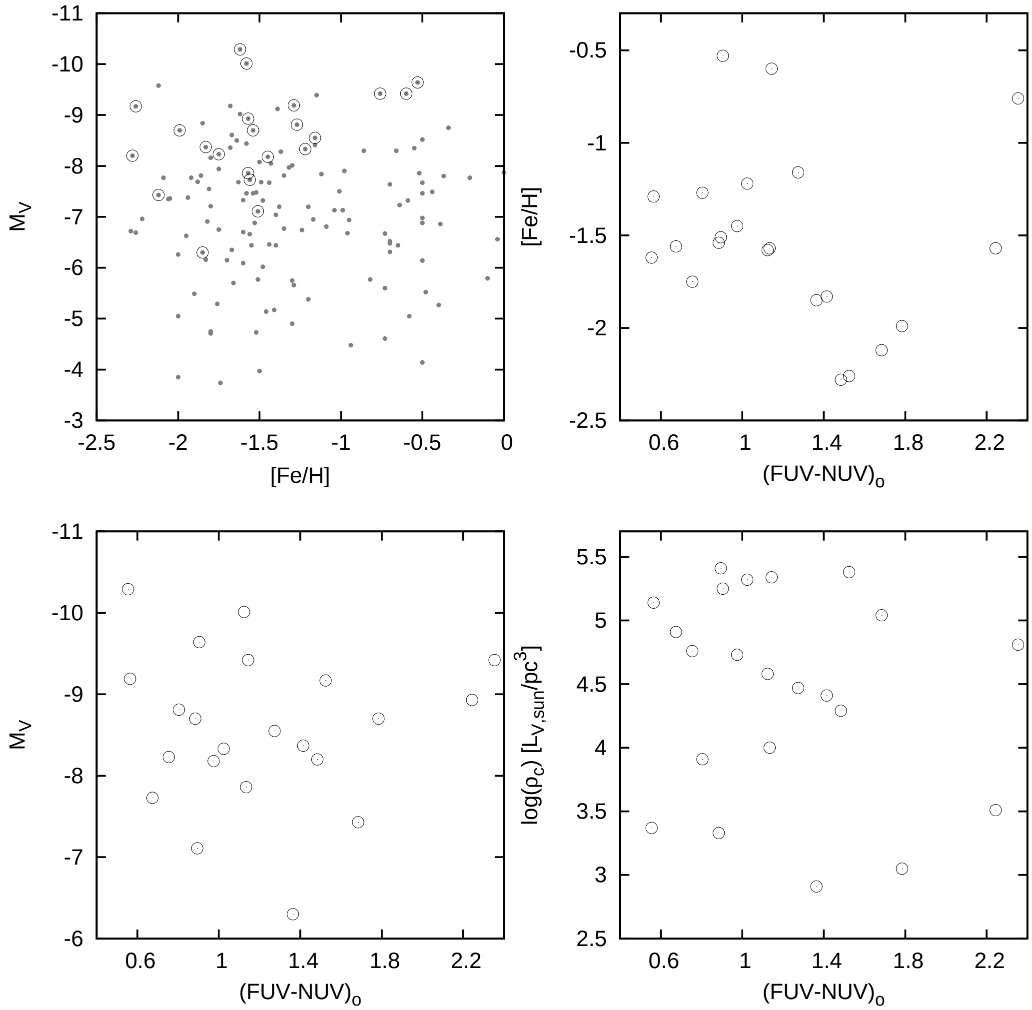

Figure 5.5: The UV properties of Milky Way GCs. UV data taken from updated table of Sohn *et al.* (2006) from the original IUE observations of Dorman *et al.* (1995). Colours are transformed into the *GALEX* filters using equation 5.3. Grey points indicate all Galactic GCs while open red circles show those with FUV and NUV data. Due to the large extinction for many of the Galactic GCs, these UV data are only available for 22 clusters.

5.4.4 Low mass X-ray binaries and other FUV-bright sources

It is generally assumed that, if BHB or EHB stars are present in a GC, then the integrated FUV luminosity of the cluster will be dominated by these stars. This is because most other stars in a cluster will be too cool to emit significantly in the FUV. However, there are other FUV bright sources in GCs. We consider the influence of these on a cluster's integrated luminosity below.

Low mass X-ray binaries (LMXBs) are found in the cores of many GCs. These objects can have very high X-ray luminosities which can irradiate the accretion

Table 5.1: FUV luminosity of selected Galactic LMXBs

Name	d [kpc]	A_{FUV}	$F_{1400Å}$ [erg/cm^2/s/Å]	$L_{1400Å}$ [10^{32}erg/s/Å]
Sco X-1[1]	2.8	2.430	2×10^{-13}	18.0
Cyg X-2[2]	8.0	3.645	5×10^{-15}	11.0
Her X-1[3]	5.5	0.405	7×10^{-14}	3.7
AC211 (M15)[4]	10.3	0.810	1.0×10^{-14}	2.4
4U1820-30 (NGC6624)[5]	7.9	-	1.8×10^{-14}	1.3
[M31 GC-B022	780	0.324	4.0×10^{-17}	40]
[M31 GC-B338	780	1.134	1.1×10^{-15}	2000]
[M31 GC-B193	780	0.891	7.8×10^{-17}	110]
[M31 GC-B225	780	0.810	4.0×10^{-16}	550]

The estimated distance to, extinction (assuming R_{FUV}=8.1), FUV flux and extinction corrected FUV luminosity of selected Galactic LMXBs. For comparison, the integrated FUV luminosity of the the faintest and brightest M31 GCs detected by Rey *et al.* (2007) are listed. Also listed are the FUV bright metal rich clusters in M31, which are known to host LMXBs. The Galactic LMXB data are taken from: [1] Vrtilek *et al.* (1991); [2] Vrtilek *et al.* (1990); [3] Boroson *et al.* (2000); [4] Dieball *et al.* (2007); [5] King *et al.* (1993).

disks and/or donor stars in the systems and heat them to very high temperatures. The result of these large, hot, accretion disks is that LMXBs can be very bright in the FUV. Indeed, the LMXB 4U1820-30 in the Galactic GC NGC 6624 dominates the total FUV luminosity of the cluster (King *et al.*, 1993). Even in the GC M15, which hosts a large population of BHB and EHB stars, the LMXB AC211 is the brightest FUV source in the cluster core (Dieball *et al.*, 2007). In table 5.1 we list the FUV luminosity of these two Galactic GC LMXBs and three other Galactic LMXBs. The fluxes of these LMXBs are highly variable. This table therefore provides only an estimate of the highest FUV fluxes reached during these observations. It can be seen that the bright LMXBs Sco X-1 and Cyg X-2 are also very bright FUV sources. However, in the context of GCs, it should be noted that GCs are unlikely to host more than one or two LMXBs in outburst. This means that, for clusters with a significant blue-HB population, a single bright LMXB is unlikely to contribute more than $\sim$ 10% to the integrated FUV luminosity of the clusters. However, for metal rich GCs (which generally lack BHB stars) LMXBs could dominate the emission. This effect will be enhanced by that fact that metal rich clusters preferentially form LMXBs (e.g. Kundu *et al.*, 2002). It can be seen from table 5.1 that a single LMXB is unlikely to explain the FUV bright, metal rich clusters, identified by Rey *et al.* (2007). However, it is interesting to note that two of the three metal rich clusters they identify do host LMXBs (B225 and B193). In particular, the cluster B225 hosts an LMXB with $L_x > 10^{38}$ergs/s (see chapter 4). Such a source will be very bright in the FUV.

Single 'UV bright' stars, such as post-AGB stars, can also contribute a significant fraction of the integrated luminosity of a cluster. However, clusters are also unlikely to host many of these sources due to their short lifetimes. It is thought that the contribution from such stars, to the integrated luminosity of a cluster, is unlikely to be more than 15% (Moehler, 2001).

In addition to these objects, there are several other hot populations in GCs. Cataclysmic Variables (CVs), the white dwarf equivalents to LMXBs, are relatively common in GCs. Because of their decreased bolometric luminosity, CVs are generally fainter than LMXBs in the FUV. However, they are more numerous and can reach FUV luminosities similar to a typical BHB star. Single white dwarf stars also emit strongly in the FUV. However, the average luminosity of both CVs and white dwarfs are thought to be too low to make a significant contribution to the integrated FUV luminosity of a cluster. The other notable FUV sources in GCs are blue straggler stars. These are very bright, blue, objects and can also reach FUV luminosities similar to BHB stars and bright CVs. However, blue stragglers this bright are likely to be very rare.

5.5 Conclusions

We have considered the FUV properties of M31's GCs. The previously identified relationships between the metallicity of a cluster and its UV brightness are confirmed. A weak anticorrelation is found between the FUV-NUV colour of a cluster and its metallicity. While this relationship is not very significant, it is in the opposite direction to the general relationship between metallicity and UV luminosity. This suggests that the metallicity of a cluster may have little effect on the blue extremes of the HB distribution.

Our data show no evidence of a relationship between either the mass or density of a cluster and its UV-optical colours. This suggests that the UV brightness of a cluster is dominated by other effects, such as metallicity. However, a significant relationship is found between the FUV-NUV colour of M31's GCs and their core densities. We interpret this result in the context of a population of EHB stars, the production of which is enhanced in dense stellar environments. This may be due to either mass loss or helium enhancement, in close encounters, or dynamical formation of tight binary systems (in which mass loss can occur, forming the EHB stars). This trend is not observed in the smaller sample of Milky Way clusters for which integrated UV colours are available. However, we note that the FUV data for the Milky Way clusters is less homogeneous and may suffer from more contamination than our M31 GC data. It should also be noted that, if such a relationship is present, it is expected to be relatively weak. It is also found that the most massive clusters considered in both M31 and the Milky Way appear to have blue UV colours. This may be related to the same mechanisms suggested for the core density relationship or it may point to an effect due to self enrichment. This luminosity trend is only identified among the brightest clusters. As such, our conclusions are limited due to the small number of clusters considered.

The relationship between cluster density and the population of EHB stars is potentially important in understanding the formation and morphology of HB stars. If a cluster's density does have a significant influence on its FUV emission, then it is important to consider this when using FUV observations to estimate the ages of globular clusters. Currently, such work does not take density effects into account.

We caution that, while these data suggest interesting correlations, the relationships observed are for a relatively small sample of M31's clusters. The FUV data are not complete and the study of the UV colours of these clusters would benefit greatly from FUV detections of more clusters. In particular it would be of great interest to detect the fainter FUV emission from more metal rich clusters. More accurate measurements of the structural parameters, metallicities and reddening of all of these clusters would also be of great benefit. However, there are no known reasons why our data should bias us towards the observed relationships.

The FUV emission from other sources in a GC are also considered. These sources are unlikely to dominate the integrated FUV emission of a cluster if it contains a significant population of BHB/EHB stars. However, bright LMXBs in these clusters are likely to contribute a significant fraction to its total FUV luminosity. These sources may also dominate the FUV output of clusters with only red HB populations (such as metal rich clusters).

6
Summary

This work has investigated the properties of M31's globular cluster system. We have presented a new catalogue of these clusters, including *ugriz* and K-band photometry, based on SDSS and WFCAM observations of the galaxy. The difficulty in studying and obtaining accurate aperture photometry of some of these clusters, due to the complex background of M31 itself, was discussed. We believe that the catalogue presented in this study contains the most reliable and homogeneous photometry of this cluster system to date. Using these data we have removed significant contamination from non-cluster sources listed in previous cluster catalogues. However, we note that there may still remain some contamination among the faint clusters in our catalogue. This study has not searched for new clusters in M31 and it is likely that the galaxy may contain a large population of over 450 old clusters. A detailed survey to identify new clusters in the galaxy, based on wide field, high spatial resolution data, remains an important project for the future.

The colours of M31's clusters were used to confirm a large population of young clusters in the galaxy. We note that, while these clusters are not believed to be massive enough to evolve into the 'normal' old cluster population, their presence and association with star forming regions is interesting in the context of cluster formation. It is likely that the photometry presented in this study will be useful for future investigation of the ages and metallicities of M31's clusters in more detail. The cluster catalogue presented here is also one of the largest, and most complete, GC datasets in the SDSS *ugriz* filters. Therefore, it should be of use in comparing with future observations of other GC systems, which are increasingly being obtained in these filters. In particular, we note that it is possible to study M31's clusters, both photometrically and spectroscopically, in greater detail than any other extragalactic clusters. As such it provides an important intermediate step between studies of Galactic and extragalactic GCs.

We have also estimated the structure of M31's old clusters by fitting PSF convolved models to their profiles. We noted the difficulty in providing accurate errors on these parameters and the limitations of this method for low signal-to-noise sources. However, from comparisons with higher spatial resolution images, it was found that these parameters are relatively reliable for those clusters with high signal-to-noise observations. In the future, this work can be extended to cover all of M31's clusters using high spatial resolution ground based images. However, to obtain more reliable parameters than those presented here would require observations that resolve the cluster cores. Currently, only a very limited sample of M31's clusters have such data. Obtaining new observations of the other clusters would require significant *HST* time ($\sim$1 orbit per cluster). While the case for obtaining such data is strong, it is likely that such observations will not be available in the near future.

Using the superb spatial coverage that is now available from archival *XMM Newton* observations of M31, we have investigated LMXBs in the M31 GC system. From these data, we confirmed a weak, but significant relationship between the metallicity and the formation of LMXBs. This effect is weaker than that observed in many elliptical galaxes. We attribute this to the relatively small population of metal rich clusters in M31, compared with typical elliptical galaxies. For such studies, it should also be noted that, there are potentially large errors on both the reddening estimates and the spectroscopic metallicities currently available for these clusters. This is something that is likely to improve in the near future. The X-ray data hint at a spectral hardening with decreasing metallicity in one of the X-ray hardness ratios. However, this result has a relatively low significance. We have demonstrated that the LMXBs are found preferentially in more luminous clusters and those with high stellar collision rates. By considering the relative effect of these parameters we have shown that LMXB hosting clusters have high stellar collision rates for their mass. This result provides strong observational evidence of dynamical formation of LMXBs in GCs, with little direct dependence on the mass of the cluster.

By considering the ultraviolet colours of M31's GCs, from published *GALEX* observations, we have identified a relationship between the UV colour of a GC and its core density. From these results we suggest that the formation of extreme horizontal branch stars may be enhanced in dense stellar environments. This is consistent with theories which predict that dynamical interactions should enhance the formation of these stars. A similar relationship has also been suggested from optical colour magnitude diagrams of GCs in the Milky Way. This result is potentially important in understanding the formation of these stars and in explaining the FUV emission of nearby globular clusters and galaxies. However, it can be seen from the data that the properties of HB stars are complex and there is significant scatter in the observed relationship. There is a clear need to extend our knowledge of HB morphology to extragalactic clusters in order to provide a better statistical sample for comparison with stellar models. While this is not easy to do, M31 represents the only realistic location to study this in detail. Deeper FUV observations of these clusters and more accurate metallicity estimates may help in making this result more significant. However, conclusive evidence of dynamical interactions playing a significant role, would be that the EHB stars should be centrally concentrated in the clusters. This is something that can be tested in the future with HST observations at FUV wavelengths.

Appendices

A

Catalogue of old clusters in M31 (table 2.1: old clusters)

This table lists all objects classified as old clusters in M31. Our classification criteria are discussed in chapter 2. We also include the previous classifications of these sources from the catalogues of Galleti *et al.* (2004) and Caldwell *et al.* (2009). Where available, we include optical and near infrared photometry of these clusters in the *u*,*g*,*r*,*i*,*z* and K-bands. Details of this catalogue are discussed in chapter 2. This table is also available in electronic form from the VizieR archive. The electronic version of this table also includes data for young (appendix B), candidate (appendix C) and previously misclassified clusters (due to space restrictions, objects that we have reclassified as non-clusters are *not* printed in these appendices. These are available from the full electronic version).

GC Name[1]	RA[2]	DEC[2]	Classification[3]			Photometry													
			f	f_{RBC}	f_{C09}	R_g^4	g	$(u-g)$	$(g-r)$	$(r-i)$	$(i-z)$	$\sigma_{g,tot}^5$	$\sigma_{(u-g)}$	$\sigma_{(g-r)}$	$\sigma_{(r-i)}$	$\sigma_{(i-z)}$	R_K^4	K_s	$\sigma_{K,tot}^5$
H1	6.69917	39.74631	1	1	old	-	-	-	-	-	-	-	-	-	-	-	-	-	-
H2	7.01367	40.04894	1	1	old	-	-	-	-	-	-	-	-	-	-	-	-	-	-
HEC2	7.13177	37.52328	1	8	old	12.0	19.300	-	0.938	0.665	-	0.076	-	0.093	0.073	-	-	-	-
H3	7.37562	41.84225	1	1	old	-	-	-	-	-	-	-	-	-	-	-	-	-	-
H4	7.43754	41.21933	1	1	old	-	-	-	-	-	-	-	-	-	-	-	-	-	-
H5	7.61375	41.60556	1	1	old	-	-	-	-	-	-	-	-	-	-	-	-	-	-
H6	7.79095	37.90000	1	1	old	10.6	16.123	1.319	0.597	0.278	0.150	0.028	0.022	0.013	0.013	0.016	-	-	-
H7	7.97715	40.11312	1	1	old	7.6	17.909	1.321	0.516	0.238	0.156	0.053	0.071	0.020	0.022	0.040	-	-	-
G001-MII	8.19389	39.57791	1	1	old	10.6	14.042	1.541	-	-	0.211	0.025	0.014	0.011	0.011	0.011	-	-	-
G002-MIII	8.39076	39.52187	1	1	old	10.6	16.067	1.230	0.547	0.265	0.164	0.021	0.021	0.013	0.013	0.017	-	-	-
H8	8.56421	39.88123	1	1	old	5.8	19.590	-	0.592	0.375	0.095	0.196	-	0.048	0.052	0.157	-	-	-
H9	8.57191	37.51195	1	1	old	6.4	18.014	1.197	0.574	0.256	0.157	0.026	0.049	0.020	0.020	0.035	-	-	-
B289	8.58700	41.79753	1	1	unknown	-	-	-	-	-	-	-	-	-	-	-	-	-	-
B290	8.58725	41.47169	1	1	unknown	-	-	-	-	-	-	-	-	-	-	-	-	-	-
H10	8.99886	35.68439	1	1	old	8.8	16.459	1.318	0.619	0.264	0.079	0.023	0.030	0.013	0.013	0.018	-	-	-
B291-G009	9.02071	42.03592	1	1	old	-	-	-	-	-	-	-	-	-	-	-	-	-	-
B292-G010	9.06941	40.97404	1	1	old	5.8	17.502	1.446	0.560	0.272	0.213	0.031	0.042	0.016	0.017	0.025	4.6	14.794	0.107
B293-G011	9.08691	40.89363	1	1	old	8.8	16.607	1.348	0.548	0.269	0.172	0.025	0.026	0.014	0.014	0.018	6.4	13.989	0.060
HEC3	9.13217	44.73797	1	8	old	-	-	-	-	-	-	-	-	-	-	-	-	-	-
B295-G014	9.19471	40.32842	1	1	old	7.6	17.002	1.228	0.558	0.278	0.177	0.021	0.032	0.015	0.015	0.024	4.6	14.458	0.038
H11	9.36717	44.19028	1	1	old	-	-	-	-	-	-	-	-	-	-	-	-	-	-
B422	9.41034	41.99995	1	1	old	5.2	18.327	1.478	0.649	0.312	0.095	0.025	0.085	0.021	0.022	0.041	-	-	-
B298-G021	9.50106	40.73223	1	1	old	8.8	16.781	1.330	0.518	0.255	0.149	0.025	0.030	0.014	0.015	0.023	5.8	14.359	0.050
SK004A	9.50564	42.06848	1	1	unknown	3.4	19.132	1.498	0.651	0.297	-	0.028	0.140	0.028	0.029	-	-	-	-
H12	9.51604	37.73350	1	1	unknown	7.6	16.814	1.100	0.540	0.254	0.075	0.028	0.030	0.014	0.014	0.019	-	-	-
HEC4	9.51919	40.74429	1	8	old	12.0	18.185	-	0.654	0.427	-	0.030	-	0.041	0.043	-	-	-	-
HEC5	9.58121	41.78747	1	8	old	12.0	18.328	-	0.548	0.203	-	0.036	-	0.051	0.058	-	-	-	-
B301-G022	9.58998	40.06029	1	1	old	7.0	17.505	1.590	0.753	0.371	0.235	0.027	0.049	0.016	0.016	0.024	4.6	14.277	0.047
B167D	9.59362	41.90974	1	1	old	5.2	18.177	1.139	0.539	0.254	0.181	0.043	0.061	0.020	0.021	0.038	-	-	-
B302-G023	9.63964	41.34790	1	1	old	5.8	17.091	1.336	0.558	0.276	0.166	0.074	0.032	0.015	0.015	0.022	4.6	14.572	0.081

H13	9.64018	41.74805	1	1	old	5.8	18.009	0.960	0.449	0.229	0.070	0.061	0.052	0.020	0.022	0.042	-	-	-
HEC6	9.64833	44.28028	1	8	old	-	-	-	-	-	-	-	-	-	-	-	-	-	-
H14	9.70587	42.37969	1	1	old	5.8	18.747	1.324	0.684	0.429	0.307	0.087	0.117	0.027	0.027	0.048	-	-	-
B304-G028	9.73726	41.17456	1	1	old	6.4	17.172	1.309	0.591	0.279	0.162	0.022	0.033	0.015	0.015	0.021	5.2	14.510	0.052
B305-D024	9.74522	40.27559	1	1	young	6.4	18.152	1.776	0.598	0.296	0.219	0.038	0.093	0.022	0.023	0.042	4.6	15.075	0.048
SK005A	9.74647	41.67426	1	1	unknown	4.6	19.771	1.095	0.728	0.213	0.434	0.081	0.178	0.047	0.053	0.099	-	-	-
B306-G029	9.78627	40.57250	1	1	old	8.8	16.880	1.890	1.125	0.606	0.395	0.021	0.047	0.014	0.013	0.016	8.2	12.521	0.030
B307-G030	9.82689	40.54948	1	1	interm	7.6	17.582	1.631	0.600	0.384	0.153	0.056	0.070	0.019	0.020	0.035	5.2	14.691	0.055
B309-G031	9.85262	40.24141	1	1	old	6.4	17.903	1.501	0.694	0.326	0.201	0.037	0.063	0.019	0.020	0.033	4.6	15.096	0.056
B310-G032	9.85724	41.39256	1	1	old	6.4	17.398	1.295	0.598	0.287	0.201	0.028	0.037	0.016	0.016	0.023	-	-	-
B436	9.87773	40.30570	1	2	interm	6.4	18.619	1.809	0.743	0.369	0.241	0.074	0.142	0.027	0.028	0.050	4.6	15.461	0.085
B181D	9.87860	41.47394	1	2	old	3.4	18.193	1.326	0.610	0.242	0.129	0.031	0.055	0.019	0.020	0.033	-	-	-
B311-G033	9.89052	40.52075	1	1	old	10.0	15.846	1.407	0.719	0.391	0.227	0.021	0.021	0.012	0.012	0.014	7.6	12.764	0.033
B312-G035	9.91738	40.95068	1	1	old	9.4	15.947	1.457	0.751	0.385	0.255	0.018	0.022	0.012	0.012	0.015	7.6	12.705	0.032
B313-G036	9.93587	40.88195	1	1	old	8.8	16.764	1.701	0.877	0.452	0.328	0.030	0.041	0.015	0.014	0.018	7.6	13.105	0.029
B001-G039	9.96253	40.96963	1	1	old	7.6	17.576	1.806	0.967	0.540	0.374	0.020	0.069	0.017	0.016	0.022	5.8	13.720	0.050
B316-G040	9.97329	40.69416	1	1	interm	9.4	17.159	1.439	0.621	0.265	0.179	0.023	0.049	0.017	0.019	0.031	5.2	14.806	0.117
B317-G041	9.98030	41.79614	1	1	old	8.8	16.915	1.277	0.537	0.252	0.141	0.019	0.029	0.015	0.015	0.021	-	-	-
B002-G043	10.01072	41.19822	1	2	old	4.6	17.857	1.289	0.516	0.283	0.160	0.025	0.053	0.019	0.021	0.040	2.8	15.469	0.099
B003-G045	10.03917	41.18478	1	1	old	5.2	17.944	1.485	0.579	0.373	0.174	0.040	0.066	0.019	0.021	0.039	4.6	15.092	0.108
H15	10.05506	35.87695	1	1	old	7.6	18.641	-	0.505	0.244	-0.094	0.065	-	0.027	0.030	0.068	-	-	-
B004-G050	10.07462	41.37787	1	1	old	5.2	17.398	1.664	0.761	0.362	0.228	0.022	0.045	0.016	0.015	0.020	4.0	14.173	0.038
B005-G052	10.08462	40.73287	1	1	old	5.8	16.123	1.744	0.803	0.419	0.284	0.019	0.026	0.013	0.012	0.015	5.8	12.561	0.028
B328-G054	10.10237	41.67289	1	1	old	3.4	18.314	1.306	0.638	0.347	0.075	0.261	0.059	0.022	0.022	0.036	-	-	-
B330-G056	10.10669	41.71497	1	2	old	4.6	18.003	1.410	0.568	0.379	0.142	0.030	0.058	0.021	0.022	0.033	-	-	-
B331-G057	10.10896	41.70118	1	1	old	3.4	18.738	1.518	0.679	0.344	0.340	0.105	0.095	0.026	0.027	0.040	-	-	-
B244	10.11020	41.30965	1	2	old	4.6	18.577	1.268	0.667	0.353	0.172	0.025	0.090	0.025	0.027	0.057	2.8	15.692	0.105
B006-G058	10.11031	41.45740	1	1	old	10.6	15.917	1.766	0.758	0.374	0.261	0.023	0.024	0.012	0.012	0.014	9.4	12.547	0.029
B333	10.12344	41.67382	1	2	old	4.0	19.199	1.140	0.736	0.506	-0.155	0.078	0.117	0.037	0.036	0.072	2.8	16.149	0.364
B008-G060	10.12613	41.26907	1	1	old	6.4	17.230	1.802	0.763	0.397	0.215	0.030	0.051	0.015	0.015	0.023	4.0	14.023	0.062
B009-G061	10.12794	41.61548	1	1	old	6.4	17.236	1.314	0.607	0.297	0.141	0.040	0.035	0.016	0.016	0.023	3.4	14.666	0.077
B010-G062	10.13154	41.23956	1	1	old	7.0	17.035	1.420	0.655	0.362	0.223	0.025	0.037	0.015	0.015	0.023	5.2	14.164	0.034
B011-G063	10.13282	41.65474	1	1	old	5.2	17.055	1.360	0.626	0.294	0.165	0.016	0.031	0.015	0.015	0.020	4.0	14.171	0.040

B012-G064	10.13525	41.36226	1	1	old	10.0	15.428	1.328	0.601	0.304	0.171	0.017	0.018	0.012	0.012	0.014	7.0	12.734	0.034
H16	10.15756	39.75831	1	1	old	8.2	17.861	1.497	0.490	0.221	-0.014	0.051	0.076	0.020	0.022	0.044	5.8	15.874	0.147
B013-G065	10.16022	41.42328	1	1	old	7.6	17.631	1.556	0.751	0.415	0.273	0.052	0.062	0.018	0.018	0.029	5.2	14.445	0.039
B335-V013	10.17365	40.64118	1	1	interm	6.4	18.408	1.759	1.099	0.605	0.388	0.126	0.120	0.026	0.023	0.031	5.2	14.071	0.102
B449-V11	10.17608	40.60120	1	2	interm	5.8	18.605	1.446	0.614	0.299	0.197	0.065	0.108	0.032	0.035	0.063	-	-	-
B015-V204	10.18757	40.99893	1	1	old	5.2	18.615	2.126	1.186	0.725	0.444	0.037	0.202	0.028	0.023	0.030	4.6	13.674	0.112
B016-G066	10.18821	41.36939	1	1	old	5.2	17.990	1.989	0.813	0.434	0.318	0.038	0.100	0.019	0.019	0.031	4.0	14.443	0.096
DAO38	10.19581	40.68278	1	2	interm	4.6	19.065	1.478	0.620	0.406	0.105	0.039	0.149	0.041	0.045	0.087	3.4	16.117	0.211
B336-G067	10.19837	42.14503	1	1	old	6.4	18.137	1.224	0.543	0.246	0.137	0.046	0.057	0.021	0.022	0.041	3.4	15.855	0.125
B337-G068	10.20202	42.20304	1	1	old	5.8	17.136	1.362	0.631	0.323	0.184	0.018	0.036	0.015	0.015	0.020	4.0	14.359	0.044
B017-G070	10.20303	41.20197	1	1	old	8.8	16.478	1.790	0.969	0.541	0.375	0.024	0.033	0.013	0.013	0.015	6.4	12.527	0.029
B019-G072	10.21887	41.31483	1	1	old	8.2	15.427	1.663	0.781	0.404	0.253	0.014	0.019	0.012	0.012	0.013	6.4	12.039	0.028
KHM31-74	10.22055	40.58880	1	-	interm	6.4	18.512	1.767	0.668	0.332	0.298	0.139	0.141	0.032	0.034	0.057	-	-	-
B020-G073	10.23026	41.69037	1	1	old	9.4	15.290	1.521	0.697	0.328	0.192	0.016	0.017	0.012	0.012	0.013	7.6	12.167	0.028
B338-G076	10.24530	40.59659	1	1	old	10.6	14.559	1.408	0.627	0.333	0.194	0.022	0.015	0.011	0.011	0.012	-	-	-
B021-G075	10.24591	41.09414	1	1	old	7.0	18.010	1.835	1.045	0.571	0.341	0.064	0.119	0.025	0.024	0.033	4.0	14.053	0.107
B022-G074	10.24616	41.41172	1	1	old	5.8	17.739	1.371	0.566	0.293	0.118	0.051	0.054	0.018	0.020	0.038	3.4	15.277	0.042
B339-G077	10.25296	39.93169	1	1	old	6.4	17.301	1.759	0.737	0.401	0.296	0.025	0.052	0.015	0.015	0.020	5.2	13.877	0.044
B023-G078	10.25494	41.22938	1	1	old	10.6	14.790	1.821	0.990	-	-	0.017	0.017	0.011	0.011	0.012	10.6	10.744	0.028
B247	10.25926	41.00876	1	1	interm	8.2	17.664	1.487	0.741	0.393	0.300	0.064	0.074	0.023	0.023	0.036	4.6	13.960	0.172
SK019A	10.27068	41.47720	1	1	na	2.8	19.723	-	1.106	0.462	0.060	0.100	-	0.036	0.032	0.073	2.8	15.262	0.050
B248	10.28309	40.88359	1	1	old	4.0	18.616	-	0.798	0.385	0.314	0.078	-	0.029	0.031	0.048	2.8	15.300	0.107
B341-G081	10.28813	40.59805	1	1	old	7.0	16.763	1.651	0.727	0.375	0.207	0.018	0.033	0.015	0.015	0.019	5.8	13.547	0.064
B017D	10.29175	40.96978	1	2	interm	5.8	18.323	1.722	0.557	0.375	0.219	0.048	0.123	0.030	0.033	0.058	4.6	15.405	0.278
B024-G082	10.29938	41.76369	1	1	old	5.8	17.294	1.680	0.772	0.372	0.227	0.036	0.043	0.015	0.015	0.020	4.6	13.984	0.046
B025-G084	10.30230	41.00781	1	1	old	4.0	17.276	1.515	0.807	0.403	0.221	0.016	0.044	0.017	0.017	0.023	4.0	13.924	0.058
SK020A	10.30564	41.16170	1	1	na	2.8	20.279	-	0.763	0.527	0.277	0.109	-	0.081	0.087	0.148	2.8	16.243	0.160
B027-G087	10.31055	40.93081	1	1	old	5.2	16.050	1.446	0.698	0.346	0.201	0.047	0.023	0.013	0.013	0.016	4.0	12.982	0.058
B026-G086	10.31057	41.41116	1	1	old	5.2	18.025	1.945	0.856	0.471	0.362	0.024	0.100	0.019	0.019	0.029	4.6	14.331	0.069
B028-G088	10.31871	40.98422	1	1	old	5.2	17.312	1.442	0.660	0.383	0.238	0.026	0.043	0.017	0.018	0.026	4.0	14.239	0.129
B020D-G089	10.32182	41.13588	1	1	old	4.0	18.113	1.692	0.964	0.478	0.379	0.063	0.092	0.023	0.023	0.032	4.0	14.411	0.064
B029-G090	10.32433	41.00640	1	1	old	6.4	17.211	1.980	0.876	0.502	0.354	0.043	0.061	0.017	0.016	0.020	5.8	13.235	0.057
B030-G091	10.32806	40.95434	1	1	old	3.4	18.198	-	1.248	0.651	0.490	0.050	-	0.021	0.018	0.021	3.4	13.341	0.045

B031-G092	10.33716	40.98449	1	1	old	3.4	18.410	-	1.007	0.501	0.325	0.051	-	0.024	0.022	0.032	2.8	14.494	0.039
B032-G093	10.33965	41.29170	1	1	old	4.6	18.207	1.848	1.028	0.560	0.355	0.085	0.119	0.027	0.027	0.036	3.4	14.019	0.043
SK026A	10.35263	40.60104	1	1	unknown	2.8	19.869	1.618	0.829	0.384	0.095	0.155	0.229	0.041	0.040	0.080	2.8	17.095	1.433
B033-G095	10.35999	41.00382	1	1	old	3.4	18.365	1.457	0.806	0.425	0.268	0.130	0.081	0.024	0.024	0.040	2.8	15.244	0.175
B034-G096	10.36715	40.89714	1	1	old	7.6	15.898	1.693	0.771	0.399	0.274	0.015	0.023	0.013	0.013	0.014	6.4	12.421	0.042
B457-G097	10.37170	42.31032	1	1	old	9.4	17.338	1.277	0.604	0.287	0.141	0.036	0.041	0.017	0.017	0.028	6.4	14.846	0.109
B035	10.38578	41.64238	1	1	old	5.2	17.886	1.552	0.775	0.380	0.297	0.033	0.066	0.019	0.019	0.031	3.4	14.582	0.078
B036	10.38677	41.43478	1	1	old	4.0	17.916	1.649	0.842	0.413	0.284	0.051	0.071	0.018	0.018	0.029	4.0	14.427	0.085
B037-V327	10.39570	41.24859	1	1	old	7.0	17.962	2.343	2.007	1.143	0.824	0.086	0.159	0.023	0.015	0.015	8.8	10.999	0.024
B038-G098	10.39979	41.32077	1	1	old	4.6	16.975	1.542	0.801	0.403	0.250	0.047	0.039	0.017	0.017	0.023	3.4	13.733	0.030
B039-G101	10.40779	41.34716	1	1	old	7.6	16.643	2.016	1.089	0.591	0.389	0.031	0.046	0.015	0.014	0.017	7.6	12.377	0.029
B041-G103	10.42006	41.24597	1	1	old	4.0	18.725	1.492	0.473	0.294	0.179	0.083	0.133	0.045	0.060	0.106	2.8	16.490	0.106
B042-G104	10.42367	41.12394	1	1	old	4.6	17.039	2.320	1.421	0.678	0.452	0.021	0.065	0.015	0.013	0.015	4.6	12.201	0.030
B044-G107	10.42876	41.33505	1	1	old	5.8	17.319	1.717	0.971	0.497	0.332	0.050	0.056	0.019	0.019	0.024	-	-	-
B343-G105	10.42958	40.20623	1	1	old	8.8	16.597	1.357	0.562	0.268	0.196	0.031	0.028	0.014	0.014	0.018	5.2	14.014	0.042
B045-G108	10.42961	41.57224	1	1	old	7.6	16.235	1.641	0.778	0.397	0.232	0.018	0.027	0.013	0.013	0.016	6.4	12.919	0.030
B046-G109	10.43593	41.77450	1	1	old	4.0	18.262	1.298	0.644	0.323	0.135	0.039	0.063	0.021	0.021	0.036	2.8	15.330	0.081
B048-G110	10.43965	41.22517	1	1	old	5.2	17.069	1.710	0.842	0.466	0.312	0.028	0.046	0.017	0.018	0.022	-	-	-
B047-G111	10.43982	41.70107	1	1	old	5.2	17.798	1.274	0.632	0.286	0.213	0.029	0.052	0.018	0.020	0.035	4.0	15.015	0.056
B050-G113	10.44285	41.53846	1	1	old	5.8	17.246	1.741	0.763	0.398	0.233	0.026	0.049	0.015	0.015	0.023	3.4	13.900	0.046
B051-G114	10.44454	41.42199	1	1	old	8.2	16.738	1.818	1.004	0.517	0.338	0.021	0.039	0.014	0.013	0.016	-	-	-
SK035A	10.44700	41.87620	1	1	unknown	2.8	20.470	1.063	1.268	0.422	0.385	0.087	0.226	0.053	0.040	0.066	2.8	15.682	0.110
SK036A	10.44742	40.85227	1	1	na	2.8	20.269	-	0.950	0.472	0.116	0.332	-	0.068	0.069	0.128	2.8	16.391	0.340
B054-G115	10.44867	41.01539	1	1	old	3.4	18.682	1.932	0.789	0.521	0.287	0.079	0.133	0.029	0.029	0.043	2.8	14.496	0.086
B055-G116	10.45994	41.20341	1	1	old	5.2	17.314	2.509	1.155	0.628	0.457	0.127	0.103	0.018	0.017	0.020	-	-	-
B254	10.46055	41.27391	1	2	old	3.4	19.117	1.720	0.680	0.413	0.365	0.049	0.193	0.048	0.057	0.086	-	-	-
B056-G117	10.46322	40.96118	1	1	old	5.2	17.739	1.983	0.860	0.500	0.402	0.023	0.077	0.020	0.020	0.025	4.0	13.618	0.092
B057-G118	10.47005	40.86805	1	1	old	5.2	17.887	1.291	0.582	0.296	0.155	0.021	0.053	0.022	0.026	0.042	3.4	15.313	0.097
B058-G119	10.47083	40.78602	1	1	old	8.2	15.356	1.471	0.645	0.318	0.196	0.016	0.017	0.012	0.012	0.013	5.8	12.392	0.035
B059-G120	10.47539	41.18354	1	1	old	4.0	17.850	1.920	1.007	0.543	0.333	0.046	0.092	0.023	0.022	0.029	-	-	-
B060-G121	10.48750	41.08735	1	1	old	5.2	17.066	1.251	0.581	0.309	0.189	0.025	0.034	0.017	0.018	0.027	4.0	14.222	0.087
B061-G122	10.50050	41.49328	1	1	old	7.0	17.251	1.950	1.055	0.551	0.383	0.039	0.058	0.015	0.014	0.018	5.2	12.977	0.038
B063-G124	10.50360	41.48602	1	1	old	7.6	16.313	1.888	1.063	0.574	0.397	0.014	0.031	0.013	0.012	0.014	7.0	12.008	0.030

B064-G125	10.50799	41.18541	1	1	old	5.8	16.665	1.361	0.641	0.343	0.221	0.043	0.030	0.016	0.017	0.023	-	-	-
B065-G126	10.50807	40.67026	1	1	old	7.0	17.253	1.549	0.655	0.325	0.136	0.035	0.042	0.016	0.016	0.023	4.0	14.474	0.045
B344-G127	10.51239	41.86726	1	1	old	7.0	16.281	1.476	0.676	0.311	0.183	0.020	0.023	0.013	0.013	0.015	5.2	13.313	0.034
B067-G129	10.51326	41.07326	1	1	old	5.2	17.564	1.332	0.572	0.294	0.170	0.048	0.045	0.020	0.023	0.036	3.4	15.021	0.127
B068-G130	10.51336	40.98062	1	1	old	6.4	16.931	2.043	1.052	0.560	0.394	0.025	0.046	0.015	0.014	0.016	5.8	12.619	0.032
B257-V219	10.51371	40.97052	1	2	old	4.6	18.491	2.256	1.226	0.682	0.461	0.044	0.174	0.026	0.022	0.027	4.0	13.680	0.096
B461-G131	10.51773	42.05738	1	1	old	5.2	17.818	1.531	0.729	0.328	0.232	0.037	0.055	0.018	0.017	0.025	4.6	14.721	0.116
B041D	10.51969	41.27972	1	1	old	2.8	19.064	1.916	1.247	0.615	0.364	0.096	0.183	0.034	0.030	0.040	-	-	-
B070-G133	10.52876	41.13233	1	1	old	4.0	17.220	1.298	0.626	0.341	0.165	0.025	0.039	0.019	0.021	0.031	-	-	-
B071	10.52968	41.20336	1	1	old	2.8	18.592	1.955	0.925	0.388	0.325	0.071	0.127	0.028	0.030	0.043	-	-	-
B073-G134	10.53048	40.98925	1	1	old	7.0	16.412	1.733	0.756	0.379	0.266	0.022	0.029	0.014	0.014	0.017	5.2	13.001	0.084
B072	10.53087	41.37990	1	1	old	4.6	18.302	2.641	1.419	0.753	0.501	0.069	0.255	0.028	0.023	0.025	-	-	-
B074-G135	10.53354	41.72269	1	1	old	7.0	17.007	1.413	0.636	0.321	0.193	0.027	0.035	0.015	0.015	0.023	4.6	14.177	0.037
B075-G136	10.53668	41.33922	1	1	old	4.0	17.955	1.574	0.865	0.418	0.210	0.062	0.078	0.026	0.027	0.039	-	-	-
MITA140	10.53956	41.29600	1	-	old	2.8	18.007	-	1.490	0.779	0.530	0.031	-	0.020	0.016	0.018	-	-	-
B045D	10.54115	41.35397	1	1	old	2.8	19.752	1.598	1.146	0.657	0.362	0.078	0.256	0.060	0.052	0.070	-	-	-
B076-G138	10.54264	41.08946	1	1	old	4.6	17.203	1.460	0.704	0.372	0.173	0.042	0.038	0.017	0.018	0.025	4.0	14.187	0.069
B077-G139	10.54640	41.12612	1	1	old	4.0	17.961	-	0.998	0.540	0.325	0.082	-	0.022	0.021	0.027	-	-	-
B078-G140	10.55068	41.29969	1	2	old	3.4	18.546	2.294	1.341	0.677	0.384	0.030	0.195	0.029	0.024	0.030	-	-	-
B080-G141	10.55160	41.31685	1	1	old	4.6	17.917	2.103	1.131	0.582	0.390	0.076	0.116	0.024	0.022	0.028	-	-	-
B345-G143	10.55888	40.29345	1	1	old	6.4	17.045	1.359	0.583	0.305	0.200	0.035	0.034	0.015	0.015	0.021	5.2	14.259	0.033
B462	10.56134	42.02681	1	1	old	5.2	18.377	1.323	0.564	0.289	0.141	0.042	0.072	0.023	0.024	0.042	3.4	15.886	0.079
B082-G144	10.56597	41.02069	1	1	old	7.6	16.359	2.611	1.451	0.753	0.450	0.023	0.047	0.013	0.012	0.013	7.6	11.378	0.029
B083-G146	10.56852	41.75572	1	1	old	6.4	17.454	1.387	0.664	0.337	0.202	0.037	0.046	0.017	0.017	0.028	4.0	14.579	0.042
B084	10.57267	41.31552	1	2	old	2.8	18.866	-	1.163	0.607	0.364	0.113	-	0.033	0.029	0.038	-	-	-
B085-G147	10.57599	40.66588	1	1	old	5.8	17.212	1.296	0.637	0.289	0.174	0.025	0.035	0.016	0.016	0.022	4.6	14.459	0.055
B086-G148	10.57773	41.23389	1	1	old	6.4	15.426	1.259	0.578	0.298	0.174	0.041	0.018	0.012	0.013	0.015	-	-	-
B259	10.57903	41.70415	1	2	interm	3.4	19.556	1.453	0.866	0.498	0.153	0.075	0.200	0.038	0.037	0.082	2.8	16.002	0.141
SK049A	10.58117	40.87288	1	1	na	2.8	20.481	-	0.767	0.404	-0.167	0.124	-	0.087	0.097	0.235	-	-	-
B087	10.58250	41.63788	1	1	old	3.4	19.123	1.628	0.810	0.361	0.192	0.080	0.160	0.030	0.031	0.066	-	-	-
B051D	10.58562	41.07720	1	2	interm	4.0	19.181	1.399	0.747	0.362	0.375	0.041	0.155	0.048	0.055	0.084	4.0	15.377	0.125
B088-G150	10.58777	41.53729	1	1	old	10.6	15.945	1.640	0.986	0.529	0.360	0.024	0.024	0.012	0.012	0.014	-	-	-
B090	10.58779	41.04932	1	1	old	4.0	18.852	1.680	0.706	0.401	0.256	0.040	0.148	0.039	0.044	0.070	2.8	15.191	0.084

B092-G152	10.59323	41.13574	1	1	old	4.6	17.375	1.476	0.682	0.335	0.172	0.035	0.042	0.018	0.020	0.029	-	-	-
B347-G154	10.59537	41.90760	1	1	old	7.6	16.744	1.284	0.568	0.268	0.158	0.022	0.027	0.014	0.014	0.019	5.2	14.217	0.052
B348-G153	10.59550	41.87455	1	1	old	4.6	17.393	1.630	0.762	0.352	0.233	0.027	0.044	0.016	0.015	0.020	4.0	14.023	0.030
B093-G155	10.59639	41.36207	1	1	old	4.0	17.271	1.587	0.834	0.456	0.229	0.047	0.048	0.019	0.019	0.026	-	-	-
H17	10.59870	37.24308	1	1	old	6.4	18.022	1.328	0.570	0.247	0.261	0.037	0.056	0.019	0.019	0.030	-	-	-
B094-G156	10.60434	40.95489	1	1	old	8.2	15.989	1.789	0.787	0.427	0.290	0.023	0.025	0.013	0.013	0.015	5.8	12.467	0.038
B095-G157	10.60748	41.09343	1	1	old	4.6	-	-	-	-	-	0.052	0.039	0.015	0.014	0.016	4.0	12.784	0.070
B096-G158	10.60863	41.32072	1	1	old	4.6	17.083	2.370	1.009	0.568	0.364	0.127	0.076	0.017	0.017	0.020	-	-	-
B098	10.61408	40.99333	1	1	old	4.6	16.703	1.658	0.750	0.358	0.223	0.047	0.032	0.015	0.015	0.019	4.0	13.486	0.091
B097-G159	10.61438	41.42561	1	1	old	4.0	17.420	1.726	0.912	0.442	0.276	0.023	0.057	0.019	0.019	0.026	-	-	-
B099-G161	10.61495	41.16747	1	1	old	4.6	17.217	1.391	0.671	0.355	0.255	0.029	0.037	0.019	0.021	0.028	-	-	-
B515	10.61687	41.55681	1	1	old	-	-	-	-	-	-	-	-	-	-	-	-	-	-
B056D	10.61820	41.57421	1	1	na	3.4	19.311	-	0.995	0.479	0.414	0.078	-	0.032	0.030	0.052	-	-	-
B350-G162	10.61847	40.41423	1	1	old	8.2	16.949	1.409	0.580	0.299	0.196	0.026	0.034	0.015	0.015	0.020	5.2	14.270	0.059
B100-G163	10.62071	40.83220	1	1	old	4.0	18.231	1.627	0.780	0.376	0.303	0.041	0.083	0.022	0.022	0.032	3.4	14.908	0.034
B101-G164	10.62093	41.13767	1	1	old	5.8	17.268	1.393	0.646	0.337	0.285	0.047	0.040	0.020	0.022	0.030	-	-	-
B103-G165	10.62390	41.29928	1	1	old	5.2	15.685	1.817	0.821	0.454	0.307	0.026	0.023	0.013	0.013	0.014	-	-	-
B104-NB5	10.62473	41.29045	1	1	old	5.2	17.649	1.502	0.683	0.287	0.055	0.068	0.063	0.024	0.028	0.046	-	-	-
B105-G166	10.62810	41.50759	1	1	old	5.2	17.707	1.528	0.768	0.441	0.195	0.030	0.062	0.021	0.023	0.033	-	-	-
B106-G168	10.62934	41.20513	1	1	old	5.8	16.568	1.732	0.801	0.419	0.264	0.020	0.032	0.015	0.015	0.019	-	-	-
B108-G167	10.62996	41.14763	1	2	old	4.6	17.850	1.881	0.806	0.459	0.337	0.025	0.081	0.024	0.026	0.034	-	-	-
B107-G169	10.63022	41.32748	1	1	old	4.0	16.292	1.568	0.808	0.398	0.220	0.024	0.027	0.014	0.014	0.017	-	-	-
B109-G170	10.63401	41.17442	1	1	old	4.6	16.923	1.871	0.837	0.442	0.365	0.031	0.042	0.016	0.017	0.020	-	-	-
B110-G172	10.63793	41.05787	1	1	old	7.0	15.607	1.631	0.711	0.374	0.241	0.015	0.020	0.012	0.012	0.014	6.4	12.233	0.031
NB16	10.63800	41.33800	1	1	old	-	-	-	-	-	-	-	-	-	-	-	-	-	-
B111-G173	10.63822	41.00733	1	1	old	4.0	17.173	1.381	0.641	0.328	0.158	0.031	0.035	0.017	0.019	0.026	3.4	14.312	0.095
B260	10.63829	41.52351	1	2	old	4.0	19.448	-	1.496	0.889	0.650	0.149	-	0.050	0.035	0.038	-	-	-
B112-G174	10.63853	41.29511	1	1	old	5.8	16.805	2.096	0.929	0.522	0.376	0.133	0.052	0.016	0.016	0.019	-	-	-
B114-G175	10.64292	41.21247	1	1	old	4.6	17.364	1.372	0.592	0.350	0.313	0.047	0.041	0.020	0.023	0.031	-	-	-
B117-G176	10.64321	40.95259	1	1	old	6.4	16.722	1.314	0.602	0.280	0.185	0.037	0.028	0.015	0.016	0.022	3.4	14.100	0.087
NB17-AU014	10.64333	41.29206	1	1	na	-	-	-	-	-	-	-	-	-	-	-	-	-	-
B115-G177	10.64337	41.23387	1	1	old	4.0	16.552	2.141	0.801	0.537	0.394	0.021	0.043	0.015	0.015	0.017	-	-	-
B116-G178	10.64390	41.54760	1	1	old	4.6	17.613	2.078	1.322	0.681	0.498	0.058	0.086	0.019	0.016	0.019	-	-	-

NB35-AU4	10.64396	41.31122	1	2	interm	-	-	-	-	-	-	-	-	-	-	-	-	-	-
B064D-NB6	10.64805	41.24284	1	1	old	5.2	16.660	1.596	0.684	0.345	0.233	0.031	0.034	0.016	0.017	0.022	-	-	-
B119-NB14	10.65043	41.29322	1	1	old	2.8	17.976	1.646	0.903	0.480	0.353	0.138	0.064	0.022	0.022	0.028	-	-	-
SK052A	10.65548	41.84822	1	1	unknown	4.0	18.796	1.252	0.638	0.300	0.083	0.085	0.104	0.029	0.032	0.076	2.8	15.964	0.137
B351-G179	10.65821	42.19192	1	1	old	5.2	17.935	1.320	0.642	0.265	0.204	0.022	0.052	0.018	0.019	0.030	4.6	15.218	0.050
NB21-AU5	10.65825	41.26636	1	1	old	-	-	-	-	-	-	-	-	-	-	-	-	-	-
B352-G180	10.65911	42.03696	1	1	old	8.2	16.836	1.260	0.571	0.284	0.127	0.020	0.027	0.014	0.014	0.019	4.6	14.244	0.037
B122-G181	10.66703	41.56299	1	1	old	4.0	18.592	-	1.408	0.758	0.426	0.063	-	0.029	0.023	0.028	-	-	-
B123-G182	10.66941	41.17595	1	1	old	5.2	17.721	1.485	0.754	0.440	0.232	0.034	0.057	0.023	0.025	0.035	-	-	-
SK053A	10.67003	40.29801	1	1	unknown	4.0	18.960	1.322	0.799	0.445	0.303	0.047	0.123	0.028	0.026	0.046	4.0	15.569	0.086
B124-NB10	10.67261	41.25663	1	1	old	4.6	15.020	1.994	0.737	-	-	0.152	0.019	0.012	0.012	0.013	-	-	-
B125-G183	10.67612	41.09197	1	1	old	6.4	16.814	1.273	0.581	0.288	0.144	0.033	0.029	0.017	0.018	0.024	5.2	13.969	0.134
DAO55	10.67715	40.49079	1	2	old	5.8	19.081	1.181	0.568	0.311	0.183	0.080	0.130	0.034	0.037	0.076	3.4	16.592	0.155
B126-G184	10.68205	41.21190	1	1	old	3.4	17.540	1.286	0.652	0.271	0.138	0.045	0.039	0.020	0.023	0.034	-	-	-
B127-G185	10.68550	41.24486	1	1	old	10.0	14.500	1.487	0.940	0.420	0.251	0.051	0.016	0.012	0.011	0.012	-	-	-
NB89	10.68658	41.24561	1	1	old	-	-	-	-	-	-	-	-	-	-	-	-	-	-
SK054A	10.68781	41.13753	1	1	na	4.0	18.828	1.367	0.740	0.249	-0.103	0.069	0.116	0.044	0.055	0.111	-	-	-
B072D	10.69079	41.45750	1	4	old	2.8	19.561	1.556	-	-	-0.057	0.101	0.203	-	-	0.141	-	-	-
NB18	10.69308	41.30900	1	2	old	-	-	-	-	-	-	-	-	-	-	-	-	-	-
B354-G186	10.69835	42.00712	1	1	old	5.8	18.094	1.420	0.584	0.269	0.114	0.044	0.063	0.020	0.021	0.036	3.4	15.468	0.039
B128-G187	10.69919	41.18718	1	2	old	5.8	17.405	1.689	0.766	0.404	0.379	0.026	0.053	0.020	0.022	0.028	-	-	-
B129	10.70135	41.41852	1	1	old	2.8	18.480	-	1.921	0.976	0.624	0.134	-	0.022	0.015	0.016	-	-	-
B130-G188	10.70356	41.49794	1	1	old	5.2	17.467	1.808	0.963	0.506	0.281	0.031	0.063	0.019	0.018	0.024	-	-	-
B262	10.70854	41.32447	1	2	old	-	-	-	-	-	-	-	-	-	-	-	-	-	-
BH18	10.71132	41.17596	1	2	old	3.4	18.650	1.705	0.762	0.365	0.227	0.086	0.114	0.035	0.040	0.061	-	-	-
B131-G189	10.71167	41.28542	1	1	old	5.2	15.789	1.596	0.682	0.354	0.219	0.069	0.021	0.013	0.013	0.016	-	-	-
B132-NB15	10.71421	41.26117	1	2	old	5.2	18.119	-	1.109	0.573	-	0.042	-	0.028	0.026	-	-	-	-
B134-G190	10.71522	41.23433	1	1	old	6.4	16.759	1.562	0.592	0.299	0.292	0.028	0.033	0.017	0.018	0.024	-	-	-
SK055A	10.71609	40.73608	1	1	unknown	5.2	19.041	0.918	0.717	0.341	0.221	0.081	0.097	0.035	0.038	0.067	3.4	15.455	0.078
B078D	10.71629	41.36811	1	2	old	-	-	-	-	-	-	-	-	-	-	-	-	-	-
B135-G192	10.71653	41.51895	1	1	old	6.4	16.441	1.531	0.778	0.399	0.234	0.030	0.029	0.014	0.014	0.018	5.2	13.140	0.045
B264-NB19	10.72162	41.27067	1	2	old	-	-	-	-	-	-	-	-	-	-	-	-	-	-
B136-G194	10.72336	41.32626	1	1	old	4.6	17.220	1.472	0.553	0.314	0.274	0.023	0.044	0.020	0.023	0.032	-	-	-

B137-G195	10.72495	41.53732	1	1	old	4.0	18.406	-	1.058	0.556	0.335	0.031	-	0.028	0.027	0.037	3.4	14.256	0.160
HEC7	10.72917	43.95778	1	8	old	-	-	-	-	-	-	-	-	-	-	-	-	-	-
AU010	10.74212	41.28132	1	1	old	5.8	17.570	2.054	0.675	0.356	0.378	0.146	0.090	0.025	0.029	0.038	-	-	-
B140-G196	10.74478	41.14799	1	1	old	5.2	17.880	1.868	0.834	0.376	0.244	0.043	0.085	0.025	0.027	0.039	-	-	-
B087D	10.74546	41.15242	1	2	old	4.0	17.997	1.508	0.660	0.383	0.130	0.043	0.068	0.027	0.031	0.048	-	-	-
B141-G197	10.74703	41.54651	1	1	old	4.6	17.412	1.504	0.828	0.436	0.242	0.021	0.048	0.018	0.018	0.025	3.4	14.073	0.137
B143-G198	10.74850	41.32206	1	1	old	6.4	16.485	1.997	0.821	0.451	0.276	0.043	0.036	0.015	0.015	0.018	-	-	-
B144	10.74942	41.26829	1	1	old	4.0	17.254	1.955	0.830	0.508	0.358	0.034	0.056	0.019	0.019	0.024	-	-	-
B090D	10.75508	41.26955	1	1	old	2.8	17.944	2.039	0.881	0.535	0.444	0.047	0.075	0.021	0.022	0.026	-	-	-
B091D-D058	10.75598	41.50481	1	1	old	5.2	15.863	1.750	0.795	0.474	0.233	0.028	0.024	0.013	0.013	0.015	4.6	12.300	0.063
B145	10.75659	41.20747	1	2	old	4.0	18.518	1.443	0.678	0.333	0.238	0.116	0.096	0.037	0.044	0.068	-	-	-
B265	10.75814	40.88396	1	1	old	3.4	18.964	1.440	0.817	0.361	0.204	0.054	0.112	0.029	0.029	0.049	-	-	-
B146	10.76212	41.25630	1	1	old	4.0	17.421	1.656	0.782	0.449	0.341	0.018	0.051	0.020	0.022	0.027	-	-	-
B147-G199	10.76375	41.35604	1	1	old	7.6	16.137	1.959	0.831	0.397	0.297	0.020	0.032	0.013	0.014	0.016	-	-	-
B266	10.76465	41.67541	1	1	old	3.4	19.004	1.678	1.060	0.588	0.328	0.079	0.162	0.034	0.031	0.044	2.8	14.794	0.070
B148-G200	10.76607	41.30136	1	1	old	4.0	16.263	1.435	0.678	0.350	0.221	0.038	0.024	0.014	0.015	0.018	-	-	-
B149-G201	10.77280	41.57421	1	1	old	5.8	17.503	1.653	0.892	0.475	0.281	0.020	0.059	0.018	0.018	0.025	4.6	13.846	0.054
B467-G202	10.77679	42.03033	1	1	old	5.8	17.819	1.464	0.623	0.249	0.118	0.027	0.054	0.018	0.019	0.030	4.0	15.242	0.039
B268	10.77997	41.19677	1	2	old	2.8	18.878	-	0.839	0.530	0.348	0.041	-	0.034	0.036	0.048	-	-	-
B269	10.78072	41.45907	1	2	old	4.6	19.176	-	1.203	0.534	0.451	0.117	-	0.046	0.042	0.057	2.8	15.229	0.112
B150-G203	10.78128	41.33883	1	2	old	3.4	17.234	1.888	0.831	0.454	0.332	0.024	0.047	0.017	0.018	0.022	-	-	-
PHF6-1	10.78325	41.30506	1	-	old	3.4	18.125	2.090	0.808	0.415	0.358	0.185	0.105	0.026	0.029	0.038	-	-	-
B151-G205	10.78976	41.35892	1	1	old	4.6	15.456	2.022	1.023	0.534	0.345	0.036	0.022	0.012	0.012	0.013	-	-	-
B152-G207	10.79167	41.30447	1	1	old	5.2	16.570	1.605	0.745	0.458	0.250	0.037	0.030	0.015	0.016	0.019	-	-	-
B356-G206	10.79316	41.84199	1	1	old	5.8	17.415	1.469	0.746	0.386	0.240	0.018	0.046	0.016	0.016	0.025	5.2	14.186	0.057
B153	10.79421	41.24760	1	1	old	4.0	16.688	1.809	0.804	0.438	0.333	0.030	0.035	0.016	0.016	0.019	-	-	-
SK060A	10.79939	40.93483	1	1	na	4.0	19.742	-	1.050	0.395	0.227	0.094	-	0.049	0.045	0.081	-	-	-
B154-G208	10.80183	41.26806	1	1	old	3.4	17.312	1.754	0.803	0.352	0.246	0.059	0.046	0.018	0.019	0.026	-	-	-
B468	10.80228	39.79926	1	1	old	5.8	18.372	1.530	0.668	0.368	0.278	0.054	0.081	0.024	0.023	0.038	-	-	-
B357-G209	10.80513	40.18236	1	1	old	6.4	17.009	1.607	0.723	0.366	0.265	0.024	0.038	0.014	0.014	0.018	-	-	-
B155-G210	10.80576	41.05782	1	1	old	3.4	18.451	1.735	0.843	0.463	0.292	0.021	0.094	0.022	0.021	0.030	-	-	-
SK061A	10.80641	41.64102	1	1	unknown	2.8	20.036	1.274	0.589	0.342	-0.086	0.061	0.234	0.070	0.087	0.201	-	-	-
B156-G211	10.80719	41.02159	1	1	old	5.8	17.275	1.413	0.637	0.318	0.194	0.048	0.038	0.016	0.016	0.023	-	-	-

B157-G212	10.80821	41.18880	1	1	old	4.0	17.913	1.171	0.574	0.238	0.073	0.049	0.051	0.026	0.033	0.055	-	-	-
B158-G213	10.80996	41.12253	1	1	old	7.6	15.079	1.623	0.734	0.359	0.232	0.016	0.017	0.012	0.012	0.013	-	-	-
SK062A	10.81053	41.89633	1	1	unknown	2.8	19.869	1.451	0.515	0.329	-0.081	0.096	0.218	0.046	0.054	0.164	-	-	-
B159	10.81099	41.42040	1	1	old	3.4	18.111	2.227	1.042	0.554	0.342	0.032	0.125	0.022	0.021	0.028	-	-	-
B160-G214	10.81224	41.02652	1	1	old	4.6	18.232	1.158	0.520	0.274	0.043	0.027	0.060	0.023	0.026	0.048	-	-	-
B161-G215	10.81421	41.19027	1	1	old	4.6	16.725	1.406	0.666	0.326	0.216	0.031	0.029	0.016	0.017	0.022	-	-	-
B162-G216	10.81834	41.40127	1	1	old	4.6	18.007	1.706	0.827	0.441	0.355	0.040	0.089	0.024	0.026	0.036	-	-	-
B163-G217	10.82346	41.46252	1	1	old	8.8	15.497	1.935	0.850	0.459	0.338	0.015	0.023	0.012	0.012	0.013	8.2	11.575	0.032
B358-G219	10.82438	39.82032	1	1	old	10.6	15.383	1.254	0.499	0.245	0.150	0.023	0.016	0.012	0.012	0.014	-	-	-
B164-V253	10.82553	41.20813	1	1	old	3.4	18.366	1.896	0.855	0.473	0.348	0.069	0.109	0.029	0.031	0.042	-	-	-
B165-G218	10.82590	41.18186	1	1	old	5.8	16.762	1.243	0.547	0.275	0.180	0.028	0.028	0.017	0.019	0.025	-	-	-
SK064A	10.82668	40.98994	1	1	unknown	2.8	20.361	1.159	0.701	0.517	0.227	0.054	0.239	0.065	0.066	0.115	-	-	-
B167	10.83802	41.23563	1	1	old	4.0	17.824	1.826	0.823	0.454	0.278	0.025	0.077	0.024	0.026	0.035	-	-	-
B168	10.84385	41.73489	1	1	old	3.4	18.770	1.782	1.340	0.750	0.514	0.066	0.145	0.026	0.021	0.025	3.4	13.625	0.065
B169	10.84579	41.25704	1	1	old	5.2	17.732	2.046	0.930	0.465	0.286	0.097	0.090	0.023	0.024	0.032	-	-	-
B170-G221	10.84787	40.84489	1	1	old	5.2	17.848	-	0.777	0.397	0.212	0.025	-	0.019	0.019	0.027	3.4	14.620	0.039
SK066A	10.85032	41.64507	1	1	na	3.4	20.030	-	0.765	0.553	0.487	0.201	-	0.057	0.051	0.091	3.4	15.623	0.176
B272-V294	10.85623	41.61995	1	1	old	4.0	18.871	2.283	0.947	0.656	0.339	0.089	0.281	0.035	0.033	0.047	4.0	14.497	0.153
B171-G222	10.85665	41.26032	1	1	old	7.0	15.733	1.821	0.805	0.415	0.294	0.021	0.023	0.013	0.013	0.015	-	-	-
B172-G223	10.85832	41.35884	1	2	old	5.2	17.154	1.662	0.764	0.432	0.347	0.034	0.044	0.019	0.020	0.025	-	-	-
B173-G224	10.86983	41.37699	1	2	old	2.8	18.138	1.624	0.780	0.450	0.312	0.104	0.063	0.022	0.023	0.030	-	-	-
B174-G226	10.87623	41.64896	1	1	old	8.2	15.949	1.642	0.845	0.434	0.256	0.017	0.025	0.013	0.012	0.015	8.2	12.390	0.037
B176-G227	10.87690	40.81964	1	1	old	7.0	16.886	1.367	0.597	0.297	0.165	0.037	0.032	0.015	0.015	0.021	5.8	14.170	0.033
B177-G228	10.87713	41.09509	1	2	old	4.0	18.651	1.255	0.764	0.413	0.333	0.027	0.086	0.027	0.027	0.040	3.4	15.602	0.168
B178-G229	10.87825	41.35459	1	1	old	8.8	15.362	1.359	0.621	0.311	0.198	0.013	0.018	0.012	0.013	0.015	-	-	-
B179-G230	10.87960	41.30407	1	1	old	7.6	15.739	1.502	0.690	0.308	0.194	0.018	0.021	0.013	0.013	0.016	-	-	-
B180-G231	10.88221	41.12952	1	1	old	6.4	16.540	1.566	0.763	0.367	0.220	0.017	0.028	0.013	0.013	0.016	-	-	-
B181-G232	10.88523	41.48537	1	2	old	5.8	17.351	1.599	0.778	0.393	0.257	0.025	0.051	0.018	0.019	0.026	4.0	13.852	0.049
H18	10.90012	44.98314	1	1	old	-	-	-	-	-	-	-	-	-	-	-	-	-	-
B182-G233	10.90280	41.13670	1	1	old	10.0	15.838	1.600	0.826	0.427	0.274	0.016	0.022	0.012	0.012	0.014	-	-	-
B183-G234	10.90388	41.03396	1	1	old	7.0	16.441	1.745	0.800	0.406	0.267	0.026	0.029	0.013	0.013	0.015	5.8	12.926	0.034
B185-G235	10.90534	41.24543	1	1	old	5.2	16.040	1.695	0.767	0.394	0.253	0.023	0.024	0.013	0.014	0.016	-	-	-
B184-G236	10.90626	41.60961	1	1	old	6.4	17.796	2.261	0.914	0.503	0.342	0.032	0.119	0.021	0.021	0.028	5.2	13.734	0.079

B186	10.90923	41.60681	1	2	old	4.6	18.670	-	0.981	0.563	0.296	0.078	-	0.031	0.030	0.044	4.6	14.444	0.044
B187-G237	10.91093	41.49634	1	1	old	4.6	17.724	1.644	0.882	0.453	0.275	0.043	0.067	0.020	0.020	0.028	3.4	14.127	0.047
B188-G239	10.92297	41.40721	1	1	old	5.2	17.364	1.332	0.564	0.293	0.200	0.031	0.040	0.019	0.022	0.032	-	-	-
B189-G240	10.92663	41.58984	1	1	old	7.0	17.558	2.216	0.910	0.479	0.327	0.038	0.098	0.019	0.019	0.026	5.2	13.485	0.146
B190-G241	10.93074	41.56832	1	1	old	7.6	17.235	1.474	0.733	0.398	0.213	0.033	0.045	0.018	0.018	0.026	4.6	14.176	0.089
B194-G243	10.93828	41.10239	1	1	old	4.6	17.555	1.380	0.613	0.325	0.177	0.029	0.044	0.017	0.018	0.026	4.0	14.849	0.056
B193-G244	10.93962	41.61601	1	1	old	10.6	15.781	1.939	0.831	0.446	0.290	0.028	0.027	0.012	0.012	0.014	8.8	12.067	0.048
SK071A	10.94336	41.65794	1	1	na	3.4	20.282	-	1.088	0.538	0.191	0.241	-	0.074	0.066	0.122	3.4	16.037	0.575
SK072A	10.94450	41.37451	1	1	na	5.2	17.958	1.915	0.815	0.440	0.340	0.088	0.092	0.024	0.025	0.034	-	-	-
B103D-G245	10.94804	41.45221	1	1	old	4.0	18.170	1.718	0.752	0.429	0.182	0.071	0.090	0.027	0.029	0.043	-	-	-
B472-D064	10.95173	41.44809	1	1	old	8.8	15.549	1.425	0.667	0.302	0.185	0.017	0.019	0.012	0.013	0.015	-	-	-
SK073A	10.95221	41.13006	1	1	na	4.0	18.611	1.562	0.840	0.466	0.348	0.030	0.106	0.026	0.025	0.036	-	-	-
B196-G246	10.95239	40.71025	1	1	old	5.2	17.719	1.348	0.686	0.355	0.232	0.026	0.051	0.017	0.017	0.026	4.0	14.630	0.065
B197-G247	10.95716	41.50281	1	1	old	4.6	18.269	2.241	0.888	0.546	0.320	0.026	0.151	0.027	0.026	0.036	3.4	14.259	0.097
B199-G248	10.95759	40.97071	1	1	old	5.8	17.884	1.337	0.583	0.311	0.149	0.039	0.054	0.020	0.021	0.034	4.0	15.178	0.045
B198-G249	10.95874	41.53133	1	1	old	4.6	18.191	1.463	0.682	0.372	0.048	0.056	0.083	0.026	0.029	0.052	2.8	15.345	0.113
B200	10.96007	41.48960	1	1	old	3.4	19.014	2.006	0.894	0.512	0.245	0.047	0.197	0.039	0.039	0.058	2.8	15.730	0.181
B201-G250	10.97016	41.16611	1	1	old	7.0	16.464	1.478	0.652	0.327	0.190	0.049	0.027	0.014	0.014	0.017	-	-	-
B202-G251	10.97784	41.00895	1	1	old	4.6	18.203	1.545	0.703	0.335	0.150	0.056	0.077	0.022	0.023	0.037	4.0	15.265	0.083
B203-G252	10.98260	41.54306	1	1	old	5.2	17.151	1.602	0.713	0.335	0.210	0.038	0.040	0.017	0.018	0.024	3.4	14.028	0.110
B204-G254	10.98510	41.36747	1	1	old	5.2	16.152	1.687	0.740	0.367	0.229	0.018	0.025	0.013	0.014	0.016	-	-	-
B361-G255	10.98787	40.23375	1	1	old	8.8	17.247	1.257	0.555	0.262	0.161	0.039	0.038	0.016	0.016	0.024	5.2	14.778	0.046
B205-G256	10.99239	41.41065	1	1	old	8.2	15.819	1.484	0.681	0.342	0.211	0.020	0.021	0.013	0.013	0.015	-	-	-
B206-G257	10.99424	41.50502	1	1	old	8.2	15.432	1.467	0.665	0.309	0.201	0.016	0.018	0.012	0.012	0.014	4.6	12.454	0.032
B110D-V296	10.99638	41.61153	1	2	old	3.4	18.785	1.890	0.594	0.391	0.176	0.219	0.160	0.031	0.034	0.062	2.8	15.397	0.359
B207-G258	10.99776	41.10297	1	1	old	4.6	17.702	1.404	0.622	0.291	0.137	0.034	0.049	0.018	0.019	0.030	3.4	15.020	0.083
B208-G259	11.00032	41.38654	1	1	old	4.0	18.359	1.675	0.858	0.451	0.371	0.038	0.101	0.029	0.030	0.041	4.0	14.663	0.140
M009	11.00348	41.28679	1	2	old	4.6	18.225	1.293	0.630	0.286	0.366	0.108	0.070	0.029	0.035	0.050	3.4	15.140	0.082
G260	11.00352	42.58008	1	1	old	9.4	17.264	1.449	0.610	0.301	0.176	0.029	0.041	0.016	0.016	0.023	5.2	14.677	0.040
B209-G261	11.01097	41.42406	1	1	old	5.8	17.000	1.511	0.664	0.317	0.159	0.018	0.036	0.017	0.018	0.025	3.4	14.131	0.074
B211-G262	11.01214	41.33464	1	1	old	5.8	16.925	1.267	0.579	0.292	0.176	0.038	0.031	0.017	0.019	0.026	4.0	14.178	0.078
B212-G263	11.01281	41.08231	1	1	old	10.0	15.774	1.285	0.587	0.281	0.137	0.019	0.019	0.012	0.012	0.015	6.4	13.109	0.033
B213-G264	11.01463	41.51075	1	1	old	4.6	17.362	1.612	0.778	0.398	0.234	0.028	0.045	0.018	0.018	0.025	4.0	13.840	0.049

B214-G265	11.01641	41.43850	1	1	old	4.0	18.048	1.273	0.668	0.328	0.242	0.028	0.059	0.026	0.029	0.044	3.4	14.841	0.042
B215-G266	11.02663	41.52882	1	1	old	6.4	17.608	1.922	0.765	0.430	0.289	0.064	0.070	0.020	0.021	0.028	4.0	14.131	0.066
SK083A	11.04164	41.85794	1	1	unknown	2.8	20.010	1.163	0.966	0.473	0.305	0.118	0.205	0.053	0.052	0.088	2.8	16.317	0.136
G268	11.04174	42.78273	1	3	old	9.4	16.966	1.674	0.760	0.397	0.289	0.021	0.037	0.014	0.014	0.018	7.0	13.532	0.068
B217-G269	11.04416	41.39752	1	1	old	7.0	16.905	1.545	0.733	0.392	0.227	0.030	0.036	0.016	0.017	0.022	5.2	13.657	0.072
B218-G272	11.05968	41.32206	1	1	old	10.0	15.079	1.567	0.703	0.364	0.237	0.026	0.017	0.012	0.012	0.013	8.2	11.833	0.024
H19	11.06212	38.42848	1	1	old	6.4	17.754	1.472	0.588	0.279	0.149	0.035	0.061	0.018	0.018	0.026	-	-	-
B219-G271	11.06263	40.94646	1	1	old	7.0	16.867	1.665	0.760	0.373	0.281	0.026	0.037	0.014	0.014	0.017	5.8	13.543	0.028
B363-G274	11.07179	40.55972	1	1	old	5.8	18.143	1.225	0.523	0.256	0.125	0.052	0.066	0.021	0.022	0.039	4.0	15.705	0.088
B220-G275	11.08102	41.50969	1	1	old	5.8	16.946	1.307	0.622	0.287	0.174	0.027	0.031	0.016	0.017	0.024	4.0	14.232	0.075
B221-G276	11.09609	41.55177	1	1	old	5.8	17.237	1.565	0.755	0.390	0.231	0.026	0.042	0.017	0.018	0.024	5.2	13.865	0.099
SK086A	11.10863	41.58734	1	1	na	5.8	18.341	-	0.872	0.478	0.303	0.066	-	0.031	0.031	0.045	5.2	14.792	0.136
B224-G279	11.11286	41.48049	1	1	old	10.6	15.592	1.287	0.599	0.278	0.156	0.032	0.020	0.013	0.013	0.016	7.6	13.025	0.036
B279-D068	11.11671	41.73623	1	2	old	4.6	18.977	1.784	0.879	0.551	0.543	0.045	0.203	0.036	0.035	0.048	4.0	14.302	0.067
B225-G280	11.12316	41.35993	1	1	old	8.8	14.590	1.736	0.767	0.396	0.288	0.016	0.016	0.011	0.011	0.012	7.0	11.031	0.023
B228-G281	11.13842	41.69107	1	1	old	5.2	17.277	1.622	0.820	0.405	0.232	0.038	0.048	0.016	0.016	0.023	4.0	13.789	0.043
B229-G282	11.14085	41.64127	1	1	old	9.4	16.745	1.213	0.568	0.274	0.170	0.020	0.029	0.016	0.017	0.024	6.4	14.301	0.098
B230-G283	11.14660	40.95342	1	1	old	8.2	16.325	1.272	0.544	0.260	0.177	0.024	0.023	0.013	0.013	0.017	6.4	13.823	0.039
B365-G284	11.15185	42.28902	1	1	old	8.2	16.985	1.303	0.624	0.302	0.167	0.029	0.034	0.015	0.015	0.024	5.2	14.232	0.082
B231-G285	11.16079	41.46302	1	1	old	4.6	17.696	1.400	0.686	0.354	0.195	0.024	0.050	0.020	0.022	0.033	2.8	14.800	0.053
B232-G286	11.16762	41.25012	1	1	old	7.0	15.994	1.341	0.605	0.303	0.156	0.020	0.020	0.013	0.013	0.015	4.6	13.279	0.028
B233-G287	11.17549	41.73180	1	1	old	5.8	16.220	1.405	0.654	0.355	0.223	0.022	0.024	0.013	0.013	0.016	5.8	13.071	0.036
B281-G288	11.17858	41.33570	1	1	interm	6.4	18.072	1.624	0.728	0.433	0.217	0.103	0.084	0.022	0.022	0.034	4.0	14.597	0.048
B234-G290	11.19334	41.48827	1	1	old	5.2	17.272	1.659	0.756	0.355	0.236	0.019	0.045	0.017	0.018	0.024	3.4	13.895	0.041
B366-G291	11.19452	42.06399	1	1	old	7.6	16.500	1.319	0.575	0.316	0.110	0.071	0.029	0.014	0.014	0.021	7.0	13.940	0.065
B255D-D072	11.20232	42.10370	1	1	na	6.4	18.474	1.735	0.763	0.391	0.275	0.060	0.134	0.024	0.025	0.049	4.6	15.557	0.076
B283-G296	11.23083	41.28332	1	1	old	4.6	18.256	1.637	0.781	0.404	0.160	0.043	0.087	0.022	0.022	0.035	4.6	14.842	0.065
B235-G297	11.24136	41.48998	1	1	old	6.4	16.736	1.516	0.693	0.405	0.277	0.015	0.031	0.015	0.015	0.019	5.8	13.259	0.042
SK093A	11.24356	41.94375	1	1	unknown	3.4	20.342	-	0.713	0.411	0.128	0.231	-	0.086	0.091	0.200	-	-	-
B236-G298	11.28712	40.84132	1	1	old	6.4	17.702	1.409	0.569	0.236	0.180	0.050	0.057	0.018	0.018	0.029	5.2	15.148	0.068
B237-G299	11.28852	41.37624	1	1	old	8.8	17.489	1.316	0.650	0.325	0.162	0.047	0.046	0.018	0.019	0.028	6.4	14.811	0.133
B370-G300	11.31000	41.96132	1	1	old	7.6	16.613	1.442	0.733	0.386	0.245	0.017	0.030	0.014	0.014	0.018	5.8	13.473	0.038
B238-G301	11.31121	41.32694	1	1	old	6.4	16.905	1.561	0.753	0.381	0.205	0.026	0.034	0.014	0.014	0.018	5.2	13.679	0.031

B239-M74	11.31499	41.58809	1	1	old	4.6	17.600	1.599	0.683	0.332	0.200	0.042	0.052	0.019	0.020	0.030	3.4	14.524	0.063
B240-G302	11.35437	41.10616	1	1	old	10.6	15.534	1.359	0.611	0.285	0.182	0.018	0.019	0.012	0.012	0.014	8.8	12.780	0.030
HEC8	11.36205	40.22977	1	8	old	12.0	19.402	-	0.639	0.561	-	0.110	-	0.135	0.117	-	-	-	-
B287	11.36873	41.50128	1	2	old	4.6	18.294	1.438	0.534	0.351	0.237	0.087	0.078	0.024	0.026	0.042	4.6	15.622	0.249
B372-G304	11.38908	42.00678	1	1	old	5.8	16.934	1.388	0.675	0.324	0.179	0.030	0.034	0.015	0.015	0.022	5.2	14.009	0.040
B373-G305	11.42436	41.75929	1	1	old	7.6	16.095	1.731	0.793	0.428	0.295	0.021	0.025	0.013	0.013	0.015	5.8	12.511	0.038
SK104A	11.43463	41.95772	1	1	unknown	4.0	18.357	1.545	0.782	0.300	0.275	0.039	0.085	0.024	0.025	0.041	2.8	15.056	0.068
V129-BA4	11.43624	41.86657	1	5	old	5.8	17.352	1.373	0.613	0.305	0.155	0.056	0.039	0.017	0.018	0.027	3.4	14.642	0.077
B375-G307	11.43983	41.66175	1	1	old	4.6	18.038	1.687	0.775	0.352	0.178	0.027	0.077	0.022	0.023	0.037	4.0	14.827	0.086
B377-G308	11.45114	40.63456	1	1	old	5.8	17.437	1.436	0.564	0.264	0.174	0.022	0.038	0.016	0.016	0.025	-	-	-
H20	11.46881	39.93116	1	1	old	7.0	18.980	-	0.429	0.198	0.025	0.056	-	0.033	0.038	0.088	-	-	-
B378-G311	11.48848	41.89188	1	1	old	4.6	17.945	1.278	0.570	0.311	0.115	0.029	0.053	0.021	0.023	0.039	3.4	15.334	0.069
B379-G312	11.49511	40.70873	1	1	old	8.2	16.561	1.748	0.751	0.384	0.299	0.022	0.034	0.013	0.013	0.015	-	-	-
B381-G315	11.52728	41.34969	1	1	old	10.0	16.046	1.566	0.711	0.326	0.209	0.020	0.024	0.013	0.012	0.015	-	-	-
B486-G316	11.53571	40.96769	1	1	old	5.2	17.953	1.244	0.551	0.259	0.195	0.028	0.056	0.019	0.019	0.032	-	-	-
B382-G317	11.54312	41.62790	1	1	old	4.6	17.714	1.282	0.618	0.265	0.099	0.023	0.045	0.018	0.019	0.031	3.4	14.964	0.043
B383-G318	11.54978	41.32822	1	1	old	7.6	16.195	1.702	0.764	0.407	0.286	0.019	0.026	0.013	0.012	0.014	-	-	-
B384-G319	11.59138	40.28322	1	1	old	7.0	16.293	1.680	0.755	0.374	0.252	0.017	0.024	0.013	0.012	0.014	-	-	-
B386-G322	11.61255	42.03132	1	1	old	8.2	15.973	1.549	0.678	0.342	0.223	0.015	0.022	0.013	0.012	0.015	5.8	12.925	0.025
B387-G323	11.63959	40.73711	1	1	old	8.2	17.318	1.321	0.551	0.274	0.149	0.042	0.035	0.016	0.016	0.025	-	-	-
G327-MVI	11.70622	42.74636	1	1	old	7.6	16.272	1.341	0.593	0.301	0.162	0.020	0.024	0.013	0.013	0.017	6.4	13.594	0.043
B391-G328	11.74205	41.56579	1	1	old	6.4	17.596	1.447	0.677	0.295	0.170	0.024	0.049	0.017	0.017	0.026	4.0	14.584	0.175
B393-G330	11.75501	41.40185	1	1	old	8.2	17.300	1.527	0.708	0.319	0.237	0.029	0.047	0.016	0.016	0.023	7.0	14.296	0.058
SK109A	11.82022	41.05324	1	1	unknown	4.0	19.490	0.865	0.574	0.190	0.133	0.051	0.137	0.039	0.044	0.103	4.0	16.129	0.134
B396-G335	11.85482	40.36168	1	1	old	5.8	17.603	1.262	0.499	0.252	0.135	0.063	0.039	0.017	0.018	0.028	-	-	-
B397-G336	11.86348	41.20290	1	1	old	6.4	16.763	1.400	0.626	0.291	0.191	0.024	0.031	0.014	0.014	0.018	5.2	13.926	0.037
G339-BA30	11.95927	43.15457	1	1	star	10.0	17.528	1.278	0.647	0.312	0.223	0.037	0.043	0.017	0.017	0.025	-	-	-
SK110A	11.98245	41.45902	1	1	unknown	2.8	19.839	-	0.570	0.216	0.316	0.060	-	0.039	0.043	0.087	-	-	-
B398-G341	11.99074	41.81264	1	1	old	5.2	17.970	1.866	0.758	0.424	0.267	0.024	0.082	0.019	0.018	0.027	4.0	14.454	0.036
B399-G342	11.99811	41.59126	1	1	old	6.4	17.654	1.200	0.525	0.272	0.153	0.035	0.044	0.017	0.018	0.031	4.0	15.190	0.091
B400-G343	12.00599	42.42583	1	1	old	7.6	16.839	1.466	0.668	0.334	0.199	0.023	0.030	0.014	0.014	0.019	5.2	13.857	0.056
B401-G344	12.03546	41.67830	1	1	old	7.0	17.100	1.240	0.518	0.260	0.166	0.037	0.033	0.015	0.015	0.023	4.6	14.658	0.095
SK111A	12.06096	41.48873	1	1	unknown	3.4	19.600	-	0.794	0.267	0.161	0.081	-	0.036	0.036	0.076	-	-	-

B402-G346	12.15023	42.02624	1	1	unknown	7.0	17.707	1.468	0.706	0.385	0.266	0.041	0.054	0.017	0.017	0.025	5.2	14.423	0.063
BA11	12.19003	42.39384	1	1	old	6.4	18.035	1.288	0.609	0.264	0.068	0.043	0.058	0.020	0.021	0.041	3.4	15.443	0.067
H21	12.21081	41.14340	1	1	old	5.8	19.165	1.614	0.786	0.296	0.287	0.122	0.176	0.037	0.035	0.067	-	-	-
B337D	12.29681	41.12245	1	2	old	4.0	18.476	1.462	0.606	0.308	0.144	0.054	0.078	0.024	0.024	0.044	-	-	-
B403-G348	12.32344	41.58564	1	1	old	7.6	16.698	1.607	0.752	0.352	0.261	0.022	0.033	0.014	0.013	0.016	-	-	-
B405-G351	12.41585	41.59160	1	1	old	8.8	15.493	1.388	0.608	0.291	0.182	0.017	0.019	0.012	0.012	0.013	6.4	12.660	0.028
H22	12.43605	38.31052	1	1	old	7.6	17.371	1.523	0.561	0.261	0.142	0.034	0.048	0.016	0.016	0.023	-	-	-
B407-G352	12.54149	41.68366	1	1	old	8.2	16.515	1.738	0.759	0.401	0.280	0.026	0.033	0.013	0.013	0.015	5.8	13.101	0.032
G353-BA13	12.57577	42.59559	1	1	unknown	8.2	17.469	1.367	0.535	0.283	0.090	0.046	0.044	0.017	0.017	0.028	-	-	-
MGC1	12.67688	32.91631	1	1	old	-	-	-	-	-	-	-	-	-	-	-	-	-	-
HEC9	12.69137	41.69264	1	8	old	12.0	19.035	-	0.731	0.171	-	0.077	-	0.092	0.100	-	-	-	-
EXT8	13.31045	41.55686	1	1	unknown	10.0	15.873	1.114	0.545	0.222	0.106	0.018	0.020	0.012	0.012	0.015	-	-	-
H23	13.60396	39.71554	1	1	old	7.0	17.205	1.555	0.693	0.302	0.155	0.022	0.045	0.015	0.015	0.019	-	-	-
HEC10	13.65148	44.97887	1	8	old	12.0	19.316	-	0.487	0.179	-	0.081	-	0.118	0.147	-	-	-	-
HEC11	13.82202	38.85081	1	8	old	8.0	18.872	-	0.540	0.225	-	0.043	-	0.055	0.064	-	-	-	-
H24	13.93309	42.77114	1	1	old	7.6	18.244	1.625	0.705	0.296	0.199	0.032	0.088	0.023	0.023	0.040	-	-	-
HEC12	14.56425	38.05056	1	8	old	-	-	-	-	-	-	-	-	-	-	-	-	-	-
HEC13	14.57054	37.23081	1	8	old	-	-	-	-	-	-	-	-	-	-	-	-	-	-
H26	14.86404	37.69281	1	1	old	-	-	-	-	-	-	-	-	-	-	-	-	-	-
H25	14.89392	44.09412	1	1	old	8.2	17.197	1.319	0.577	0.295	0.164	0.058	0.039	0.016	0.016	0.023	-	-	-
B517	14.99961	41.90184	1	1	unknown	10.6	16.892	1.203	0.642	0.295	0.131	0.031	0.033	0.015	0.014	0.022	-	-	-
H27	16.85958	35.77958	1	1	old	-	-	-	-	-	-	-	-	-	-	-	-	-	-

[1]Cluster name, taken from the Revised Bologna Catalogue (Galleti *et al.*, 2004)

[2]Position of object in SDSS *r*-band image [J2000, degrees]

[3]Classification of source as described in chapter 2. Options for flag, f: 1-old globular cluster; 2-candidate cluster (21-candidate old cluster, 23-candidate young cluster); 3-young cluster; 4-galaxy; 5-HII region; 6-stellar source. Flags f_{RBC} and f_{C09} indicate the previous classifications of the source from the RBC v3.5 of Galleti *et al.* (2004) and from the catalogue of Caldwell *et al.* (2009), respectively.

[4]Aperture size used to measure the total magnitude of the cluster [arcsec]

[5]Error on the total magnitude, includes the statistical, calibration and systematic errors

B
Catalogue of young clusters in M31 (table 2.1: young clusters)

This table lists all objects classified as young clusters in M31. Our classification criteria are discussed in chapter 2. We also include the previous classifications of these sources from the catalogues of Galleti *et al.* (2004) and Caldwell *et al.* (2009). Where available, we include optical and near infrared photometry of these clusters in the *u*,*g*,*r*,*i*,*z* and K-bands. Details of this catalogue are discussed in chapter 2.

GC Name[1]	RA[2]	DEC[2]	Classification[3]			Photometry													
			f	f_{RBC}	f_{C09}	R_g^4	g	$(u-g)$	$(g-r)$	$(r-i)$	$(i-z)$	$\sigma^5_{g,tot}$	$\sigma_{(u-g)}$	$\sigma_{(g-r)}$	$\sigma_{(r-i)}$	$\sigma_{(i-z)}$	R_K^4	K_s	$\sigma^5_{K,tot}$
B431-G027	9.72821	40.58231	3	1	young	5.8	17.709	1.226	0.224	0.273	-0.084	0.092	0.053	0.021	0.024	0.057	3.4	15.964	0.287
SK007A	9.93363	40.85526	3	1	unknown	4.0	17.724	0.238	-0.082	0.086	-0.012	0.031	0.028	0.023	0.031	0.073	2.8	15.932	0.130
B314-G037	9.93581	40.23553	3	7	young	7.6	17.647	1.354	0.375	0.171	0.247	0.054	0.052	0.020	0.023	0.041	4.0	16.269	0.268
B315-G038	9.95223	40.52513	3	1	young	10.0	16.314	0.961	0.235	0.150	0.183	0.026	0.021	0.014	0.015	0.021	5.2	14.393	0.041
DAO30	9.96162	40.30409	3	1	young	5.8	18.596	1.558	0.611	0.226	0.306	0.050	0.113	0.028	0.031	0.057	3.4	15.814	0.232
KHM31-22	9.99457	40.59006	3	-	young	3.4	19.997	1.008	0.465	0.364	0.506	0.213	0.193	0.074	0.085	0.137	-	-	-
WH2	9.99996	40.55755	3	-	young	4.6	18.763	0.939	0.033	-0.199	0.034	0.077	0.080	0.042	0.074	0.188	-	-	-
B318-G042	10.00358	40.56890	3	1	young	6.4	16.859	0.762	0.010	0.031	-0.117	0.022	0.023	0.017	0.021	0.041	-	-	-
B319-G044	10.01279	40.56620	3	1	young	6.4	17.466	0.911	0.115	0.154	0.178	0.027	0.034	0.021	0.025	0.045	-	-	-
KHM31-37	10.04573	40.60316	3	-	young	3.4	18.162	0.692	0.060	0.026	-0.368	0.035	0.039	0.026	0.036	0.104	-	-	-
B321-G046	10.06409	40.46276	3	1	young	7.6	17.637	1.105	0.174	0.100	0.110	0.058	0.043	0.021	0.026	0.053	-	-	-
B189D-G047	10.06455	40.66653	3	1	young	6.4	18.024	0.842	0.229	-0.112	0.216	0.031	0.047	0.026	0.038	0.075	3.4	16.178	0.109
B322-G049	10.07186	40.65123	3	1	young	5.8	17.523	0.716	0.003	-0.028	-0.195	0.043	0.032	0.022	0.030	0.074	2.8	17.107	0.154
B323	10.07620	40.54580	3	2	young	7.0	17.639	1.558	0.272	0.115	0.128	0.076	0.065	0.023	0.029	0.056	-	-	-
B442-D033	10.08081	40.62475	3	2	young	6.4	18.038	1.156	0.268	0.114	0.296	0.036	0.058	0.026	0.033	0.059	-	-	-
B324-G051	10.08529	41.68036	3	1	young	-	-	-	-	-	-	-	-	-	-	-	-	-	-
B443-D034	10.08661	40.55615	3	6	young	3.4	18.464	0.938	0.052	0.049	0.099	0.065	0.055	0.030	0.043	0.093	-	-	-
B325	10.09632	40.51310	3	1	young	10.6	17.070	1.376	0.519	0.279	0.231	0.053	0.045	0.019	0.020	0.031	-	-	-
B327-G053	10.10047	40.60620	3	1	young	8.2	16.531	0.641	0.113	0.100	0.192	0.021	0.020	0.015	0.017	0.026	-	-	-
VDB0-B195D	10.12250	40.60414	3	1	young	10.6	14.878	0.601	0.059	0.117	0.124	0.029	0.014	0.012	0.013	0.016	-	-	-
BH05	10.12714	40.75814	3	2	young	5.8	15.700	0.398	-0.127	-0.005	0.065	0.012	0.015	0.013	0.015	0.022	6.4	14.125	0.059
B196D	10.14498	40.44369	3	2	young	5.2	18.527	0.026	-0.035	-0.304	0.033	0.090	0.038	0.034	0.059	0.165	-	-	-
B448-D035	10.15211	40.67088	3	1	young	7.0	17.823	1.312	0.434	0.182	0.198	0.115	0.066	0.026	0.031	0.057	4.6	15.639	0.220
BH09	10.15481	40.55596	3	2	young	2.8	20.032	-	0.584	0.235	0.154	0.060	-	0.062	0.072	0.152	-	-	-
B006D-D036	10.15576	40.81265	3	1	young	5.2	18.437	1.286	0.134	0.206	0.112	0.069	0.091	0.034	0.046	0.100	4.0	15.934	0.160
BH10	10.18705	40.88559	3	2	young	4.6	19.371	1.663	0.474	0.231	0.198	0.157	0.260	0.053	0.068	0.146	2.8	15.578	0.082
PHF7-1	10.19342	40.86136	3	-	old	3.4	18.688	1.182	0.263	0.149	0.107	0.181	0.084	0.032	0.043	0.094	3.4	15.802	0.145
V202	10.19906	40.92631	3	2	young	3.4	19.116	1.181	0.099	-	-	0.073	0.118	0.049	-	-	2.8	17.128	0.715
B452-G069	10.20138	40.58498	3	2	young	6.4	17.793	1.024	0.099	0.107	-0.002	0.033	0.045	0.024	0.032	0.068	-	-	-
PHF7-2	10.20155	40.86618	3	-	young	6.4	17.967	0.696	0.131	0.140	0.237	0.058	0.044	0.026	0.035	0.068	2.8	15.252	0.047

B018-G071	10.20583	40.69220	3	1	young	6.4	17.849	1.540	0.634	0.394	0.195	0.059	0.065	0.022	0.023	0.036	4.6	14.675	0.132
B010D	10.21280	41.25136	3	2	young	4.0	19.110	1.687	0.492	0.215	0.130	0.114	0.193	0.036	0.044	0.114	2.8	17.069	0.259
B011D	10.21508	40.73504	3	2	young	4.6	17.872	0.951	0.662	0.717	0.718	0.076	0.042	0.021	0.020	0.023	4.6	13.035	0.045
B012D-D039	10.21776	40.97812	3	1	young	4.6	19.033	1.566	0.558	0.341	0.323	0.052	0.180	0.044	0.051	0.089	4.6	15.735	0.304
SK018A	10.22351	41.27076	3	1	young	4.0	19.661	1.683	0.668	0.372	0.405	0.204	0.310	0.048	0.054	0.111	2.8	16.014	0.122
KHM31-77	10.22368	40.61405	3	-	young	2.8	20.200	-	0.814	0.609	0.303	0.148	-	0.064	0.060	0.098	-	-	-
KHM31-81	10.23226	40.58955	3	-	young	2.8	19.746	0.443	0.168	0.229	0.442	0.157	0.088	0.059	0.080	0.139	-	-	-
KHM31-85	10.23597	40.57361	3	-	young	4.0	18.880	-	0.130	0.165	-0.331	0.036	-	0.043	0.059	0.180	-	-	-
KHM31-97	10.24505	40.57337	3	-	young	3.4	19.216	1.082	0.105	0.090	0.234	0.057	0.107	0.048	0.071	0.146	-	-	-
B014D	10.25437	41.10911	3	2	young	2.8	19.046	1.496	0.552	0.359	-	0.044	0.123	0.036	0.044	-	2.8	16.104	0.126
B015D-D041	10.26137	41.11007	3	1	young	5.2	18.696	1.699	0.685	0.303	0.287	0.091	0.159	0.037	0.044	0.075	3.4	16.002	0.135
KHM31-113	10.26147	40.57895	3	-	young	5.2	18.455	1.119	0.071	-0.135	-0.098	0.081	0.074	0.035	0.060	0.157	2.8	16.859	0.144
BH12	10.26208	40.58287	3	2	young	3.4	18.220	0.980	-0.007	0.035	-0.008	0.090	0.047	0.027	0.039	0.090	2.8	16.725	0.184
B453-D042	10.26379	41.01539	3	6	young	4.6	18.250	0.904	-0.527	-0.262	0.478	0.110	0.058	0.045	0.090	0.170	2.8	16.359	0.611
LGS04105.6...-SK067B	10.27338	41.12849	3	2	young	2.8	19.174	1.722	0.918	0.476	0.205	0.042	0.164	0.035	0.035	0.059	2.8	15.684	0.055
B200D-D043	10.27856	40.57466	3	2	young	4.0	18.586	0.884	0.006	0.082	0.286	0.032	0.063	0.037	0.056	0.108	2.8	16.520	0.155
B201D-D044	10.28451	40.54778	3	2	young	4.0	18.913	1.533	0.475	0.362	0.069	0.074	0.131	0.032	0.035	0.070	2.8	15.365	0.044
V031	10.30100	41.09133	3	1	young	6.4	18.048	1.572	0.444	0.355	0.532	0.086	0.097	0.030	0.037	0.052	4.0	14.877	0.214
G083-V225	10.30177	41.16369	3	2	young	4.0	18.854	-	0.409	0.296	-0.036	0.233	-	0.044	0.057	0.127	2.8	15.977	0.245
G085-V015	10.30333	40.57144	3	2	young	8.2	17.405	0.970	0.102	0.219	0.218	0.030	0.035	0.019	0.022	0.036	4.0	14.999	0.055
V014	10.30755	40.56607	3	2	young	6.4	17.485	0.976	0.156	0.103	0.003	0.051	0.035	0.019	0.022	0.042	4.0	16.064	0.092
B342-G094	10.35046	40.61310	3	1	young	6.4	17.878	0.927	0.048	-0.033	-0.465	0.047	0.044	0.023	0.031	0.098	3.4	16.457	0.136
DAO47	10.37284	40.75470	3	1	young	3.4	19.214	1.301	0.295	0.198	0.193	0.080	0.124	0.046	0.063	0.124	2.8	16.030	0.093
LGS04131.1_404612	10.37977	40.77027	3	-	young	4.0	18.938	1.407	0.271	0.165	0.142	0.112	0.123	0.043	0.060	0.124	-	-	-
G099-V022	10.40333	40.79010	3	2	back	6.4	17.535	1.465	0.477	0.343	0.186	0.050	0.051	0.020	0.023	0.036	4.6	14.469	0.056
B040-G102	10.41198	40.68176	3	1	young	6.4	17.380	0.936	0.193	0.136	0.071	0.035	0.033	0.018	0.021	0.038	3.4	15.913	0.165
PHF8-1	10.41460	40.67594	3	-	young	3.4	19.252	0.967	0.245	0.347	0.130	0.031	0.098	0.040	0.048	0.096	2.8	15.910	0.191
B206D-D048	10.41909	40.83523	3	1	young	4.6	18.737	1.420	0.360	0.032	-0.148	0.089	0.109	0.037	0.054	0.139	-	-	-
B521-SK034A	10.42387	40.86712	3	2	young	4.0	19.272	1.629	0.611	0.439	0.019	0.101	0.196	0.049	0.057	0.112	2.8	15.587	0.057
B043-G106	10.42629	40.71111	3	1	young	6.4	16.980	0.925	0.153	0.092	0.107	0.030	0.026	0.017	0.021	0.036	2.8	15.075	0.068
B458-D049	10.43595	40.85628	3	1	young	7.0	17.989	1.381	0.293	0.196	-0.082	0.086	0.067	0.028	0.037	0.079	2.8	16.899	0.486
B049-G112	10.43987	40.83194	3	1	young	5.8	17.708	1.493	0.371	0.244	0.222	0.110	0.057	0.022	0.027	0.044	3.4	15.203	0.183
B032D	10.44150	41.21706	3	2	young	-	-	-	-	-	-	-	-	-	-	-	-	-	-

B035D	10.45999	41.33424	3	2	young	4.0	18.677	1.375	0.411	0.360	0.324	0.111	0.118	0.048	0.061	0.093	-	-	-
KHM31-345	10.47437	40.83594	3	-	young	-	-	-	-	-	-	-	-	-	-	-	-	-	-
KHM31-151	10.48560	40.76650	3	-	young	3.4	19.891	0.828	-0.012	0.252	0.612	0.208	0.149	0.090	0.135	0.208	2.8	16.960	0.292
KHM31-152	10.48714	40.77571	3	-	young	3.4	19.705	-	0.339	0.360	0.188	0.090	-	0.064	0.082	0.159	2.8	16.874	0.268
B255	10.50003	40.80945	3	2	young	5.8	18.187	1.585	0.424	0.367	0.329	0.094	0.085	0.027	0.032	0.050	5.2	14.938	0.074
B066-G128	10.51287	40.74642	3	1	young	7.0	17.438	0.726	0.010	-0.231	0.296	0.022	0.030	0.020	0.029	0.051	4.0	16.521	0.180
B040D	10.51789	41.30204	3	2	young	2.8	19.103	1.774	0.458	0.438	0.365	0.264	0.170	0.048	0.059	0.085	-	-	-
B069-G132	10.52297	41.43594	3	1	young	5.8	18.305	1.247	0.283	0.128	0.034	0.056	0.088	0.043	0.063	0.123	-	-	-
B081-G142	10.55664	40.81083	3	1	young	5.8	17.205	1.540	0.418	0.350	0.286	0.030	0.040	0.016	0.017	0.024	4.6	14.024	0.030
B091-G151	10.59046	41.36817	3	1	young	4.0	17.915	1.357	0.213	0.159	0.144	0.127	0.065	0.032	0.045	0.078	-	-	-
B349	10.60053	40.62886	3	2	young	4.0	18.497	1.337	0.606	0.433	0.309	0.052	0.082	0.025	0.026	0.040	2.8	15.018	0.039
B061D	10.63564	41.36164	3	2	young	2.8	19.291	1.199	-0.284	0.147	-0.014	0.085	0.126	0.087	0.147	0.312	-	-	-
B067D	10.66247	41.61204	3	2	young	4.0	19.386	1.203	0.552	0.374	0.196	0.044	0.163	0.042	0.049	0.114	-	-	-
B133-G191	10.71516	41.39167	3	6	young	5.2	17.491	0.509	0.208	0.264	0.262	0.091	0.031	0.024	0.031	0.048	-	-	-
B081D	10.72996	41.05205	3	6	young	4.0	18.177	1.084	0.420	0.181	0.142	0.046	0.056	0.028	0.037	0.066	-	-	-
B095D	10.80850	41.14579	3	2	young	2.8	19.362	-	0.415	0.470	0.429	0.117	-	0.057	0.071	0.097	-	-	-
B097D	10.81976	41.10927	3	2	young	4.6	18.770	-	0.746	0.413	0.288	0.120	-	0.043	0.050	0.074	-	-	-
B098D	10.82230	41.52483	3	2	young	5.2	18.746	1.335	0.149	0.094	0.548	0.096	0.123	0.047	0.074	0.116	2.8	17.075	0.171
B089D	10.82250	41.52500	3	2	young	2.8	19.277	1.195	-	-	-0.035	0.075	0.120	-	-	0.147	-	-	-
B271	10.84620	41.42395	3	2	young	3.4	19.046	1.639	0.799	0.481	0.241	0.085	0.167	0.040	0.044	0.069	-	-	-
B192-G242	10.93547	41.62417	3	2	young	4.6	18.245	1.149	0.068	0.147	-0.140	0.067	0.068	0.031	0.043	0.109	2.8	16.746	0.506
M001	10.93786	41.30334	3	2	young	2.8	19.254	1.104	0.200	0.409	-0.036	0.115	0.103	0.062	0.085	0.159	-	-	-
B195	10.95231	41.04101	3	2	young	5.2	18.745	1.414	0.423	0.242	0.351	0.047	0.110	0.032	0.039	0.064	2.8	16.180	0.068
M003	10.97613	41.23659	3	2	young	4.0	18.603	0.694	0.384	0.373	0.313	0.100	0.063	0.046	0.061	0.089	-	-	-
B106D	10.97687	41.25381	3	2	young	4.0	18.320	1.205	0.347	0.282	0.216	0.073	0.072	0.039	0.053	0.084	-	-	-
B108D-SK150B	10.98793	41.75911	3	2	young	5.8	18.565	1.615	0.397	0.331	0.133	0.074	0.134	0.034	0.042	0.082	5.8	15.148	0.244
M005	10.99167	41.35933	3	2	young	3.4	19.759	1.265	0.233	-0.079	-0.356	0.198	0.201	0.089	0.162	0.482	-	-	-
LGS04359.1_413843	10.99655	41.64549	3	-	young	5.8	18.125	1.148	-0.180	-0.004	-0.276	0.065	0.066	0.034	0.054	0.165	2.8	16.842	0.588
B210-M11	11.01159	41.24013	3	1	young	6.4	17.725	1.208	0.383	0.192	0.133	0.046	0.046	0.020	0.023	0.039	2.8	15.417	0.201
B111D-D065	11.02040	41.65158	3	1	young	5.2	17.972	0.873	0.050	-0.047	0.051	0.061	0.048	0.027	0.041	0.093	2.8	16.540	0.451
B240D-D066	11.02866	41.67444	3	1	young	5.2	17.827	-0.037	-0.251	-0.137	-0.123	0.068	0.028	0.028	0.048	0.129	2.8	15.787	0.196
M016	11.03352	41.39839	3	2	young	3.4	19.579	-	0.205	0.067	0.357	0.149	-	0.079	0.130	0.218	2.8	16.268	0.218
B216-G267	11.03659	41.63217	3	7	young	8.2	17.190	1.157	0.315	-0.056	0.076	0.057	0.039	0.019	0.025	0.048	4.0	15.699	0.197

M020	11.05811	41.37188	3	2	young	4.0	18.588	0.276	-0.134	0.093	0.016	0.029	0.047	0.052	0.086	0.178	3.4	16.231	0.172
M023	11.07884	41.35267	3	2	young	5.2	18.550	1.515	0.177	0.033	-0.255	0.045	0.113	0.045	0.073	0.186	2.8	17.184	0.772
M025	11.08197	41.40248	3	2	young	4.0	18.919	1.285	0.026	0.117	-0.116	0.064	0.117	0.060	0.097	0.224	-	-	-
B112D-M27	11.08825	41.31949	3	2	young	3.4	18.900	1.390	0.491	0.415	0.331	0.049	0.108	0.030	0.033	0.051	3.4	15.431	0.190
B278-M30	11.09718	41.58440	3	2	young	2.8	19.121	1.370	0.233	0.230	0.209	0.049	0.105	0.043	0.060	0.105	4.0	16.337	0.202
M031	11.10113	41.56615	3	2	young	4.0	19.092	1.064	0.361	0.381	0.201	0.059	0.109	0.052	0.066	0.113	3.4	15.692	0.489
B222-G277	11.10563	41.23665	3	1	young	8.2	17.741	1.532	0.495	0.354	0.224	0.028	0.062	0.020	0.022	0.034	3.4	14.613	0.092
B223-G278	11.11271	41.57699	3	7	young	5.2	17.714	1.103	0.079	0.006	0.153	0.027	0.043	0.026	0.038	0.068	2.8	15.679	0.183
M039	11.13061	41.50129	3	2	young	3.4	19.015	1.329	0.181	0.118	-0.099	0.041	0.110	0.047	0.072	0.164	2.8	17.783	0.386
M040	11.13128	41.46537	3	2	young	5.8	19.564	-	0.539	0.832	0.327	0.090	-	0.080	0.082	0.110	4.0	15.804	0.236
M042	11.14153	41.35081	3	2	young	5.8	18.855	1.104	0.199	-0.005	0.134	0.082	0.098	0.038	0.057	0.123	-	-	-
M043	11.14310	41.38657	3	2	young	3.4	19.957	-	0.378	0.309	0.535	0.150	-	0.091	0.118	0.182	2.8	15.750	0.157
DAO69	11.14500	41.89090	3	2	young	6.4	17.325	0.766	-0.000	-0.546	0.202	0.031	0.031	0.020	0.035	0.077	2.8	15.719	0.107
M045	11.15156	41.59253	3	2	young	4.6	19.216	-	0.831	0.539	0.139	0.043	-	0.044	0.045	0.077	4.0	15.934	0.545
B118D-M049	11.16540	41.40774	3	1	young	4.6	18.468	1.119	0.346	0.286	0.186	0.137	0.073	0.035	0.046	0.078	2.8	15.494	0.120
M050	11.16948	41.50181	3	2	young	6.4	18.610	1.569	0.325	0.285	-0.114	0.131	0.135	0.045	0.060	0.131	4.0	16.661	0.342
B367-G292	11.19654	42.09218	3	1	young	5.2	18.203	1.069	0.310	0.169	0.253	0.027	0.060	0.023	0.028	0.061	2.8	16.260	0.161
B368-G293	11.19917	41.85252	3	1	young	4.0	18.003	0.598	-0.147	-0.074	-0.048	0.140	0.040	0.028	0.043	0.114	2.8	16.705	0.155
KHM31-234	11.20572	41.32654	3	-	young	3.4	20.564	-	0.182	0.334	0.605	0.081	-	0.112	0.150	0.228	2.8	16.283	0.178
KHM31-246	11.22806	41.48093	3	-	interm	2.8	20.125	1.089	0.256	0.156	0.002	0.091	0.192	0.090	0.138	0.302	2.8	16.300	0.098
B475-V128	11.23356	41.90021	3	1	young	8.8	17.408	1.482	0.300	0.281	0.263	0.050	0.059	0.021	0.024	0.041	3.4	15.952	0.127
B256D	11.24469	41.91020	3	2	young	4.6	17.234	0.845	0.439	0.400	0.326	0.022	0.030	0.017	0.018	0.025	4.0	13.646	0.031
B257D-D073	11.24791	41.91301	3	1	young	5.8	18.049	1.316	0.091	0.155	-0.155	0.052	0.069	0.027	0.036	0.093	2.8	16.782	0.372
M057	11.26150	41.78396	3	2	young	3.4	20.319	-	0.928	0.687	0.158	0.108	-	0.081	0.073	0.123	2.8	16.835	0.472
M059	11.26696	41.77242	3	2	young	3.4	19.087	1.625	0.514	0.336	0.130	0.075	0.144	0.039	0.046	0.086	2.8	16.384	0.181
KHM31-264	11.27445	41.59535	3	-	young	4.0	20.254	1.863	0.743	0.356	0.358	0.207	0.571	0.098	0.114	0.190	2.8	16.337	0.474
M062	11.28185	41.75857	3	2	young	2.8	20.187	0.899	0.437	0.542	0.144	0.171	0.170	0.076	0.088	0.160	2.8	16.300	0.197
B477-D075	11.28471	41.66053	3	2	young	4.6	18.202	1.319	0.118	-0.049	-	0.045	0.067	0.031	0.048	-	2.8	17.152	1.036
V133	11.29383	42.00334	3	2	young	5.2	18.187	-0.054	0.084	-0.413	-0.186	0.028	0.032	0.027	0.047	0.165	-	-	-
M068	11.29581	41.64897	3	6	young	4.0	19.175	0.429	-0.365	0.278	0.047	0.090	0.073	0.079	0.122	0.262	3.4	16.864	0.568
M069	11.29696	41.82214	3	2	young	4.6	19.647	1.659	0.391	0.515	0.343	0.265	0.299	0.074	0.087	0.139	4.0	15.935	0.097
WH28	11.30597	41.62666	3	-	young	4.6	17.531	0.989	0.321	0.177	0.035	0.036	0.035	0.020	0.025	0.044	2.8	15.820	0.220
M072-SK167C	11.30754	41.70733	3	2	young	4.0	18.570	1.301	0.116	0.093	0.067	0.068	0.085	0.037	0.054	0.115	2.8	17.424	0.514

M073	11.31303	41.79223	3	2	young	2.8	20.092	0.975	0.362	0.279	0.529	0.199	0.167	0.074	0.098	0.151	2.8	16.785	0.481
M076-SK170C	11.31711	41.72280	3	2	young	2.8	20.176	1.253	0.248	-	-	0.303	0.224	0.084	-	-	-	-	-
M078	11.32401	41.69791	3	2	young	2.8	20.321	1.185	0.077	0.464	0.213	0.142	0.239	0.104	0.137	0.249	2.8	16.951	1.193
M079	11.32418	41.68276	3	2	young	4.6	19.453	1.144	0.258	-0.164	-0.256	0.125	0.163	0.068	0.121	0.375	-	-	-
M080	11.33168	41.80842	3	2	young	4.6	18.942	0.779	0.092	0.176	0.373	0.235	0.081	0.050	0.073	0.126	2.8	16.085	0.076
M081	11.34281	41.79913	3	2	young	2.8	20.628	-	0.622	0.173	-	0.300	-	0.099	0.131	-	2.8	16.814	0.573
M082	11.35931	41.76446	3	2	young	4.0	19.436	1.007	0.241	-0.029	0.412	0.066	0.135	0.064	0.104	0.187	2.8	16.345	0.080
B371-G303	11.36314	41.72908	3	1	young	9.4	17.790	1.335	0.315	0.094	-0.009	0.047	0.064	0.026	0.035	0.074	2.8	16.891	0.343
M085	11.36672	41.70101	3	2	young	2.8	19.715	1.530	0.444	0.245	0.083	0.041	0.190	0.053	0.069	0.143	2.8	17.098	0.272
M086	11.36870	41.82488	3	2	young	8.2	18.289	1.411	0.386	0.018	0.181	0.036	0.093	0.033	0.047	0.092	2.8	16.651	0.313
M087	11.38363	41.82557	3	2	young	5.8	18.577	1.655	0.692	0.440	0.473	0.099	0.118	0.030	0.033	0.045	4.0	14.947	0.103
M088	11.38546	41.72522	3	2	young	5.8	18.895	1.509	0.735	0.502	0.326	0.102	0.148	0.039	0.041	0.063	3.4	14.985	0.050
M091	11.38792	41.70533	3	2	young	3.4	19.375	1.655	0.517	0.379	0.222	0.090	0.188	0.047	0.055	0.098	2.8	15.699	0.116
M092	11.39824	41.75502	3	2	young	4.0	19.545	-	0.608	0.385	0.190	0.048	-	0.058	0.067	0.123	3.4	15.801	0.131
M093	11.40607	41.66979	3	2	young	3.4	20.057	-	0.688	0.115	-0.452	0.177	-	0.072	0.095	0.320	-	-	-
B374-G306	11.43550	41.69863	3	1	young	5.2	18.399	1.239	0.390	0.122	-0.058	0.046	0.074	0.030	0.040	0.089	2.8	16.240	0.188
B480-V127	11.43981	41.76458	3	1	young	5.2	18.169	1.285	0.162	0.119	0.043	0.057	0.065	0.029	0.041	0.083	2.8	15.500	0.188
M101	11.44282	41.80580	3	2	young	3.4	19.622	1.618	0.537	0.410	0.316	0.143	0.221	0.051	0.057	0.100	3.4	15.845	0.066
B376-G309	11.45161	41.71108	3	1	young	5.2	18.144	1.010	0.262	0.130	0.050	0.062	0.053	0.028	0.037	0.074	2.8	16.236	0.107
M104	11.45339	41.80560	3	2	young	4.6	18.786	1.342	0.301	0.030	-0.158	0.059	0.104	0.036	0.052	0.140	-	-	-
M105	11.45705	41.65729	3	2	interm	4.0	19.398	1.549	0.630	0.437	0.069	0.122	0.199	0.042	0.044	0.090	3.4	16.947	0.354
DAO84	11.46803	41.71360	3	1	young	4.0	19.329	0.909	0.363	0.236	-0.707	0.096	0.115	0.055	0.074	0.293	-	-	-
B484-G310	11.47457	41.79362	3	1	young	4.0	18.503	1.512	0.379	0.235	-0.129	0.080	0.093	0.029	0.036	0.084	2.8	16.277	0.071
B483-D085	11.47472	42.03834	3	1	young	5.8	18.436	1.379	0.200	0.294	0.295	0.071	0.097	0.030	0.037	0.073	2.8	16.412	0.076
B380-G313	11.52583	42.01472	3	7	young	8.2	17.040	1.398	0.213	0.115	0.090	0.031	0.036	0.017	0.020	0.035	3.4	15.407	0.101
B392-G329	11.75383	41.91236	3	6	young	9.4	17.073	1.415	0.469	0.208	0.169	0.017	0.038	0.016	0.017	0.026	5.8	14.868	0.059

[1]Cluster name, taken from the Revised Bologna Catalogue (Galleti *et al.*, 2004)

[2]Position of object in SDSS *r*-band image [J2000, degrees]

[3]Classification of source as described in chapter 2. Options for flag, f: 1-old globular cluster; 2-candidate cluster (21-candidate old cluster, 23-candidate young cluster); 3-young cluster; 4-galaxy; 5-HII region; 6-stellar source. Flags f_{RBC} and f_{C09} indicate the previous classifications of the source from the RBC v3.5 of Galleti *et al.* (2004) and from the catalogue of Caldwell *et al.* (2009), respectively.

[4]Aperture size used to measure the total magnitude of the cluster [arcsec]

[5]Error on the total magnitude, includes the statistical, calibration and systematic errors

C

Catalogue of candidate clusters in M31 (table 2.1: candidate clusters)

This table lists all potential (but unconfirmed) clusters in M31. Our classification criteria are discussed in chapter 2. We also include the previous classifications of these sources from the catalogues of Galleti *et al.* (2004) and Caldwell *et al.* (2009). Where available, we include optical and near infrared photometry of these clusters in the *u*,*g*,*r*,*i*,*z* and K-bands. Details of this catalogue are discussed in chapter 2.

GC Name[1]	RA[2]	DEC[2]	Classification[3]			Photometry													
			f	f_{RBC}	f_{C09}	R_g^4	g	$(u-g)$	$(g-r)$	$(r-i)$	$(i-z)$	$\sigma^5_{g,tot}$	$\sigma_{(u-g)}$	$\sigma_{(g-r)}$	$\sigma_{(r-i)}$	$\sigma_{(i-z)}$	R_K^4	K_s	$\sigma^5_{K,tot}$
SK002C	8.31599	40.00704	2	2	unknown	5.2	19.389	-	1.310	0.467	0.394	0.128	-	0.033	0.026	0.041	-	-	-
SK001B	8.34617	40.07819	2	2	unknown	5.2	18.650	1.617	0.827	0.386	0.296	0.061	0.110	0.024	0.023	0.038	-	-	-
SK002B	8.38421	39.85920	2	2	unknown	5.2	18.138	0.975	0.360	0.253	-0.039	0.082	0.049	0.021	0.023	0.048	-	-	-
SK004C	8.39568	40.13807	2	2	unknown	4.6	20.008	-	1.277	0.590	0.465	0.165	-	0.048	0.036	0.056	-	-	-
SK003B	8.40440	39.68317	2	2	unknown	8.8	17.147	1.278	0.702	0.343	0.295	0.033	0.037	0.015	0.015	0.023	-	-	-
SK005C	8.40866	39.59334	2	2	unknown	5.8	19.509	-	1.240	0.534	0.313	0.122	-	0.037	0.029	0.062	-	-	-
SK006C	8.44221	39.81025	2	2	unknown	5.8	19.281	1.883	0.940	0.410	0.350	0.118	0.259	0.034	0.031	0.053	-	-	-
SK007C	8.47779	39.57689	2	2	unknown	5.2	19.468	-	1.508	0.591	0.344	0.133	-	0.035	0.024	0.045	-	-	-
B133D	8.54579	39.84726	2	2	star	7.6	18.361	1.230	0.880	0.393	0.280	0.053	0.085	0.022	0.021	0.041	-	-	-
SK009C	8.55076	40.10846	2	2	unknown	5.8	18.884	2.090	1.256	0.508	0.316	0.065	0.214	0.026	0.021	0.031	-	-	-
SK010C	8.61195	39.90169	2	2	unknown	4.0	19.459	-	0.978	0.408	0.354	0.034	-	0.034	0.031	0.068	-	-	-
SK004B	8.64255	40.04724	2	2	unknown	4.6	19.986	-	1.124	0.452	0.318	0.048	-	0.050	0.040	0.074	-	-	-
SK011C	8.71320	39.92606	2	2	unknown	4.6	19.863	-	1.207	0.500	0.533	0.077	-	0.044	0.035	0.066	-	-	-
SK012C	8.78661	40.12594	2	2	unknown	3.4	19.926	1.502	0.868	0.389	0.314	0.058	0.245	0.043	0.040	0.075	3.4	15.979	0.068
SK013C	8.78840	40.09463	2	2	unknown	5.2	19.720	-	1.084	0.461	0.303	0.131	-	0.043	0.037	0.085	-	-	-
B413	8.80411	41.48547	2	2	unknown	7.0	18.648	1.903	1.049	0.508	0.369	0.095	0.180	0.025	0.021	0.033	-	-	-
BA22	8.80672	39.76033	2	2	unknown	5.8	18.812	1.147	0.752	0.413	0.322	0.074	0.104	0.026	0.026	0.052	-	-	-
SK014C	8.81215	39.69452	2	2	unknown	4.6	19.501	1.647	1.208	0.480	0.420	0.083	0.272	0.035	0.028	0.054	-	-	-
SK015C	8.83561	39.58459	2	2	unknown	6.4	19.160	-	1.238	0.474	0.429	0.154	-	0.031	0.025	0.046	-	-	-
SK005B	8.83833	41.92572	2	2	unknown	-	-	-	-	-	-	-	-	-	-	-	-	-	-
SK016C	8.84167	41.82983	2	2	unknown	-	-	-	-	-	-	-	-	-	-	-	-	-	-
SK017C	8.86887	39.54045	2	2	unknown	2.8	20.217	-	1.196	0.475	0.228	0.071	-	0.043	0.034	0.078	-	-	-
SK018C	8.87217	41.70925	2	2	unknown	-	-	-	-	-	-	-	-	-	-	-	-	-	-
B134D	8.87612	40.74031	2	2	unknown	6.4	18.381	1.138	0.735	0.414	0.217	0.048	0.067	0.022	0.022	0.037	4.6	14.560	0.082
SK006B	8.89266	41.19814	2	2	unknown	4.0	19.524	1.869	0.846	0.503	0.150	0.125	0.323	0.037	0.034	0.066	-	-	-
SK007B	8.93874	39.65600	2	2	unknown	4.6	19.747	-	1.057	0.479	0.113	0.128	-	0.042	0.035	0.092	-	-	-
SK020C	8.95725	41.83400	2	2	unknown	-	-	-	-	-	-	-	-	-	-	-	-	-	-
SK021C	8.96204	39.60028	2	2	unknown	4.6	19.417	1.607	1.052	0.431	0.374	0.068	0.243	0.034	0.029	0.060	-	-	-
SK022C	8.96564	40.90338	2	2	unknown	5.2	19.357	1.423	1.322	0.487	0.347	0.047	0.167	0.032	0.025	0.040	5.2	14.343	0.102
SK023C	8.97125	41.85658	2	2	unknown	-	-	-	-	-	-	-	-	-	-	-	-	-	-

SK024C	8.97429	41.72850	2	2	unknown	-	-	-	-	-	-	-	-	-	-	-	-	-	-
SK025C	8.97592	41.78161	2	2	unknown	-	-	-	-	-	-	-	-	-	-	-	-	-	-
SK008B	8.99246	39.62658	2	2	unknown	5.2	18.780	1.722	0.988	0.444	0.433	0.070	0.160	0.025	0.022	0.039	-	-	-
SK009B	9.00095	40.93885	2	2	unknown	3.4	20.266	-	1.274	0.522	0.351	0.087	-	0.050	0.038	0.065	3.4	15.346	0.196
SK010B	9.00721	39.81411	2	2	unknown	5.2	19.092	1.740	0.958	0.479	0.235	0.102	0.216	0.030	0.026	0.056	-	-	-
SK011B	9.00846	41.24552	2	2	unknown	5.2	19.724	1.337	0.629	0.398	0.031	0.079	0.268	0.049	0.050	0.120	-	-	-
SK012B	9.02122	40.92229	2	2	unknown	7.0	18.724	1.772	1.300	0.524	0.385	0.060	0.147	0.025	0.020	0.029	6.4	13.856	0.077
SK026C	9.02335	39.96814	2	2	unknown	4.0	19.867	-	1.044	0.569	0.220	0.068	-	0.045	0.037	0.085	-	-	-
SK028C	9.07066	41.42682	2	2	unknown	3.4	19.822	1.054	0.942	0.475	0.229	0.088	0.179	0.040	0.035	0.065	-	-	-
SK029C	9.09281	39.86804	2	2	unknown	5.8	19.631	-	1.295	0.528	0.503	0.163	-	0.042	0.031	0.058	-	-	-
B139D	9.10324	39.75210	2	2	unknown	2.8	18.862	1.161	0.607	0.247	0.162	0.042	0.078	0.023	0.024	0.055	-	-	-
SK030C	9.11409	41.58738	2	2	unknown	2.8	22.240	-	1.632	0.808	0.540	0.504	-	0.194	0.094	0.144	-	-	-
SK031C	9.13096	42.10683	2	2	unknown	-	-	-	-	-	-	-	-	-	-	-	-	-	-
SK013B	9.13220	41.19494	2	2	unknown	4.0	19.491	0.998	1.105	0.505	0.368	0.037	0.149	0.035	0.028	0.046	-	-	-
SK032C	9.13911	41.50093	2	2	unknown	2.8	20.747	-	1.355	0.412	0.420	0.133	-	0.061	0.043	0.076	-	-	-
B142D	9.14113	41.15224	2	2	unknown	4.6	19.152	1.208	0.794	0.302	0.338	0.092	0.139	0.031	0.031	0.055	-	-	-
SK002A	9.14580	41.01902	2	1	unknown	2.8	19.553	1.290	0.548	0.196	0.092	0.075	0.123	0.033	0.038	0.086	-	-	-
B144D	9.15270	41.61775	2	2	unknown	3.4	18.442	-	0.953	0.425	0.287	0.039	-	0.020	0.018	0.027	-	-	-
SK033C	9.15787	42.24617	2	2	unknown	-	-	-	-	-	-	-	-	-	-	-	-	-	-
SK034C	9.18104	39.58239	2	2	unknown	6.4	18.810	2.002	1.115	0.479	0.403	0.094	0.196	0.026	0.022	0.036	-	-	-
SK035C	9.19442	41.44004	2	2	unknown	2.8	20.554	-	1.169	0.508	0.308	0.065	-	0.055	0.042	0.076	-	-	-
SK036C	9.19671	40.06954	2	2	unknown	3.4	20.205	-	1.283	0.581	0.411	0.160	-	0.049	0.035	0.069	-	-	-
SK037C	9.20509	39.66226	2	2	unknown	4.6	19.282	-	1.331	0.542	0.385	0.060	-	0.030	0.023	0.037	-	-	-
B150D	9.24949	41.42505	2	1	unknown	4.6	17.777	1.284	0.518	0.249	0.169	0.037	0.050	0.018	0.018	0.030	-	-	-
SK039C	9.25410	39.55779	2	2	unknown	2.8	20.652	-	1.384	0.862	0.500	0.300	-	0.056	0.036	0.052	-	-	-
SK040C	9.26421	41.55619	2	2	unknown	2.8	20.498	-	1.034	0.462	0.164	0.072	-	0.054	0.044	0.093	-	-	-
SK041C	9.27127	40.01866	2	2	unknown	4.0	19.747	-	1.107	0.567	0.307	0.148	-	0.041	0.033	0.070	-	-	-
SK042C	9.27616	41.74697	2	2	unknown	4.6	18.708	1.764	0.911	0.450	0.338	0.109	0.146	0.024	0.022	0.036	-	-	-
SK043C	9.28791	39.81965	2	2	unknown	2.8	19.987	-	0.913	0.304	0.382	0.067	-	0.039	0.038	0.074	-	-	-
SK045C	9.30386	41.44353	2	2	unknown	2.8	19.504	0.646	0.524	0.435	0.161	0.056	0.086	0.032	0.033	0.065	-	-	-
SK046C	9.37058	41.91742	2	2	unknown	2.8	20.706	-	1.360	0.816	0.505	0.061	-	0.058	0.037	0.054	-	-	-
SK017B	9.37687	40.61236	2	2	unknown	6.4	18.816	-	1.117	0.463	0.285	0.059	-	0.026	0.023	0.044	5.8	14.369	0.050
SK018B	9.37844	40.30691	2	2	unknown	4.0	19.553	-	0.825	0.500	0.222	0.081	-	0.042	0.039	0.085	3.4	15.419	0.084

SK019B	9.38949	40.09152	2	2	unknown	5.2	19.466	-	1.113	0.441	0.296	0.068	-	0.037	0.032	0.066	4.6	15.103	0.074
SK020B	9.39873	40.58752	2	2	unknown	4.0	19.940	-	1.369	0.507	0.321	0.099	-	0.046	0.033	0.071	4.0	14.933	0.071
SK048C	9.40504	40.09456	2	2	unknown	5.8	18.526	1.634	1.127	0.489	0.405	0.079	0.126	0.023	0.020	0.032	5.2	14.010	0.052
SK049C	9.40540	41.90131	2	2	unknown	2.8	21.035	-	1.786	0.560	0.351	0.270	-	0.071	0.038	0.068	-	-	-
SK050C	9.42196	40.07878	2	2	unknown	2.8	19.982	-	1.205	0.548	0.469	0.070	-	0.039	0.030	0.053	2.8	15.229	0.071
SK051C	9.42418	40.08856	2	2	unknown	2.8	19.911	1.018	1.195	0.424	0.444	0.050	0.160	0.037	0.030	0.057	2.8	15.396	0.124
SK021B	9.47169	41.51939	2	2	unknown	2.8	19.939	0.759	0.525	0.203	0.301	0.095	0.131	0.042	0.048	0.099	-	-	-
SK022B	9.47630	40.29102	2	2	unknown	4.0	19.571	-	1.468	0.529	0.317	0.073	-	0.038	0.027	0.049	5.8	14.376	0.072
B423	9.48630	40.95987	2	1	unknown	6.4	18.164	1.410	0.581	0.305	0.216	0.074	0.069	0.021	0.022	0.036	4.6	15.570	0.132
SK052C	9.49212	41.39358	2	2	unknown	2.8	20.050	0.994	0.492	0.122	0.232	0.062	0.146	0.046	0.057	0.129	-	-	-
SK023B	9.50189	41.57107	2	2	unknown	2.8	19.463	1.171	0.525	0.218	0.188	0.052	0.123	0.032	0.035	0.073	-	-	-
SK053C	9.50333	42.04930	2	2	unknown	4.0	19.915	-	1.306	0.498	0.414	0.139	-	0.044	0.033	0.056	-	-	-
SK054C	9.52545	40.40861	2	2	unknown	2.8	18.618	2.115	0.866	0.345	0.138	0.031	0.137	0.021	0.021	0.038	2.8	15.558	0.044
SK055C	9.55368	41.87998	2	2	unknown	2.8	21.079	-	1.068	0.567	0.235	0.283	-	0.082	0.063	0.127	-	-	-
SK056C	9.59388	40.84925	2	2	unknown	3.4	19.489	1.691	0.952	0.468	0.397	0.055	0.228	0.034	0.031	0.060	3.4	15.370	0.059
SK057C	9.68138	41.97742	2	2	unknown	2.8	21.039	-	1.544	0.440	0.419	0.202	-	0.074	0.046	0.081	-	-	-
SK058C	9.70177	40.05055	2	2	unknown	4.0	19.701	-	1.010	0.439	0.302	0.062	-	0.043	0.038	0.073	4.0	15.524	0.130
SK060C	9.72457	40.64424	2	2	unknown	2.8	20.064	-	0.706	0.304	-	0.079	-	0.052	0.058	-	-	-	-
DAO23	9.72640	40.44623	2	1	star	5.2	19.940	2.140	1.370	0.471	-	0.080	0.690	0.060	0.028	-	3.4	15.750	0.053
SH05	9.73000	41.17444	2	2	noobject	-	-	-	-	-	-	-	-	-	-	-	-	-	-
SK061C	9.74662	41.73293	2	2	unknown	2.8	19.996	1.621	0.841	0.245	0.291	0.083	0.281	0.040	0.039	0.079	-	-	-
SK062C	9.75514	42.06519	2	2	unknown	4.6	19.925	-	1.252	0.502	0.370	0.055	-	0.047	0.035	0.059	-	-	-
SK063C	9.78073	40.67038	2	2	unknown	3.4	19.057	0.980	0.106	0.272	0.280	0.098	0.094	0.039	0.050	0.108	-	-	-
SK064C	9.79051	41.58769	2	2	unknown	4.0	19.511	-	1.016	0.432	0.433	0.071	-	0.036	0.032	0.052	4.0	15.416	0.048
SK028B	9.80708	41.96444	2	2	unknown	3.4	19.286	0.964	0.537	0.432	0.249	0.084	0.107	0.032	0.032	0.060	-	-	-
SK066C	9.81334	42.38080	2	2	unknown	2.8	19.224	1.634	0.738	0.312	0.186	0.089	0.142	0.026	0.027	0.052	-	-	-
SH06	9.83042	41.17472	2	2	noobject	-	-	-	-	-	-	-	-	-	-	-	-	-	-
SK067C	9.83263	40.63327	2	2	unknown	4.0	19.039	1.485	1.211	0.661	0.407	0.050	0.159	0.030	0.024	0.037	4.6	14.069	0.037
SK029B	9.84934	42.02704	2	2	unknown	2.8	19.619	1.235	0.539	0.179	0.077	0.059	0.148	0.035	0.039	0.092	-	-	-
SK030B	9.86286	42.11561	2	2	unknown	2.8	19.722	0.635	0.410	0.139	0.179	0.051	0.100	0.038	0.046	0.106	-	-	-
SK069C	9.86844	42.04898	2	2	unknown	4.0	19.923	-	1.355	0.522	0.272	0.097	-	0.044	0.031	0.055	-	-	-
SH07	9.90587	42.16564	2	2	unknown	10.6	16.734	0.907	0.454	0.351	0.221	0.043	0.030	0.015	0.016	0.022	-	-	-
SK032B	9.93742	42.11805	2	2	unknown	4.0	17.731	1.539	0.618	0.228	0.157	0.024	0.057	0.017	0.017	0.028	-	-	-

B001D	9.97750	41.38692	2	2	unknown	-	-	-	-	-	-	-	-	-	-	-	-	-	-
SK071C	9.99059	41.01604	2	2	unknown	4.0	19.367	1.758	1.074	0.498	0.395	0.067	0.254	0.035	0.030	0.056	2.8	14.788	0.052
B186D	10.00940	39.38665	2	2	unknown	9.4	17.945	1.563	0.696	0.344	0.201	0.052	0.084	0.020	0.020	0.034	5.2	14.863	0.046
SK073C	10.01791	40.23652	2	2	unknown	4.0	19.740	-	1.405	0.585	0.356	0.085	-	0.040	0.029	0.045	4.6	14.518	0.045
SK039B	10.02098	41.78833	2	2	unknown	2.8	19.359	0.998	0.555	0.262	0.125	0.040	0.086	0.032	0.036	0.072	-	-	-
SK074C	10.02201	41.44339	2	2	unknown	2.8	19.878	1.232	0.412	0.089	0.092	0.070	0.158	0.044	0.056	0.131	-	-	-
SK075C	10.02871	41.71941	2	2	unknown	3.4	19.739	1.478	0.551	0.038	-	0.058	0.201	0.045	0.059	-	-	-	-
SK040B	10.03156	41.96991	2	2	unknown	4.0	19.937	0.977	0.301	0.243	-0.031	0.081	0.178	0.060	0.078	0.217	-	-	-
BH02	10.04287	40.60728	2	2	unknown	4.0	18.510	0.844	0.234	0.238	0.287	0.026	0.060	0.032	0.040	0.072	-	-	-
SK042B	10.05852	41.69327	2	2	star	3.4	20.299	1.014	0.753	-	-	0.070	0.222	0.070	-	-	-	-	-
SK043B	10.06402	40.61511	2	2	-	4.0	18.300	0.903	0.107	0.140	0.363	0.084	0.054	0.030	0.040	0.070	-	-	-
SK077C	10.06427	41.90658	2	2	unknown	2.8	19.855	-	0.776	0.188	0.129	0.067	-	0.038	0.041	0.091	-	-	-
SK078C	10.06469	40.77312	2	2	unknown	2.8	19.837	1.027	0.559	0.372	0.017	0.060	0.157	0.049	0.057	0.138	2.8	16.788	0.567
SK079C	10.06914	41.56805	2	2	unknown	2.8	19.451	1.082	0.436	0.053	0.144	0.058	0.102	0.038	0.049	0.096	-	-	-
SK044B	10.07848	40.52091	2	2	unknown	4.0	19.323	-	1.186	0.649	0.463	0.084	-	0.042	0.032	0.043	-	-	-
SK080C	10.08387	41.91871	2	2	unknown	2.8	20.159	-	1.447	0.973	0.545	0.090	-	0.041	0.026	0.032	-	-	-
BH03	10.09429	41.67900	2	2	na	-	-	-	-	-	-	-	-	-	-	-	-	-	-
SK015A	10.10896	40.75886	2	1	star	-	-	-	-	-	-0.001	198.010	-	-	-	0.192	2.8	16.393	0.265
SK082C	10.11261	41.55522	2	2	unknown	2.8	19.830	1.090	0.513	0.295	0.145	0.062	0.139	0.047	0.054	0.101	2.8	17.262	0.437
BH04	10.11333	41.70664	2	2	old	-	-	-	-	-	-	-	-	-	-	-	-	-	-
SK047B	10.12079	41.70489	2	2	star	3.4	19.756	-	-	-	-	0.075	-	-	-	-	2.8	16.300	0.093
BH06	10.12768	40.74829	2	2	na	4.6	17.070	0.324	-0.218	0.140	0.306	0.027	0.022	0.018	0.023	0.040	4.0	14.579	0.204
SH08	10.13083	40.44083	2	2	noobject	-	-	-	-	-	-	-	-	-	-	-	-	-	-
SK016A	10.13229	40.76887	2	1	star	2.8	-	-	-	0.775	0.389	-	-	-	0.064	0.097	2.8	15.905	0.245
SK050B	10.14680	41.79242	2	2	unknown	2.8	20.541	-	1.157	0.345	0.231	0.111	-	0.058	0.051	0.099	2.8	16.473	0.082
SK086C	10.18106	41.59300	2	2	unknown	3.4	19.728	0.734	0.696	0.313	-0.118	0.079	0.114	0.047	0.051	0.113	3.4	16.405	0.213
SK087C	10.19316	41.68387	2	2	unknown	4.0	19.513	1.492	0.901	0.269	0.128	0.110	0.200	0.039	0.039	0.076	3.4	16.524	0.114
B450	10.19451	41.67395	2	1	noobject	4.0	21.539	-	0.084	0.769	0.953	0.315	-	0.316	0.341	0.332	3.4	16.440	0.259
SK088C	10.20030	40.67775	2	2	unknown	4.0	20.233	-	0.667	0.705	0.305	0.230	-	0.093	0.089	0.144	2.8	16.542	0.097
B009D	10.20826	41.02777	2	2	unknown	2.8	19.165	1.512	0.490	0.260	0.120	0.052	0.135	0.037	0.045	0.091	2.8	16.760	1.102
BH11	10.21183	40.67730	2	2	interm	2.8	20.475	-	0.797	0.630	0.353	0.113	-	0.080	0.074	0.118	2.8	16.622	0.127
SK054B	10.21407	41.71309	2	2	unknown	3.4	21.099	-	1.713	0.577	0.346	0.211	-	0.097	0.052	0.083	3.4	15.589	0.154
B198D	10.21441	40.55774	2	2	unknown	7.0	18.231	1.397	0.497	0.374	0.264	0.095	0.087	0.029	0.032	0.053	-	-	-

B246	10.21782	40.89900	2	2	old	6.4	18.626	-	0.793	0.537	0.097	0.058	-	0.033	0.033	0.062	3.4	15.486	0.162
SK090C	10.22113	40.01217	2	2	unknown	3.4	20.096	-	1.141	0.395	0.569	0.140	-	0.046	0.039	0.063	3.4	15.252	0.149
SK059B	10.23836	40.74192	2	2	unknown	2.8	20.490	-	0.489	0.217	0.379	0.320	-	0.091	0.119	0.218	2.8	16.818	0.495
SK091C	10.23878	40.36533	2	2	unknown	6.4	18.595	1.181	0.962	0.503	0.345	0.093	0.096	0.027	0.024	0.036	6.4	14.400	0.067
SK062B	10.24362	41.13105	2	2	unknown	2.8	21.001	-	1.521	0.497	0.398	0.445	-	0.118	0.086	0.136	2.8	16.663	0.191
SK063B	10.25506	41.74149	2	2	unknown	4.6	18.144	0.444	0.090	0.011	0.005	0.039	0.035	0.023	0.031	0.067	-	-	-
SK092C	10.26062	40.80425	2	2	unknown	5.2	19.421	-	1.272	0.624	0.579	0.098	-	0.048	0.037	0.048	5.2	14.359	0.074
SK066B	10.27334	42.21541	2	2	unknown	5.2	19.165	2.085	0.820	0.403	0.167	0.083	0.249	0.031	0.031	0.060	3.4	15.482	0.119
SK068B	10.27668	41.16035	2	2	unknown	2.8	18.991	0.869	0.026	-0.084	-0.101	0.170	0.074	0.045	0.079	0.207	-	-	-
B016D	10.28031	40.83698	2	2	maybestar	4.6	18.481	0.206	-0.026	-0.241	-0.038	0.037	0.041	0.038	0.070	0.182	-	-	-
SK095C	10.28263	41.85912	2	2	unknown	2.8	20.346	0.868	0.713	0.418	0.190	0.085	0.173	0.054	0.054	0.107	2.8	16.780	0.095
SK070B	10.28720	41.16546	2	2	unknown	5.2	18.182	1.817	1.012	0.546	0.306	0.084	0.113	0.025	0.024	0.034	4.6	14.084	0.089
SK071B	10.29552	40.38510	2	2	unknown	4.6	19.040	1.104	0.839	0.414	0.204	0.183	0.109	0.031	0.030	0.053	4.6	15.097	0.101
SK072B	10.30064	41.60291	2	2	unknown	3.4	18.969	1.143	0.394	0.105	-0.025	0.091	0.085	0.032	0.040	0.086	-	-	-
B249	10.30254	41.02000	2	2	old	5.8	18.436	1.945	1.017	0.572	0.451	0.035	0.168	0.029	0.026	0.036	5.2	15.025	0.092
SK074B	10.30288	41.66051	2	2	unknown	3.4	19.210	0.924	0.263	0.006	0.236	0.088	0.087	0.035	0.049	0.099	-	-	-
B019D	10.31727	41.08545	2	2	interm	3.4	19.384	1.760	0.772	0.506	0.515	0.043	0.242	0.048	0.051	0.073	3.4	15.049	0.064
SK097C	10.35195	42.33738	2	2	unknown	5.2	18.620	1.580	0.970	0.444	0.328	0.066	0.124	0.023	0.021	0.032	-	-	-
SK078B	10.35585	40.51484	2	2	unknown	2.8	20.739	-	1.438	0.621	0.362	0.222	-	0.066	0.044	0.068	3.4	15.543	0.137
SK080B	10.36252	40.69361	2	2	unknown	3.4	18.831	1.224	0.291	0.237	0.207	0.195	0.085	0.035	0.044	0.084	3.4	16.302	0.503
B022D	10.37504	41.28870	2	1	maybestar	2.8	18.539	1.505	0.344	0.143	0.082	0.029	0.086	0.033	0.047	0.089	2.8	16.413	0.127
B024D	10.39157	41.02353	2	2	unknown	2.8	20.140	-	0.923	0.408	0.522	0.199	-	0.069	0.073	0.109	2.8	16.230	0.733
SK085B	10.41936	40.97182	2	2	unknown	4.0	19.433	-	1.226	0.361	0.108	0.203	-	0.046	0.042	0.078	3.4	14.838	0.210
SK100C	10.42083	41.06825	2	2	unknown	2.8	19.567	2.224	1.318	0.567	0.412	0.057	0.353	0.041	0.034	0.048	2.8	14.481	0.125
BH13	10.44048	41.55697	2	2	unknown	2.8	22.169	-	2.100	0.659	0.067	0.516	-	0.206	0.084	0.206	2.8	15.943	0.183
B522-SK038A	10.46228	40.88002	2	2	old	5.8	18.688	1.443	0.684	0.496	0.391	0.042	0.118	0.036	0.039	0.057	5.8	14.717	0.056
B460	10.47824	39.59029	2	2	star	6.4	18.500	1.317	0.607	0.358	0.232	0.048	0.078	0.026	0.025	0.045	4.0	15.094	0.116
SK090B	10.48736	40.49512	2	2	unknown	3.4	20.223	-	1.128	0.498	0.396	0.106	-	0.056	0.046	0.073	3.4	15.567	0.072
B037D	10.49623	41.36611	2	2	maybestar	2.8	19.426	1.071	0.307	0.059	-0.060	0.079	0.127	0.066	0.106	0.234	-	-	-
B038D	10.50177	41.20395	2	2	unknown	3.4	19.303	1.546	0.779	0.489	0.397	0.041	0.196	0.053	0.059	0.085	-	-	-
SK104C	10.51279	40.06371	2	2	unknown	4.0	19.493	1.279	0.867	0.468	0.461	0.129	0.183	0.036	0.033	0.053	2.8	15.470	0.085
B258	10.53256	41.15737	2	2	unknown	4.0	18.532	1.512	0.560	0.072	0.151	0.116	0.115	0.038	0.054	0.103	-	-	-
B048D	10.55233	40.81051	2	2	maybestar	2.8	18.337	0.116	-0.019	-0.029	-0.082	0.038	0.029	0.024	0.034	0.079	-	-	-

SK096B	10.56891	41.41298	2	2	unknown	2.8	20.069	-	1.304	0.529	0.228	0.328	-	0.073	0.062	0.095	-	-	-
SK097B	10.56983	41.40458	2	2	-	-	-	-	-	-	-	-	-	-	-	-	-	-	-
SK102B	10.59450	40.37323	2	2	unknown	4.0	19.281	1.297	1.048	0.423	0.288	0.060	0.154	0.032	0.028	0.049	3.4	14.920	0.043
SK108C	10.59749	40.64348	2	2	unknown	3.4	21.160	-	1.922	0.655	0.449	0.388	-	0.107	0.050	0.072	3.4	15.209	0.122
SK104B	10.60392	40.60808	2	2	unknown	-	-	-	-	-	-	-	-	-	-	-	-	-	-
NB31	10.60458	41.29858	2	2	maybestar	-	-	-	-	-	-	-	-	-	-	-	-	-	-
NB66	10.60698	41.32983	2	2	maybestar	4.0	18.745	0.758	-0.247	-0.247	0.043	0.104	0.079	0.074	0.162	0.357	-	-	-
NB60	10.61117	41.30297	2	2	noobject	-	-	-	-	-	-	-	-	-	-	-	-	-	-
NB108	10.62200	41.25433	2	2	unknown	-	-	-	-	-	-	-	-	-	-	-	-	-	-
NB107	10.62614	41.25550	2	2	maybestar	3.4	18.564	1.118	0.306	-	-	0.067	0.078	0.041	-	-	-	-	-
NB77	10.62883	41.26061	2	2	maybestar	-	-	-	-	-	-	-	-	-	-	-	-	-	-
NB63	10.63016	41.33662	2	2	maybestar	5.8	17.297	1.424	0.322	0.180	0.054	0.038	0.048	0.023	0.030	0.052	-	-	-
NB24	10.63254	41.26253	2	2	unknown	-	-	-	-	-	-	-	-	-	-	-	-	-	-
SK107B	10.63777	41.18107	2	2	cluster	4.0	18.769	1.572	0.720	0.509	0.296	0.279	0.130	0.043	0.048	0.067	-	-	-
SK110C	10.63815	40.08177	2	2	unknown	4.0	20.100	-	1.206	0.388	0.245	0.191	-	0.051	0.040	0.079	-	-	-
V229	10.64375	40.92889	2	2	noobject	-	-	-	-	-	-	-	-	-	-	-	-	-	-
SK110B	10.64661	41.50514	2	2	unknown	4.0	17.965	0.248	-0.055	0.027	-0.135	0.110	0.034	0.033	0.053	0.123	-	-	-
NB29	10.64708	41.29644	2	2	na	-	-	-	-	-	-	-	-	-	-	-	-	-	-
NB57	10.65054	41.22033	2	2	noobject	-	-	-	-	-	-	-	-	-	-	-	-	-	-
B068D	10.66625	41.34442	2	2	old	-	-	-	-	-	-	-	-	-	-	-	-	-	-
NB62	10.68421	41.23975	2	2	unknown	-	-	-	-	-	-	-	-	-	-	-	-	-	-
BH16	10.69204	41.29333	2	2	unknown	-	-	-	-	-	-	-	-	-	-	-	-	-	-
B523	10.69283	41.30900	2	2	-	-	-	-	-	-	-	-	-	-	-	-	-	-	-
SK112B	10.69317	41.30917	2	2	-	-	-	-	-	-	-	-	-	-	-	-	-	-	-
SK114C	10.70062	40.30692	2	2	unknown	4.0	19.437	1.046	0.822	0.412	0.244	0.065	0.143	0.036	0.035	0.068	3.4	15.690	0.072
NB41	10.70075	41.26683	2	2	na	-	-	-	-	-	-	-	-	-	-	-	-	-	-
NB39-AU6	10.70229	41.26322	2	2	na	-	-	-	-	-	-	-	-	-	-	-	-	-	-
AU008	10.70401	41.30313	2	2	old	2.8	17.970	1.606	0.679	0.393	0.269	0.209	0.062	0.023	0.025	0.035	-	-	-
BH17	10.71188	40.97817	2	2	na	2.8	20.596	-	0.690	0.493	-0.177	0.232	-	0.110	0.124	0.280	-	-	-
NB59	10.71304	41.24350	2	2	star	-	-	-	-	-	-	-	-	-	-	-	-	-	-
SK113B	10.72955	40.99595	2	2	na	2.8	19.215	0.958	0.454	-0.006	0.071	0.058	0.085	0.043	0.065	0.133	-	-	-
B138	10.73165	41.30981	2	6	old	5.2	17.023	1.964	0.648	0.471	0.316	0.154	0.052	0.019	0.020	0.025	-	-	-
B524	10.73274	41.05361	2	2	unknown	2.8	19.605	1.530	0.457	0.115	0.182	0.092	0.179	0.056	0.082	0.154	-	-	-

SK115B	10.73529	40.68536	2	2	unknown	2.8	20.578	0.722	-	-	0.254	0.101	0.202	-	-	0.112	2.8	16.315	0.062
SK116B	10.73670	40.50349	2	2	unknown	3.4	20.348	-	1.111	0.469	0.345	0.143	-	0.057	0.047	0.086	-	-	-
B088D	10.74741	41.07149	2	2	na	4.0	18.189	1.378	-	-	-	0.152	0.071	0.035	0.058	-	-	-	-
SK117C	10.75496	40.74973	2	2	unknown	2.8	20.490	-	1.156	0.401	0.302	0.095	-	0.062	0.054	0.093	2.8	15.926	0.118
B092D	10.75684	41.21920	2	2	old	4.6	18.747	-	0.737	0.543	0.487	0.063	-	0.044	0.048	0.060	-	-	-
BH23	10.76554	41.34117	2	2	na	4.0	-	-	-	0.221	0.244	-	-	-	0.045	0.070	-	-	-
SK118C	10.77185	41.24127	2	2	cluster	4.0	18.875	2.161	0.904	0.611	0.550	0.063	0.241	0.045	0.045	0.054	-	-	-
SK120C	10.79255	41.28903	2	2	na	2.8	19.186	2.329	1.078	0.496	0.126	0.570	0.262	0.041	0.040	0.062	-	-	-
BH25	10.80000	41.04689	2	2	na	3.4	18.680	1.106	-0.025	0.113	-0.031	0.214	0.070	0.033	0.045	0.105	-	-	-
B225D	10.80599	40.02066	2	2	unknown	3.4	18.428	1.112	0.258	0.043	0.131	0.023	0.052	0.023	0.028	0.058	-	-	-
SK125B	10.82882	42.25318	2	2	unknown	5.2	16.055	1.970	0.850	0.301	0.146	0.019	0.025	0.012	0.012	0.014	3.4	13.086	0.027
SK126B	10.83885	41.32277	2	2	unknown	2.8	19.697	-	0.977	0.510	0.379	0.464	-	0.060	0.062	0.085	-	-	-
SK128B	10.84552	42.02845	2	2	unknown	5.2	19.417	-	0.980	0.579	0.219	0.065	-	0.040	0.036	0.076	4.6	15.230	0.090
SK133B	10.86192	40.41686	2	2	unknown	2.8	20.447	-	-	-	-	0.105	-	-	-	-	2.8	16.470	0.104
SK134B	10.86661	40.59998	2	2	unknown	3.4	19.453	1.033	0.703	0.510	0.141	0.050	0.127	0.035	0.034	0.067	2.8	15.429	0.039
SK126C	10.87521	40.28531	2	2	unknown	3.4	19.335	0.791	0.315	0.210	-	0.062	0.096	0.036	0.043	-	-	-	-
B274	10.91399	41.52172	2	2	unknown	3.4	19.330	-	0.812	0.346	0.149	0.074	-	0.044	0.050	0.092	2.8	15.732	0.251
SK138B	10.91400	41.16908	2	2	unknown	4.0	16.288	0.558	0.174	-0.002	0.077	0.111	0.018	0.015	0.020	0.030	-	-	-
B233D	10.92214	39.61274	2	2	unknown	9.4	16.723	1.255	0.666	0.452	0.215	0.028	0.026	0.014	0.014	0.017	-	-	-
SK128C	10.92460	40.40053	2	2	unknown	2.8	19.782	1.036	0.509	0.363	0.179	0.076	0.138	0.039	0.042	0.085	2.8	16.516	0.191
SK140B	10.92844	40.98263	2	2	unknown	2.8	20.483	-	1.155	0.448	0.345	0.082	-	0.062	0.053	0.086	2.8	16.312	0.241
B102D	10.93715	41.34098	2	2	maybestar	3.4	19.338	1.123	0.434	0.274	0.298	0.225	0.127	0.058	0.078	0.127	-	-	-
B104D-M2	10.95458	41.23770	2	2	maybestar	4.0	18.506	0.982	0.403	0.279	0.147	0.085	0.071	0.043	0.058	0.097	-	-	-
SK133C	10.96568	40.62890	2	2	unknown	3.4	20.228	0.918	1.006	0.558	0.321	0.142	0.222	0.054	0.045	0.082	2.8	15.524	0.140
SK147B	10.97160	40.33290	2	2	unknown	5.2	19.115	0.859	0.472	0.214	0.216	0.177	0.104	0.035	0.040	0.084	4.0	16.216	0.308
SK135C	11.00499	41.06827	2	2	unknown	4.6	19.810	-	1.662	0.578	0.416	0.132	-	0.048	0.031	0.043	4.6	14.348	0.135
M012	11.01181	41.36120	2	2	interm	4.6	19.032	1.436	0.768	0.506	0.555	0.111	0.152	0.048	0.051	0.065	3.4	14.899	0.120
SK136C	11.01857	40.08882	2	2	unknown	2.8	19.271	1.503	0.522	0.241	0.055	0.045	0.111	0.030	0.032	0.070	-	-	-
SK137C	11.02389	41.26443	2	2	unknown	2.8	20.201	-	1.670	0.900	0.580	0.169	-	0.074	0.043	0.049	2.8	14.324	0.087
SK138C	11.04995	42.18521	2	2	unknown	5.8	19.188	-	1.323	0.550	0.299	0.135	-	0.033	0.026	0.049	5.2	14.363	0.116
SK084A	11.05143	41.35300	2	1	na	2.8	19.684	0.775	0.931	0.560	0.238	0.166	0.110	0.053	0.052	0.078	2.8	15.511	0.265
SH14	11.06167	41.92331	2	2	missing	-	-	-	-	-	-	-	-	-	-	-	-	-	-
SK140C	11.06939	40.60742	2	2	unknown	3.4	-	-	-	0.435	0.398	-	-	-	0.051	0.093	2.8	15.730	0.095

B277-M22	11.07047	41.23772	2	2	interm	4.6	19.235	1.303	0.554	0.371	0.080	0.134	0.150	0.041	0.047	0.091	4.0	16.504	0.326
B246D	11.09512	42.07584	2	2	maybestar	7.0	16.305	0.035	-0.154	-0.135	-0.108	0.014	0.016	0.014	0.016	0.035	4.6	15.932	0.130
SK142C	11.10240	41.86272	2	2	unknown	4.0	19.958	-	1.499	0.962	0.808	0.343	-	0.060	0.038	0.039	4.0	13.512	0.072
SK167B	11.10482	40.93740	2	2	unknown	2.8	20.537	1.172	1.230	0.432	0.509	0.062	0.290	0.055	0.044	0.072	2.8	15.447	0.168
SK168B	11.10958	40.25143	2	2	unknown	4.6	18.032	1.294	0.563	0.266	0.154	0.027	0.050	0.020	0.020	0.035	4.0	14.838	0.062
B115D-M33	11.11048	41.64927	2	2	na	5.2	18.617	1.274	0.397	0.318	-0.157	0.062	0.093	0.036	0.046	0.103	3.4	15.945	0.215
SK169B	11.11103	40.71275	2	2	unknown	3.4	20.207	-	1.387	0.510	0.444	0.123	-	0.049	0.035	0.058	4.0	15.117	0.079
SK171B	11.11872	40.70669	2	2	unknown	5.8	18.837	1.641	1.065	0.524	0.414	0.066	0.152	0.027	0.023	0.035	5.8	14.276	0.060
SK147C	11.13467	40.27789	2	2	unknown	5.8	19.588	-	1.469	0.541	0.431	0.122	-	0.046	0.028	0.043	5.8	14.335	0.068
SK148C	11.13558	40.64905	2	2	unknown	6.4	18.666	1.963	1.229	0.518	0.336	0.098	0.199	0.024	0.020	0.029	6.4	13.918	0.080
SK149C	11.14321	41.85508	2	2	cluster	-	-	-	-	-	-	-	-	-	-	-	-	-	-
SK175B	11.14677	40.73143	2	2	unknown	4.0	19.658	1.044	1.054	0.360	0.655	0.074	0.166	0.040	0.036	0.055	3.4	15.472	0.056
M046	11.15278	41.45391	2	2	na	4.0	18.863	1.256	0.171	0.145	0.162	0.102	0.105	0.048	0.073	0.137	2.8	18.053	0.805
M047	11.15757	41.48115	2	2	interm	4.0	19.392	1.301	0.862	0.213	0.077	0.104	0.169	0.052	0.062	0.119	2.8	16.482	0.190
SK153C	11.16035	41.41979	2	2	cluster	7.0	16.811	0.328	0.732	-0.733	0.475	0.029	0.021	0.016	0.024	0.036	10.0	14.454	0.150
BH28	11.16280	41.74060	2	2	na	4.0	20.022	-	0.602	0.513	0.011	0.103	-	0.082	0.091	0.199	2.8	16.769	0.251
SK090A	11.17726	41.68606	2	1	unknown	3.4	19.949	-	0.644	0.187	0.037	0.301	-	0.070	0.092	0.199	2.8	16.796	1.284
SK179B	11.17866	41.55728	2	2	star	4.0	18.077	1.201	0.480	0.355	0.129	0.039	0.056	0.025	0.030	0.048	4.0	15.126	0.114
SK156C	11.19149	40.58881	2	2	unknown	2.8	21.375	-	1.664	0.664	0.308	0.200	-	0.097	0.050	0.087	2.8	15.914	0.126
SK157C	11.19305	40.55196	2	2	unknown	2.8	20.430	0.708	0.610	0.123	0.026	0.053	0.195	0.058	0.068	0.185	-	-	-
SK158C	11.20830	40.38773	2	2	unknown	3.4	20.283	-	1.470	0.615	0.304	0.082	-	0.057	0.033	0.055	3.4	14.957	0.147
SK092A	11.21481	41.84909	2	1	unknown	3.4	20.263	-	0.415	0.078	0.422	0.300	-	0.092	0.130	0.259	-	-	-
SK159C	11.22263	41.53229	2	2	cluster	2.8	20.129	-	0.595	0.046	-0.846	0.272	-	0.070	0.109	0.473	-	-	-
SK160C	11.22686	40.11235	2	2	unknown	4.0	19.619	-	1.004	0.438	0.436	0.121	-	0.042	0.033	0.052	-	-	-
SK184B	11.22808	41.87559	2	2	unknown	4.0	20.067	-	0.836	0.097	0.407	0.104	-	0.076	0.089	0.176	3.4	17.166	0.584
M053	11.23877	41.80054	2	2	interm	2.8	19.845	-	0.992	0.627	0.464	0.122	-	0.047	0.043	0.061	2.8	14.765	0.062
SK189B	11.24713	40.97279	2	2	unknown	2.8	20.226	1.510	0.574	0.372	0.288	0.092	0.300	0.052	0.057	0.117	2.8	16.857	0.146
M055	11.24835	41.56086	2	2	na	4.0	19.258	1.552	0.881	0.287	-0.525	0.044	0.183	0.044	0.049	0.149	2.8	16.904	0.953
SK190B	11.25680	40.40317	2	2	unknown	6.4	18.807	1.967	1.301	0.441	0.335	0.077	0.168	0.028	0.021	0.032	7.0	14.110	0.049
SK095A	11.25927	41.82768	2	1	unknown	2.8	19.666	1.856	0.836	0.386	0.284	0.072	0.275	0.043	0.043	0.079	2.8	16.301	0.206
SK192B	11.26602	40.49988	2	2	unknown	5.8	18.691	0.985	0.623	0.355	0.094	0.076	0.087	0.026	0.027	0.053	3.4	15.313	0.081
SK193B	11.26732	40.71878	2	2	unknown	4.6	19.240	1.321	0.981	0.378	0.387	0.068	0.169	0.032	0.028	0.047	3.4	15.246	0.144
SK194B	11.26991	40.50892	2	2	unknown	3.4	19.038	0.775	0.362	0.294	0.008	0.067	0.079	0.029	0.033	0.075	2.8	16.137	0.091

SK097A	11.27128	41.70811	2	1	unknown	3.4	19.353	1.091	0.368	0.215	0.090	0.164	0.117	0.049	0.066	0.137	2.8	15.546	0.111
SK162C	11.27824	40.73543	2	2	unknown	3.4	19.760	-	1.164	0.463	0.370	0.235	-	0.037	0.029	0.049	3.4	15.284	0.108
B476-D074	11.27992	41.67534	2	2	interm	5.2	18.818	1.505	0.731	0.404	0.247	0.152	0.130	0.036	0.040	0.065	2.8	15.992	0.306
SK197B	11.28139	41.00339	2	2	unknown	3.4	19.528	0.808	0.356	0.228	-0.232	0.071	0.111	0.041	0.050	0.157	-	-	-
M065	11.29154	41.70652	2	2	unknown	4.6	19.138	1.340	0.169	-0.219	-0.047	0.192	0.143	0.055	0.101	0.264	-	-	-
SK165C	11.29597	40.58738	2	2	unknown	4.0	20.118	-	1.022	0.430	0.500	0.128	-	0.054	0.046	0.076	-	-	-
M070	11.29910	41.67215	2	2	interm	4.0	19.718	-	0.954	0.501	0.284	0.109	-	0.059	0.059	0.094	3.4	15.418	0.122
SK172C	11.33110	41.38114	2	2	unknown	4.0	20.234	-	1.444	0.529	0.192	0.331	-	0.062	0.045	0.078	4.0	15.115	0.163
SK175C	11.33818	41.68222	2	2	unknown	2.8	19.377	1.173	0.469	0.251	-	0.036	0.109	0.042	0.053	-	2.8	16.613	0.424
SK174C	11.33841	41.50045	2	2	unknown	2.8	21.854	-	2.179	-0.649	0.717	0.406	-	0.158	0.130	0.224	2.8	16.931	0.389
SK179C	11.35571	40.31689	2	2	unknown	2.8	19.929	1.091	0.629	0.331	0.126	0.047	0.135	0.044	0.043	0.096	-	-	-
SK180C	11.36219	41.26253	2	2	unknown	3.4	20.188	1.162	0.960	0.491	0.226	0.112	0.247	0.059	0.055	0.097	2.8	15.637	0.128
SK181C	11.36343	41.69974	2	2	unknown	3.4	19.805	1.220	0.731	0.273	-0.172	0.149	0.189	0.059	0.069	0.172	-	-	-
SK182C	11.36383	41.54835	2	2	unknown	3.4	19.778	0.627	1.270	0.616	0.366	0.091	0.113	0.041	0.032	0.047	3.4	14.582	0.101
SK183C	11.36489	41.39000	2	2	unknown	6.4	18.302	1.707	0.996	0.445	0.309	0.073	0.104	0.023	0.021	0.031	6.4	14.101	0.144
SK202B	11.36845	41.51443	2	2	unknown	2.8	20.033	-	1.169	0.597	0.155	0.041	-	0.044	0.035	0.060	2.8	15.301	0.124
SK204B	11.37750	40.79954	2	2	unknown	4.0	19.983	-	1.056	0.420	0.324	0.118	-	0.049	0.041	0.074	-	-	-
SK205B	11.38863	40.28576	2	2	unknown	2.8	19.708	-	0.683	0.410	0.261	0.069	-	0.038	0.035	0.066	-	-	-
B267D	11.39946	40.59295	2	2	maybestar	3.4	17.746	1.462	0.542	0.182	0.088	0.036	0.042	0.017	0.018	0.029	-	-	-
BH29	11.40551	41.61258	2	2	na	4.0	19.805	0.840	0.399	0.171	-0.152	0.137	0.157	0.061	0.081	0.228	-	-	-
SK187C	11.40723	41.90121	2	2	unknown	4.0	19.417	1.641	0.562	0.324	0.036	0.045	0.220	0.049	0.057	0.125	2.8	17.095	0.377
SK188C	11.41167	41.89480	2	2	unknown	3.4	20.049	-	0.619	0.260	0.396	0.235	-	0.067	0.080	0.143	2.8	16.719	0.116
SK207B	11.41328	41.83201	2	2	unknown	4.0	19.263	1.999	0.679	0.395	0.264	0.089	0.261	0.042	0.045	0.080	4.0	15.666	0.084
M095	11.41611	41.74490	2	2	unknown	3.4	19.352	0.841	0.362	0.371	0.077	0.213	0.097	0.049	0.061	0.122	2.8	16.982	0.139
SK190C	11.43330	41.90752	2	2	unknown	7.0	18.642	-	1.110	0.769	0.448	0.125	-	0.034	0.027	0.035	7.0	13.617	0.074
SK210B	11.44619	40.75505	2	2	unknown	6.4	18.859	2.188	1.094	0.410	0.404	0.032	0.290	0.027	0.023	0.036	-	-	-
SK192C	11.44904	41.87146	2	2	unknown	2.8	19.894	1.633	0.430	0.096	0.089	0.131	0.237	0.056	0.076	0.177	-	-	-
B270D	11.45510	41.03032	2	2	maybestar	7.0	17.814	1.460	0.612	0.304	0.188	0.079	0.063	0.019	0.019	0.033	-	-	-
DAO83	11.45768	41.80503	2	2	maybestar	2.8	19.870	1.799	0.157	-0.175	0.004	0.050	0.267	0.062	0.110	0.297	-	-	-
SK193C	11.45822	40.08590	2	2	unknown	7.0	17.819	1.975	0.990	0.419	0.257	0.043	0.078	0.018	0.016	0.022	-	-	-
SK194C	11.45897	41.73052	2	2	back	4.0	20.029	-	1.376	0.683	0.465	0.247	-	0.066	0.048	0.064	3.4	14.604	0.144
SH18	11.46117	40.50651	2	2	-	-	-	-	-	-	-	-	-	-	-	-	-	-	-
SK195C	11.46387	40.42925	2	2	unknown	5.2	19.511	-	1.351	0.543	0.449	0.130	-	0.042	0.027	0.042	-	-	-

SK196C	11.46492	40.07886	2	2	unknown	3.4	19.680	2.143	1.113	0.409	0.340	0.087	0.316	0.039	0.030	0.048	-	-	-
SK105A	11.46608	41.96155	2	1	unknown	2.8	19.404	1.645	0.564	0.401	0.329	0.210	0.158	0.037	0.042	0.067	2.8	15.875	0.090
SK212B	11.46729	41.53054	2	2	unknown	3.4	19.814	-	0.823	0.302	0.175	0.054	-	0.047	0.049	0.096	-	-	-
SK213B	11.47449	41.68656	2	2	unknown	3.4	19.474	1.030	0.615	0.324	0.397	0.198	0.124	0.048	0.057	0.091	2.8	15.550	0.066
SK214B	11.47515	39.94646	2	2	unknown	3.4	19.942	-	1.317	0.725	0.376	0.093	-	0.036	0.026	0.036	-	-	-
SK197C	11.49022	40.28601	2	2	unknown	5.2	18.692	1.093	0.639	0.368	0.136	0.064	0.076	0.027	0.026	0.048	-	-	-
SK216B	11.51128	41.74799	2	2	unknown	2.8	18.948	-0.003	-0.285	-0.299	-	0.057	0.038	0.046	0.093	-	-	-	-
SK198C	11.51185	40.38444	2	2	unknown	2.8	21.004	-	1.632	0.498	0.337	0.246	-	0.083	0.041	0.071	-	-	-
SK199C	11.51576	41.60803	2	2	unknown	2.8	19.771	0.804	0.507	0.181	0.021	0.132	0.109	0.044	0.054	0.126	-	-	-
SK200C	11.52545	40.37388	2	2	unknown	5.8	18.950	2.151	1.285	0.439	0.452	0.118	0.233	0.031	0.022	0.032	-	-	-
SK217B	11.53930	41.48452	2	2	unknown	2.8	19.625	1.485	0.401	0.171	-0.040	0.063	0.166	0.042	0.053	0.129	-	-	-
SK218B	11.54201	40.92035	2	2	unknown	5.8	19.004	1.445	1.001	0.423	0.271	0.067	0.166	0.029	0.025	0.043	-	-	-
B276D	11.54304	40.84228	2	2	maybestar	2.8	18.264	1.444	0.617	0.209	0.083	0.018	0.063	0.019	0.019	0.032	-	-	-
SK201C	11.57144	41.60996	2	2	unknown	4.6	20.044	-	1.463	0.610	0.415	0.175	-	0.059	0.041	0.060	4.6	14.967	0.087
SK220B	11.57429	41.74560	2	2	unknown	3.4	20.400	-	0.873	0.206	0.224	0.119	-	0.067	0.071	0.153	-	-	-
SK202C	11.57638	41.78360	2	2	unknown	4.0	19.964	1.223	0.785	0.434	0.190	0.087	0.248	0.067	0.069	0.134	3.4	15.730	0.089
SK221B	11.58025	40.39502	2	2	unknown	2.8	20.858	-	0.851	0.162	-	0.112	-	0.082	0.076	-	-	-	-
B281D	11.59274	40.30234	2	2	maybestar	2.8	18.451	1.067	0.383	0.123	0.012	0.031	0.046	0.021	0.023	0.044	-	-	-
SK203C	11.59512	40.96353	2	2	unknown	3.4	19.884	-	1.081	0.443	0.391	0.177	-	0.041	0.033	0.056	3.4	15.447	0.074
SK204C	11.59561	40.34508	2	2	unknown	2.8	20.103	1.624	1.147	0.428	0.366	0.069	0.244	0.045	0.033	0.054	-	-	-
BH32	11.59820	42.01617	2	2	na	2.8	20.488	-	0.831	0.339	0.325	0.115	-	0.067	0.069	0.133	-	-	-
SK205C	11.60343	40.58572	2	2	unknown	7.0	19.011	-	1.318	0.519	0.430	0.121	-	0.035	0.025	0.037	-	-	-
B283D	11.61906	41.88487	2	2	maybestar	6.4	17.647	1.166	0.446	0.234	0.081	0.046	0.041	0.019	0.021	0.038	4.6	15.684	0.225
SK223B	11.63737	40.11049	2	2	unknown	4.0	18.234	1.933	0.694	0.267	0.152	0.065	0.112	0.019	0.019	0.031	-	-	-
SK206C	11.64457	40.51141	2	2	unknown	3.4	19.987	-	0.776	0.383	0.272	0.063	-	0.051	0.046	0.091	-	-	-
SK207C	11.65233	41.17555	2	2	unknown	3.4	19.607	1.513	0.738	0.413	0.249	0.175	0.225	0.037	0.035	0.067	3.4	15.702	0.102
SK208C	11.65352	40.71702	2	2	unknown	3.4	19.720	1.576	0.968	0.474	0.375	0.098	0.199	0.041	0.033	0.056	-	-	-
B291D	11.67221	40.05088	2	2	maybestar	3.4	18.502	1.310	0.502	0.092	0.203	0.022	0.075	0.021	0.022	0.040	-	-	-
SK226B	11.69946	42.03235	2	2	unknown	2.8	20.142	1.397	0.602	0.194	0.299	0.042	0.232	0.053	0.063	0.135	-	-	-
B293D	11.70015	40.03930	2	2	maybestar	4.6	18.160	1.230	0.402	0.243	-0.181	0.024	0.063	0.020	0.021	0.043	-	-	-
SK212C	11.72145	41.36863	2	2	unknown	4.6	19.596	-	1.309	0.562	0.451	0.117	-	0.038	0.028	0.044	4.6	14.597	0.101
SK227B	11.72700	42.01317	2	2	-	-	-	-	-	-	-	-	-	-	-	-	-	-	-
SK213C	11.74498	42.29593	2	2	unknown	5.2	19.395	1.270	0.677	0.369	0.334	0.127	0.193	0.041	0.042	0.094	2.8	16.065	0.097

SK214C	11.74550	40.90068	2	2	unknown	5.2	19.001	1.835	1.272	0.478	0.371	0.093	0.164	0.029	0.022	0.033	5.8	14.205	0.059
SK230B	11.75918	41.18207	2	2	unknown	4.0	19.659	-	1.000	0.406	0.454	0.086	-	0.040	0.034	0.057	3.4	15.625	0.102
SK215C	11.75967	41.05701	2	2	unknown	3.4	20.200	-	1.161	0.491	0.476	0.289	-	0.049	0.038	0.062	4.0	15.492	0.188
SK216C	11.76569	41.65406	2	2	unknown	4.0	19.695	-	1.166	0.466	0.342	0.038	-	0.043	0.035	0.059	4.0	15.157	0.069
SK231B	11.80885	40.37315	2	2	unknown	2.8	19.217	0.960	0.308	0.308	0.006	0.085	0.072	0.031	0.033	0.071	-	-	-
BA28	11.80924	42.36173	2	2	unknown	4.0	19.374	-	0.872	0.493	0.053	0.051	-	0.036	0.033	0.080	3.4	15.081	0.049
SK232B	11.81019	40.42749	2	2	unknown	4.0	19.259	-	0.994	0.444	0.454	0.066	-	0.034	0.027	0.040	-	-	-
SK233B	11.81332	41.02012	2	2	unknown	4.6	19.233	0.816	0.778	0.321	0.118	0.055	0.110	0.032	0.032	0.067	2.8	15.545	0.070
SK219C	11.85542	41.03929	2	2	unknown	2.8	19.687	1.084	0.398	0.220	-	0.075	0.141	0.038	0.044	-	-	-	-
SK234B	11.89690	41.02536	2	2	unknown	4.0	19.019	0.983	0.495	0.277	0.224	0.031	0.080	0.032	0.034	0.069	3.4	15.926	0.068
DAO93	11.94250	41.74861	2	2	noobject	-	-	-	-	-	-	-	-	-	-	-	-	-	-
DAO94	11.97659	42.73376	2	2	unknown	4.0	19.113	1.637	1.038	0.458	0.379	0.083	0.186	0.028	0.025	0.047	-	-	-
BA10	11.98445	42.47871	2	2	unknown	4.0	19.589	-	0.760	0.483	0.052	0.100	-	0.041	0.039	0.104	-	-	-
SK221C	11.99513	41.65929	2	2	unknown	2.8	20.223	-	0.897	0.454	0.408	0.251	-	0.047	0.043	0.077	2.8	15.909	0.056
SK222C	11.99786	41.90366	2	2	unknown	3.4	19.849	1.131	0.476	0.235	0.410	0.184	0.177	0.048	0.057	0.109	-	-	-
SK238B	12.00710	41.83245	2	2	unknown	3.4	18.770	1.096	0.288	0.121	0.080	0.059	0.073	0.027	0.033	0.074	-	-	-
SK223C	12.01921	40.14094	2	2	unknown	4.6	18.827	1.288	1.207	0.458	0.327	0.038	0.131	0.024	0.020	0.027	-	-	-
SK224C	12.03600	41.81896	2	2	unknown	4.6	18.870	1.633	1.088	0.467	0.328	0.060	0.151	0.025	0.022	0.036	5.8	14.334	0.063
SK240B	12.10062	40.11206	2	2	unknown	2.8	19.984	0.667	0.748	0.347	0.223	0.114	0.148	0.041	0.039	0.069	-	-	-
SK242B	12.11109	41.32975	2	2	unknown	5.2	20.064	-	0.555	0.385	0.323	0.153	-	0.065	0.069	0.141	-	-	-
SK243B	12.11337	42.04546	2	2	unknown	10.0	17.676	1.838	1.076	0.476	0.395	0.044	0.079	0.018	0.016	0.021	8.8	13.290	0.045
SK244B	12.11437	41.10475	2	2	unknown	3.4	20.642	-	1.296	0.392	0.209	0.106	-	0.076	0.051	0.106	-	-	-
SK225C	12.13074	42.01825	2	2	unknown	4.6	18.374	1.824	1.073	0.513	0.364	0.151	0.110	0.021	0.018	0.026	4.6	13.828	0.086
SK249B	12.13747	42.04591	2	2	unknown	5.8	18.968	1.886	1.019	0.420	0.238	0.050	0.202	0.028	0.025	0.045	4.6	14.809	0.035
SK252B	12.17169	41.53178	2	2	unknown	3.4	18.920	1.533	0.643	0.189	0.261	0.038	0.129	0.025	0.027	0.051	-	-	-
SK227C	12.18363	42.26361	2	2	unknown	3.4	19.750	-	0.934	0.405	0.364	0.060	-	0.038	0.034	0.062	3.4	15.652	0.120
B504	12.18817	40.14620	2	2	star	7.0	18.129	1.657	0.983	0.401	0.300	0.042	0.118	0.020	0.018	0.025	-	-	-
SK228C	12.19374	41.77946	2	2	unknown	2.8	20.795	0.608	0.851	0.314	0.620	0.069	0.233	0.070	0.070	0.124	2.8	16.944	0.126
B334D	12.22861	39.59899	2	2	unknown	5.8	18.166	2.104	1.161	0.453	0.303	0.123	0.147	0.020	0.017	0.022	-	-	-
SK255B	12.26248	41.91600	2	2	unknown	7.0	18.033	1.883	0.698	0.351	0.209	0.059	0.105	0.020	0.020	0.035	4.0	15.321	0.100
SK256B	12.27252	41.96070	2	2	unknown	4.6	19.818	-	1.498	0.498	0.466	0.125	-	0.042	0.029	0.047	4.6	14.697	0.075
SK229C	12.29609	41.96480	2	2	unknown	3.4	20.430	0.701	0.819	0.358	-	0.115	0.213	0.062	0.062	-	2.8	16.210	0.073
SK257B	12.31341	41.02490	2	2	unknown	2.8	19.065	1.433	0.491	0.197	0.018	0.047	0.096	0.028	0.029	0.060	-	-	-

B338D	12.31571	40.77340	2	2	unknown	8.2	18.294	-	1.049	0.455	0.380	0.077	-	0.021	0.019	0.026	-	-	-
B339D	12.32291	40.75195	2	2	unknown	8.8	18.232	-	1.124	0.497	0.322	0.065	-	0.020	0.018	0.024	-	-	-
DAO104	12.33889	42.27119	2	2	unknown	5.2	19.262	1.218	0.584	0.351	0.227	0.093	0.141	0.035	0.037	0.076	3.4	16.094	0.107
SK232C	12.35699	42.10204	2	2	unknown	4.0	19.209	2.256	0.959	0.402	0.422	0.074	0.335	0.030	0.028	0.047	4.0	15.054	0.054
B340D	12.37155	41.07558	2	2	unknown	5.8	18.498	-	1.047	0.430	0.361	0.074	-	0.024	0.020	0.028	-	-	-
SK233C	12.39852	42.19533	2	2	unknown	4.6	19.607	1.141	1.075	0.468	0.506	0.133	0.173	0.039	0.032	0.051	4.0	15.278	0.081
B344D	12.46693	41.61080	2	1	unknown	4.6	17.426	1.325	0.600	0.279	0.175	0.055	0.042	0.016	0.016	0.023	3.4	14.700	0.069
B346D	12.51556	40.62766	2	2	unknown	7.0	18.345	1.584	1.125	0.500	0.292	0.062	0.129	0.021	0.018	0.024	-	-	-
SK258B	12.57280	42.11196	2	2	unknown	4.6	19.770	-	0.971	0.375	0.462	0.041	-	0.043	0.040	0.072	3.4	15.764	0.075
B348D	12.58008	40.96753	2	2	unknown	5.2	19.094	-	1.143	0.452	0.405	0.083	-	0.027	0.022	0.032	-	-	-
B511	12.68121	40.18703	2	2	star	6.4	18.013	1.309	0.682	0.388	0.184	0.034	0.070	0.020	0.019	0.027	-	-	-
SH25	12.99458	41.58806	2	2	noobject	-	-	-	-	-	-	-	-	-	-	-	-	-	-

[1]Cluster name, taken from the Revised Bologna Catalogue (Galleti *et al.*, 2004)

[2]Position of object in SDSS *r*-band image [J2000, degrees]

[3]Classification of source as described in chapter 2. Options for flag, f: 1-old globular cluster; 2-candidate cluster (21-candidate old cluster, 23-candidate young cluster); 3-young cluster; 4-galaxy; 5-HII region; 6-stellar source. Flags f_{RBC} and f_{C09} indicate the previous classifications of the source from the RBC v3.5 of Galleti *et al.* (2004) and from the catalogue of Caldwell *et al.* (2009), respectively.

[4]Aperture size used to measure the total magnitude of the cluster [arcsec]

[5]Error on the total magnitude, includes the statistical, calibration and systematic errors

D

The structural parameters of old clusters in M31 (table 3.1)

This table contains the structural parameters for the 213 old clusters covered by our WFCAM survey of M31. These parameters are measured from King model fits to the WFCAM K-band images of these clusters, as presented in chapter 3. This table is the full version of table 3.1, it is also available in electronic form from the VizieR archive.

GC Name[1]	$\chi^2/\nu^{(2)}$	$W_0^{(3)}$	$c^{(3)}$	$K^{(4)}$	$r_c^{(5)}$	$r_h^{(5)}$	$r_t^{(5)}$	$\log(\rho_c)^{(6)}$	$\log(\Gamma)^{(6)}$	Flag[7]
B001-G039	1.07	6.25	13.70	1.31	1.25	2.71	25.9	3.87	6.00	1
B002-G043	1.07	8.10	15.34	1.86	0.34	1.93	24.8	4.55	5.90	1
B003-G045	1.15	9.55	14.91	2.25	0.24	4.05	42.7	4.82	5.99	1
B004-G050	1.69	6.45	14.18	1.37	0.92	2.13	21.4	4.05	6.01	1
B005-G052	1.20	8.25	12.54	1.91	0.36	2.27	29.1	5.57	7.47	12
B006-G058	0.85	9.60	12.64	2.26	0.20	3.47	36.2	5.97	7.55	1
B008-G060	11.15	4.30	14.04	0.89	2.16	2.77	16.8	3.31	5.63	1
B009-G061	1.35	7.40	14.63	1.65	0.56	2.00	24.6	4.35	6.02	1
B010-G062	1.02	6.00	14.00	1.25	2.70	5.37	48.2	2.79	5.05	1
B011-G063	1.28	7.00	14.20	1.52	0.63	1.84	21.1	4.44	6.26	1
B012-G064	0.95	7.25	12.69	1.60	0.91	3.00	36.1	4.52	6.70	1
B013-G065	1.06	3.35	14.47	0.73	4.90	5.08	26.1	2.21	4.70	1

B015-V204	1.33	6.30	13.48	1.33	1.78	3.91	37.9	3.50	5.74	1
B016-G066	1.14	9.10	14.41	2.14	0.21	2.59	29.6	5.29	6.60	1
B017-G070	0.92	7.70	12.49	1.74	0.72	3.09	39.4	4.81	6.93	1
B019-G072	1.12	7.65	12.01	1.72	0.64	2.67	33.9	5.16	7.36	2
B020-G073	1.17	7.20	12.17	1.58	0.84	2.72	32.4	4.83	7.10	1
B020D-G089	1.15	8.95	14.06	2.10	0.44	4.75	55.8	4.53	6.08	1
B021-G075	0.98	7.70	13.90	1.74	0.68	2.90	37.0	4.33	6.15	1
B022-G074	0.98	6.40	15.23	1.35	0.94	2.14	21.3	3.61	5.36	1
B023-G078	1.54	6.25	10.78	1.31	1.65	3.57	34.2	4.67	7.45	1
B024-G082	0.94	8.10	13.97	1.86	0.30	1.71	22.1	5.25	6.85	1
B025-G084	1.07	5.65	13.95	1.17	0.94	1.69	13.9	4.23	6.29	1
B026-G086	1.08	5.90	14.32	1.23	1.23	2.37	20.7	3.70	5.73	1
B027-G087	1.02	5.80	12.99	1.20	1.37	2.56	21.8	4.11	6.44	1
B028-G088	1.05	5.90	14.33	1.23	1.25	2.41	21.0	3.68	5.71	1
B029-G090	1.08	7.15	13.09	1.57	1.32	4.16	49.1	3.89	6.08	1
B030-G091	1.06	5.60	13.33	1.16	1.06	1.88	15.3	4.33	6.55	1
B031-G092	1.04	5.15	14.52	1.06	1.15	1.80	13.1	3.82	5.85	1
B032-G093	1.27	6.70	14.03	1.44	0.62	1.58	17.0	4.58	6.46	1
B033-G095	0.45	8.15	14.86	1.88	0.48	2.78	35.8	4.30	5.81	1
B034-G096	1.00	7.45	12.45	1.66	0.59	2.16	26.8	5.15	7.26	1
B035	1.24	7.55	14.53	1.69	0.33	1.30	16.3	5.03	6.59	1
B036	1.13	7.00	14.34	1.52	0.65	1.89	21.7	4.34	6.14	1
B037-V327	1.17	5.60	11.00	1.16	2.20	3.88	31.5	4.32	7.16	2
B038-G098	1.08	5.55	13.69	1.15	1.11	1.94	15.5	4.13	6.29	1
B039-G101	1.00	7.60	12.42	1.71	0.69	2.76	34.9	4.92	7.06	1
B041-G103	1.04	13.97	16.47	3.13	0.03	4.42	39.5	5.95	5.86	6
B042-G104	0.99	6.35	12.15	1.34	0.84	1.89	18.5	4.99	7.34	2
B045-G108	1.14	7.05	12.93	1.54	0.96	2.87	33.2	4.39	6.55	1
B046-G109	1.18	6.60	15.27	1.41	0.75	1.84	19.3	3.85	5.53	1
B047-G111	1.83	4.40	15.01	0.91	2.58	3.38	20.9	2.67	4.83	1
B050-G113	2.19	7.95	13.88	1.81	0.34	1.74	22.4	5.17	6.82	1
B054-G115	1.09	6.15	14.46	1.29	0.91	1.89	17.7	4.00	5.92	1
B056-G117	1.00	8.15	13.53	1.88	0.43	2.51	32.4	4.97	6.72	1
B057-G118	1.36	9.30	15.16	2.19	0.22	3.08	34.0	4.91	6.04	1
B058-G119	1.18	7.75	12.38	1.75	0.47	2.07	26.5	5.41	7.45	1
B060-G121	1.01	2.40	14.39	0.57	2.20	1.82	8.2	3.44	5.85	1
B061-G122	1.26	7.65	12.93	1.72	0.58	2.40	30.5	4.93	6.92	1
B063-G124	1.36	7.45	12.03	1.66	0.55	2.04	25.3	5.39	7.57	1
B065-G126	1.48	3.65	14.47	0.78	2.41	2.67	14.4	3.09	5.40	1
B067-G129	1.03	5.70	15.18	1.18	0.82	1.48	12.3	3.92	5.70	1
B068-G130	1.11	7.95	12.60	1.81	0.49	2.49	32.2	5.21	7.20	2
B073-G134	1.11	8.50	12.99	1.98	0.31	2.33	29.2	5.54	7.28	1
B074-G135	1.07	6.60	14.15	1.41	1.18	2.91	30.4	3.71	5.70	1
B076-G138	1.12	8.55	14.14	1.99	0.28	2.17	27.1	5.21	6.70	1
B082-G144	1.02	7.80	11.40	1.77	0.46	2.11	27.0	5.81	8.04	1
B083-G146	1.59	5.75	14.41	1.19	2.70	4.98	41.9	2.66	4.86	1
B085-G147	1.11	7.55	14.34	1.69	0.65	2.52	31.7	4.25	5.99	1
B090	1.08	1.80	15.22	0.47	2.81	1.95	8.2	2.90	5.25	1
B091D-D058	388.85	6.60	12.49	1.41	0.53	1.30	13.6	5.42	7.58	3
B094-G156	1.15	7.80	12.49	1.77	0.40	1.84	23.6	5.55	7.53	1
B095-G157	0.06	5.25	13.28	1.08	1.84	2.96	22.0	3.68	6.06	3
B098	1.21	7.00	13.44	1.52	0.41	1.21	13.9	5.29	7.17	1
B100-G163	1.23	4.45	14.82	0.92	2.93	3.88	24.2	2.58	4.80	1
B110-G172	1.18	7.50	12.24	1.68	0.43	1.62	20.3	5.63	7.71	1
B111-G173	1.26	6.70	14.30	1.44	0.72	1.85	19.8	4.27	6.13	1

B117-G176	1.23	7.30	14.01	1.61	0.58	1.96	23.8	4.57	6.38	1
B125-G183	1.17	10.60	14.15	2.47	0.12	3.78	34.5	5.80	6.84	1
B135-G192	1.05	7.40	13.12	1.65	0.67	2.38	29.3	4.73	6.74	1
B137-G195	1.10	8.05	13.85	1.84	1.00	5.45	70.3	3.76	5.64	1
B141-G197	1.04	8.70	13.78	2.04	0.41	3.67	44.9	4.79	6.41	1
B149-G201	1.09	8.15	13.73	1.88	0.65	3.78	48.7	4.35	6.15	1
B163-G217	0.90	9.10	11.62	2.14	0.25	3.00	34.3	6.22	8.12	1
B168	1.46	8.10	13.53	1.86	0.40	2.24	28.9	5.08	6.82	5
B170-G221	1.09	7.95	14.56	1.81	0.33	1.68	21.6	4.94	6.45	1
B174-G226	1.16	5.60	12.38	1.16	2.57	4.54	36.8	3.56	6.16	1
B176-G227	1.61	7.75	13.95	1.75	1.35	5.99	76.6	3.40	5.36	1
B177-G228	1.21	11.20	15.13	2.58	0.15	6.52	57.0	4.96	5.78	1
B181-G232	1.01	6.90	13.82	1.50	0.78	2.17	24.4	4.33	6.28	1
B183-G234	1.62	8.10	12.92	1.86	0.47	2.62	33.7	5.12	7.02	2
B184-G236	1.15	6.50	13.72	1.38	1.20	2.83	28.9	3.88	5.98	1
B187-G237	1.28	2.10	14.21	0.52	4.10	3.12	13.5	2.76	5.36	1
B189-G240	1.16	6.20	13.49	1.30	1.74	3.69	34.9	3.53	5.78	1
B190-G241	1.05	7.45	14.17	1.66	0.61	2.24	27.8	4.41	6.18	1
B193-G244	1.02	8.10	12.15	1.86	0.36	2.03	26.2	5.76	7.76	1
B194-G243	1.18	7.70	14.78	1.74	0.40	1.70	21.6	4.68	6.21	1
B196-G246	1.75	6.65	14.55	1.42	1.13	2.83	29.9	3.60	5.51	1
B197-G247	1.02	8.75	13.97	2.05	0.35	3.27	39.6	4.90	6.45	1
B198-G249	1.04	3.40	15.46	0.73	1.73	1.82	9.4	3.16	5.22	1
B199-G248	1.13	5.70	15.24	1.18	1.06	1.92	16.0	3.56	5.39	1
B200	1.07	3.80	15.74	0.80	3.08	3.53	19.5	2.24	4.34	6
B202-G251	4.39	6.80	15.28	1.47	0.65	1.73	19.0	4.00	5.63	1
B203-G252	1.53	14.00	13.85	3.14	0.05	6.98	62.4	6.41	6.94	6
B206-G257	1.05	5.65	12.43	1.17	1.57	2.81	23.1	4.18	6.66	1
B207-G258	1.23	6.30	15.00	1.33	0.99	2.18	21.2	3.64	5.46	1
B208-G259	0.99	8.40	14.32	1.95	0.64	4.52	57.2	4.07	5.72	1
B209-G261	1.05	6.00	14.16	1.25	0.73	1.44	13.0	4.44	6.38	1
B211-G262	0.99	6.80	14.24	1.47	0.93	2.48	27.2	3.96	5.87	1
B212-G263	1.15	7.45	13.10	1.66	0.79	2.91	36.1	4.50	6.55	1
B213-G264	1.11	6.90	13.92	1.50	0.50	1.40	15.7	4.87	6.70	1
B214-G265	1.06	9.25	14.82	2.18	0.20	2.72	30.2	5.17	6.37	1
B215-G266	1.08	7.10	14.09	1.55	0.74	2.26	26.4	4.26	6.12	1
B217-G269	1.09	5.50	13.74	1.13	1.39	2.39	18.9	3.83	6.03	1
B218-G272	1.03	8.45	11.85	1.96	0.44	3.19	40.2	5.55	7.60	1
B219-G271	1.23	7.50	13.54	1.68	0.57	2.15	26.8	4.75	6.63	1
B220-G275	1.00	6.00	14.12	1.25	2.05	4.08	36.6	3.10	5.27	1
B221-G276	1.19	6.30	14.06	1.33	1.08	2.37	23.0	3.91	5.93	1
B224-G279	1.03	4.45	13.11	0.92	5.24	6.95	43.4	2.50	5.19	1
B225-G280	1.08	7.20	11.02	1.58	0.66	2.12	25.2	5.62	8.06	1
B228-G281	1.65	3.45	13.83	0.74	2.68	2.84	14.8	3.24	5.72	1
B229-G282	3.51	3.80	14.26	0.80	6.21	7.11	39.3	1.92	4.46	1
B230-G283	0.94	7.90	13.86	1.80	0.43	2.08	26.8	4.91	6.62	1
B231-G285	1.58	7.05	14.69	1.54	0.65	1.93	22.4	4.20	5.92	1
B232-G286	1.00	7.55	13.21	1.69	0.62	2.43	30.5	4.75	6.71	1
B233-G287	1.36	6.60	13.06	1.41	1.07	2.64	27.5	4.27	6.47	1
B234-G290	1.10	7.20	13.79	1.58	0.77	2.48	29.6	4.30	6.23	1
B235-G297	1.31	7.95	13.26	1.81	0.42	2.10	27.2	5.17	6.99	1
B236-G298	1.09	2.50	15.37	0.59	2.84	2.40	10.9	2.71	4.96	1
B237-G299	1.00	7.60	14.60	1.71	1.42	5.72	72.2	3.11	4.96	1
B238-G301	0.98	7.40	13.55	1.65	0.97	3.46	42.7	4.07	6.07	1
B239-M74	1.12	8.10	14.36	1.86	0.39	2.17	28.0	4.79	6.36	1

B240-G302	0.95	7.85	12.80	1.78	0.63	2.99	38.5	4.83	6.84	2
B247	1.02	3.90	13.96	0.82	9.77	11.45	64.4	1.43	4.13	6
B248	1.17	6.10	15.11	1.28	1.65	3.38	31.1	2.98	4.90	1
B255D-D072	1.43	3.35	14.98	0.73	6.62	6.87	35.3	1.62	4.07	1
B257-V219	1.01	7.50	13.69	1.68	0.43	1.62	20.2	5.05	6.84	1
B266	247.44	4.50	14.96	0.93	1.36	1.82	11.5	3.52	5.55	1
B269	0.99	9.90	14.91	2.33	0.24	5.01	49.9	4.76	5.88	1
B272-V294	1.04	6.65	14.38	1.42	1.95	4.90	51.8	2.96	5.02	1
B279-D068	1.31	7.90	13.90	1.80	1.03	5.03	64.8	3.74	5.64	1
B281-G288	1.10	2.25	14.57	0.54	3.91	3.10	13.7	2.65	5.16	1
B283-G296	1.12	5.60	14.82	1.16	1.95	3.44	27.9	2.95	5.00	1
B292-G010	0.90	6.75	14.74	1.45	1.12	2.94	31.8	3.51	5.37	1
B293-G011	0.94	7.15	13.96	1.57	1.06	3.33	39.4	3.83	5.79	1
B295-G014	0.93	6.10	14.41	1.28	1.52	3.12	28.7	3.36	5.40	1
B298-G021	0.96	7.05	14.35	1.54	0.93	2.78	32.2	3.86	5.73	1
B301-G022	1.16	6.20	14.25	1.30	1.22	2.58	24.4	3.70	5.72	1
B302-G023	0.92	4.50	14.54	0.93	3.42	4.58	28.9	2.48	4.79	1
B304-G028	1.03	6.80	14.44	1.47	1.22	3.26	35.8	3.51	5.44	1
B305-D024	1.06	9.25	15.22	2.18	0.21	2.91	32.3	4.93	6.05	56
B306-G029	0.97	7.90	12.51	1.80	0.57	2.81	36.2	5.05	7.10	1
B307-G030	1.36	9.35	14.37	2.20	0.33	4.83	52.7	4.67	6.05	52
B309-G031	2.94	3.40	15.11	0.73	4.89	5.13	26.6	1.95	4.30	1
B311-G033	1.16	7.65	12.76	1.72	0.61	2.52	32.0	4.94	6.98	1
B312-G035	1.08	7.25	12.65	1.60	1.08	3.59	43.1	4.31	6.53	1
B313-G036	1.11	8.05	13.04	1.84	0.62	3.38	43.5	4.71	6.65	1
B316-G040	1.03	6.15	14.58	1.29	3.03	6.33	59.0	2.38	4.53	1
B333	1.07	13.55	15.97	3.04	0.07	8.32	73.2	5.17	5.40	1
B335-V013	1.18	6.65	13.85	1.42	2.18	5.47	57.8	3.02	5.21	1
B336-G067	0.95	2.95	16.03	0.66	2.55	2.41	11.7	2.50	4.57	1
B337-G068	0.96	5.75	14.36	1.19	1.16	2.14	18.0	3.79	5.81	1
B339-G077	0.94	8.25	13.82	1.91	0.38	2.37	30.4	5.00	6.65	1
B341-G081	1.41	7.50	13.57	1.68	0.62	2.37	29.6	4.61	6.50	1
B343-G105	0.88	8.35	13.95	1.94	0.40	2.73	34.8	4.83	6.47	1
B344-G127	1.04	7.45	13.28	1.66	0.67	2.46	30.6	4.65	6.62	1
B345-G143	1.66	7.50	14.27	1.68	0.57	2.18	27.2	4.44	6.17	1
B347-G154	1.11	7.35	14.08	1.63	0.99	3.47	42.4	3.83	5.73	1
B348-G153	426.75	8.20	13.99	1.89	0.28	1.68	21.6	5.34	6.90	1
B350-G162	0.88	6.25	14.18	1.31	2.14	4.62	44.1	2.98	5.13	1
B351-G179	0.95	6.15	14.97	1.29	2.06	4.30	40.1	2.73	4.72	1
B352-G180	1.04	7.35	14.15	1.63	0.75	2.63	32.1	4.16	5.99	5
B354-G186	1.05	1.50	15.47	0.41	4.74	2.97	12.1	2.18	4.62	2
B356-G206	1.30	7.55	14.10	1.69	0.65	2.54	32.0	4.33	6.12	1
B361-G255	0.94	6.65	14.69	1.42	1.31	3.30	34.9	3.35	5.26	1
B363-G274	0.98	2.65	15.89	0.61	2.08	1.83	8.5	2.87	4.94	1
B365-G284	3.42	6.30	14.23	1.33	1.76	3.88	37.6	3.20	5.30	1
B366-G291	1.65	4.15	14.01	0.86	3.40	4.21	24.8	2.75	5.19	1
B370-G300	1.38	8.05	13.39	1.84	0.51	2.74	35.3	4.84	6.67	1
B372-G304	1.44	6.80	13.95	1.47	1.30	3.46	37.9	3.63	5.68	6
B373-G305	1.43	7.55	12.48	1.69	0.49	1.92	24.1	5.35	7.40	1
B375-G307	1.57	9.65	14.34	2.27	0.28	5.14	53.2	4.81	6.12	1
B378-G311	1.58	7.75	15.03	1.75	0.70	3.10	39.6	3.82	5.42	1
B382-G317	1.44	5.25	14.97	1.08	1.28	2.06	15.4	3.48	5.44	1
B386-G322	1.74	7.85	12.86	1.78	0.48	2.29	29.5	5.15	7.09	1
B391-G328	0.95	5.25	14.72	1.08	1.69	2.71	20.2	3.22	5.29	1
B393-G330	0.93	6.10	14.32	1.28	2.21	4.54	41.8	2.90	5.05	1

B397-G336	2.33	7.80	13.94	1.77	0.48	2.19	28.1	4.74	6.47	1
B398-G341	0.97	5.05	14.41	1.04	2.02	3.08	21.9	3.15	5.33	1
B399-G342	1.11	7.55	15.00	1.69	0.94	3.68	46.3	3.49	5.18	1
B400-G343	1.00	8.00	13.86	1.83	0.38	2.00	25.8	5.03	6.71	1
B401-G344	1.07	8.05	14.50	1.84	0.62	3.39	43.7	4.12	5.77	1
B402-G346	1.23	4.60	14.44	0.95	2.36	3.24	20.9	2.99	5.23	1
B405-G351	0.97	6.75	12.60	1.45	1.47	3.83	41.5	4.02	6.37	1
B407-G352	0.97	6.90	13.07	1.50	0.87	2.42	27.1	4.49	6.61	1
B436	1.20	5.75	15.38	1.19	2.20	4.06	34.2	2.54	4.50	1
B457-G097	2.81	2.20	15.23	0.54	6.09	4.77	20.9	1.82	4.30	1
B461-G131	0.95	7.10	14.70	1.55	0.73	2.25	26.3	4.02	5.76	1
B462	0.94	7.35	15.80	1.63	0.99	3.45	42.2	3.15	4.71	1
B467-G202	1.02	7.50	15.34	1.68	0.96	3.64	45.5	3.34	4.98	1
BA11	1.06	10.55	15.46	2.46	0.11	3.42	31.3	5.38	6.15	2
DAO38	1.14	9.60	16.20	2.26	0.19	3.31	34.5	4.60	5.46	1
DAO55	0.91	2.80	17.52	0.64	1.69	1.54	7.3	2.47	4.16	1
G260	0.97	7.20	14.55	1.58	1.35	4.34	51.7	3.27	5.17	1
G268	1.01	6.25	13.58	1.31	1.69	3.65	34.9	3.53	5.75	1
G327-MVI	0.98	6.80	13.54	1.47	1.39	3.72	40.7	3.71	5.85	1
H16	0.90	5.80	15.30	1.20	5.70	10.67	91.0	1.32	3.50	1
M009	1.05	6.15	15.22	1.29	1.26	2.64	24.6	3.27	5.10	1
SK019A	1.10	7.90	15.23	1.80	0.31	1.49	19.2	4.79	6.16	1
SK020A	1.14	3.30	16.21	0.72	2.71	2.78	14.2	2.29	4.31	1
SK026A	1.79	5.70	16.80	1.18	0.46	0.84	7.0	4.01	5.35	1
SK035A	1.11	6.75	15.63	1.45	0.76	1.98	21.4	3.67	5.26	1
SK036A	1.10	4.05	16.73	0.84	1.30	1.57	9.1	2.93	4.63	1
SK052A	1.74	4.45	15.93	0.92	1.65	2.19	13.7	2.88	4.76	1
SK053A	1.09	9.95	15.50	2.33	0.15	3.32	32.8	5.09	5.99	1
SK055A	1.18	5.25	15.38	1.08	2.53	4.07	30.3	2.43	4.45	1
SK066A	1.11	10.05	15.66	2.36	0.14	3.33	32.4	5.08	5.93	1
SK071A	1.06	5.20	16.09	1.07	1.94	3.07	22.6	2.50	4.33	1
SK083A	1.25	9.95	16.23	2.33	0.09	2.02	20.0	5.44	6.09	1
SK086A	1.10	5.05	14.85	1.04	3.18	4.86	34.5	2.37	4.57	1
SK104A	1.48	6.35	14.99	1.34	0.70	1.56	15.4	4.10	5.84	1
SK109A	1.15	8.10	15.89	1.86	0.79	4.44	57.2	3.25	4.66	1
V129-BA4	1.48	5.20	14.63	1.07	1.49	2.36	17.4	3.43	5.49	1

This table is available in electronic form from the VizieR archive.

[1]Cluster names are taken from table 2.1 and are the same as those in the Revised Bologna Catalogue of M31 GCs (Galleti *et al.*, 2004).

[2]The χ^2 per degree of freedom for the best fitting model to the cluster profile.

[3]The central potential (W_0) and concentration parameter [$c = \log(r_t/r_c)$] of the cluster.

[4]The K-band magnitude of the cluster (from profile fits *not* aperture photometry) [mag].

[5]The core, half light and tidal radii of the cluster (assuming the distance of M31 to be 780 kpc McConnachie *et al.*, 2005) [pc].

[6]The cluster core density [$L_{K,\odot}pc^{-3}$] and stellar encounter rate [as defined by equation 1.6; $L^2_{K,\odot}pc^{-3}km^{-1}s$].

[7]Flag based on visual examination of the cluster image and its residual after subtraction of the best fitting model. Flags are: 1-clean cluster image and residual; 2-elliptical profile; 3-poor residual after subtraction; 4-bright source close to the cluster which may potentially influence its profile; 5-potential asterism; 6-potentially stellar profile/ unphysical parameters.

Bibliography

Aarseth S. J., Heggie D. C., 1998, MNRAS, 297, 794

Adelman-McCarthy J. K., *et al.*, 2007, ApJs, 172, 634

An D., Johnson J. A., Clem J. L., Yanny B., Rockosi C. M., Morrison H. L., Harding P., Gunn J. E., Allende Prieto C., Beers T. C., Cudworth K. M., Ivans I. I., Ivezić Ž., Lee Y. S., Lupton R. H., Bizyaev D., Brewington H., Malanushenko E., Malanushenko V., Oravetz D., Pan K., Simmons A., Snedden S., Watters S., York D. G., 2008, ApJs, 179, 326

Angelini L., Loewenstein M., Mushotzky R. F., 2001, ApJ, 557, L35

Ashman K. M., Zepf S. E., 1992, ApJ, 384, 50

Ashman K. M., Zepf S. E., 1998, *Globular Cluster Systems*

Barmby P., Holland S., Huchra J. P., 2002, AJ, 123, 1937

Barmby P., Huchra J. P., 2001, AJ, 122, 2458

Barmby P., Huchra J. P., Brodie J. P., Forbes D. A., Schroder L. L., Grillmair C. J., 2000, AJ, 119, 727

Barmby P., McLaughlin D. E., Harris W. E., Harris G. L. H., Forbes D. A., 2007, AJ, 133, 2764

Barmby P., Perina S., Bellazzini M., Cohen J. G., Hodge P. W., Huchra J. P., Kissler-Patig M., Puzia T. H., Strader J., 2009, ArXiv e-prints

Barnard R., 2003, in *XMM-Newton Proposal ID #02022304*, pp. 120–+

Bassa C., Pooley D., Homer L., Verbunt F., Gaensler B. M., Lewin W. H. G., Anderson S. F., Margon B., Kaspi V. M., van der Klis M., 2004, ApJ, 609, 755

Bassino L. P., Richtler T., Dirsch B., 2006, MNRAS, 367, 156

Battistini P., Bonoli F., Braccesi A., Federici L., Fusi Pecci F., Marano B., Borngen F., 1987, A&AS, 67, 447

Battistini P. L., Bonoli F., Casavecchia M., Ciotti L., Federici L., Fusi-Pecci F., 1993, A&A, 272, 77

Baum W. A., 1955, PASP, 67, 328

Beasley M. A., Brodie J. P., Strader J., Forbes D. A., Proctor R. N., Barmby P., Huchra J. P., 2004, AJ, 128, 1623

Becker W., Swartz D. A., Pavlov G. G., Elsner R. F., Grindlay J., Mignani R., Tennant A. F., Backer D., Pulone L., Testa V., Weisskopf M. C., 2003, ApJ, 594, 798

Bellazzini M., Pasquali A., Federici L., Ferraro F. R., Pecci F. F., 1995, ApJ, 439, 687

Bellazzini M., Pecci F. F., Ferraro F. R., Galleti S., Catelan M., Landsman W. B., 2001, AJ, 122, 2569

Bertin E., Arnouts S., 1996, A&AS, 117, 393

Bohlin R. C., Dickinson M. E., Calzetti D., 2001, AJ, 122, 2118

Boroson B., Kallman T., Vrtilek S. D., Raymond J., Still M., Bautista M., Quaintrell H., 2000, ApJ, 529, 414

Bradt H., Levine A. M., Remillard R. A., Smith D. A., 2000, ArXiv Astrophysics e-prints

Bregman J., 2005, in *XMM-Newton Proposal ID #04040602*, pp. 151–+

Brodie J. P., Huchra J. P., 1991, ApJ, 379, 157

Brodie J. P., Strader J., 2006, ARA&A, 44, 193

Brown T. M., Ferguson H. C., Smith E., Kimble R. A., Sweigart A. V., Renzini A., Rich R. M., VandenBerg D. A., 2004, ApJ, 613, L125

Brown T. M., Sweigart A. V., Lanz T., Landsman W. B., Hubeny I., 2001, ApJ, 562, 368

Brown W. R., Geller M. J., Kenyon S. J., Diaferio A., 2010, AJ, 139, 59

Bruzual G., Charlot S., 2003, MNRAS, 344, 1000

Buonanno R., Corsi C., Bellazzini M., Ferraro F. R., Pecci F. F., 1997, AJ, 113, 706

Caldwell N., Harding P., Morrison H., Rose J. A., Schiavon R., Kriessler J., 2009, AJ, 137, 94

Cardelli J. A., Clayton G. C., Mathis J. S., 1989, ApJ, 345, 245

Carlson M. N., Holtzman J. A., 2001, PASP, 113, 1522

Carpenter J. M., 2001, AJ, 121, 2851

Carretta E., Bragaglia A., Gratton R. G., Leone F., Recio-Blanco A., Lucatello S., 2006, A&A, 450, 523

Casares J., 2007, in V. Karas & G. Matt (ed.), *IAU Symposium*, vol. 238 of *IAU Symposium*, pp. 3–12

Casares J., Charles P. A., Naylor T., 1992, Nature, 355, 614

Catelan M., 2000, ApJ, 531, 826

Catelan M., 2009, Ap&SS, 320, 261

Clark G. W., 1975, ApJ, 199, L143

Code A. D., 1969, PASP, 81, 475

Cohen J. G., Hsieh S., Metchev S., Djorgovski S. G., Malkan M., 2007, AJ, 133, 99

Cohen J. G., Matthews K., Cameron P. B., 2005, ApJ, 634, L45

Côté P., Blakeslee J. P., Ferrarese L., Jordán A., Mei S., Merritt D., Milosavljević M., Peng E. W., Tonry J. L., West M. J., 2004, ApJs, 153, 223

Côté P., Marzke R. O., West M. J., 1998, ApJ, 501, 554

Côté P., West M. J., Marzke R. O., 2002, ApJ, 567, 853

Cox A. N., 2000, *Allen's astrophysical quantities*

Davies M. B., Piotto G., de Angeli F., 2004, MNRAS, 349, 129

D'Cruz N. L., Dorman B., Rood R. T., O'Connell R. W., 1996, ApJ, 466, 359

de Jong J. A., van Paradijs J., Augusteijn T., 1996, A&A, 314, 484

de Vaucouleurs G., de Vaucouleurs A., Corwin Jr. H. G., Buta R. J., Paturel G., Fouque P., 1991, *Third Reference Catalogue of Bright Galaxies*

di Stefano R., 2003, in *XMM-Newton Proposal ID #02047910*, pp. 255–+

Di Stefano R., Kong A. K. H., Garcia M. R., Barmby P., Greiner J., Murray S. S., Primini F. A., 2002, ApJ, 570, 618

Dieball A., Knigge C., Zurek D. R., Shara M. M., Long K. S., Charles P. A., Hannikainen D., 2007, ApJ, 670, 379

Dirsch B., Richtler T., Geisler D., Forte J. C., Bassino L. P., Gieren W. P., 2003, AJ, 125, 1908

Dirsch B., Schuberth Y., Richtler T., 2005, A&A, 433, 43

Djorgovski S., Meylan G., 1994, AJ, 108, 1292

Dorman B., O'Connell R. W., Rood R. T., 1995, ApJ, 442, 105

Dorman B., Rood R. T., O'Connell R. W., 1993, ApJ, 419, 596

Dye S., Warren S. J., Hambly N. C., Cross N. J. G., Hodgkin S. T., Irwin M. J., Lawrence A., Adamson A. J., Almaini O., Edge A. C., Hirst P., Jameson R. F., Lucas P. W., van Breukelen C., Bryant J., Casali M., Collins R. S., Dalton G. B., Davies J. I., Davis C. J., Emerson J. P., Evans D. W., Foucaud S., Gonzales-Solares E. A., Hewett P. C., Kendall T. R., Kerr T. H., Leggett S. K., Lodieu N., Loveday J., Lewis J. R., Mann R. G., McMahon R. G., Mortlock D. J., Nakajima Y., Pinfield D. J., Rawlings M. G., Read M. A., Riello M., Sekiguchi K., Smith A. J., Sutorius E. T. W., Varricatt W., Walton N. A., Weatherley S. J., 2006, MNRAS, 372, 1227

Fabian A. C., Pringle J. E., Rees M. J., 1975, MNRAS, 172, 15P

Fall S. M., Zhang Q., 2001, ApJ, 561, 751

Fan Z., Ma J., de Grijs R., Yang Y., Zhou X., 2006, MNRAS, 371, 1648

Fan Z., Ma J., de Grijs R., Zhou X., 2008, MNRAS, 385, 1973

Fan Z., Ma J., Zhou X., Chen J., Jiang Z., Wu Z., 2005, PASP, 117, 1236

Ferraro F. R., Montegriffo P., Origlia L., Fusi Pecci F., 2000, AJ, 119, 1282

Forbes D. A., Brodie J. P., Grillmair C. J., 1997, AJ, 113, 1652

Forbes D. A., Lasky P., Graham A. W., Spitler L., 2008, MNRAS, 389, 1924

Frank J., King A., Raine D. J., 2002, *Accretion Power in Astrophysics: Third Edition*

Freeman K. C., Norris J., 1981, ARA&A, 19, 319

Fruchter A. S., Hook R. N., 2002, PASP, 114, 144

Fukugita M., Ichikawa T., Gunn J. E., Doi M., Shimasaku K., Schneider D. P., 1996, AJ, 111, 1748

Fusi Pecci F., Battistini P., Bendinelli O., Bonoli F., Cacciari C., Djorgovski S., Federici L., Ferraro F. R., Parmeggiani G., Weir N., Zavatti F., 1994, A&A, 284, 349

Fusi Pecci F., Bellazzini M., 1997, in A. G. D. Philip, J. Liebert, R. Saffer, & D. S. Hayes (ed.), *The Third Conference on Faint Blue Stars*, pp. 255–+

Fusi Pecci F., Bellazzini M., Buzzoni A., De Simone E., Federici L., Galleti S., 2005, AJ, 130, 554

Fusi Pecci F., Ferraro F. R., Bellazzini M., Djorgovski S., Piotto G., Buonanno R., 1993, AJ, 105, 1145

Fusi-Pecci F., Renzini A., 1978, in A. G. D. Philip & D. S. Hayes (ed.), *The HR Diagram - The 100th Anniversary of Henry Norris Russell*, vol. 80 of *IAU Symposium*, pp. 225–+

Galleti S., Bellazzini M., Federici L., Buzzoni A., Fusi Pecci F., 2007, A&A, 471, 127

Galleti S., Federici L., Bellazzini M., Buzzoni A., Fusi Pecci F., 2006, A&A, 456, 985

Galleti S., Federici L., Bellazzini M., Fusi Pecci F., Macrina S., 2004, A&A, 416, 917

Geisler D., Lee M. G., Kim E., 1996, AJ, 111, 1529

Grimm H., Gilfanov M., Sunyaev R., 2002, A&A, 391, 923

Grindlay J. E., Heinke C., Edmonds P. D., Murray S. S., 2001a, Sci, 292, 2290

Grindlay J. E., Heinke C. O., Edmonds P. D., Murray S. S., Cool A. M., 2001b, ApJ, 563, L53

Grindlay J. E., Hertz P., 1985, in D. Q. Lamb & J. Patterson (ed.), *Cataclysmic Variables and Low-Mass X-ray Binaries*, vol. 113 of *Astrophysics and Space Science Library*, pp. 79–91

Han Z., 2008, A&A, 484, L31

Han Z., Podsiadlowski P., Lynas-Gray A. E., 2007, MNRAS, 380, 1098

Han Z., Podsiadlowski P., Maxted P. F. L., Marsh T. R., 2003, MNRAS, 341, 669

Han Z., Podsiadlowski P., Maxted P. F. L., Marsh T. R., Ivanova N., 2002, MNRAS, 336, 449

Hannikainen D. C., Charles P. A., van Zyl L., Kong A. K. H., Homer L., Hakala P., Naylor T., Davies M. B., 2005, MNRAS, 357, 325

Harris W. E., 1991, ARA&A, 29, 543

Harris W. E., 1996, AJ, 112, 1487

Harris W. E., 2009, ApJ, 703, 939

Harris W. E., Harris G. L. H., Barmby P., McLaughlin D. E., Forbes D. A., 2006, AJ, 132, 2187

Harris W. E., van den Bergh S., 1981, AJ, 86, 1627

Heber U., Kudritzki R. P., Caloi V., Castellani V., Danziger J., 1986, A&A, 162, 171

Heinke C. O., Budac S. A., 2009, The Astronomer's Telegram, 2139, 1

Heinke C. O., Grindlay J. E., Lugger P. M., Cohn H. N., Edmonds P. D., Lloyd D. A., Cool A. M., 2003, ApJ, 598, 501

Hempel M., Geisler D., Hoard D. W., Harris W. E., 2005, A&A, 439, 59

Hempel M., Zepf S., Kundu A., Geisler D., Maccarone T. J., 2007, ApJ, 661, 768

Henze M., Pietsch W., Haberl F., Sala G., Quimby R., Hernanz M., Della Valle M., Milne P., Williams G. G., Burwitz V., Greiner J., Stiele H., Hartmann D. H., Kong A. K. H., Hornoch K., 2009, A&A, 500, 769

Hewett P. C., Warren S. J., Leggett S. K., Hodgkin S. T., 2006, MNRAS, 367, 454

Hills J. G., Day C. A., 1976, 17, 87

Hobbs G., Lorimer D. R., Lyne A. G., Kramer M., 2005, MNRAS, 360, 974

Hodgkin S. T., Irwin M. J., Hewett P. C., Warren S. J., 2009, MNRAS, 394, 675

Hogg D. E., 1964, JRASC, 58, 203

Hoyle F., Schwarzschild M., 1955, ApJs, 2, 1

Hubble E., 1932, ApJ, 76, 44

Huchra J. P., Brodie J. P., Kent S. M., 1991, ApJ, 370, 495

Hut P., Verbunt F., 1983, Nature, 301, 587

Huxor A. P., Tanvir N. R., Ferguson A. M. N., Irwin M. J., Ibata R., Bridges T., Lewis G. F., 2008, MNRAS, 385, 1989

Huxor A. P., Tanvir N. R., Irwin M. J., Ibata R., Collett J. L., Ferguson A. M. N., Bridges T., Lewis G. F., 2005, MNRAS, 360, 1007

Hynes R. I., Horne K., O'Brien K., Haswell C. A., Robinson E. L., King A. R., Charles P. A., Pearson K. J., 2006, ApJ, 648, 1156

Irwin J. A., Bregman J. N., 1999, ApJ, 510, L21

Ivanova N., 2006, ApJ, 636, 979

Ivanova N., Heinke C. O., Rasio F. A., Belczynski K., Fregeau J. M., 2008, MNRAS, 386, 553

Jester S., Schneider D. P., Richards G. T., Green R. F., Schmidt M., Hall P. B., Strauss M. A., Vanden Berk D. E., Stoughton C., Gunn J. E., Brinkmann J., Kent S. M., Smith J. A., Tucker D. L., Yanny B., 2005, AJ, 130, 873

Jiang L., Ma J., Zhou X., Chen J., Wu H., Jiang Z., 2003, AJ, 125, 727

Jordán A., Blakeslee J. P., Côté P., Ferrarese L., Infante L., Mei S., Merritt D., Peng E. W., Tonry J. L., West M. J., 2007a, ApJs, 169, 213

Jordán A., Côté P., Blakeslee J. P., Ferrarese L., McLaughlin D. E., Mei S., Peng E. W., Tonry J. L., Merritt D., Milosavljević M., Sarazin C. L., Sivakoff G. R., West M. J., 2005, ApJ, 634, 1002

Jordán A., Côté P., Ferrarese L., Blakeslee J. P., Mei S., Merritt D., Milosavljević M., Peng E. W., Tonry J. L., West M. J., 2004, ApJ, 613, 279

Jordán A., Peng E. W., Blakeslee J. P., Côté P., Eyheramendy S., Ferrarese L., Mei S., Tonry J. L., West M. J., 2009, ApJs, 180, 54

Jordán A., Sivakoff G. R., McLaughlin D. E., Blakeslee J. P., Evans D. A., Kraft R. P., Hardcastle M. J., Peng E. W., Côté P., Croston J. H., Juett A. M., Minniti D., Raychaudhury S., Sarazin C. L., Worrall D. M., Harris W. E., Woodley K. A., Birkinshaw M., Brassington N. J., Forman W. R., Jones C., Murray S. S., 2007b, ApJ, 671, L117

Kaaret P., 2002, ApJ, 578, 114

Kaaret P., Ford E. C., Chen K., 1997, ApJ, 480, L27+

Katz J. I., 1975, Nature, 253, 698

Kaviraj S., Sohn S. T., O'Connell R. W., Yoon S., Lee Y. W., Yi S. K., 2007, MNRAS, 377, 987

Kim D., Fabbiano G., 2004, ApJ, 611, 846

Kim E., Kim D., Fabbiano G., Lee M. G., Park H. S., Geisler D., Dirsch B., 2006, ApJ, 647, 276

Kim S. C., Lee M. G., Geisler D., Sarajedini A., Park H. S., Hwang H. S., Harris W. E., Seguel J. C., von Hippel T., 2007, AJ, 134, 706

King A. R., 1999, Physical Reports, 311, 337

King A. R., Kolb U., Burderi L., 1996, ApJ, 464, L127+

King I. R., 1966, AJ, 71, 64

King I. R., Stanford S. A., Albrecht R., Barbieri C., Blades J. C., Boksenberg A., Crane P., Disney M. J., Deharveng J. M., Jakobsen P., Kamperman T. M., Macchetto F., Mackay C. D., Paresce F., Weigelt G., Baxter D., Greenfield P., Jedrzejewski R., Nota A., Sparks W. B., Sosin C., 1993, ApJ, 413, L117

Kissler-Patig M., 2000, in R. E. Schielicke (ed.), *Reviews in Modern Astronomy*, vol. 13 of *Reviews in Modern Astronomy*, pp. 13–+

Knigge C., Leigh N., Sills A., 2009, Nature, 457, 288

Kong A., 2005, in *XMM-Newton Proposal ID #04035301*, pp. 138–+

Kong A. K. H., Bassa C., Pooley D., Lewin W. H. G., Homer L., Verbunt F., Anderson S. F., Margon B., 2006, ApJ, 647, 1065

Kong A. K. H., Garcia M. R., Primini F. A., Murray S. S., Di Stefano R., McClintock J. E., 2002, ApJ, 577, 738

Kundu A., Maccarone T. J., Zepf S. E., 2002, ApJ, 574, L5

Kundu A., Maccarone T. J., Zepf S. E., 2007, ApJ, 662, 525

Kundu A., Maccarone T. J., Zepf S. E., Puzia T. H., 2003, ApJ, 589, L81

Kundu A., Whitmore B. C., 1998, AJ, 116, 2841

Kundu A., Whitmore B. C., 2001, AJ, 121, 2950

Kundu A., Zepf S. E., 2007, Astrophys. J. Lett., 660, L109

Kundu A., Zepf S. E., Hempel M., Morton D., Ashman K. M., Maccarone T. J., Kissler-Patig M., Puzia T. H., Vesperini E., 2005, ApJ, 634, L41

Larsen S. S., Brodie J. P., Huchra J. P., Forbes D. A., Grillmair C. J., 2001, AJ, 121, 2974

Larsen S. S., Richtler T., 2000, A&A, 354, 836

Lattimer J. M., Prakash M., 2004, Science, 304, 536

Lee H., Yoon S., Lee Y., 2000, AJ, 120, 998

Lee Y., Demarque P., Zinn R., 1994, ApJ, 423, 248

Lee Y., Joo S., Han S., Chung C., Ree C. H., Sohn Y., Kim Y., Yoon S., Yi S. K., Demarque P., 2005, ApJ, 621, L57

Leigh N., Sills A., Knigge C., 2007, ApJ, 661, 210

Lewin W. H. G., van der Klis M., 2006, *Compact stellar X-ray sources*

Lightman A. P., Shapiro S. L., 1978, Reviews of Modern Physics, 50, 437

Liu Q. Z., van Paradijs J., van den Heuvel E. P. J., 2001, A&A, 368, 1021

Lyne A. G., Brinklow A., Middleditch J., Kulkarni S. R., Backer D. C., 1987, Nature, 328, 399

Maccarone T. J., Kundu A., Zepf S. E., 2004, ApJ, 606, 430

Mackey A. D., Huxor A., Ferguson A. M. N., Tanvir N. R., Irwin M., Ibata R., Bridges T., Johnson R. A., Lewis G., 2006, ApJ, 653, L105

Magnier E. A., 1993, *A study of M31*, Ph.D. thesis, AA(Massachusetts Inst. of Tech.)

Maraston C., 2005, MNRAS, 362, 799

Margon B., Anderson S. F., Downes R. A., Bohlin R. C., Jakobsen P., 1991, ApJ, 369, L71

Marín-Franch A., Aparicio A., Piotto G., Rosenberg A., Chaboyer B., Sarajedini A., Siegel M., Anderson J., Bedin L. R., Dotter A., Hempel M., King I., Majewski S., Milone A. P., Paust N., Reid I. N., 2009, ApJ, 694, 1498

Massey P., Olsen K. A. G., Hodge P. W., Strong S. B., Jacoby G. H., Schlingman W., Smith R. C., 2006, AJ, 131, 2478

Maxted P. f. L., Heber U., Marsh T. R., North R. C., 2001, MNRAS, 326, 1391

McClintock J. E., Remillard R. A., 1986, ApJ, 308, 110

McConnachie A. W., Irwin M. J., Ferguson A. M. N., Ibata R. A., Lewis G. F., Tanvir N., 2005, MNRAS, 356, 979

McCrea W. H., 1964, MNRAS, 128, 147

McLaughlin D. E., 1999, AJ, 117, 2398

McLaughlin D. E., Barmby P., Harris W. E., Forbes D. A., Harris G. L. H., 2008, MNRAS, 384, 563

Mengel J. G., Gross P. G., 1976, Ap&SS, 41, 407

Miller B. W., Lotz J. M., Ferguson H. C., Stiavelli M., Whitmore B. C., 1998, ApJ, 508, L133

Mirabel I. F., Dhawan V., Mignani R. P., Rodrigues I., Guglielmetti F., 2001, Nature, 413, 139

Mirabel I. F., Rodrigues I., 2003, A&A, 398, L25

Mochejska B. J., Kaluzny J., Krockenberger M., Sasselov D. D., Stanek K. Z., 1998, AcA, 48, 455

Moehler S., 2001, PASP, 113, 1162

Moni Bidin C., Catelan M., Altmann M., 2008, A&A, 480, L1

Moni Bidin C., Moehler S., Piotto G., Momany Y., Recio-Blanco A., 2009, A&A, 498, 737

Morrissey P., Schiminovich D., Barlow T. A., Martin D. C., Blakkolb B., Conrow T., Cooke B., Erickson K., Fanson J., Friedman P. G., Grange R., Jelinsky P. N., Lee S., Liu D., Mazer A., McLean R., Milliard B., Randall D., Schmitigal W., Sen A., Siegmund O. H. W., Surber F., Vaughan A., Viton M., Welsh B. Y., Bianchi L., Byun Y., Donas J., Forster K., Heckman T. M., Lee Y., Madore B. F., Malina R. F., Neff S. G., Rich R. M., Small T., Szalay A. S., Wyder T. K., 2005, ApJ, 619, L7

Murphy B. W., Cohn H. N., Hut P., 1990, MNRAS, 245, 335

Naylor T., Charles P. A., Drew J. E., Hassall B. J. M., 1988, MNRAS, 233, 285

O'Connell R. W., 1999, ARA&A, 37, 603

Oke J. B., Gunn J. E., 1983, ApJ, 266, 713

Ostriker J. P., Weaver R., Yahil A., McCray R., 1976, ApJ, 208, L61

Ostrov P., Geisler D., Forte J. C., 1993, AJ, 105, 1762

Paczynski B., 1976, in P. Eggleton, S. Mitton, & J. Whelan (ed.), *Structure and Evolution of Close Binary Systems*, vol. 73 of *IAU Symposium*, pp. 75–+

Peacock M. B., Maccarone T. J., Knigge C., Kundu A., Waters C. Z., Zepf S. E., Zurek D. R., 2010, MNRAS, 402, 803

Peacock M. B., Maccarone T. J., Waters C. Z., Kundu A., Zepf S. E., Knigge C., Zurek D. R., 2009, MNRAS, 392, L55

Peng E. W., Jordán A., Côté P., Blakeslee J. P., Ferrarese L., Mei S., West M. J., Merritt D., Milosavljević M., Tonry J. L., 2006, ApJ, 639, 95

Peng E. W., Jordán A., Côté P., Takamiya M., West M. J., Blakeslee J. P., Chen C., Ferrarese L., Mei S., Tonry J. L., West A. A., 2008, ApJ, 681, 197

Perets H. B., Fabrycky D. C., 2009, ApJ, 697, 1048

Perina S., Federici L., Bellazzini M., Cacciari C., Fusi Pecci F., Galleti S., 2009, ArXiv e-prints

Perrett K. M., Bridges T. J., Hanes D. A., Irwin M. J., Brodie J. P., Carter D., Huchra J. P., Watson F. G., 2002, AJ, 123, 2490

Peterson R. C., 1982, ApJ, 258, 499

Peterson R. C., 1985, ApJ, 294, L35

Pfahl E., Rappaport S., Podsiadlowski P., 2002, ApJ, 573, 283

Pietsch W., 2008, Astronomische Nachrichten, 329, 170

Piotto G., Bedin L. R., Anderson J., King I. R., Cassisi S., Milone A. P., Villanova S., Pietrinferni A., Renzini A., 2007, ApJ, 661, L53

Piotto G., King I. R., Djorgovski S. G., Sosin C., Zoccali M., Saviane I., De Angeli F., Riello M., Recio-Blanco A., Rich R. M., Meylan G., Renzini A., 2002, A&A, 391, 945

Pogson N., 1860, MNRAS, 21, 32

Pooley D., Hut P., 2006, ApJ, 646, L143

Pooley D., Lewin W. H. G., Anderson S. F., Baumgardt H., Filippenko A. V., Gaensler B. M., Homer L., Hut P., Kaspi V. M., Makino J., Margon B., McMillan S., Portegies Zwart S., van der Klis M., Verbunt F., 2003, ApJ, 591, L131

Pooley D., Lewin W. H. G., Homer L., Verbunt F., Anderson S. F., Gaensler B. M., Margon B., Miller J. M., Fox D. W., Kaspi V. M., van der Klis M., 2002a, ApJ, 569, 405

Pooley D., Lewin W. H. G., Verbunt F., Homer L., Margon B., Gaensler B. M., Kaspi V. M., Miller J. M., Fox D. W., van der Klis M., 2002b, ApJ, 573, 184

Primini F. A., Forman W., Jones C., 1993, ApJ, 410, 615

Puzia T. H., Perrett K. M., Bridges T. J., 2005, A&A, 434, 909

Puzia T. H., Zepf S. E., Kissler-Patig M., Hilker M., Minniti D., Goudfrooij P., 2002, A&A, 391, 453

Quimby R., Mondol P., Wheeler J. C., Rykoff E., Yuan F., Akerlof C., Shafter A., Ofek E., Kasliwal M., 2007, ATel, 1118, 1

Racine R., 1968, PASP, 80, 326

Racine R., 1991, AJ, 101, 865

Randall S. W., Sarazin C. L., Irwin J. A., 2004, ApJ, 600, 729

Reed L. G., Harris G. L. H., Harris W. E., 1992, AJ, 103, 824

Reed L. G., Harris G. L. H., Harris W. E., 1994, AJ, 107, 555

Reed M. D., Stiening R., 2004, PASP, 116, 506

Rey S., Rich R. M., Lee Y., Yoon S., Yi S. K., Bianchi L., Sohn Y., Friedman P. G., Barlow T. A., Byun Y., Donas J., Forster K., Heckman T. M., Jee M. J., Jelinsky P. N., Kim S., Lee J., Madore B. F., Malina R. F., Martin D. C., Milliard B., Morrissey P., Neff S. G., Rhee J., Schiminovich D., Siegmund O. H. W., Small T., Szalay A. S., Welsh B. Y., Wyder T. K., 2005, ApJ, 619, L119

Rey S., Rich R. M., Sohn S. T., Yoon S., Chung C., Yi S. K., Lee Y., Rhee J., Bianchi L., Madore B. F., Lee K., Barlow T. A., Forster K., Friedman P. G., Martin D. C., Morrissey P., Neff S. G., Schiminovich D., Seibert M., Small T., Wyder T. K., Donas J., Heckman T. M., Milliard B., Szalay A. S., Welsh B. Y., 2007, ApJs, 173, 643

Rey S., Yoon S., Lee Y., Chaboyer B., Sarajedini A., 2001, AJ, 122, 3219

Rhode K. L., Zepf S. E., 2004, AJ, 127, 302

Rhode K. L., Zepf S. E., Kundu A., Larner A. N., 2007, AJ, 134, 1403

Rhode K. L., Zepf S. E., Santos M. R., 2005, ApJ, 630, L21

Rich R. M., Corsi C. E., Cacciari C., Federici L., Fusi Pecci F., Djorgovski S. G., Freedman W. L., 2005, AJ, 129, 2670

Rich R. M., Sosin C., Djorgovski S. G., Piotto G., King I. R., Renzini A., Phinney E. S., Dorman B., Liebert J., Meylan G., 1997, ApJ, 484, L25+

Rood R. T., 1973, ApJ, 184, 815

Rutledge R. E., Bildsten L., Brown E. F., Pavlov G. G., Zavlin V. E., 2002, ApJ, 578, 405

Salaris M., Weiss A., 2002, A&A, 388, 492

Sandage A., 1961, *The Hubble atlas of galaxies*

Sandage A., Wallerstein G., 1960, ApJ, 131, 598

Santos M. R., 2003, in M. Kissler-Patig (ed.), *Extragalactic Globular Cluster Systems*, pp. 348–+

Sarazin C. L., Kundu A., Irwin J. A., Sivakoff G. R., Blanton E. L., Randall S. W., 2003, ApJ, 595, 743

Schlegel D. J., Finkbeiner D. P., Davis M., 1998, ApJ, 500, 525

Searle L., Zinn R., 1978, ApJ, 225, 357

Servillat M., Dieball A., Webb N. A., Knigge C., Cornelisse R., Barret D., Long K. S., Shara M. M., Zurek D. R., 2008, A&A, 490, 641

Shafter A. W., Quimby R. M., 2007, ApJ, 671, L121

Shapley H., 1918, PASP, 30, 42

Shara M. M., Zurek D. R., Baltz E. A., Lauer T. R., Silk J., 2004, ApJ, 605, L117

Sharov A. S., Alksnis A., 1995, AstL, 21, 579

Sharov A. S., Liutyi V. M., 1983, Ap&SS, 90, 371

Sharov A. S., Lyutyj V. M., Esipov V. F., 1987, PAZh, 13, 643

Sharov A. S., Lyutyj V. M., Ikonnikova N. P., 1992, SvAL, 18, 41

Shirey R., Soria R., Borozdin K., Osborne J. P., Tiengo A., Guainazzi M., Hayter C., La Palombara N., Mason K., Molendi S., Paerels F., Pietsch W., Priedhorsky W., Read A. M., Watson M. G., West R. G., 2001, A&A, 365, L195

Smits M., Maccarone T. J., Kundu A., Zepf S. E., 2006, A&A, 458, 477

Sohn S. T., O'Connell R. W., Kundu A., Landsman W. B., Burstein D., Bohlin R. C., Frogel J. A., Rose J. A., 2006, AJ, 131, 866

Spitzer Jr. L., Thuan T. X., 1972, ApJ, 175, 31

Stoughton C., *et al.*, 2002, AJ, 123, 485

Strader J., Brodie J. P., Spitler L., Beasley M. A., 2006, AJ, 132, 2333

Strader J., Smith G. H., Larsen S., Brodie J. P., Huchra J. P., 2009, AJ, 138, 547

Suda T., Tsujimoto T., Shigeyama T., Fujimoto M. Y., 2007, ApJ, 671, L129

Supper R., Hasinger G., Lewin W. H. G., Magnier E. A., van Paradijs J., Pietsch W., Read A. M., Trümper J., 2001, A&A, 373, 63

Supper R., Hasinger G., Pietsch W., Truemper J., Jain A., Magnier E. A., Lewin W. H. G., van Paradijs J., 1997, A&A, 317, 328

Sutantyo W., 1975, A&A, 44, 227

Tabur V., Kiss L. L., Bedding T. R., 2009, ApJ, 703, L72

Tamura N., Sharples R. M., Arimoto N., Onodera M., Ohta K., Yamada Y., 2006a, MNRAS, 373, 588

Tamura N., Sharples R. M., Arimoto N., Onodera M., Ohta K., Yamada Y., 2006b, MNRAS, 373, 601

Tanvir N., 2006, in *XMM-Newton Proposal ID #05059004*, pp. 212–+

Tauris T. M., van den Heuvel E., 2003, ArXiv Astrophysics e-prints

Trinchieri G., Fabbiano G., 1991, ApJ, 382, 82

Trudolyubov S., Priedhorsky W., 2004, ApJ, 616, 821

van den Bergh S., Morbey C., Pazder J., 1991, ApJ, 375, 594

van den Heuvel E. P. J., Heise J., 1972, Nature, 239, 67

van der Klis M., 2000, ARA&A, 38, 717

van Leeuwen J., Stappers B. W., 2010, A&A, 509 (26), A260000+

van Paradijs J., 1996, Astrophys. J. Lett., 464, L139+

Verbunt F., Hut P., 1987, in D. J. Helfand & J.-H. Huang (ed.), *The Origin and Evolution of Neutron Stars*, vol. 125 of *IAU Symposium*, pp. 187–+

Verbunt F., Lewin W. H. G., 2006, *Globular cluster X-ray sources*, pp. 341–379

Vetešnik M., 1962, Bulletin of the Astronomical Institutes of Czechoslovakia, 13, 180

Vrtilek S. D., Penninx W., Raymond J. C., Verbunt F., Hertz P., Wood K., Lewin W. H. G., Mitsuda K., 1991, ApJ, 376, 278

Vrtilek S. D., Raymond J. C., Garcia M. R., Verbunt F., Hasinger G., Kurster M., 1990, A&A, 235, 162

Warner B., 1995, *Cataclysmic variable stars*

Waters C. Z., 2007, *High resolution analysis of extragalactic globular clusters*, Ph.D. thesis, AA(Michigan State University)

Watson M. G., Schröder A. C., Fyfe D., Page C. G., Lamer G., Mateos S., Pye J., Sakano M., Rosen S., Ballet J., Barcons X., Barret D., Boller T., Brunner H., Brusa M., Caccianiga A., Carrera F. J., Ceballos M., Della Ceca R., Denby M., Denkinson G., Dupuy S., Farrell S., Fraschetti F., Freyberg M. J., Guillout P., Hambaryan V., Maccacaro T., Mathiesen B., McMahon R., Michel L., Motch C., Osborne J. P., Page M., Pakull M. W., Pietsch W., Saxton R., Schwope A., Severgnini P., Simpson M., Sironi G., Stewart G., Stewart I. M., Stobbart A., Tedds J., Warwick R., Webb N., West R., Worrall D., Yuan W., 2009, A&A, 493, 339

Wehlau A., Butterworth S., Hogg H. S., 1990, AJ, 99, 1159

West M. J., 1993, MNRAS, 265, 755

White N. E., Angelini L., 2001, ApJ, 561, L101

White R. E., Sarazin C. L., Kulkarni S. R., 2002, ApJ, 571, L23

Whitmore B. C., Schweizer F., 1995, AJ, 109, 960

Williams B. F., Garcia M. R., Kong A. K. H., Primini F. A., King A. R., Di Stefano R., Murray S. S., 2004, ApJ, 609, 735

Worthey G., 1994, ApJs, 95, 107

Zepf S. E., Ashman K. M., 1993, MNRAS, 264, 611

Zucker D. B., Kniazev A. Y., Bell E. F., Martínez-Delgado D., Grebel E. K., Rix H., Rockosi C. M., Holtzman J. A., Walterbos R. A. M., Ivezić Ž., Brinkmann J., Brewington H., Harvanek M., Kleinman S. J., Krzesinski J., Lamb D. Q., Long D., Newman P. R., Nitta A., Snedden S. A., 2004, ApJ, 612, L117